The impact of *Candida rugosa* lipase in the gut microbiome in health and Alzheimer's disease and identification of allosteric modulators

Ariane Menden, M.Sc.

A thesis submitted for the degree of Doctor of Philosophy in the discipline of neuroscience

Supervised by: Dr. Ghania Ait-Ghezala, Dr. Stefan Crynen, Dr. Michael Mullan

Submitted: May 2021

Roskamp Institute
2040 Whitfield Ave
Sarasota, FL, 34243
USA

The Open University
Walton Hall
Milton Keynes, MK76 AA
UK

Declaration

I hereby declare that the work presented in this thesis is my own, except where stated. This work has not been submitted for any other degree or professional qualification.

Ariane Menden

Acknowledgements

I would like to express my sincere gratitude to the following people, which provided continuous support and guidance to me and enabled the completion of this research.

First of all, I would like to thank my primary supervisor Dr. Ait-Ghezala, who never hesitated to discuss and support my research efforts. Her encouragement of my professional and personal development has always been greatly appreciated and enabled the achievements of this thesis. She has been a role model and I consider myself very lucky to have her as my supervisor on this venture.

In addition, I would like to thank my secondary supervisors Dr. Crynen and Dr. Mullan. Dr. Crynen has always been approachable to discuss and develop new ideas advancing the work of my thesis. Dr. Mullan has always kept my research investigations on track, while sharing his comprehensive knowledge, which advanced the assessment and interpretation of results in detail and in the bigger picture.

Thank you all for supporting and encouraging my ideas and preparing with me this thesis and the associated publications.

I would also like to thank the Roskamp Institute and Enzymedica, Inc, who initiated and sponsored this project. Thank you to Scott Sensenbrenner, who collaborated with us and provided Candida rugosa lipase for all experiments.

Furthermore, I would like to express my sincere gratitude to Dr. Crawford, who leads among many other programs the PhD program at the Roskamp institute. Thank you for giving me and many others the opportunity to advance their professional development in a highly innovative and inspiring environment. Also, thank you to Dr. Crawford and Dr. Mullan for keeping the institute safe in an unprecedented global pandemic, which allowed completion of my PhD without experiencing any hardship or delay.

Special thank you goes to our external collaborators Prof. Dr. Klatt and Ms. Broedlow from the University of Minnesota, who provided the 16S sequencing platform and assisted with analysing gut microbiome data in R and Qiime. In addition, I would like to thank Dr. V Venkatarajan Mathura, who supported the *in silico* analysis.

I would also like to thank the other PIs of the Roskamp institute, Dr. Evans, Dr. Paris, Dr. Abdullah, Dr. Ferguson, Dr. Mouzon, Dr. Bachmeier and Dr. Ojo, who were always willing to discuss research and to help when needed. Thank you to my fellow PhD students and all technicians, which accompanied me on this journey. Special thank you goes to Davane, Coral, Andrew, Teresa and Utsav, who actively contributed to this thesis.

Finally, I would like to thank my family and friends, which always enabled me to achieve my goals and fulfill my dreams.

Danke an meine Freunde und Familie, die mir trotz der Distanz immer das Gefuehl geben ein Teil meines und ihres Lebens zu sein.
Danke Mama und Papa. Euch widme ich diese Arbeit, denn diese waere ohne euch nicht moeglich gewesen. Weiterer Dank geht an meinen Bruder Marian, meine Nichte Vivi und meinen Neffen Dari sowie Lydia, Bodo und Oli; durch euch alle weiss ich, was Familie bedeutet.

- Freundschaft und Familie bilden das Seil das haelt, wenn alle Stricke reissen. -

Thank you to my friends and family back home, who always gave me the feeling to be part of their life and them being part of mine. Thank you, Mama and Papa. This thesis is dedicated to you, since this would have not been possible without you. Additional thank you goes to my brother Marian, my niece Vivi and my nephew Dari as well as Lydia, Bodo and Oli, due to you, I know what family means.

- Friendship and family form the rope that will hold you, when all else is failing. -

Thank you to my second family Maureen, George, Peter, Andrea, Jen, Tony, Declan, Mary, Marshall, Dawn, Bill, Katie, and Cullen, who have always given me the feeling of being home, far away from home.
Finally, thank you to my husband Mike, who has taken on the craziest challenge with me called life. Thank you for being so patient and loving throughout the past five years, which included caring for Kaja, numerous travel adventures, four visa processes, two theses, several moves, furniture shopping and Florida during a global pandemic. I think we might be invincible. I love you.

Publications

Franke AA, Li X, **Menden A**, Lee MR & Lai JF. *Oxytocin analysis from human serum, urine, and saliva by orbitrap liquid chromatography-mass spectrometry*. Drug testing and analysis, 2019, *11*(1), 119–128. https://doi.org/10.1002/dta.2475

Menden A, Hall D, Paris D, Mathura V, Crawford F, Mullan M, Crynen S & Ait-Ghezala G. *A fast, miniaturised in-vitro assay developed for quantification of lipase enzyme activity*, Journal of enzyme inhibition and medicinal chemistry, 2019, *34*(1), 1474–1480. https://doi.org/10.1080/14756366.2019.1651312 (Chapter II, IV)

Menden A, Hall D, Broedlow CA, Darcey T, Crawford F, Klatt N, Crynen S, Mullan M, Ait-Ghezala G. *Candida rugosa lipase alters the gastrointestinal environment in wild-type mice*. Journal of Biomedicine and Pharmacotherapy. 2020, 130:110579. https://doi.org/10.1016/j.biopha.2020.110579 (Chapter II)

Menden A, Crynen S, Mathura V, Paris D, Crawford F, Mullan M, & Ait-Ghezala G. *Novel, natural allosteric inhibitors, and enhancers of Candida rugosa lipase activity.* Bioorganic Chemistry.2020,
https://doi.org/10.1016/j.bioorg.2021.104732 (Chapter IV)

Poster

Franke AA, **Menden A**, Li X. *Determination of Total Oxytocin in Human Serum by Traditional LCMS*, Experimental Biology, 2017, Chicago, CO

Franke AA, Li X, **Menden A**, Lai J. *Basal Serum Oxytocin Levels in Healthy Non-Pregnant/Lactating Humans Are Below 10 pg/ml and Not Detectable by Traditional Orbitrap LCMS*, Experimental Biology, 2018, San Diego, CA

Menden A, Ringland C, Broedlow CA, Hall D, Crawford F, Crynen S, Bachmeier C, Klatt N, Mullan M, Ait-Ghezala G. *APOE4 and E4FAD gut microbiome analysis infers that the ApoE4 allele drives AD microbiome changes*, 3rd Microbiome Movement: Gut-Brain Axis Summit, 2019, Boston, MA

Menden A, Hall D, Hahn-Townsend C, Broedlow CA, Crawford F, Klatt N, Crynen S, Mullan M, Ait-Ghezala G. *Candida rugosa lipase administration alters Alzheimer's disease pathology.* 6th Translational Microbiome Conference, 2020, virtual

Menden A, Hall D, Hahn-Townsend C, Broedlow CA, Crawford F, Klatt N, Crynen S, Mullan M, Ait-Ghezala G. *Candida rugosa lipase administration modulates gut-brain axis in Alzheimer's disease-like pathology.* Cold Spring Harbor Laboratory - Microbiome, 2020, virtual

Menden A, Hall D, Hahn-Townsend C, Broedlow CA, Crawford F, Klatt N, Crynen S, Mullan M, Ait-Ghezala G. *Candida rugosa lipase administration modulates gut-brain axis in Alzheimer's disease-like pathology.* SfN Connectome, 2021, virtual

Menden A, Hall D, Hahn-Townsend C, Broedlow CA, Crawford F, Klatt N, Crynen S, Mullan M, Ait-Ghezala G. *Candida rugosa lipase administration modulates gut-brain axis in Alzheimer's disease-like pathology.* Keystone Symposia – Harnessing the Microbiome for Disease Prevention and Therapy, 2021, virtual

Presentations

Menden A, *Optimization of allosteric modulation of digestive enzymes and the potential impact in the gut microbiome*, The Human Microbiome Symposium (EMBL), 2018, Heidelberg, Germany

Abstract

Alzheimer's disease (AD) affects more than 50 million people worldwide. Despite the continual identification of new disease features, treatment options are limited due to failure of clinical trials to identify effective treatments. Consequently, novel therapeutic strategies arising from other areas of research, such as the gut microbiome, are being considered due to their potential to modulate AD pathology. The gut microbiome is regarded as a symbiotic physiological regulator of human health via the bidirectional gut–brain axes. Several studies have revealed a persistent compositional imbalance in the gut microbiome of both AD patients and in animal models of AD potentially contributing to AD pathology. Conversely, it has been suggested that normalization of the gut microbial composition might ameliorate AD pathology in animal models and in humans. In healthy individuals, shifts of the gut microbiota primarily occur in response to dietary changes such as administration of exogenous enzymes. These enzymes can evoke shifts in the composition of the gut microbiota by increasing enzymatic activity in the digestive tract and therefore the release of metabolites from dietary macromolecules. Lipases are one subclass of digestive enzymes which can elevate gut availability of fatty acids and glycerol. Some of these cleavage products can promote growth and metabolite production of specific bacterial species changing the gut microbial composition. Hence, we hypothesized that **"Oral administration of an exogenous lipase in AP/PS1 mice normalizes gut microbiome and metabolite composition, and rescues AD pathology and aberrant behavior**".

To this end, three hypotheses were examined: **(1)** Oral lipase administration in C67BL/6J (Wt) mice will alter free fatty acid and glycerol release in the gut; **(2)** oral lipase administration in APPsw/PS1-de9 (APP/PS1) mice will normalize the gut microbiota and metabolite composition that correlates with improved AD-like pathology; and **(3)** that a combined use of a positive allosteric modulator with the exogenous lipase will enhance the expected effects from hypotheses (1) and (2).

The studies revealed that exogenous lipase administration is correlated with normalization of gut microbiome and metabolite composition in Wt and APP/PS1 animals. Furthermore, administration of exogenous lipase correlated with reduced AD-like pathology and behavior in APP/PS1 animals. In addition, we provided evidence that the treatment-dependent shifts in the gut microbiome and metabolite composition of APP/PS1 mice caused the observed improvement of memory in these animals. Collectively, this work advances our understanding of how CRL could be used to reduce AD pathology and might present novel treatment options for AD patients.

Table of contents

Figures

CHAPTER I

CHAPTER II

CHAPTER III

CHAPTER IV

Tables

CHAPTER II

CHAPTER IV

Abbreviations

4-MU	4-methylumbelliferone
4-MUB	4-methylumbelliferyl butyrate
4-MUP	4-methylumbelliferyl palmitate
5HT	serotonin
AAALAC	Association for Assessment and Accreditation of Laboratory Animal Care International
Aβ	amyloid
AD	Alzheimer's disease
AhR	aryl hydrocarbon receptor
AICD	protein intracellular C-terminal domain
ABX	antibiotic-induced microbiome-depleted
ALS	amyotrophic lateral sclerosis
ANCOM	analysis of composition of microbiomes
ANOVA	analysis of variance
ApoE	apolipoprotein E
APP	amyloid precursor protein
APP/PS1	APPsw/PS1-de9
ASV	amplicon sequence variant
AUC	area under the curve
BACE	β-secretase
BBB	blood-brain barrier
B-cells	B lymphocyte
BLI	biolayer interferometry
BMI	body mass index
CCK	cholecystokinin
CCL	C-C Motif Chemokine Ligand
CNS	central nervous system
CR1	complement receptor type 1
CRL	*Candida rugosa* lipase
CSF	cerebrospinal fluid
DAMP	danger-associated molecular pattern
DC	dendritic cell

DIABLO	Data Integration Analysis for Biomarker discovery using a latent component method for Omics
DMSO	dimethyl sulfoxide
EEC	enteroendocrine cells
FAD	familial form of AD
FBS	fetal bovine serum
FC	fold change
FDR	false discovery rate
FIP	*Fédération Internationale Pharmaceutique*
FITC	fluorescein isothiocyanate
FMT	fecal matter transplant
FFA	free fatty acid
FFAR	free fatty acid receptor
GABA	γ-aminobutyric acid
GBA	gut-brain axis
GCMS	gas-chromatography mass spectrometry
GF	germ-free
GFAP	glial fibrillary acidic protein
GLP-1	glucagon-like protein 1
GOS	galactooligosaccharide
GPR	G-protein coupled receptor
GRAS	Generally Recognized as Safe
GWAS	genome-wide association studies
HDL	high-density lipoprotein
HD	Huntington's disease
IBD	inflammatory bowel diseases
IFNγ	interferon γ
IACUC	Institutional Animal Care and Use Committee
Iba1	ionized calcium-binding adapter molecule 1
IgA	immunoglobulin A
IL	interleukin
Km	Michaelis-Menten constant
LCMS	liquid-chromatography mass spectrometry

LEfSe	Linear discriminant analysis Effect Size
LLOQ	lower limit of quantification
LPS	lipopolysaccharides
M1	neurotoxic microglia
M2	phagocytic microglia
MCI	mild cognitive impairment
MS	multiple sclerosis
NFT	neurofibrillary tangles
NLRP3	NOD-, LRR- and pyrin domain-containing protein 3
PAGE	polyacrylamide gel electrophoresis
PAM	positive allosteric modulator
PAMP	pathogen-associated molecular pattern
PB	phosphate buffer
PBS	phosphate buffered saline
PD	Parkinson's disease
PERMANOVA	permutational multivariate analysis of variance
PERT	pancreatic enzyme replacement therapy
PFA	paraformaldehyde
PSEN	Presenilin 1
PYY	peptide YY
RBC	red blood cells
ROS	reactive oxygen species
rdCV-RF	repeated double cross validation random forest
SAD	sporadic form of AD
SCAP	cleavage-activating protein
SCFA	short-chain fatty acids
SDS	sodium dodecyl sulfate
SFA	saturated fatty acid
SI	small intestine
SREBP	sterol regulatory element-binding protein
T-cell	T lymphocyte
Th	T-helper cell
TGFβ	transforming growth factor β

TGR5	G-protein-coupled bile acid receptor, Gpbar1
TNFα	tumor necrosis factor
Treg	regulatory T-cell
TREM2	triggering receptors expressed on myeloid cells 2
UFA	unsaturated fatty acid
ULOQ	lower limit of quantification
V0	initial velocity
VLDL/LDL	very-low-density lipoprotein/low-density lipoprotein
Vmax	maximal velocity
Wt	C57BL/6J

Chapter I: Introduction

1.1 Alzheimer's disease

Alzheimer's disease (AD) was first reported by Alois Alzheimer in 1907, who conducted behavioral studies and investigated the brain pathology of AD patients. He identified the main pathological hallmarks of the disease as extra-cellular aggregation of amyloid into plaques and neurofibrillary tangles [1]. AD is a multifactorial disease and is the most prevalent form of dementia in the elderly. Almost 50 million people worldwide are affected by AD or other dementias, but occurrence can strongly vary by location [2]. AD is associated with environmental and genetic risk factors. Most AD cases are a sporadic form of AD (SAD), which accounts for more than 90% of all AD cases with an average age onset around the age of 65 (late-onset) [3]. Although no obvious inheritance pattern has been identified in SAD, certain risk factors such as the presence of the Apolipoprotein E (ApoE) 4 allele have been noted [4]. Although the ApoE gene is primarily present in peripheral organs such as liver, kidney, and spleen, it plays a critical role in the central nervous system (CNS) by transporting lipids, cholesterol and vitamins to neuronal receptors. It is polymorphic, with three alleles: ApoE2, 3 and 4 [5]. ApoE3 carriers have no higher risk for SAD development. However, heterozygous ApoE4 carriers have a 2-3 fold increased risk of AD development (homozygous carriers: 12-fold), while carriers of the protective ApoE2 allele exhibit a reduced risk of SAD development even in the heterogenic form with ApoE4 [4, 6]. In AD, ApoE has been suggested to have differing effects - dependent on the present isoforms - in Aβ aggregation, clearance, neurotoxicity and neuroinflammation, but it has not been fully understood how ApoE isoforms can favor or protect from AD development [7].

The familial form of AD (FAD) accounts for less than 5% of all AD cases; it is inherited in an autosomal dominant manner. Its onset typically occurs before the age of 65 (early-onset) and is caused by a mutation in one of the following three genes: the Amyloid Precursor Protein (APP),

Presenilin 1 (PSEN1) or PSEN2 [8]. APP is expressed in various cell types including neurons, where it has been reported to promote neuronal cell migration during early development [9]. Investigation of mutations in the APP allele revealed 50 different mutations accounting for 10% of FAD cases. PSEN1 encodes for the proteolytic subunit of γ-secretase with more than 150 identified mutations accounting for 70% of FAD cases. Mutation of this gene promotes the cleavage of APP into a longer, toxic amyloid (Aβ) species. PSEN2 encodes for another catalytic component of γ-secretase with only 14 known mutations, generating the same toxic cleavage product and accounting for under 5% of FAD cases (figure 1.1) [10]. The common pathological hallmarks, which are induced by the respective genetic mutations and environmental factors in both FAD and SAD, can be detected in several regions of the brain (hippocampus, hypothalamus, amygdala, cerebellum, frontal, parietal and occipital lobe, corpus callosum and the thalamus) [11]. Depending on the extent of progression, different pathological features can be dominant such as neurodegeneration, neuroinflammation, increased oxidative stress, mitochondrial damage, reactive glial and microglial changes [12, 13].

1.1.1: AD pathology

The main pathological characteristics in AD, which are associated with cognitive decline and behavioral changes include the aggregation of the longer extracellular amyloid fragments, the hyperphosphorylation of intracellular tau, and neuroinflammation [14, 15].

1.1.1.1: Amyloid hypothesis

APP has eight isoforms, of which APP695 is the most commonly expressed in neurons [16]. α- and β-secretase enzymes process APP through extra-cellular cleavage of the N-terminal domain (figure 1.1). While α-secretase cleaves APP releasing extracellular soluble APPs-α and the membrane-bound C83 (non-amyloidogenic pathway), β-secretase (BACE) cleavage causes the release of APPs-β and the longer C99 fragment (amyloidogenic pathway, figure 1.1). Both membrane-bound fragments C83 and C99 can be further processed by γ-secretase, which causes

the intracellular release of the amyloid precursor protein intracellular C-terminal domain (AICD, figure 1.1). The remaining extracellular fragment is released, consisting of either the shorter p3 fragment from C83 after additional γ-secretase cleavage (non-amyloidogenic pathway) or Aβ from C99 (amyloidogenic pathway, figure 1.1).

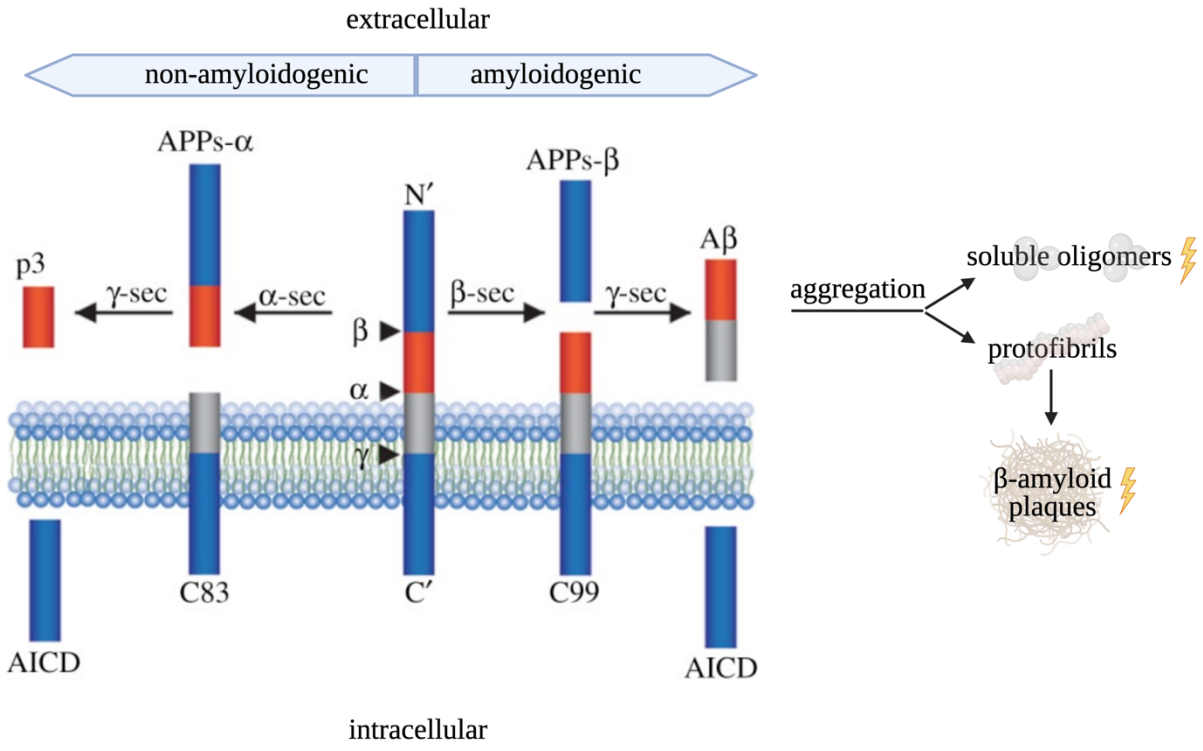

Figure 1.1: Amyloidogenic and non-amyloidogenic pathway of APP processing adapted from Frost et al [17]. α-secretase and/or β-secretase cleavage determines the resulting fragment with pivotal consequences. While p3 has no known harmful effects in AD, the resulting Aβ aggregates, which further assemble to either soluble oligomers or protofibrils and plaques have detrimental consequences.

The length of Aβ varies between 40-42 amino acids. Aβ42 represents the most toxic fragment with the highest potential to accumulate and form amyloid-like structures [18-21]. In recent years there has been an increasing focus on the smaller, more soluble aggregates of Aß, referred to as oligomers, whose formation can also be enhanced by several mutations [22-27]. These soluble oligomers are now widely regarded as the more toxic species and show an increased correlation with cognitive decline similar to that shown with the development of tau pathology, the second pathological hallmark of AD [28].

Over the past decade the amyloid hypothesis has become increasingly controversial in part due to several failed clinical trials and new evidence suggesting amyloid is not the primary mechanistic driver of AD pathology. Numerous AD clinical trials testing antibodies targeting APP aggregates to enhance clearance such as gantenerumab or bapineuzumab failed to improve cognitive measures, even though Aβ levels were drastically reduced [29, 30]. Other strategies such as inhibition of the amyloidogenic pathway to reduce Aβ production through BACE1 inhibitors such as verubecestat or atabecestat even worsened patient's health status [31]. Finally, a case study has been presented where a 73-year old carrier of a familial PSEN1 E280A mutation, which normally leads to fast progression of AD and early death, did not exhibit cognitive impairment [32]. She was identified as a homozygous carrier of the APOE3 Christchurch mutation, and analysis of the brain by PET scan showed increased amyloid depositions in the AD-affected areas of the brain and fewer areas of tau accumulation [32]. The study suggested that the presence of the homozygous APOE isoform protected her from the familial PSEN1 mutation and raised questions about amyloid's impact on cognitive decline [32]. Hence, other disease hypotheses such as tau phosphorylation, ApoE isoforms, neuroinflammation, or dysbiosis of the gut microbiota (aberrant composition of the gut microbiota throughout an extended period) have gained increased focus as drivers of disease pathology.

1.1.1.2: Neuroinflammation

Neuroinflammation is a critical contributor to AD pathology. While initial research has focused on the neurodegenerative components of the disease such as amyloid plaques or neurofibrillary tangles, the role of neuroinflammation is recognized as an independent mechanism rather than a consequence of the former in the recent decade.

In healthy individuals, the gastrointestinal cell walls (endocrine cells, Paneth cells, goblet cells, neuroendocrine cells) and the blood-brain barrier (BBB, endothelial cells, pericytes, astrocytes)

provide a physical barrier against pathogen-associated molecular patterns (PAMPs) such as lipopolysaccharides, flagellin, ssRNA or lipoproteins and danger-associated molecular patterns (DAMPs) from the gut to prevent vast inflammation [33]. The brain is further protected against potential threats by resident glial cells, namely microglia and astrocytes. These are activated when the physical barriers fail to retain the microbial-derived PAMPs and DAMPs in the gut or when other threats are encountered such as brain injuries or toxic metabolites. Activation of the resident glia cells results in activation of the endogenous inflammatory cascades to eradicate the identified threats. Genome-wide association studies (GWAS) support the pivotal role of these two glial cell types in AD by identifying 25 loci that showed a robust association between glia and AD. Some of these genes are exclusively or preferentially expressed by microglia and astrocytes such as ApoE, triggering receptors expressed on myeloid cells 2 (TREM2), or CD33 [34-36].

Microglia are the brain's resident macrophages and are, through the BBB, secluded to maintain tissue homeostasis in the brain. They act as the host´s brain immune defense by recognizing and eliminating pathogens and positively impacting brain development through pruning of synapses and the secretion of neurotrophic factors [37-39]. Depending on surrounding cytokine and metabolite expression, microglia can be activated and subsequently differentiated into two subtypes, although it has been shown that this simplistic subgrouping does not reflect the microglial populations [40]. However, many studies have maintained the common stratification to reduce complexity when analyzing and interpreting the associated data. The pro-inflammatory, neurotoxic subtype of microglia (M1) can be favored by cytokines such as interleukin (IL)-1β, tumor necrosis factor α (TNFα) or interferon γ (IFNγ), while the anti-inflammatory and neuroprotective microglia subtype (M2) differentiates when IL-4, IL-10 and IL-13 are present. Additionally, M2 microglia can express IL-4, IL-10 and transforming growth factor β (TGFβ), which inhibits the pro-inflammatory M1 subtype [41]. Chronic stimulation of

microglia, due to a reduction in BBB integrity and the presence of amyloid fibrils, can harm neuronal function and result in neurodegeneration over time. In AD patients, reactive microglia surround Aβ depositions and express neurotoxic factors such as IL-1β, TNFα and reactive oxygen species (ROS), all of which cause progressive neuronal damage [1, 36, 42]. Reactive microglia express increased levels of ionized calcium-binding adapter molecule 1 (Iba1) and cluster of differentiation 45 (CD45) [43]. Additionally, the abundance of microglia is proportionally associated with plaque size in both animal models as well as humans [44]. Furthermore, the presence of cortical activated microglia is associated with cognitive decline in AD patients [44]. Finally, it was shown that phagocytosis of amyloid fibrils by reactive microglia was impaired with prolonged break down of amyloid fibrils and secretion of undigested peptides, which was proposed to enhance amyloid plaque formation in AD patients [44].

Astrocytes are the second contributors to brain homeostasis due to their proximal connectivity to synaptic junctions and blood vessels, and their ability to provide metabolic and trophic support to neurons. Diseases of the brain and injury can trigger astrocytosis, an astrocyte state which enables their immunogenic response mechanisms. Astrocytosis is characterized by astrocytes that express glial fibrillary protein (GFAP), vimentin and nestin. Astrocytes are in direct interaction with neurons and can activate immune responses if exposed to triggers such as PAMPs and DAMPs [45]. In AD, reactive astrocytes can undergo excessive proliferation and process interdigitation, increase inflammatory cytokine and ROS secretion, as well as contribute to the break-down of the BBB. This leads to disturbance of their networks, interference with their functions and harm of surrounding cells including neurons [45, 46]. Similar to microglia, astrocytes expressing reactive astrocytosis markers occur commonly around plaques and correlate with plaque quantity and distribution [45]. In addition, reactive astrocytes and associated molecular patterns were determined to correlate with neurofibrillary tangle (NFT)

density but not with amyloid pathology, which could suggest an association between tau and astroglia rather than amyloid [47, 48]. Furthermore, reactive astrocytes have been shown to upregulate BACE1 production enhancing production of the more toxic amyloid species.

All together microglia and astrocytes are found to be highly activated in AD patients. In AD, they fail to perform their endogenous protective functions, while exacerbating AD pathology through their long-lasting immunogenic responses. This is also shown in various animal models, which share some of the pathological features of AD.

1.1.2: Animal Models

The development of a reliable and disease-reflective *in vivo* model of AD has been a necessary requirement to investigate human disease pathology and potential treatments. Several transgenic mouse models have been developed based on human familial mutations. Depending on the implemented mutations and promotors, different characteristics of AD pathology occur in the selected mouse model, but no model covers all properties of AD. Hence, multiple mutations have been combined to enhance pathological characteristics that more closely replicate human pathology such as the 5xFAD, 3xTg and APPsw/PS1-de9 (APP/PS1) mouse model.

In this study, the transgenic APP/PS1 mouse model, which expresses chimeric mouse/human APP with the Swedish mutations (K670N/M671L) and the human PS1 gene without Exon9 on a C57BL/6J (Wt) background was used [49]. Amyloid deposits are abundant in the hippocampus and cortex by nine months [50]. In addition, mice exhibit microglial activation around amyloid deposits as well as increased astrocytosis from six months on and cognitive impairment by twelve months of age [51, 52]. Implementation of these familial mutations for studying AD pathology is necessary to induce AD-like pathology in mice, which do not naturally develop AD.

1.1.3: Current treatments

Currently no pharmaceutical or alternative treatment strategies are available for both FAD or SAD, likely due to both the complex and heterogeneous nature of the disease. Most of the available pharmaceuticals approved for AD target symptoms such as anxiety and depression, rather than counteracting the actual pathology [53]. Experimental treatment approaches range from antibodies designed to activate the endogenous immune system to clear Aβ deposits to BACE1 inhibitors and neurotransmitter internalization inhibition [54]. Many of these strategies have failed due to occurrence of severe side effects or inability to prove efficacy in clinical trials [30, 54]. In addition, numerous clinical trials focused on targets derived from the amyloid hypothesis such as amyloid plaque removal or β-secretase inhibition, both of which seem to be less central than presumed. Hence, alternative treatments have been investigated, including: regular exercise, administration of natural compounds (Ginkgo biloba, melatonin, curcumin, vitamin C/E, etc.), dietary changes (Mediterranean diet) and cognitive training [55-57]. These studies demonstrated a reduction in the risk for SAD or ameliorated symptoms like cognitive decline and have been partly associated with changes in the composition of the gut microbiota [58]. In accordance with these investigations and results from other fields, this eventually led to examination of the contribution and role of the gut microbiome in AD. After an initial studies found disturbances of the microbiota composition in a murine model of AD, a human study concluded similar results [59, 60].

1.2 Microbiome

The human body hosts symbiotic microbial communities of bacteria, viruses, archaea, yeast, and fungi in the gut, collectively known as the gut microbiota. The cellular abundance of the gut microbiota exceeds the number of human cells by at least one order of magnitude. In humans, the gastrointestinal tract is estimated to house around two hundred trillion microbes,

most of them belonging to the Bacteria domain. In the gut, *Firmicutes*, *Bacteroidetes*, *Actinobacteria*, *Proteobacteria*, *Fusobacteria*, and *Verrucomicrobia* comprise the most prominent phyla; the *Bacteroidetes* and *Firmicutes* represent 90% of gut microbiota, but this can vary dependent on the geographical location [61]. These bacteria colonize the intestinal tissue in spatially organized networks exchanging metabolites and competing for ecological niches [62, 63]. When sampling the gut microbiome, this spatial organization is often neglected, and samples represent a mixture rather than a location-specific composition of the total gut microbiome. This is particularly true for fecal samples, which allow to assess non-invasively the gut microbiota status in animals and humans, but certain scientific questions cannot be investigated. For the following studies fecal samples were selected to assess changes in the total gut microbiota composition post treatment since this will be easily translatable to human studies. Typical assessed parameters for diversity among the microbial community include α- and β-diversity, which measure and describe differences within microbial communities of each sample (α) and within samples (β). Furthermore, the microbial communities have numerous interconnections with other complex networks of the human body such as the immune system, endocrine system and the brain with potential effects on cardiovascular and mental health [64]. It is presumed that the collective metabolic activity of the microbiota is equivalent to that of a virtual organ within the gastrointestinal lumen, highlighting its unique function.

Although numerous diseases have been associated with gut dysbiosis, the impact beyond the gut is not fully understood. Interest in the gut microbiome as it relates to the field of neuroscience intensified when researchers found a correlation between intestinal disturbances in Parkinson's disease (PD) patients decades prior to the onset of the disorder [65]. This caused the initiation of numerous other studies in brain-related diseases such as AD with particular focus on the gut microbial composition, the function of commensal and pathogenic bacterial strains, as well as its impact on signaling and transmission pathways throughout the host organism.

1.2.1: Gut-brain axes (GBA)

Several hypotheses about the communication pathways from the gut to the brain have been described, including neuronal (vagus nerve) and endocrine (glucagon-like protein 1 (GLP-1), serotonin (5-HT), corticosterone, etc.). Furthermore, the metabolic (lipopolysaccharides (LPS), peptidoglycans, short-chain fatty acids (SCFA), etc.) and immunological (cell abundance, differentiation, and activation of T-helper cell 1 (Th1), Th2, Th17, regulatory T-cells (Tregs), etc.) have been identified. The GBA were defined as bidirectional pathways involving the enteric microbiota, the CNS, and the sympathetic and parasympathetic nervous system [66]. Furthermore, the endocrine system, the enteric nervous system, the metabolic system, and the immune system have all been shown to be connected with the enteric microbiota, which represent together the major links between the microbiota in the gut and the brain (figure 1.2) [66].

1.2.1.1: Neuronal axis

The vagus nerve is the major physical connection between the brain and the intestinal system and is considered one of the central transmission axes. It maintains parasympathetic control of the lungs, heart and intestines and is the longest nerve in the autonomic nervous system. It has been shown that specialized cells of the intestinal cell wall, EECs, or L-cells, form basal cytoplasmic processes (neuropods). The neuropods are connected to cell bodies of afferent neurons in the nodose ganglia of the vagus nerve, which creates a neuroepithelial circuit by glutamate-dependent transduction [67]. Signal transduction can be triggered by stimuli in the intestinal lumen induced by receptor binding to the apical site of EECs such as FFAR3 or FFAR2. Their activation can cause the release of GLP-1 or 5-HT, both of which possess numerous receptors on enteric vagal afferent fibers. Hence, their release induces vagal afferent signaling to the brain [68, 69]. In mouse models of neurodegenerative disease and stress, the role of vagal transmission has been demonstrated by application of sub-diaphragmatic

vagotomy, which actively disrupts the vagal signaling route. This includes the prevention of the spread of toxic α-synuclein from the gut to the brain [70-72].

1.2.1.2: Endocrine axis

The second GBA, the endocrine axis, comprises the neuroendocrine system responding to stress but also regulating other processes in the organism such as the immune system, metabolism, emotions, and digestion. Bravo et al. found that mice that have previously undergone a stress paradigm but ingested *L.rhamnosus* showed reduced stressed response indicated by lower corticosterone levels when compared to control mice [73]. This has provided evidence together with other studies that the hypothalamus-pituitary-adrenal axis, which upon activation releases corticosterone might be modulated by specific bacterial species in the gut [73]. Furthermore, it has been determined that direct or indirect microbial changes can affect other endocrine metabolites such as neurotransmitters and neurohormones, which can be secreted by certain bacterial species in the specific genera including γ-aminobutyric acid (GABA, *Lactobacillus, Bifidobacterium*), 5-HT (*Candida, Streptococcus, Escherichia, Enterococcus*) and dopamine (*Bacillus, Serratia*) [74, 75], [76, 77]. All possess pivotal functions in the brain, although it remains to be elucidated whether these enteric produced metabolites can reach the brain and emphasize the endocrine axis as second potential transmission route for AD pathology. Similarly, to the neuronal axis, this axis might play a role in the development and progression of AD pathology and contains potential treatment targets.

1.2.1.3: Immunological axis

The third GBA, the immunological axis, comprises the innate and adaptive immune responses, which maintain homeostasis by preventing pathogen infiltration within the luminal and intestinal interfaces and interacts directly with the luminal microbiota and their metabolites [78]. Memory and activated T-cells remain in commensal-colonized tissue awaiting, among other things, microbial signals, which induce their proliferation and expression of IL-17 (Th17) or

IFNγ (Th1), both of which initiate the inflammatory cascades to prevent host infection [79-81]. Furthermore, macrophages which reside in the lamina propria and recognize translocated bacteria enable live transport and activation of DCs [82, 83]. DCs can further activate immune cascades of T- and B- cells in Peyer's Patches, inducing B-cell differentiation and T-cell maturation (figure 1.2) [84]. Binding of microbial-derived butyrate or other SCFAs in the gut lumen to DCs or epithelial cell surface receptor GPR109A can cause DC-dependent IL-10 and epithelial TGFβ secretion in the lamina propria, - which can increase Treg levels in the lymph nodes [85, 86]. Tregs have specific functions in the gastro-intestinal (GI) tract where they initiate the response to orally ingested antigens, maintain mucosal homeostasis, act as immune-suppressors and prevent systemic fatal autoimmunity through IL-10, IL-35 and TGFβ expression [87, 88]. They can control Th1 and Th2 immune responses [89]. Imbalances in this fragile system, such as gut dysbiosis, can result in vast inflammatory signaling and immune cell differentiation driving reduced BBB integrity and potentially contributing to diseases such as AD [90].

1.2.1.4: Metabolic axis

The metabolic axis represents the last identified GBA. The gut microbiota can produce, metabolize, or release various substances from the luminal content; induce metabolite secretion in enteric cells; or metabolize luminal secreted substances from the host (figure 1.2). While a functional gut barrier allows selective transport of microbial metabolites preventing particular PAMPs such as LPS to travel beyond the gut, microbial dysbiosis has been shown to increase gut permeability as shown in IBDs or colon cancer [91, 92]. It remains controversial what contribution an increased gut permeability has in onset and progression of neurodegenerative diseases, but it has been positively correlated with increased age, inflammation and reduced BBB integrity [93, 94]. Furthermore, a link between gut permeability, AD, and its progressive neurodegeneration has been suggested but needs to be further investigated [95, 96]. However,

the gut microbiome does not only contribute to the harmful pool of metabolites but also to numerous metabolite levels associated with host health such as SCFA; indole derivatives; neurohormones such as 5-HT or GABA; oligosaccharides; 2°BA; metabolites of the Krebs cycle.

In this series of studies SCFA and indoles were of particular interest due to their ability to interact with glial receptors (figure 1.2):

First, SCFA's—in particular, acetate, propionate, and butyrate—are by-products of bacterial saccharolytic fermentation of complex carbohydrates and bacterial degradation of long-chain fatty acid released from the gut luminal content. These metabolites improve host health. Butyrate possesses anti-inflammatory properties and binds to the microglial receptor GPR109A inducing the anti-inflammatory state in microglia [97, 98]. In addition, it has been shown that butyrate is an energy-resource of colonocytes and inhibits histone deacetylases [99]. SCFAs interact through various receptors such as FFAR2/3 or GPR109A to impact host homeostasis [100]. It was shown that, butyrate binding to EEC's FFAR2/3 receptor resulted in secretion of gut hormones including GLP-1, peptide YY (PYY) and cholecystokinin (CCK) [101]. These hormones have been shown to inhibit appetite by activating signaling pathways in the brain [101]. Furthermore, binding of butyrate to dendritic and microglia cells' GPR109A have been shown to promote anti-inflammatory effects by enhancing Treg differentiation and the anti-inflammatory microglia state [102, 103].

Second, indole derivatives are produced as a by-product of bacterial metabolism. Tryptophan has been shown to be metabolized by bacteria of the genera *Bacteroides* and *Clostridium* to indole derivatives such as indole, indole propionic acid or indole acetic acid [104]. Previous studies have shown that these metabolites can impact brain homeostasis by enhancing mucosal homeostasis, activating glial cells and preventing brain damage by increasing antioxidant activity [105]. Furthermore, they have shown that these metabolites can interact with aryl

hydrocarbon receptor (AhR) receptors, which are ligand-activated transcription factor activated by environmental, dietary, metabolic and microbial signals [106]. These receptors are expressed on immune and brain cells, where binding was proposed to potentially counteract age-related systemic inflammation (figure 1.2) [107].

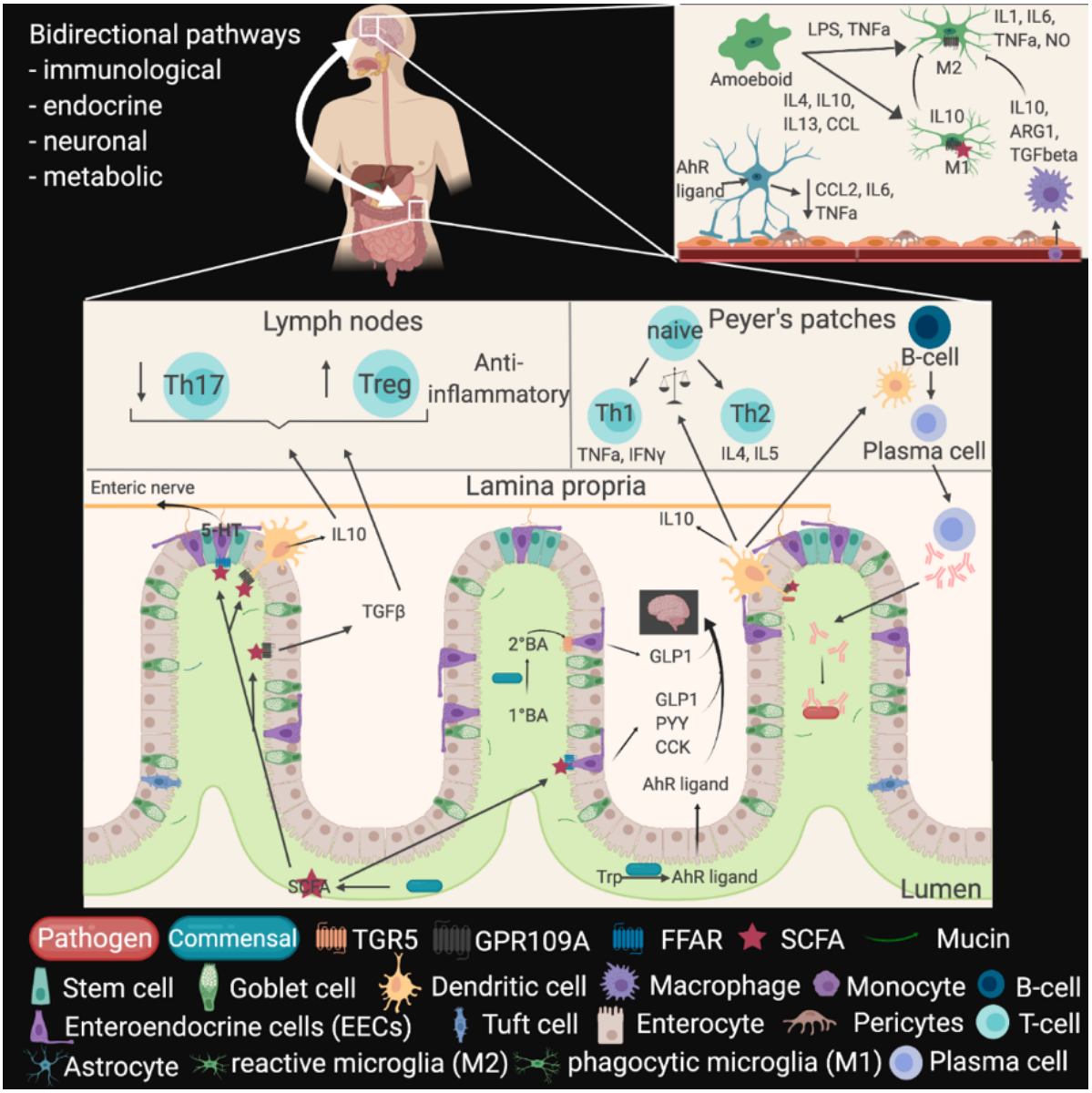

Figure 1.2: Microbial impact on the human organism.
Bacteria produce SCFA through saccharolytic fermentation in the gut lumen, which can interact with numerous G-protein coupled receptors (GPR109A, free fatty acid receptors (FFARs)). On the luminal epithelial layer, the receptors are primarily expressed by enteroendocrine cells, dendritic cells (DCs) and enterocytes, which cause the release of anti-inflammatory cytokines such as IL-10 and TGFβ as well as gut hormones such as GLP-1, peptide YY (PYY) and CCK. While the gut hormones can travel in the brain to inhibit for instance appetite, the cytokines and activated DCs can travel through the endocrine and lymphatic system to interact with T and B lymphocytes (T- and B- cells), which causes their maturation promoting anti-inflammatory signaling. In the lymph nodes the Treg to Th17 ratio is increased, while in the Peyer's Patches the balance of differentiated Th1 and Th2 cells is maintained. DC's can activate the differentiation of B-cells into plasma cells, which travel to the lamina propria

and release immunoglobulin As (IgAs) in the gut lumen, where they bind to microbial pathogens and enable defense mechanism against their infiltration. Commensal bacteria also deconjugate conjugated bile acids and enable the generation of secondary bile acids, which can bind for instance to G-protein-coupled bile acid receptor 1 (Gpbar1, TGR5) on enteroendocrine cells (EECs), which contributes to the gut hormone pool of GLP-1. In the brain microglia carry the SCFA receptor GPR109A, whose activation shifts the microglia subtype towards M2. The microbial-dependent conversion of tryptophan in the gut lumen causes the generation of AhR ligands, which can further travel in the brain, where the AhR ligands can bind receptors expressed on astrocytes, which, upon activation, decrease the inflammatory responses of astrocytes.

1.2.2: Microbiome and the brain

These investigations of the four axes demonstrate how microbial composition and microbial-derived metabolites in the gut lumen could potentially alter host homeostasis in parts of the body distal to the gut, such as the brain [108]. The anatomical proximity of the small intestine (SI) to the portal vein and the expressed receptors on enteric, neuronal, and glial cells with high affinity to microbial metabolites facilitate propagation of microbial signals into the circulatory system (figure 1.2). In addition, show small intestine and colon different receptor and cell profiles that allow responses to different metabolite signatures [109-111]. To enter the brain, molecules using the metabolic and immunological axes need to overcome not only the intestinal barrier but also the BBB. Animals studies in rodents that have been raised germ-free (GF) have demonstrated that the absence of the gut microbiome decreased expression of tight junction protein and impacted BBB integrity, emphasizing the connection between the gut microbiome and the brain [112]. Nevertheless, the exact mechanism on how microbiota-derived metabolites enter the brain has not been elucidated yet

Upon entering the brain, microbial-derived metabolites such as butyrate and indole propionic acid can target different cell types and pathways in the brain, potentially altering glial activation states [113-115]. Butyrate and its isoforms are common ligands of the receptors mitigating the inflammatory responses of microglia. Furthermore, they can promote development of the anti-inflammatory M2 microglia sub-type by inhibition of the NOD-, LRR- and pyrin domain-containing protein 3 (NLRP3) inflammasome in the periphery [97, 116-118]. In addition, Lee et al. as well as Rothhammer et al. described that dietary tryptophan that is metabolized by the

gut microbiota into indole derivatives (indole propionic acid) evokes anti-inflammatory effects in astrocytes through activation of AhR by reducing C-C Motif Chemokine Ligand 2 (CCL2), IL-6 and TNFα expression [106, 119, 120]. However, the precise mechanism on how gut derived metabolites could induce these described changes in the brain remains to be shown. Nevertheless, both microglia and astrocytes have pivotal roles in neuroinflammation and maintenance of BBB integrity, which highlights their critical role in neurodegenerative diseases such as AD [121, 122].

1.2.3: Microbiome in diseases

The discovery of the GBA and its complex networks emphasizes the importance of the gut microbiota composition in health and disease [123-125]. Brain disorders have a far more distant relationship to the gut microbiota than, for instance, inflammatory bowel diseases (IBD); nevertheless, microbial diversity is a pivotal component in the development of neurodegeneration throughout ageing [95, 126]. Inflammation represents one connective link between the progression of neurodegeneration during ageing and the composition of the gut microbiota [127]. Additionally, early human studies of mental and neurodegenerative disorders reported gastrointestinal disturbances caused by inflammation, which have been linked to the initiation and/or progression of neurodegeneration [128]. While gut disturbances have been a very persistent symptom prior to onset of PB, reports in AD were less consistent but still reported [129]. Furthermore, patients with mental disorders such as autism and depression showed improvement in cognition when their microbial composition was targeted by probiotics such as *Bifidobacterium* and *Lactobacillus*, which can promote butyrate producing genera in the gut through cross-feeding, or fecal matter transplants (FMT) [130-133]. Hence, the microbial metabolites and activated immune system may contribute to development and progression of brain disorders, which emphasizes the opportunity to target the gut microbiome as a treatment for neurodegenerative diseases.

1.2.3.1: Microbiome in AD

AD has been shown to possess numerous connections to the gut microbiome. First, ageing, which is the biggest risk factor for AD, influences gut health and function (figure 1.3) [134]. In addition, ageing has been shown to reduce gut motility, enzyme activity and gut microbiota diversity [135-137]. These alterations can lead to malnutrition and dysbiosis, which potentially harm peripheral and brain homeostasis [135-137]. A study by Thevaranjan et al. has shown that ageing can facilitate the development of an imbalanced gut microbiome, while others have shown that FMT with fecal matter of healthy mice can reduce these trends [138, 139]. In addition, it has been shown that FMT from old into young mice can reduce functions in young mice such as memory similar to old mice [140]. Furthermore, ageing has been associated with reduced diversity and abundance of beneficial genera such as *Bifidobacterium* as well as increased gut permeability and systemic inflammation [138].

Inflammation represents the second direct link between an imbalanced gut microbial composition and AD pathology (figure 1.3). Previous studies have shown that various cytokines and chemokines are secreted abnormally in the gut of AD patients. Additionally, inflammation has been proposed to contribute to reduction of the BBB's integrity, harming brain homeostasis and increasing glial activation [141-143].

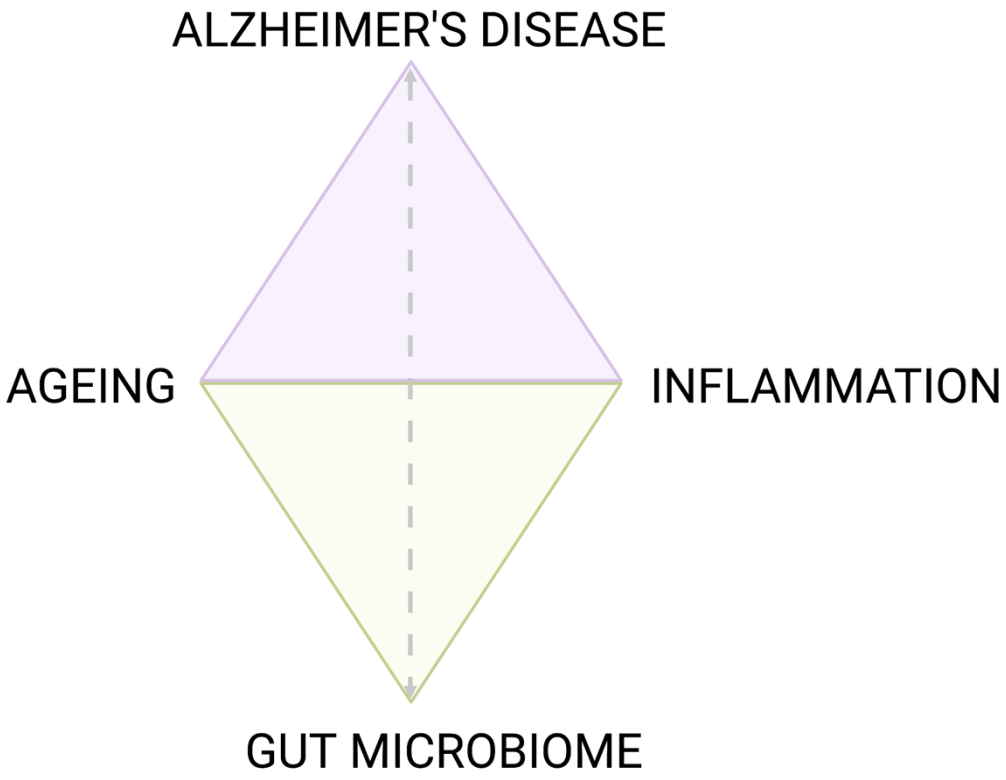

Figure 1.3: Link between AD and the gut microbiome.
Inflammation and ageing represent the major links between AD and gut microbiota. Both have been shown to negatively alter brain and gut health potentially facilitating disease development and progression. However, the precise mechanism remains unknown.

In a controlled and healthy environment, activation of the immune system represents an endogenous protective mechanism. However, under diseased conditions and dysbiosis, these mechanisms could contribute to systemic inflammation harming the host's health. For instance, it has been demonstrated in mouse models of AD that GF APP/PS1 mice show reduced aggregation and pathology compared to conventionally raised APP/PS1 mice at 8 months of age [59]. In addition, microbe-dependent secretion of metabolites like LPS or amyloids result in severe systemic inflammation, and are associated in *in vitro* and *in vivo* studies with AD pathology [144].

Finally, it has been observed that AD patients exhibit an imbalanced microbial composition, which increases intestinal permeability and subsequently facilitates systemic infiltration of gut-derived metabolites and PAMPs [60, 145]. Furthermore, an investigation of cerebrospinal fluid

(CSF) in AD or mild cognitively impaired (MCI) patients have shown a correlation between decreased microbial diversity and increased AD pathology [60]. This has given support to the hypothesis stated above since decreased microbial diversity has been implicated as a biomarker of instability of the ecosystem, which can evoke impairment of pivotal ecological functions and has been observed in IBDs [146]. Specifically, the microbiota diversity analysis of fecal matter from AD patients has shown significant reduction in richness, α-diversity, as well as β-diversity when compared to age-matched and sex-matched control individuals [60]. Moreover, *Lachnospiraceae*, *Bacteroidaceae* and *Streptococcaceae* levels increase, while *Ruminococcaceae* levels decrease, which altogether suggest gut dysbiosis in these AD patients, but can slightly vary dependent on the study, respectively [60].

In conclusion, neurodegeneration, inflammation, and the gut microbiota have numerous associations, all of which support our hypothesis that microbial dysbiosis and/or immune dysfunction combined with ageing drive AD disease pathology through the GBA.

1.2.4: Microbiome-targeted therapies and their potential in AD

Patients living with AD rely on a broad variety of pharmaceuticals, including antidepressants, antipsychotics, anxiolytics, and mood stabilizers. Approved drugs including cholinesterase inhibitors (e.g. donepezil) and a glutamate receptor antagonist (memantine) exhibited moderate effects in clinical trials of AD and cause side effects such as decreased blood pressure, insomnia, and impaired vision. In addition, it has been shown that some of these drugs can cause severe gastrointestinal problems such as rivastigmine [147]. These drugs mostly target symptoms rather than root causes of AD pathology. Given that the amyloid hypothesis centered clinical trials have failed in the last decade, AD researchers' interests have been directed towards new treatment targets such as the gut microbiome. Microbiota-altering treatment strategies have been shown to reverse dysbiosis and recover gut homeostasis. This recovery of homeostasis could result in reduction of inflammatory signals through reduction of PAMP levels or release of anti-

inflammatory metabolites, but could also be dependent on the administration time-point in the disease progression [132, 148, 149]. Furthermore, these alterations could potentially modulate the immune system by decreasing systemic inflammation as has been shown in studies of autism and depression [132, 148, 149]. Consequently, several approaches have been applied to restore a healthy gut environment including pre- and probiotics, FMT and enzyme supplements.

1.2.4.1: Prebiotics and probiotics

Prebiotics are composed of molecules, which promote the growth of beneficial bacteria of the gut microbiota by altering the balance of bacteria and their metabolites. Prebiotics are most commonly composed of fructans and various oligosaccharides [150-152]. For instance, it has been shown that supplementation with galactooligosaccharides (GOSs) leads to a 100-fold increase in *Bifidobacterium* abundance [153]. This can indirectly increase butyrate production, protect from pathogens and enhance anti-oxidant activity [153].

Probiotics are live bacteria that colonize the gut and can replace pathogens, while contributing to the gut metabolome. Furthermore, these bacteria can promote the growth and metabolite secretion of other strains in the gut by providing nutritional metabolites such as lactic acid to these strains. In addition, they can directly interact with the immune system or produce metabolites to decrease inflammation [154, 155]. The diet has the largest impact on the microbial composition of the gut and it is also the greatest source of pre- and probiotics [156]. Hence, supplementation with pre- and probiotics represents one approach for altering the gut microbiota in healthy and diseased individuals. This has been shown to restore and support a healthy gut environment, but manifestation of changes can be a lengthy process [157-159].

1.2.4.2: Antibiotics and FMTs

Antibiotics are anti-bacterial pharmaceuticals traditionally used for suppression of pathogenic strains to treat infections and rehabilitate a healthy gut microbiota composition [160, 161]. Antibiotics often lack specificity, which leads to elimination of commensal residential strains

of the gut microbiota. Frequent use of antibiotics can, therefore, lead to short- and long-term gastric dysbiosis which could result in the development of IBDs [162]. But broad depletion of bacteria can be also used to facilitate implementation and/or renewal of the gut microbiota. This can expedite rebuilding of a healthy gut microbiome when FMTs or probiotics are additionally or subsequently are administered with antibiotics [163, 164].

FMTs are intended to replace gut dysbiosis by re-establishing a microbiome resistant to pathogenic strains. FMTs can be collected from healthy donors, or from so-called super-donors, which have been shown to improve the gut microbial composition specifically in individuals with recurring *C.difficile* infections [165-167]. In human studies of autistic children, FMTs from healthy individuals have improved the children's gut microbial composition, which enhanced their development [132, 168]. Furthermore, this benefit has been shown in a follow-up study to have persisted for two years post FMT, although results were based on a small study cohort [132, 168]. Thus, the use of FMTs have shown the potential to improve long-term cognitive function by reorganizing the gut microbial composition. Conversely, it has been shown that PD and AD pathological features can be transferred through human-derived fecal matter in animals highlighting not only the great opportunity but also the potential danger of FMTs [59, 128].

1.2.4.3: Enzyme supplementation

Digestive enzyme supplements can affect gut health similarly to prebiotics by altering gut luminal metabolite and microbiota composition. Proteases, glycosidases, and lipases are commonly used in enzyme supplement formulations. While prebiotics are exogenous substances, which can be directly metabolized by certain bacterial species, digestive enzymes are dependent on the presence of macromolecules in the intestinal tract to release cleavage products. These enzyme cleavage products have beneficial effects on the host through direct absorption or by favoring growth of certain bacterial species due to increased nutritional availability of distinct metabolite classes. In the clinic, pancreatic enzyme replacement therapy

(PERT) has been used as treatment strategy in diseases such as cystic fibrosis or exocrine pancreatic deficiency. Patients of these diseases lack endogenous enzyme activity due to hindered expression or secretion in the gut lumen and treatments have been shown to decrease macromolecular content in feces such as triglyceride levels [169-171]. Ageing, the main risk factor of AD, has been associated with decreased enzyme activity in the gut lumen, which could favor malnutrition and contribute to development gut dysbiosis [172, 173]. Furthermore, it has been reported that digestion efficacy and gut health can detrimentally change the gut microbial composition or vice versa emphasizing the potential link between ageing, inflammation, gut microbiota composition and AD [136, 173-176]. In addition, metabolic and lipid pathways, which rely on nutritional supply, have been shown to be disturbed in AD patients emphasizing again the connection between functionality of the gut and AD development [60, 177-179]. Hence, enzyme supplements could represent a great potential way to support gut health and rebalance the gut microbiota, while enhancing the nutritional supply. A recent study has been shown that an enzyme supplement (Pancrealipase) comprising several enzyme classes has altered the gut microbiota in Wt mice [180]. Although the beneficial effects could not be attributed to the individual enzyme classes, some of the observed effects could be attributed to lipase activity which hydrolyze lipids [180-182].

1.3 Candida rugose lipase (CRL)

Candida is classified as single cell fungi in the genus of yeast and is found on sugar-rich materials as well as in hosts' microenvironments as pathogens, endosymbionts or commensals [183]. Candida tropicalis, Candida antarctica, Candida cylindracea, Candida parapsilopsis, Candida deformans, Candida curvata and Candida rugosa [184] are terrestrial species and express a broad variety of lipases with common structural features [185]. Their lipases (triacylglycerol acyl hydrolases; EC 3.1.1.3) catalyze the hydrolysis of triacylglycerol to release

fatty acids and glycerol [186-189]. CRL is frequently used in the nutraceutical and biotechnological industry due to the unique activity, selectivity, and specificity within its lipase isoforms.

1.3.1: CRL isoforms

Candida rugosa secretes at least five isoenzymes, which are encoded in the lipase gene family [190] consisting of a polypeptide chain of 543 amino acids for each isoenzyme. They are hydrophobic N-glycosylated proteins with an apparent molecular weight of 60 kDa and belong to the subclass of carboxylic ester hydrolases with a conserved α-/ß-hydrolase fold. The five lipase isoforms CRL1 to CRL5 share 77% identity, with conserved domains comprising the binding site within the catalytic triad, the binding tunnel, and the loop region- which is capable of opening and closing the binding site upon conformational changes [191]. Differences in the binding site tunnel and the loop region impact the enzyme's activity and substrate specificity and has been shown to be further modified by site directed mutagenesis [190, 192] [193-195]. In addition, it has been shown that CRL isoforms' activity are sensitive to pH and temperature changes [196, 197].

1.3.2: Catalytic mechanism

Structural differences between the CRL isoforms have been further elucidated through sequencing approaches and X-ray crystallography [191]. The structures of the open, closed, and inhibitor-bound conformation (PDB: 1CRL, 1TRH, 1LPN, 1LPM, 1LPO) of CRL1 and CRL3 support the identification of conformational changes and revealed the underlying mechanism [191, 198]. The catalytic cleavage is directed through the highly conserved catalytic triad (Ser209-Glu341-His449). In the closed conformation the amphipathic loop lays flat on the enzyme's surface, covering the entrance of the hydrophobic tunnel and the catalytic triad. The encompassed distorted helical turn and α-helix (Glu66 to Pro92), which comprise the loop

region, can be further fixed through a disulfide bond and a hydrogen bond (Cys60-Cys97, Glu 95-Arg37), which stabilizes the closed conformation.

In contrast, the open conformation exposes a large hydrophobic region, where the loop moves at almost a 90° angle upwards. Therefore, residues 86-90 refold into a short α-helix, while the longer α-helix shifts towards the N-terminus by two amino acids and travels overall 19Å [191]. This directs the ester bond of the substrate (e.g. lipid) into the oxyanion hole and the connected hydrophobic acyl group in the hydrophobic tunnel for stabilization. The triad cleaves the ester in three consecutive steps: (1) formation of a tetrahedral intermediate, due to a nucleophilic attack of Ser209 on the ester bond, stabilized by His449. Subsequently the glyceride is released, (2) and an incoming water molecule de-acylates Ser209 through formation of the second tetrahedral intermediate; (3) the fatty acid is released, and all involved amino acids remain unchanged. The oxyanion hole stabilizes the oxyanion with H-bonds to allow complete cleavage [198]. The varying specificity within the isoforms is caused by sequential differences in the described conserved loop and tunnel domain, which determines the activity and specificity of the respective isoforms in regards to fatty acid length and cleavage position preference (figure 1.4) [192-194].

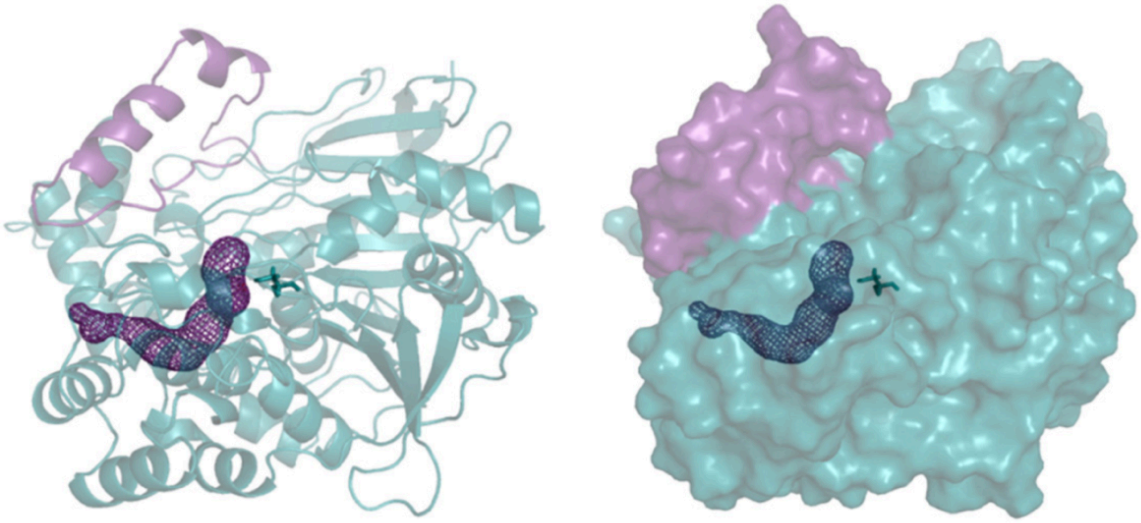

Figure 1.4:CRL 3 in the open conformation adapted from Barriuso et al. [185].
The dark purple area highlights the flexible loop, which opens and closes the binding site. Also, the catalytic serine is indicated next to the L-shaped tunnel area (purple mesh), where the fatty acid will be enclosed.

This enables the hydrolysis of fatty acids by CRL's isoforms preferentially from position 1 or 3 on the glyceride with an additional preference for medium- and long-chain fatty acid, but no preference between saturated and unsaturated fatty acids or cholesterol esters [194, 199-201].

1.3.3: Allosteric enhancement

Most of the industrial strategies to enhance CRL activity are limited because of toxic and nonspecific effects [202, 203]. Allosteric modulation of CRL activity represents a competitive alternative method since toxicity, specificity and efficacy are important criteria to achieve enhanced treatment effects *in vivo*. We hypothesized that the allosteric enhancer of CRL activity would increase the enzyme's hydrolysis activity in the gut resulting in elevated levels of fatty acids and glycerol when administered together. Furthermore, this might enhance direct absorption of long-chain and omega fatty acids by the host and/or promote growth and metabolite secretion (e.g. SCFA, reuterin) of selective bacterial strains in the gut through increased availability of nutritional metabolites [204-206]. Bacterial-derived metabolites such as reuterin/acrolein (bacterial glycerol digestion) or butyrate can support the host's health status by rebuilding a healthy gut microbiome and reducing systemic inflammation [113, 207]. Nevertheless, we cannot exclude the possibility to observe opposite effects by enhancing growth of for instance pathobionts, which was aimed to investigate in the first study.

The identification of allosteric sites has been simplified through pre-screening of potential allosteric modulators by computational analysis; it pre-sorts and reduces the pool of screening components reducing the complexity and cost-intensity of the endeavor [208-210]. The *in silico* approach relies on availability of high quality structures of the selected enzyme. For the *in silico* screening, potential allosteric sites on the enzyme's surface need to be identified satisfying specific characteristics including deep, distinct, and in proximity to the binding site with

characteristic interaction groups. Next, compound libraries are built that are composed of molecules of natural origin to enhance tolerability of the positive allosteric modulator (PAM) when tested *in vivo*. Then, the compound libraries are fitted into the selected allosteric sites on the enzyme's surface that yield in a selected set of potential modulating compounds [208, 209]. Finally, the theoretically identified distinct group of modulators is evaluated *in vitro*.

1.4 Hypothesis and synopsis of following chapters

The study of the gut microbiome provides opportunities to deepen our understanding of pathogenesis and discovery of novel treatment strategies for CNS disorders. The apparent connections between the gut microbiota composition and the brain warrants the assessment of gut microbiota-based treatment strategies a valid approach for the treatment of neurodegenerative diseases. In AD, both mouse models and patients with AD pathology exhibit an altered gut composition, which has been suggested to contribute to disease pathogenesis [59, 60, 211-213]. The experiments performed in this thesis therefore assessed whether rebalancing of the gut microbiota composition can ameliorate AD pathology, while determining the potential causal relationships between AD neuropathology and gut dysbiosis or vice versa. For this purpose, we selected CRL, a lipase with a broad specificity range, that has been frequently used in the nutraceutical and food industry, to alter the gut microbiota composition to profiles that are associated with normal gut health through increased lipid hydrolysis products [214, 215]. Thus, we hypothesized that:

"Oral administration of an exogenous lipase in APP/PS1 mice normalizes gut microbial and metabolite composition, and rescues AD pathology and aberrant behavior".

Three hypotheses were tested in this thesis:

(1) Oral lipase administration in Wt mice will alter free fatty acid (FFA) and glycerol release in the gut;

(2) oral lipase administration in APP/PS1 mice will normalize the gut microbiota and metabolite composition that correlates with improved AD-like pathology; and

(3) that a combined use of a PAM with the exogenous lipase will enhance the expected effects from hypotheses (1) and (2).

1.5 Summary of the upcoming chapters

In Chapter II, hypothesis (1) was investigated by examining CRL's treatment effects in Wt mice. Firstly, it was assured for the subsequent animal studies that CRL could be delivered in an active state into the gastrointestinal tract. Secondly, short- and long-term effects in the gut of Wt mice during and post CRL administration were examined. In chapter III, hypothesis (2) was tested by determining the potential beneficial effects of CRL treatment on the gut microbiota and metabolome of APP/PS1 mice and subsequently AD-like pathology. In addition, it was assessed whether the neuropathological benefits were evoked by the alterations of the gut microbiota and metabolite composition. In Chapter IV, PAMs of CRL activity were identified by *in silico* and *in vitro* screening to finally examine hypothesis (3).

Chapter II: The impact of oral administration of CRL on the gastrointestinal environment of Wt mice

2.1 Introduction

The gut microbiome resides in symbiosis with the host and has a distinct composition in each person that is mostly shaped by diet [216]. The gut microbiota have pivotal functions in the host organism including nutritional supply, protection against pathogens and immune system modulation [217, 218]. Compositional shifts of the gut microbiota can affect metabolite composition, digestion, and signaling pathways in the host, influencing the organism's resiliency and general health status [219-222]. For instance, microbial imbalances, or dysbiosis, have been associated with numerous diseases such as IBD, colorectal cancer, obesity and PD [223-225]. In AD, it has been reported that animal models as well as AD patients exhibit an apparent gut dysbiosis [60, 211, 212]. Hence, it has been suggested that reduction of gut dysbiosis by dietary changes may decrease the contribution of the gut microbiome to disease pathogenesis and consequently ameliorate AD pathology (hypothesis (2)).

Therefore, in this chapter we assessed, as a prerequisite of the investigation of hypothesis (2) whether exogenous administration of the digestive enzyme CRL can alter the gut microbial and metabolite composition in Wt mice (hypothesis (1)). CRL activity in the gastrointestinal tract was proposed to modulate gut microbial communities by increasing break-down of dietary macromolecules and subsequent nutrient availability [180, 226]. These hydrolysis products can include glycerol, long-chain fatty acids and omega-3 fatty acids, which have been reported to exert anti-inflammatory and anti-bacterial properties reportedly benefitting the host's health [227, 228]. Furthermore, the increased levels of these metabolites can favor growth of specific bacterial species, which have the genetic basis to metabolize, for instance, glycerol into the anti-

biotic compound acrolein [182, 229, 230]. These compounds can alter the gut microbiota composition and have been shown to reduce the inflammatory state of the host [231, 232].

In this thesis, we selected CRL for investigation due to its known broad range of specificity and wide use in nutraceutical applications, where it has been recognized as Generally Recognized as Safe (GRAS; GRA 000081) in humans. In addition, CRL's catalytic mechanism has been described and X-ray crystallography structures are available, which were pivotal for the investigation of hypothesis (3). In addition, lipases have been clinically applied in diseases where digestive enzyme secretion is disturbed, such as cystic fibrosis or pancreatic insufficiency, to restore nutritional supply and absorption through PERT [170, 233]. Furthermore, Nishiyama et al. administered one of these PERTs (Pancrealipase) containing proteases, amylases and lipases in Wt mice to investigate their effect on the gut microbiota in a healthy gut environment [180]. They have shown that the enzyme's activity caused an increase in beneficial bacterial species such as *L.reuteri* and *A.muciniphila*, which have been associated with lipid hydrolysis (*L.reuteri*) and gut health (*A.muciniphila*) [229, 234-236]. Despite these findings, they have not been able to specify which of the components within the enzyme mixture have evoked the observed effects, respectively, although increase of *L.reuteri* could be attributed to release of glycerol through lipase activity [180].

For this study, we therefore used Candida rugosa lipase alone to investigate CRL's specific effects. This study was subdivided into three sections: (1) First, we assessed the enzyme's purity and stability and if CRL could be delivered in an active state to the gastrointestinal tract. Second, we examined the short-term (2) and finally, the long-term (3) effects of CRL treatment on gut microbiota and metabolite composition in Wt mice, which enabled the investigation of CRL's treatment effects in an environment that is considered "healthy" and independent of the effects potentially induced by genetic modifications.

2.2 Material and methods

2.2.1: Animal models

Animals were kept in the Association for Assessment and Accreditation of Laboratory Animal Care International (AAALAC) accredited vivarium of the Roskamp Institute. Revision and approval for experiments with mice were reviewed and approved by the Institutional Animal Care and Use Committee (IACUC) of the Roskamp Institute before implementation and conducted in compliance with the National Institutes of Health Guidelines for the Care and Use of Laboratory Animals. Wt mice were obtained from the Jackson Laboratories (#000664) or from in-house breeding. Mice lived on a 12h/12h light/dark cycle and received food and water ad-libitum. Mice were weighed and monitored before and throughout procedures.

2.2.2: Stability of CRL

CRL (1 mg/mL) was incubated in water for six days at room temperature and samples were collected after 0, 1, 3, 5 and 6 day. Subsequently, the collected samples were analysed by sodium dodecyl sulfate (SDS) poly-acrylamide gel electrophoresis (PAGE) and the CRL activity assay developed in Chapter IV to investigate stability and purity of CRL. **SDS PAGE**. 10 µg of each sample were combined 1:1 2x Laemmli buffer (Bio-Rad, Hercules, CA) and incubated at 95 ºC for 10 min. Subsequently, samples were loaded as well as PlusProtein Unstained Protein Standard (Bio-Rad, Hercules, CA) on a Criterion TGX Stain-Free gel (Bio-Rad, Hercules, CA) and separated at 150 V for 40 min. Finally, the gel was developed using the Plastic Bio-Rad Gel Doc EZ imaging system (Bio-Rad, Hercules, CA). **CRL enzyme activity assay**. The activity assay was conducted in Phosphate Buffer (PB) pH 7. Samples were diluted to 10 ng/mL in PB. The substrate 4-Methylumbelliferyl butyrate (4MUB) was prepared as 100 mM stock in dimethyl sulfoxide (DMSO) and diluted to 0.25 mM. Finally, 50 µL of sample, buffer and substrate were added in triplicates on a 96-well µ-clear black round bottom plate (Greiner, Monroe, NC). Samples were incubated for 30 min at 37 ºC. The reaction was stopped using 50

μL of 10 % o-phosphoric acid for each well. The fluorescence was immediately measured with the BioTek Cytation 3 system at λ=326/472 with a gain of 72.

2.2.3: Purity of CRL

50 μg of CRL (1 mg/mL stock) were loaded in triplicate on a Criterion TGX stain-free gel (BioRad, Hercules, CA). The SDS PAGE ran for 40 min at 150V. Subsequently, gel bands were excised and incubated for 5 min in 500 μL of acetonitrile. Liquid was removed and gel samples incubated in 50 μL of dithiothreitol (100 mM in 100 mM ammonium bicarbonate) at 56°C for 30 min. Next, 500 μL acetonitrile was added and samples were incubated for 10 min at room temperature. Fifty μL of iodoacetamide (55 mM in 100 mM ammonium bicarbonate) was added and samples were incubated for 20 min at room temperature protected from light. Finally, 500 μL of acetonitrile were added and incubated at room temperature for 10 min to complete reduction and alkylation of the protein. Next, 100 μL of trypsin (13 ng/μL) were added for in-gel digestion and incubated at 4 °C for 2h. Subsequently, the tubes were incubated at 37 °C, overnight. For extraction, 100 μL of extraction reagent (1:2 (V/V 5% formic acid in acetonitrile) was added to the samples and incubated at 37 °C for 15 min. Supernatant was collected and extracts were dried down in a Speedvac. Next, 42 μL of 5% formic acid were added and shaken at 37 °C for 15 min. Subsequently, the samples were filtered (0.45 μm) and transferred into autosampler vials for liquid chromatography mass spectrometry (LCMS) analysis. Samples were analysed using a Thermo Scientific Q Exactive Hybrid Quadrupole Orbitrap mass spectrometer (Thermo Fisher, Waltham, MA) and Thermo Scientific EASY-nLC 1000 Liquid Chromatograph (Thermo Fisher, Waltham, MA). 12 μL of samples were injected and separated on an Acclaim PrepMap 3 μm, 0.075 mm x 15 cm column with an Acclaim PrepMap 3 μm, 0.075 mm x 2 cm pre-column with a flow rate of 300 nL/min. Solvent A: 0.1 % formic acid in water and B: 0.1 % acetonitrile were used for gradient and isocratic elution: 0 to 25 min from 2 to 30 % increasing B, 25.1 to 35.1 min 80 % B and 35.2 to 45 min 2 % B. Samples were analysed

using Full-MS and $ddMS^2$ in positive mode from 300 to 2000 m/z. Finally, chromatograms were analysed using Proteome Discoverer Software (Thermo Fisher, Waltham, MA), which aligned samples with the yeast proteome to identify the measured protein fragments.

2.2.4: *In vivo* kinetic study of biotin-labeled CRL

Biotin labeling. 1 mg/mL CRL (300000 *Fédération Internationale Pharmaceutique* (FIP)/g, Enzymedica, Venice, FL, USA) in water was performed according to the manufacturer's protocol with EZ-Link Sulfo-NHS-Biotin (Thermo Fisher, #A39256) for 2h on ice and subsequently stored at -20°C. This allowed the measurement without interference of endogenous active lipases. **Treatment of animals**. Female Wt mice (aged 5 months, n=4/group) were obtained from an internal breeding protocol, randomly subdivided in four groups (n=4/group) and group housed. Mice received 5000 FIP/kg body weight (38.5 μM/kg) of biotin-labeled CRL in 200 μL water via oral gavage. Four groups received either biotinylated CRL at 90, 30 and 0 min prior to euthanasia, or water at 0 min before euthanasia. Mice were anaesthetized with isoflurane (3% in 1.5 L/min O_2; Patterson Veterinary, Greeley, CO) delivered to an induction chamber via a calibrated vaporizer equipped with a waste-gas scavenger device. Once deeply anaesthetized mice were humanely euthanized by cardiac puncture-induced exsanguination and subsequently perfused with phosphate buffered saline (PBS) in accordance with the approved IACUC protocol. After collection of the intestinal tract, the SI was subdivided into three sections: proximal, medial, and distal SI before storage at -80ºC. Each section was homogenized and mixed with an equal amount of 0.1M PB. Subsequently, the samples were centrifuged for 10 min at 4°C, and the supernatant was collected for analysis. **Biotinylated CRL activity assay**. A 1:1000 dilution of each sample (in triplicate) was incubated on 96-well streptavidin-coated plates (Thermo Fisher, #15219) at 4°C for 16h, followed by two washes with 1x wash buffer (Thermo Fisher, #WB01) and two washes with PB. The PB wash removed excess detergent from the wash buffer, which could interfere with the subsequent enzyme

activity measurement [237]. Finally, the substrate (0.25 M 4-methylumbelliferyl butyrate in PB) was added to measure lipase activity in the crude extracts at 37°C for 25 min. **FFA assay**. 20 µL of supernatant were added to 200 µL of chloroform with 1% Triton X-100, thoroughly mixed and centrifuged at 20000g for 5 min at 4°C. The lower phase was collected and dried under vacuum in a Speedvac. Dried extracts were reconstituted in the provided assay buffer of the FFA Assay Kit (Abcam, Cambridge, MA). Samples were diluted 1:10 (stomach), 1:25 (cecum), 1:100 (SI) and analysed according to the manufacturer's protocol. Data was normalized to tissue weight and analysed with one-way analysis of variance (ANOVA) and Tukey's post-hoc test in GraphPad Prism. SI and cecum data were not normally distributed and therefore log-transformed for statistical analysis.

2.2.5: Short-term effect of CRL on the gut microbiome

Female Wt mice (aged 6 months, n=3/group) were obtained from an internal breeding protocol, group housed and randomly assigned to the four groups: 1000, 5000 or 10000 FIP/kg (7.7, 38.5 or 77.7 µM/kg) per day in drinking water or water alone for 3 days. In addition, cage bedding was collected from all cages two times a week, mixed and evenly distributed between cages to counteract cage effects starting three weeks prior to the study. After three days, mice were anaesthetized with isoflurane (3% in 1.5 L/min O_2; Patterson Veterinary, Greeley, CO) delivered to an induction chamber via a calibrated vaporizer equipped with a waste-gas scavenger device. Once deeply anaesthetized, mice were humanely euthanized by cardiac puncture-induced exsanguination in accordance with the approved IACUC protocol. Subsequently, mice were perfused with phosphate buffered saline (PBS) and the intestinal tract was subdivided into small intestine, cecum, and colon and immediately frozen in liquid nitrogen prior to storage at -80°C.

2.2.6: Long-term effect of CRL on the gut microbiome

Male Wt mice (aged 6 months, n=10/group) were obtained from Jackson Laboratory (#000664), single housed and acclimatized for 3 weeks. Subsequently, mice were trained for two weeks for

fecal collection prior to the start of the study. In addition, cage bedding was collected from all cages two times a week, mixed and evenly distributed between cages to counteract cage effects starting three weeks prior to the study and within groups throughout the study to reduce confounding effects due to single-housing. Mice received 1000 FIP/kg (7.7 μM /kg) CRL per day in drinking water or water (n=10/group) for 30 days, which was then discontinued 30 days prior to euthanasia. The 30 day washout period was selected to allow the gut microbiota to readjust to the new environment in the gut to then measure compositional changes that would persist after 30 days of treatment discontinuation. Supplemented water or water alone was changed twice a week as determined in 2.3.1. Feces were collected on day 0, 30 (after treatment) and 60 (after washout) of the study. Feces were kept on dry ice during collection and then stored at -80°C for long-term storage. At 8 months of age, mice were anaesthetized with isoflurane (3% in 1.5 L/min O_2; Patterson Veterinary, Greeley, CO) delivered to an induction chamber via a calibrated vaporizer equipped with a waste-gas scavenger device. Once deeply anaesthetized, mice were humanely euthanized by cardiac puncture-induced exsanguination in accordance with the approved IACUC protocol. Subsequently, mice were perfused with PBS, and the SI, colon and cecum were collected. The tissue was stored at -80°C or emptied and flushed with 1 mL of PBS before rolled into Swiss rolls and transfer into tissue embedding cassettes. Then, the tissue was incubated in 4% paraformaldehyde (PFA) for 24 h before tissue processing.

2.2.7: SCFA analysis

Cecal samples were sent to Duke University School of Medicine, Proteomics and Metabolomics Shared Resource facility for short-chain fatty acid analysis using gas-chromatography mass spectrometry (GCMS) analysis.

2.2.8: DNA Extraction

Feces (20-100 mg/pellet) and cecum (30 mg) samples were extracted using the Fast DNA stool mini kit (Qiagen, #51604) according to the manufacturer's protocol. Volumes were adjusted to account for lower sample weight.

2.2.9: Illumina MiSeq 16S rRNA gene sequencing

Fecal and cecal DNA extracts were analysed by V3-V4 region 16S rRNA gene sequencing using the Illumina MiSeq sequencing platform (Prof. Dr. Klatt, University of Miami) following the Earth Microbiome Project protocols (http://press.igsb.anl.gov/earthmicrobiome/protocols-and-standards/16s/) with the following modifications. Platinum™ II Hot-Start PCR Master Mix (2X) (ThermoFisher Scientific, #14000013) was used with the 515FB-806RB primer pair for DNA amplification of the V4 variable region in the 16S rRNA gene resulting in approximately 400 bp amplicons. The reaction was performed in triplicate and pooled once the LabChip GX (Agilent, #5067-5582) confirmed pure PCR results. The pools were subsequently quantified with the Qubit dsDNA High Sensitivity Assay Kit (ThermoFisher Scientific, #Q32854) and the concentrations unified. The library pools were combined (0.4 ng per sample) into a single sample and purified using the QIAquick PCR Purification Kit (Qiagen, #28104). After purification, the KAPA Library Quantification Kit (KAPA Biosystems, #KK4842) was used to quantify the total library pool. Finally, the 300-cycle Illumina MiSeq Kit (Illumina, #MS-102-200) was used to analyse 8 pM of pooled library with 30% PhiX Control v3 Library (Illumina, #FC-110-3001) as control following the EMP protocol.

2.2.10: Data availability and analysis of 16S rRNA gene sequencing

Authors did not use custom code or software for the described analysis of this manuscript. The sequencing data (paired end reads in FASTQ), the respective manifest and metadata files as well as unfiltered taxonomic classification of each study and specimen are available in the Mendeley repository [238]. The sequencing data was processed with the Qiime 2-2019.01 software

packages. Paired end reads were demultiplexed, trimmed, corrected for chimera, merged, and filtered with the demux and dada2 plugin. α-diversity (Shannon index and Simpson index) and β-diversity (Bray-Curtis dissimilarity and longitudinal volatility) were determined, and the significance was tested with Kruskal Wallis H test (α-diversity), permutational multivariate analysis of variance analysis (PERMANOVA, β-diversity) and 2-way ANOVA with multiple t-testing. Sequence classification was performed with the Naïve Bayes classifier trained on Greengenes 13_8 and subsequently binned into amplicon sequence variant (ASVs) at 99% sequence similarity. The Greengenes 13_8 was then used to classify ASVs and to determine relative abundance at various taxonomic levels allowing visualization and statistical analyses with analysis of composition of microbiomes (ANCOM). Plots of taxonomies were acquired in Qiime 2 and GraphPad Prism.

2.2.11: Immunofluorescence staining

After fixation of tissue in 4% PFA, the tissue was dehydrated and embedded in paraffin. 10 μm longitudinal sections were prepared for immunofluorescence staining. Slides were deparaffinized in histo-clear, rehydrated and rinsed. Antigen retrieval was then performed, followed by incubation in Sudan black for 30 min. The slides were subsequently rinsed and blocked for 1 hour with blocking serum at room temperature. The slides were incubated for 16h at 4°C with either the α-Claudin 2 primary antibody (1:200, ab53032, Abcam, Cambridge, MA)—detecting the tight junction protein Claudin-2 which is predominately expressed in leaky epithelial cells—or α-Zonula occludens-1 (ZO1) primary antibody (1:200, ab216880, Abcam, Cambridge, MA), which plays a role in cross-linking cells and anchoring tight junctions, all performed in super sensitive wash buffer. Subsequently, slides were rinsed and incubated in AlexaFluor 488 secondary antibody (1:66.6, A21206, Invitrogen, Carlsbad, CA) for 1 hour at room temperature. Finally, slides were rinsed and mounted in Fluoroshield mounting media with DAPI dye (ab104139, Abcam, Cambridge, MA). Slides were stored upon analysis at 4°C.

Analysis was performed using a ZEISS LSM 800 confocal microscope using channels AF405 and AF488 for DAPI and green fluorescence, respectively. Five animals per group were analyzed using four sections that were 90 μm apart were randomly chosen per animal and three pictures were randomly taken per section. Pictures were processed with ZEN 2.3 and quantified with ImageJ 1.8.0 software.

2.2.12: Statistical analysis

Statistical analysis of enzymatic activity, short-chain fatty acids and immunofluorescence quantification was determined in GraphPad Prism v8.3.0 using 2-way ANOVA and multiple t-testing. Statistical analysis of microbial parameters was performed by Qiime2. For α-diversity Kruskal-Wallis H test was performed with subsequent pairwise comparisons. To statistically analyse β-diversity dissimilarity, PERMANOVA was performed, while compositional differential abundance was determined by ANCOM and W-statistics. For visualization, data was plotted in GraphPad Prism or Qiime2. Data is presented as mean ± standard deviation, and p-values <0.05 were considered significant: *p< 0.05, **p< 0.01, ***p< 0.001, ****p< 0.0001, *****p<0.00001.

2.3 Results

2.3.1: CRL purity and stability

Firstly, the used CRL extract was characterized *in vitro* by SDS-PAGE and LCMS to investigate which of CRL's isoforms were contained in the extract and to identify potential impurities. LCMS analysis revealed the presence of CRL isoforms 1, 2 and 3 in the main band (60 kDa) of the SDS-PAGE as depicted by the number of identified representative peptides as well as additional fragments in the lower bands, which suggested CRL degradation products but no impurities (table 2.1, figure 2.1).

Table 2.1: LCMS analysis of Enzymedica's CRL extract to identify the contained components.
Numbers indicate the amount of detected peptide fragments in the respective gel bands. The primary band was detected at 60 kDa, but several others less intense bands were identified as evident in figure 2.1. These bands were further investigated to assure purity of the obtained extract. Lipase 1 and 3 had the greatest coverage in all investigated bands, while lipase 2 was solely detected in the dominant band (60 kDa).

Molecular weight of band	60 kDa	50 kDa	40 kDa	35 kDa
Liapse1	23	11	11	11
Lipase2	5	-	-	-
Lipase3	17	9	6	9
Lipase4	-	-	-	-
Lipase 5	-	-	-	-
Actin	1	-	-	-

Next, the stability of CRL in water was determined over six days at room temperature to identify potential impurities in the extract that were below the detection limit of the LCMS analysis and could potentially degrade the enzyme in solution. We used an in-house developed CRL activity assay that used 4-MUB as a substrate for CRL and upon hydrolysis releases the fluorescent dye 4-MU. This allowed us to measure the activity of CRL throughout the 6 days of sampling, while the SDS PAGE can identify enzyme degradation by an increase in unspecific bands and decrease of the main band at 60 kDa (figure 2.1, figure 2.2).

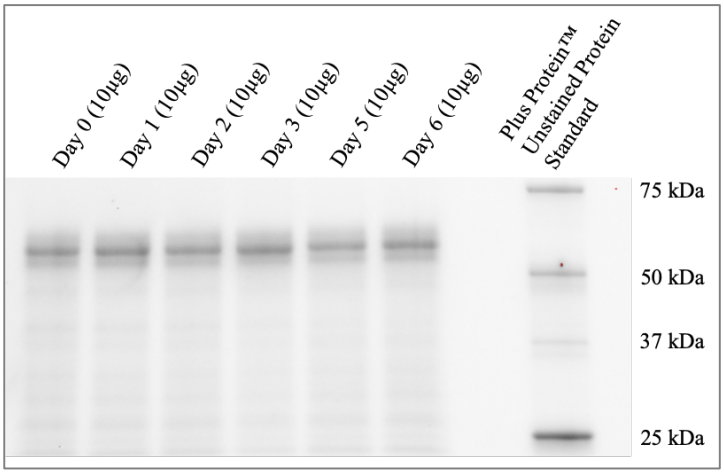

Figure 2.1: Stability of CRL throughout six days in water at room temperature.
The SDS PAGE was used to monitor CRL's stability in water at room temperature throughout six days. CRL has a molecular weight of 60 kDa. No increase of degradation was observed throughout the 6 days.

The SDS PAGE analysis revealed no quantifiable degradation of CRL. Although, the enzyme activity assay showed a slightly decreasing activity over the six-day period indicating auto-degradation or presence of proteases that were below the detection limit of the method used for evaluation, the enzyme extract was considered clean and stable for three days (figure 2.2).

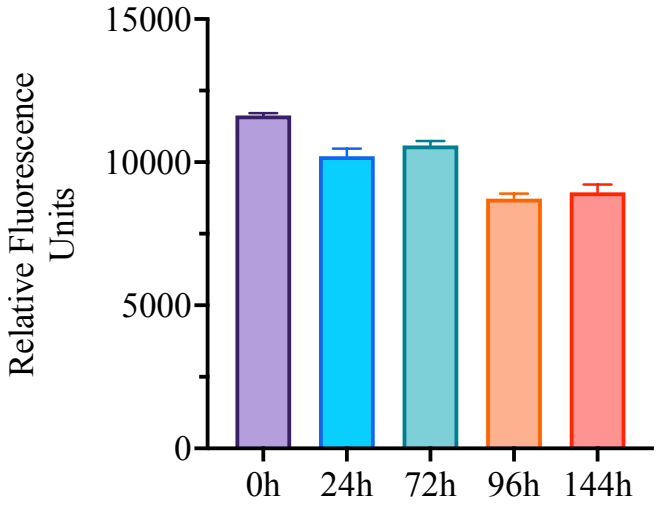

Figure 2.2: Investigation of CRL's activity throughout six days in water at room temperature.
The in-house developed activity assay was used to determine for each sampled day the enzyme's activity, which showed a 20% decrease of CRL's activity over time. The enzyme was incubated at a concentration of 1 mg/mL.

2.3.2: CRL activity in the gut lumen

After assessment of CRL's quality, we examined whether orally administered CRL could reach the gastrointestinal tract in an active state. The administration of biotinylated CRL into mice via oral gavage (to control for dose and time-point of administration) allowed monitoring of the enzyme's presence and activity in the intestinal tract for 90 min at a dose approximately equivalent to the recommended daily dose in humans. Biotinylated CRL showed the same activity in the assay when compared to the non-biotinylated enzyme (post-biotinylation and purification, figure 2.3).

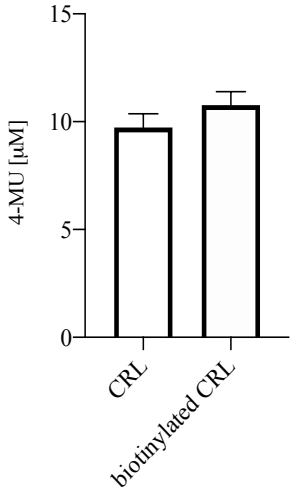

Figure 2.3: CRL's activity before and after biotinylation.
Comparison of CRL activity before and after biotinylation. No significant difference between biotinylated and non-biotinylated enzyme was determined. Values are displayed +/- standard deviation, and significance was tested by one-way ANOVA and student's t-test.

The data showed that delivery of 5000 FIP/kg of biotinylated CRL via oral gavage allowed monitoring of CRL's passing through the mouse digestive system over time. The biotin label aided to separate CRL specifically from endogenous lipases, which are present in the gut lumen. At 0 min, CRL was detected in the stomach and proximal SI ($p=4.50*10^{-5}$ and $p= 2.29*10^{-2}$, respectively, figure 2.4). Subsequently, the enzyme moved into the medial SI at 30 min ($p=1.54*10^{-2}$, figure 2.4) and cecum at 90 min ($p=5.98*10^{-2}$, figure 2.4).

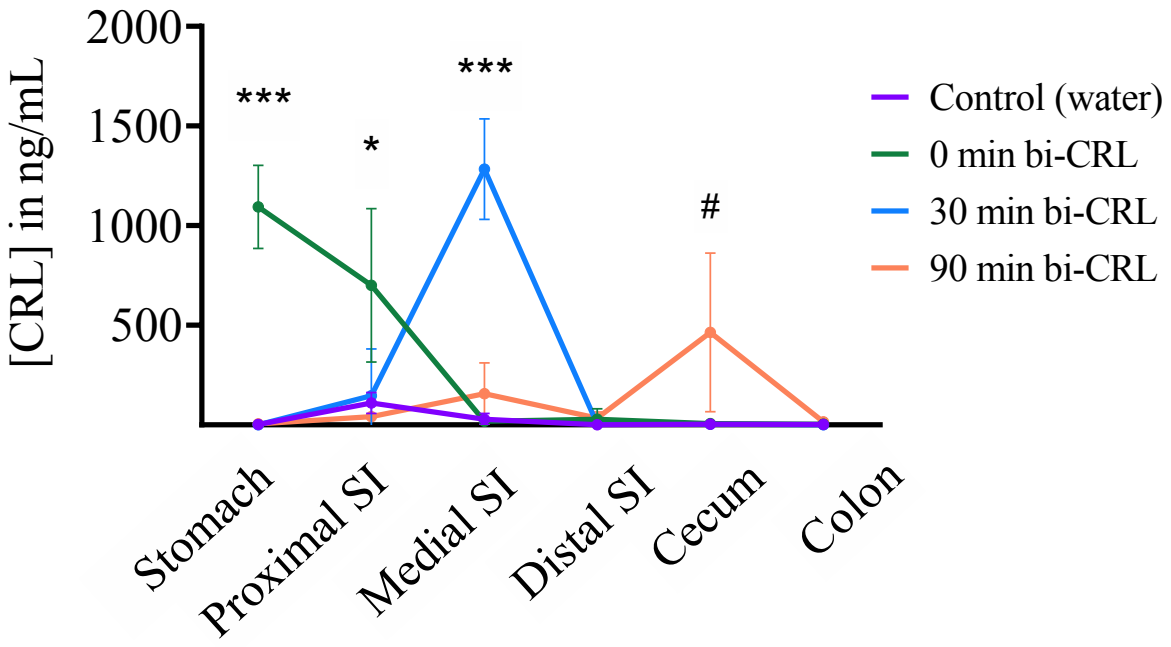

Figure 2.4: Oral administration of CRL in mice.
*CRL movement through the mouse intestine monitored with biotinylated CRL throughout 90 min confirms travelling of the enzyme in an active state. The control, which received water at 0 min before anesthesia, showed negligible activity in the SI (purple). At 0 min CRL's activity can be measured in the stomach and proximal SI (green). At 30 min a dominant signal could be measured in the medial SI (blue), while at 90 min most of CRL's activity can be measured in the cecum (orange). Significance was analysed with a 2-way ANOVA and corrected for multiple t-testing applying Tukey post-hoc: $^{\#}$<0.01, * p<0.05, ** p<0.01, *** p<0.001.*

In addition, we investigated CRL's activity in the gut lumen by determining changes in cleavage product in the intestinal tract. We administered a low-to-medium dose (when compared to human doses) of unbiotinylated CRL (1000 FIP/kg) or water with glyceryl trioctanoate and determined FFA levels in the stomach, SI and cecum normalized to the weight of the tissue segment at different time-points. While no differences in FFAs in the stomach were shown, a time-point dependent increase in FFAs in the SI and cecum were observed compared to mice receiving water (figure 2.5).

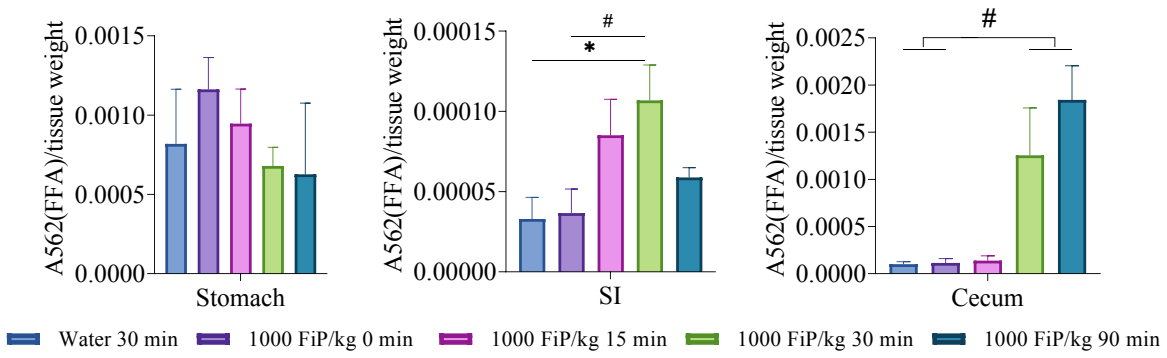

Figure 2.5: Determination of FFA levels to measure CRL's activity in the gastrointestinal tract.
*Mice received 1000 FIP/kg CRL and glycerol trioctanoate via oral gavage. While no difference was observed in the stomach, the SI showed 30 min post administration a significant increase in FFAs compared to the water group and trend when compared to 0 min. The 15 min and 90 min time-point showed a similar trend. In cecum only 30 and 90 min showed a trend for increased FFA concentration in the cecum. Values are displayed +/- standard error of mean, and significance was tested by one-way ANOVA and post-hoc Tukey-test. Significance: #p<0.1, *p<0.05.*

While we showed *in vitro* that CRL and its activity were stable in water for up to 6 days, this is the first time it has been demonstrated that administration of CRL in drinking water can be used to deliver active CRL beyond the stomach into the digestive system to hydrolyze triglycerides. This route of CRL administration allowed for subsequent studies to investigate the short- and long-term effects of CRL on the gut microbiota.

2.3.3. CRL short-term administration (cecum)

In the short-term study, we examined whether supplementation of three different concentrations of CRL would result in short-term effects on the abundance of bacterial genera and potentially species in the cecum. Wt mice (n=12) were divided into four groups receiving 1000 FIP/kg (low-to-medium), 5000 FIP/kg (medium) or 10000 FIP/kg (high) CRL in drinking water or water alone for control animals (n=3/group, figure 2.6A). No differences in water consumption and animal weight were determined. The administered doses were extrapolated from the clinically suggested dose range in humans. Following three days of supplementation, animals were euthanized and the ceca were collected for investigation of α-diversity, which describes the average species diversity in each individual based on evenness and richness in samples by the Simpson- and Shannon-indices [239]. While the Simpson index was significantly decreased

in all three treatment groups compared to control animals (p=0.049), the Shannon-index only showed a significant decrease for 1000 and 10000 FIP/kg CRL (p=0.049), although administration of 5000 FIP/kg showed a similar trend (p=0.12, figure 2.6B).

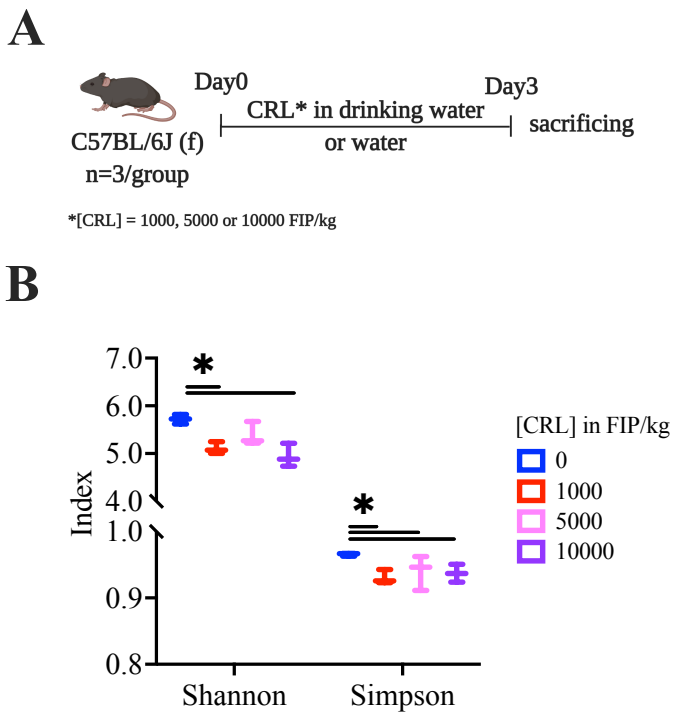

Figure 2.6: Short-term treatment effect of CRL on cecal α-diversity in Wt mice.
*A. Study design of short-term CRL administration study applying three doses: 1000, 5000 and 10000 FIP/kg CRL. B. Shannon and Simpson indices describing decreased α-diversity in all treatment groups compared to control animals. Significance was analysed with Kruskal-Wallis H test and pairwise Kruskal-Wallis post-hoc: *p<0.05.*

When analysing β-diversity, which describes the diversity within one group of animals compared to all other groups, here described by Bray-Curtis dissimilarity, all three doses showed a trend of separation when compared to control animals. In addition, PERMANOVA was applied to test whether centroid distances between the groups overlapped (p=0.096, p=0.113, p=0.095 for 1000, 5000 and 10000 FIP/kg CRL, respectively, figure 2.7A/B). The data indicated that the distances between all groups show a trend to separate from the control group; although not significantly, suggesting composition and abundance differences in the gut microbiota (figure 2.7A/B).

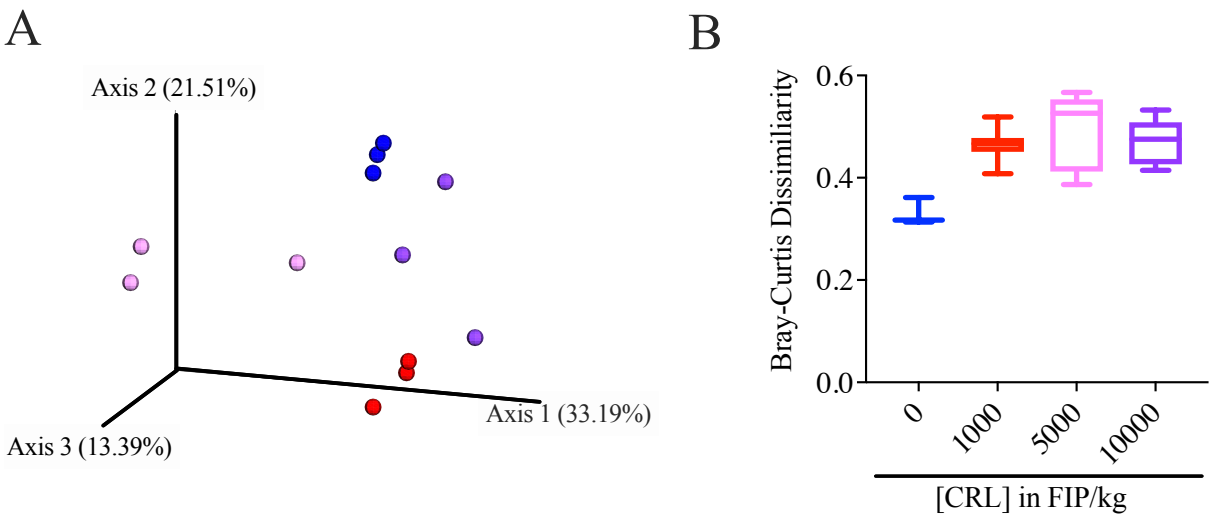

Figure 2.7: Short-term treatment effect of CRL on cecal β-diversity in Wt mice.
*A. Principle Coordinate analysis plot of Bray-Curtis distances. B. Statistical analysis of Bray-Curtis dissimilarity between groups. Significance was analysed with PERMANOVA: *p<0.05.*

Furthermore, to determine the bacterial taxa driving the significant difference in α-diversity, taxonomic classification was assigned using the Greengenes library. At the phylum level, a higher *Bacteroidetes* and lower *Tenericutes* level was observed in all three treatment groups when compared to the control group. In addition, *Verrucomicrobia* and *Proteobacteria* levels were higher at 10000 FIP/kg CRL, while *Actinobacteria* was lower at this dose compared to the other groups (figure 2.8).

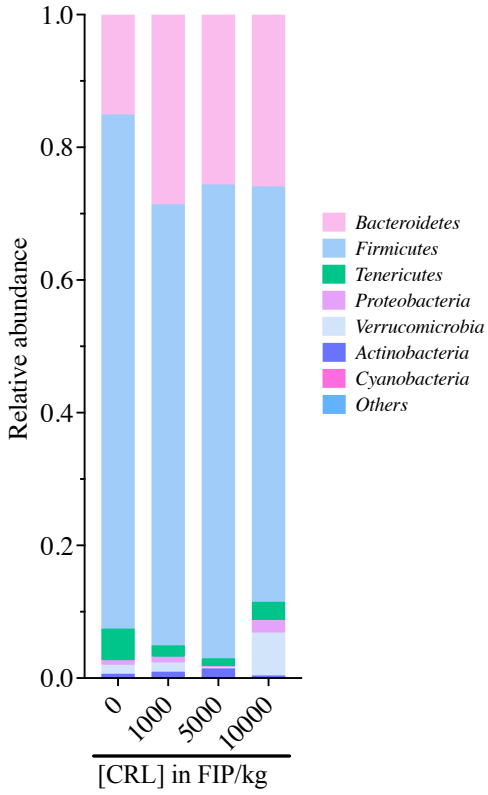

Figure 2.8: Short-term treatment effect of CRL on cecal taxonomy on the phyla level in Wt mice. Taxa assignment with the Greengenes database yielded in determination of phyla differences between treatment groups and control group.

Next, a compositional abundance analysis was applied to determine which taxa were driving the observed differences in the taxa bar plots. The pairwise ANCOM analysis determined three bacterial genera to be significantly altered: *Bifidobacterium pseudolongum, Rikenellaceae* and *Allobaculum* (figure 2.9, supplementary figure 2.1.1A). While the 5000 FIP/kg group showed significant higher levels of *Bifidobacterium pseudolongum* (significance level<0.05, W=26) when compared to 1000 FIP/kg and a trend when compared to the control group, 10000 FIP/kg CRL showed a trend of higher levels of *Bifidobacterium pseudolongum* when compared to the control group (figure 2.9). No changes were detected for the 1000 FIP/kg group (figure 2.9). *Rikenellaceae* and *Allobaculum* displayed significant changes for 5000 FIP/kg and 10000 FIP/kg CRL (significance level<0.05, W=28 and W=29, respectively, figure 2.9), respectively, when compared to the 1000 FIP/kg and a trend when compared to control groups (figure 2.9). All other taxa in the feature heatmap did not show significant changes following CRL

supplementation (figure 2.9, supplementary figure 2.1.1A). However, the short duration of supplementation probably did not reflect the long-term effects of CRL treatment on the microbiota.

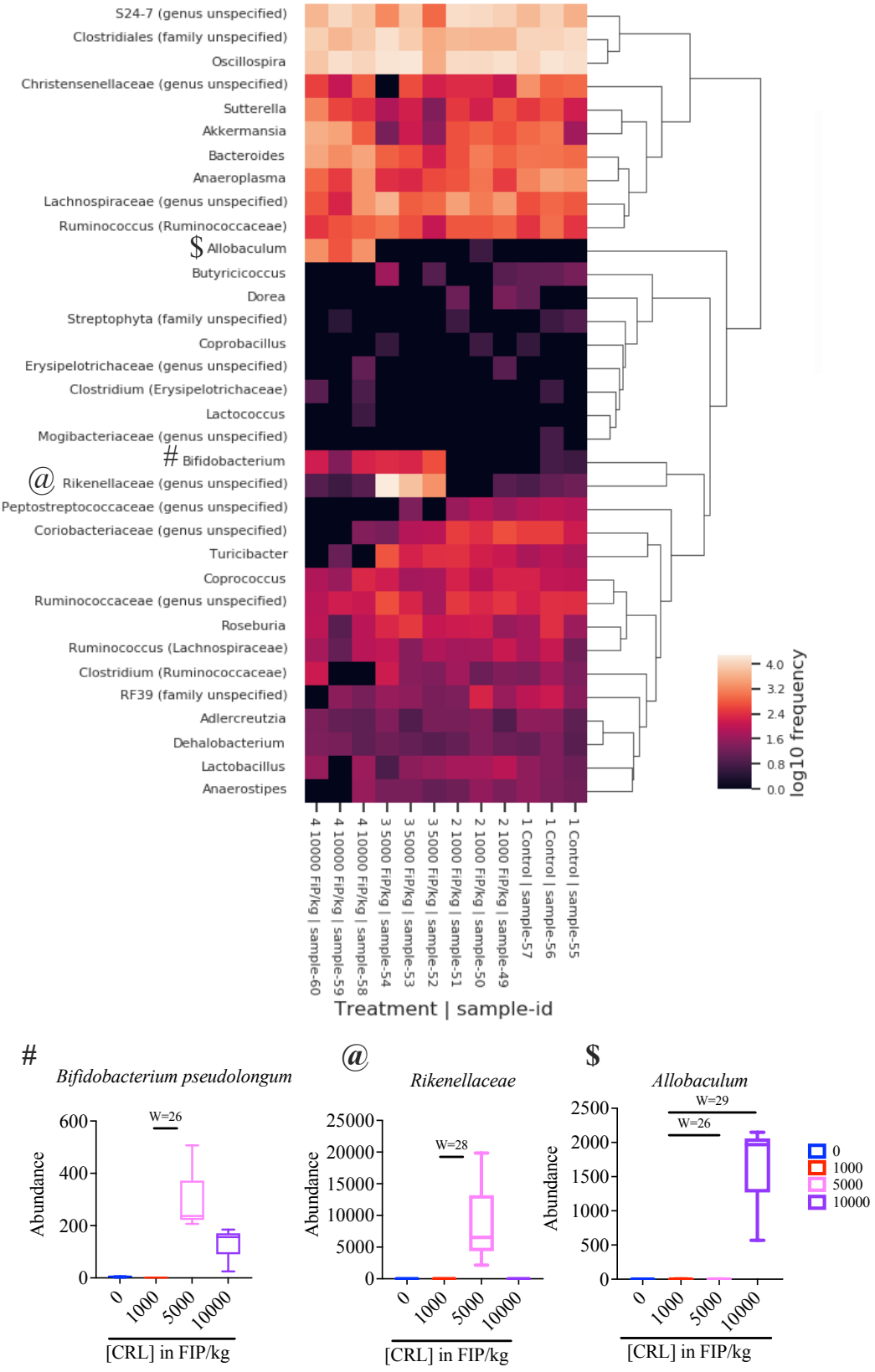

*Figure 2.9: Heatmap of cecal bacterial taxa and pairwise ANCOM comparison to determine significant features. The analysis resulted in three taxa with significant changes due to CRL administration: Bifidobacterium, Rikenellaceae and Allobaculum. #, @, *: significance level<0.05 when W-value indicated.*

Finally, short-chain fatty acids (SCFA) levels were measured in the cecum content to investigate metabolic alterations in the gut environment following CRL supplementation. While no significant differences between treatment groups and short-chain fatty acids level were determined, we detected a dose-dependent trend of decrease for acetic acid (C2-C8, figure 2.10).

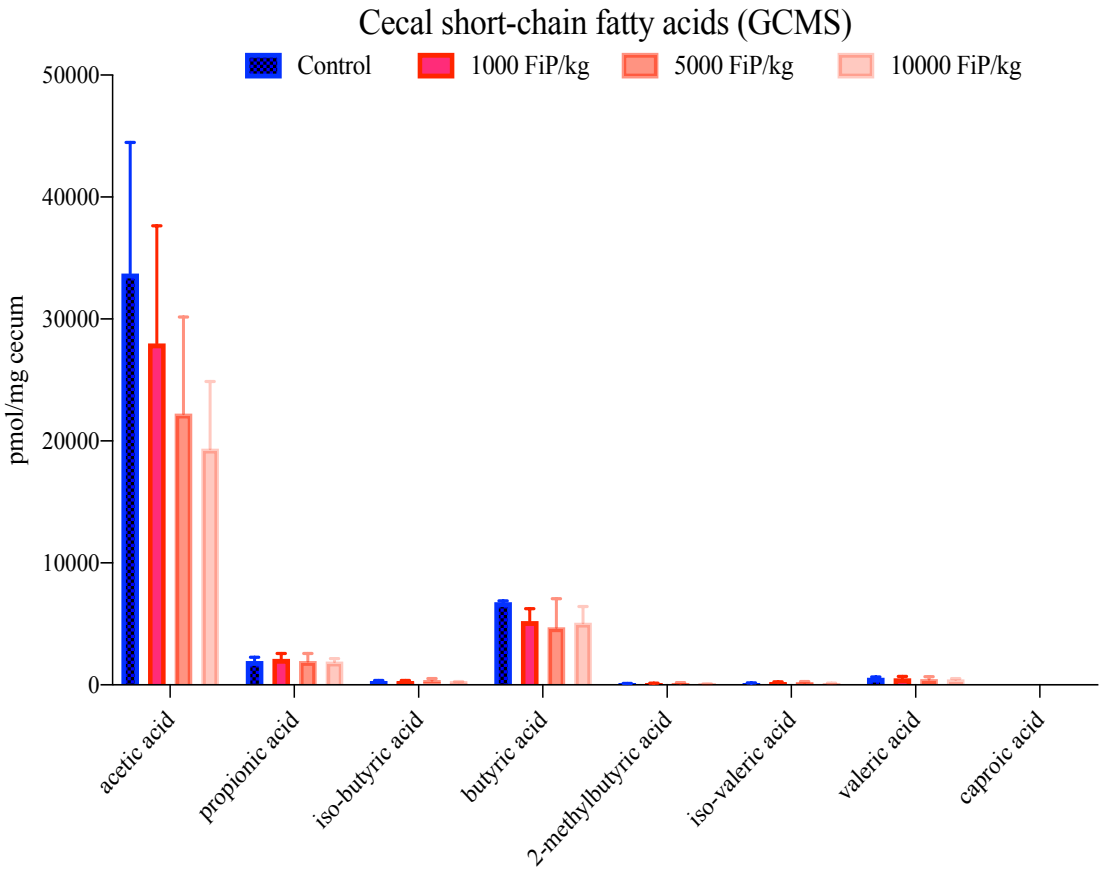

*Figure 2.10: Lipid profiles and short-chain fatty acid levels in cecal matter determined by GCMS. No significant difference could be determined for short-chain fatty acid levels in cecal content, although a dose-dependent decrease trend of acetic acid was observed. Significance was determined by applying a linear mixed regression model and post-hoc Fisher's LSD in SPSS. Data is displayed with standard error of mean. Significance: * $p<0.05$.*

This dose-dependent trend might also explain why we did not see dose-dependent results in the microbial communities. Reduced levels of metabolites such as acetic acid, can detrimentally alter the microbial composition and metabolome. This could also affect the time it takes the microbial community to reorganize and adapt to the new environmental conditions induced by CRL treatment.

2.3.4: CRL long-term administration (feces and cecum)

In the long-term study, we investigated the effects of 1000 FIP/kg CRL in Wt mice to determine CRL's impact on the gut microbiota and intestinal barrier integrity. In addition, we examined whether changes in the microbiota composition would be sustained after discontinuation of supplementation (figure 2.11A). For the long-term study, we selected the lowest dose from the short-term study to prevent potential harm to the intestines during long-term administration of one of the higher doses. No differences in water consumption and animal weight were determined. No significant difference in α-diversity between fecal samples of treatment and control groups or between the three time-points was observed (figure 2.11B).

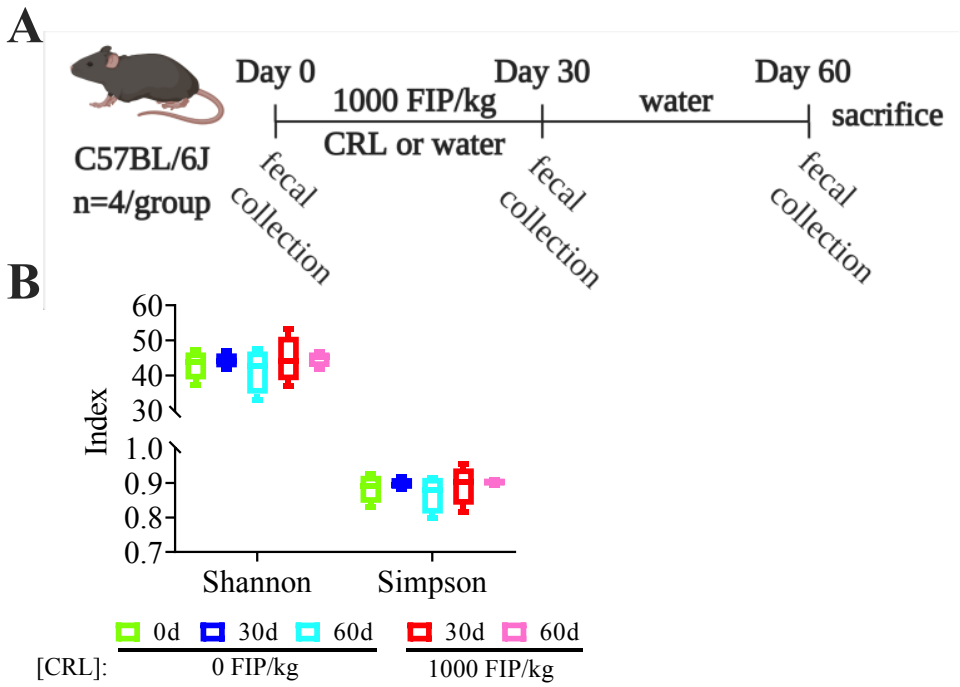

Figure 2.11: Long-term CRL treatment effect on fecal α-diversity.
A. Study design of long-term CRL administration study with 1000 FIP/kg CRL. B. Determination of differences in α-diversity in lipase-receiving animals compared to controls at three different time points analysed with Shannon- and Simpson-index showed no differences. Significance was analysed with Kruskal-Wallis H test and pairwise Kruskal-Wallis.

When investigating β-diversity, significant differences were observed between each time-point of the treatment group compared to each time-point in the control group (figure 2.12A). This was further confirmed by PERMANOVA (p(30 days)=0.032 and p(60 days)=0.029, figure

2.12B) and longitudinal volatility analysis (p(30 days)=0.000015 and p(60 days)=0.00004, figure 2.12C). While axes 2 and 3 did not demonstrate the separation between the treatment and time-points of the groups (figure 2.12C), axis 1 emphasized the significant distribution described by the PERMANOVA analysis (figure 2.12B/C).

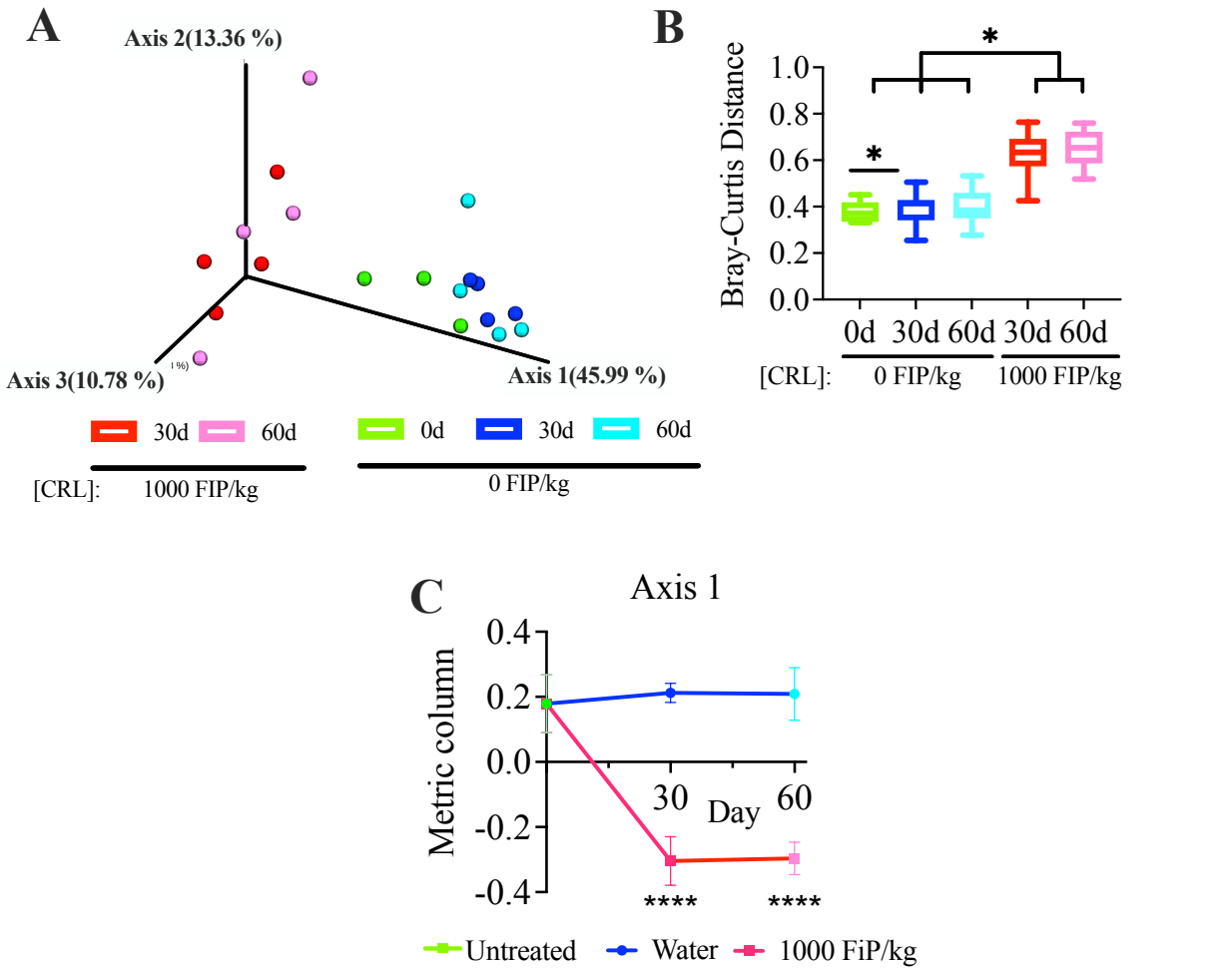

Figure 2.12: Long-term CRL treatment effect on fecal β-diversity.
*A. Principle Coordinate analysis plot of Bray-Curtis dissimilarity analysis to determine β-diversity, which showed a significant separation between treatment time points compared to controls. B. PERMANOVA analysis of Bray-Curtis dissimilarity showed signficant differences between treatment and control groups. C. Longitudinal volatility of β-diversity (Bray-Curtis dissimilarity) along Axis 1 emphasized the results of A/B. Significance was analysed with and PERMANOVA (B) and 2-way ANOVA with multiple t-testing (C): * p<0.05, ** p<0.01, *** p<0.001, ****p<0.0001.*

Therefore, the results of the β-diversity analysis emphasize that compositional microbial differences occur not only after 30 days of treatment but were also maintained after 30 days of

discontinuation of CRL treatment. Subsequently, taxa assignment was performed to assess which taxa were causing the observed diversity differences (figure 2.13).

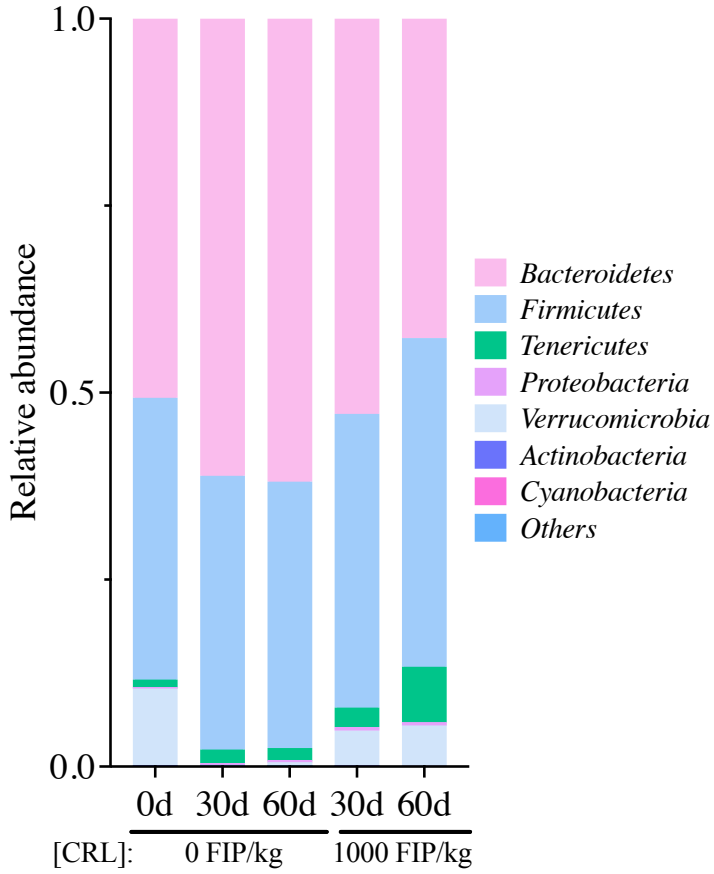

Figure 2.13: Long-term CRL treatment effect on fecal taxonomy.
*Taxonomy assignment with Greengenes database to analyse effects in treated compared to control animals, which showed maintained Verrucomicrobia levels in treated groups. Significance was analysed with Kruskal-Wallis H test and pairwise Kruskal-Wallis (B) and PERMANOVA (D): * $p<0.05$, ** $p<0.01$, *** $p<0.001$.*

On the phylum level, *Verrucomicrobia* were maintained in the treatment group while almost disappearing in the 30- and 60-day control groups, similar to the detected changes in the short-term study- although no changes of diet and water supply were applied in the control group. *Tenericutes* showed higher levels in both treatment groups compared to all control time-points. To analyse the significant differences on the species level a taxa heatmap was created and significant taxa identified with pairwise ANCOM analysis (figure 2.14, supplementary figure 2.1.1B). While the heatmap indicated numerous common traits between the time-points and treatment groups, *Anaerostipes* was only detected in the treatment group at 30 and 60 days but

in none of the control time-points (significance level<0.05, W=18 and W=15 compared to control time-points, respectively, figure 2.14). Additionally, *A.muciniphila* was detected at the 0 min time-point but was significantly reduced after 30 days (significance level<0.05, W=26) and showed a trend after 60 days. Furthermore, this species was significantly higher compared to respective control time-point after 30 days (significance level<0.05, W=28) and displayed a trend after 60 days when CRL was supplemented in the drinking water (figure 2.14).

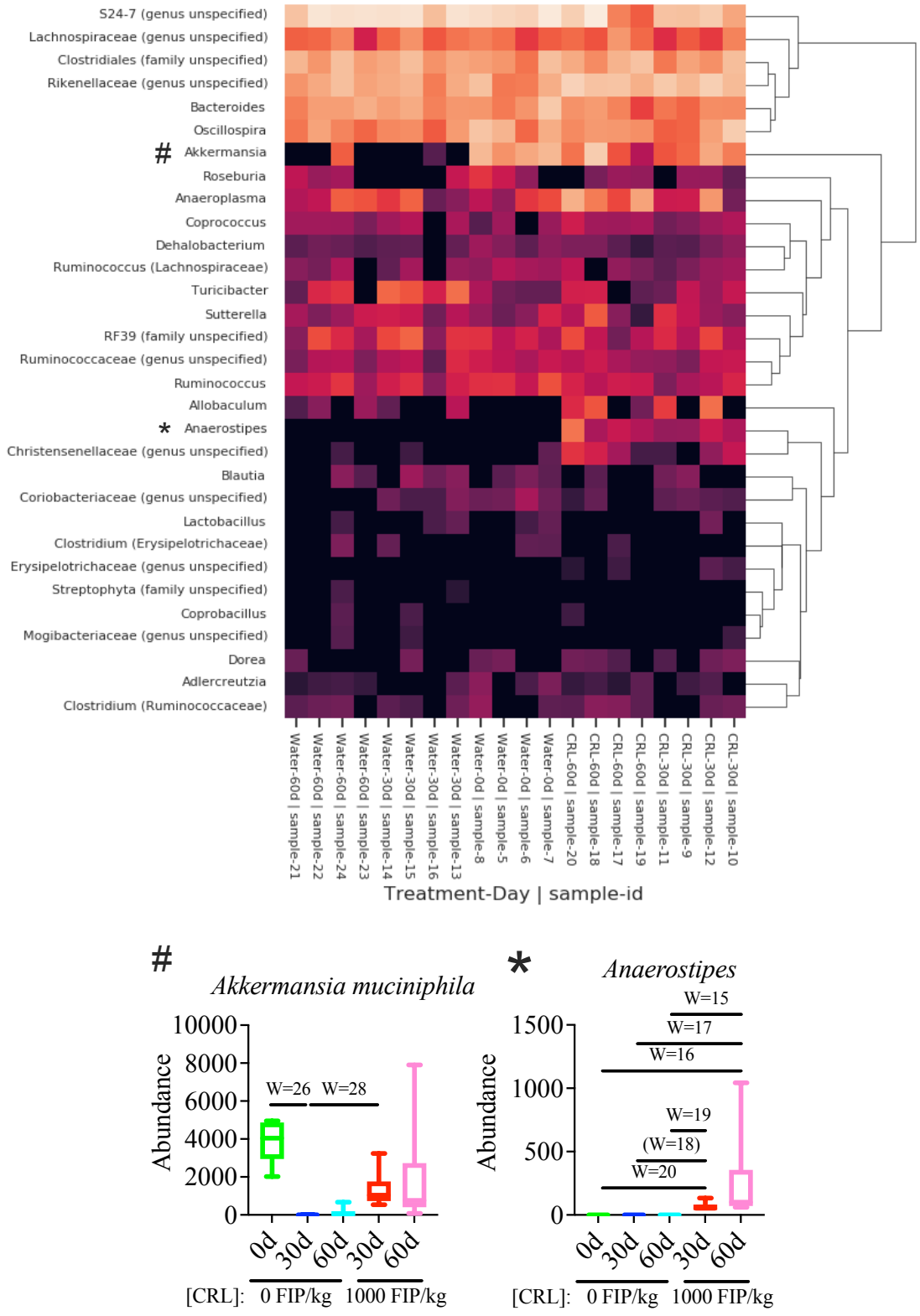

*Figure 2.14: Heatmap of fecal bacterial taxa and pairwise ANCOM comparison to determine significant features. The feature heatmap illustrates the most important taxa determined in feces samples, elucidating two significantly different taxa. While A.muciniphila was significantly reduced at 30 and showed a trend of reduction at 60 days in Wt mice, it was higher in both treatment time-points. Anaerostipes was significantly different in treated groups only compared to all control time-points. #, *: significant level<0.05 when W-value indicated, brackets indicate trends.*

Finally, microbial changes in the cecum were investigated after 30 days of CRL supplementation followed by 30 days of supplementation discontinuation. The treatment group showed a higher (p=0.083 and p=0.021, respectively) α-diversity for the Shannon and Simpson indices after supplementation and subsequent one-month wash out compared to control animals (figure 2.15A). β-diversity analysis (PERMANOVA) assessed a significant separation (p=0.031) between treated and non-treated animals, emphasizing the enzyme's impact on the gastrointestinal environment (figure 2.14B/C).

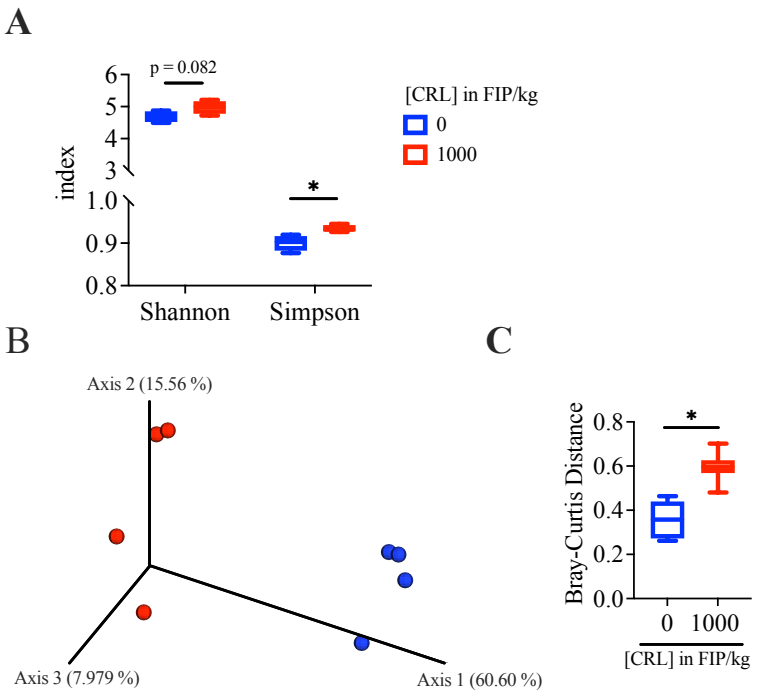

Figure 2.15: Long-term administration of CRL in Wt mice and the effect on cecal diversity.
*A. Shannon and Simpson index analyses showed increased α-diversity in treatment groups compared to control animals. B/C. Principle Coordinate analysis plot of Bray-Curtis dissimilarity analysis determined a significant dissimilarity between treatment and control group. Significance was analysed with Kruskal-Wallis H test and pairwise Kruskal-Wallis (A) and PERMANOVA (C): * p<0.05, ** p<0.01, *** p<0.001.*

Next, taxonomy assignment with the Greengenes database was performed to extract the phylogenetic information in the data set. After treatment discontinuation for 30 days, lower phyla levels of *Bacteroidetes* and higher levels of both *Verrucomicrobia* and *Tenericutes*

abundance were detected (figure 2.16), similar to the changes observed in the fecal samples when compared to controls.

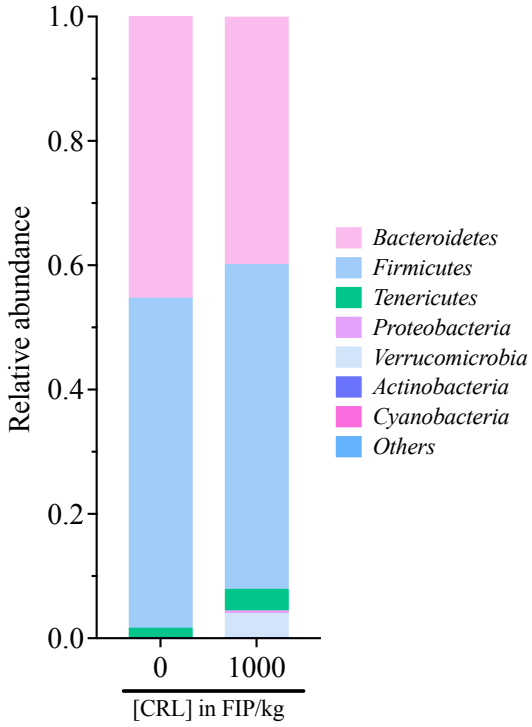

Figure 2.16: Long-term administration of CRL in Wt mice and the effect on cecal taxonomy on the phyla level. Taxa assignment with the Greengenes database to measure phyla differences between treatment groups and control group determined decreased Bacteroidetes and increased Verrucomicrobia levels post treatment

Analysis of lower phylogenetic levels (family, genera, and species) indicated more differences between treatment and control groups, but complexity of the results had to be reduced by differential abundance analysis in order to analyse significant differences of individual taxa in the data set. The data was summarized at the genera-level heatmap to emphasize these significant differences (figure 2.17). While most taxa remained unchanged and are therefore considered treatment independent, ANCOM analysis identified two species that were significantly induced by treatment: *A.muciniphila* and *Christensenellaceae* (significance level<0.05, W=10 and W=19, respectively, figure 2.17, supplementary figure 2.1.1C).

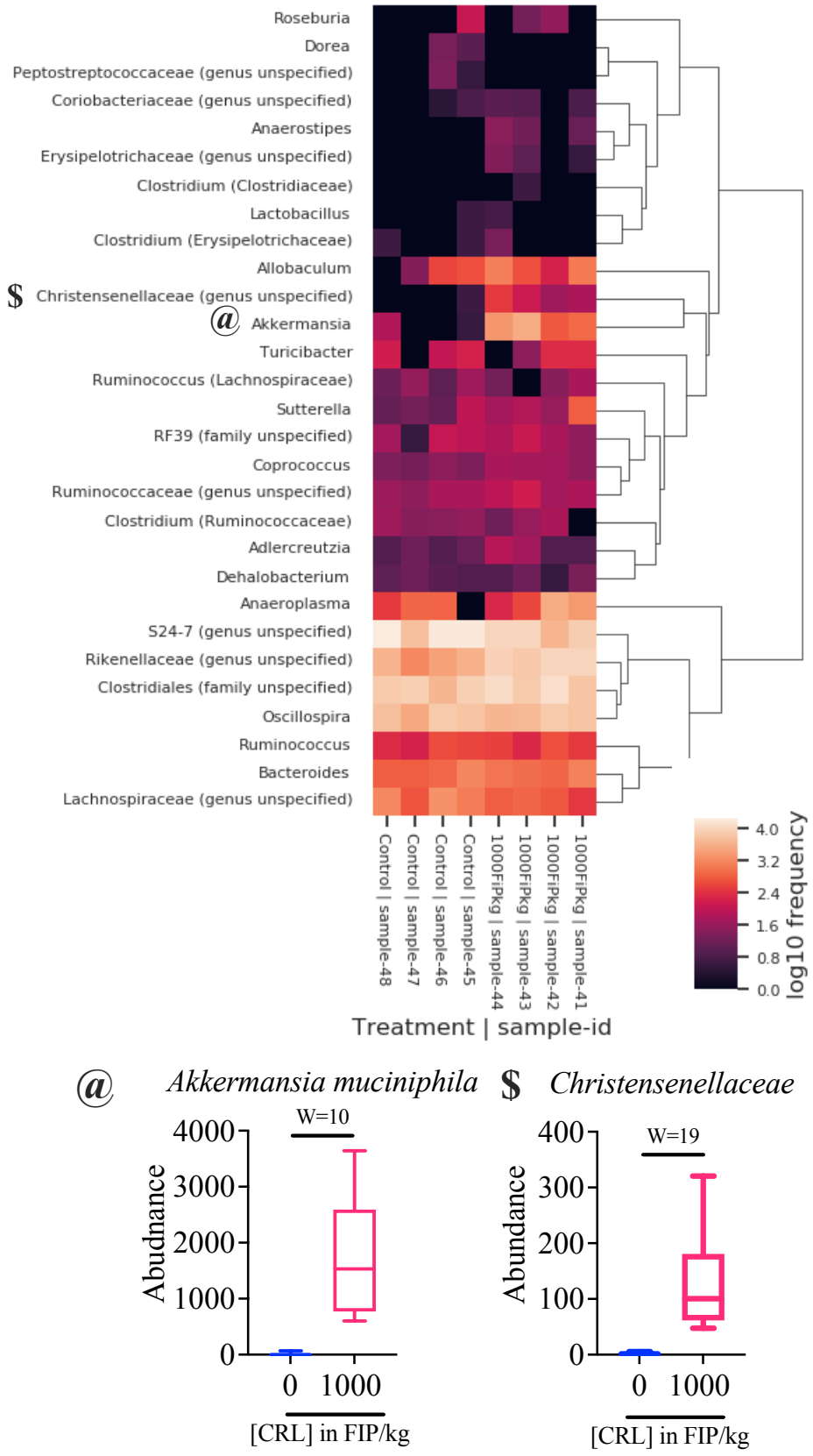

Figure 2.17: Heatmap of cecal bacterial taxa and pairwise ANCOM analysis.
The taxa heatmap highlights taxa causing differences between the treatment groups. Differential abundance analysis (pairwise ANCOM) determined significant taxa changes in cecum. A.muciniphila and Christensenellaceae were both significantly higher in the treatment groups. @, $: significance level<0.05 when W-value indicated.

These determined changes are CRL administration dependent; however, most other families remain unchanged or showed marginal differences. Although CRL treatment was discontinued for 30 days after 30 days of treatment, changes in the gut microbiota were persistent even after the 30 days of washout, suggesting a sustained effect on the microbial environment after CRL treatment.

2.3.5: Immunohistochemistry of SI and colon after long-term supplementation

Since the results showed that CRL was active beyond the stomach and that it did alter the gut microbial composition in the short- and long-term, it was analysed whether long-term supplementation with CRL negatively affects gut barrier integrity. Claudin-2 and Zonula occludens-1 (ZO-1), which are tight junction proteins determining gut barrier integrity, were used for immunofluorescent staining in the SI and colon (figure 2.18). The subsequent quantification and comparison of treated and untreated animals did not reveal any significant differences for either ZO-1 or Claudin-2 expression relative to the DAPI signal in the tissue of the SI and colon. Therefore, the gut barrier was considered intact and unharmed by treatment.

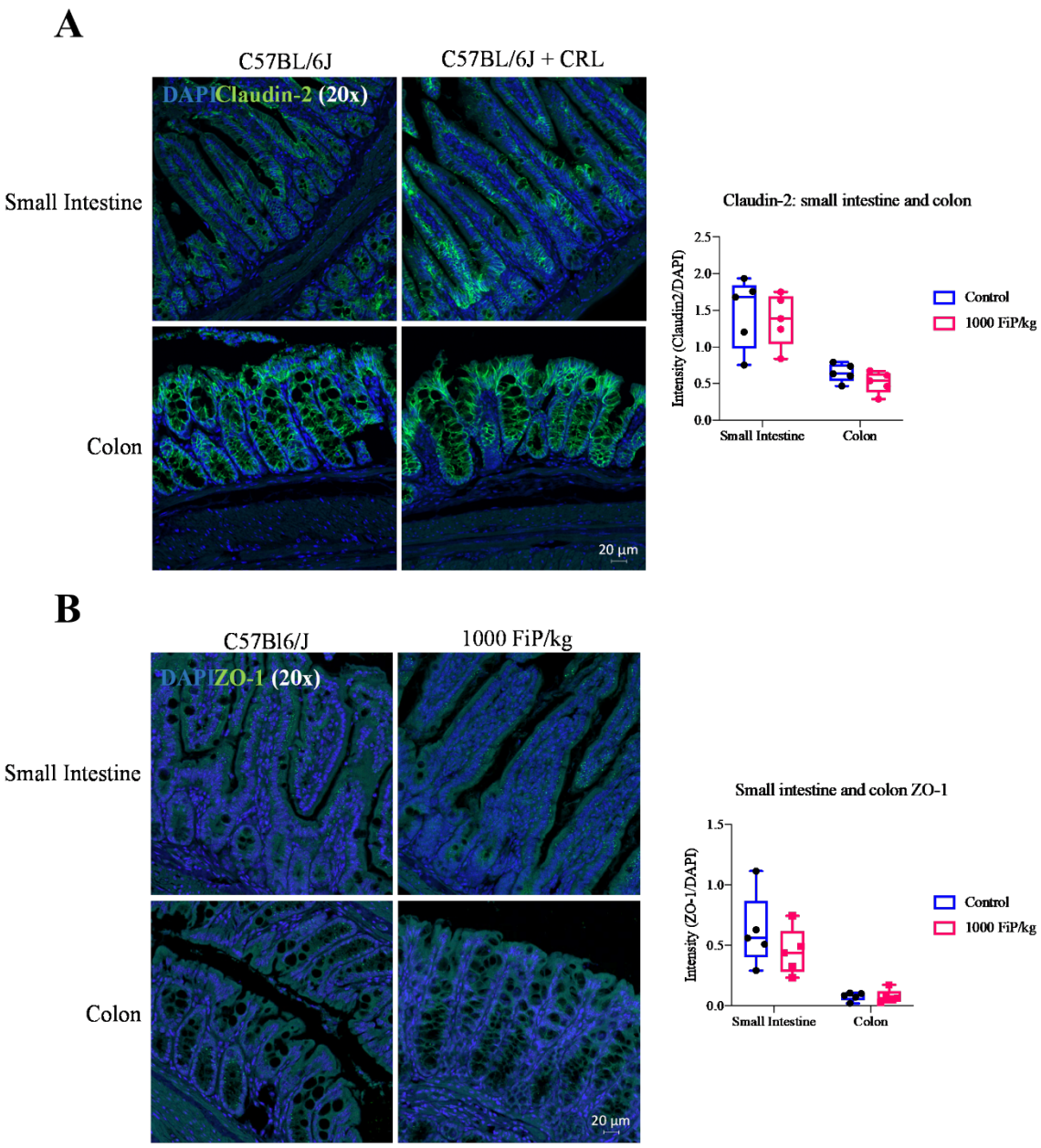

Figure 2.18: Immunofluorescent staining of tight junction proteins in SI and colon.
A. Claudin-2 staining, and quantification showed no significant differences between treated and control animals. B. ZO-1 staining, and quantification resulted in no significant differences between treated and control animals. SI quantitation comprises the sum of the three subsegments of the SI. Data is displayed with standard deviation.

2.4 Discussion

Diet has the greatest impact on the gut microbial composition [240, 241]. We hypothesized that administration of an exogenous digestive enzyme, CRL, alters the gut microbiota and metabolite composition by changing nutritional levels of glycerol and fatty acids in the gut lumen

(hypothesis (1)). First, we demonstrated that CRL is pure and stable, which assured measurement of treatment specific effects without interference of impurities. Next, the transfer of active CRL in the gastrointestinal tract of mice was assessed when the enzyme was supplemented in their drinking water despite the acidic environment of the stomach (pH 3-4) [242]. We observed that differences in CRL activity *ex vivo* (biotinylated CRL) and cleavage product levels *in vivo* (FFA levels) were dependent on CRL treatment. While administration of biotinylated CRL confirmed CRL's presence and maintained activity throughout the intestinal tract, the administration of CRL with pure triglyceride, which allowed us to control the simultaneous food intake of all animals, demonstrated the activity of CRL directly in the gut lumen (FFA levels). This revealed for the first time that the enzyme is active far beyond the stomach and therefore can be delivered unprotected in the drinking water of mice in the subsequent studies.

Next, the short- and long-term effects of CRL treatment were investigated in two separate studies to test our null hypothesis that CRL's activity in the gut does not increase the abundance of bacteria beneficial to the host. For the short-term study, CRL was administered for three days in three different concentrations in drinking water. Subsequently, we demonstrated that exogenous CRL induced biological changes in the gut environment by alteration of α- and β-diversity in the gut microbiota. Significant changes in bacterial taxa associated with CRL administration further supported this hypothesis. Among the species present, there was a change in *Bifidobacterium pseudolongum*; a commensal bacteria in the gut that has been implicated in supporting gut health by both maintaining gut integrity and enabling digestion of hydrolysis-resistant starch [243, 244]. In addition, two other bacterial strains- *Rikinellaceae* and *Allobaculum*, were elevated in the medium and high dose studies, respectively. These two species are also abundant in humans: low abundances of *Rikenellaceae* have been associated with obesity and high abundance with high-fat diets; while a high abundance of *Allobaculum*

has been observed with normal diets [245-247]. This supported the hypothesis that CRL favors the abundance of bacteria which preferably digest fats such as *Firmicutes* and *Proteobacteria*. However, the observed changes in the gut microbiota occurred after a short supplementation period. Hence, the data might reflect the transient adaptation of the gut microbiota to the changed gut environment rather than a dose-dependency observed in pharmacokinetics due to the changing presence of, and interaction between, bacterial taxa. This might also explain both the observed inconsistencies in α-diversity and β-diversity between the three doses as well as the lack of significant change in SCFA levels. Nevertheless, despite the absence of a traditional dose effect that one might see with a pharmaceutical agent, this study strongly supports the hypothesis that CRL activity impacts the host's gut environment.

Subsequently, the long-term effects of CRL intake on the gut microbiota were analysed throughout and after the study to determine the more chronic effects of CRL supplementation in the treatment-adapted gut microbiota. Despite minor differences, α-diversity did not reach statistical significance across treatment and control groups at different time-points and within groups in feces. However, β-diversity was significantly different when comparing control and treatment groups. These differences were unexpectedly maintained even after discontinuation of CRL administration, which emphasizes that CRL's activity in the gut lumen has a detrimental impact on the gut microbial composition. It remains unclear how these changes persist after discontinuation but is hypothesized to be based on a potential feedback loop that has not been elucidated yet. When examining the significantly changing taxa between the treatment groups, two species were determined to be changed: *A.muciniphila* and *Anaerostipes*. *A.muciniphila* levels drastically decreased at 30 and 60 days in the control groups compared to day 0. However, in the treatment group higher levels were detected at 30 days and at 60 days when compared to controls at the same time points. The abundance of *A.muciniphila* before the study began and the apparent subsequent loss of this species in the control group was probably an artifact of the

acclimatization period of the mice to their new environment, which needs to be investigated further. After 30 days in the study the levels of *A.muciniphila* in controls receded, while the treatment group maintained the species abundance. Although *A.muciniphila* is inversely associated with numerous diseases such as obesity, metabolic disorder and low-grade inflammation, and hence is considered beneficial [248], its role remains controversial. For instance, higher levels of *A.muciniphila* were associated with Parkinson's disease [249], whereas it has been shown that treatment with miR-30d from feces of multiple sclerosis (MS) patients led to higher levels of *A.muciniphila*- which improved pathology [250]. It was suggested that *A.muciniphila* exert their beneficial effect by digesting mucin and regulating DCs and therefore increase Treg abundance. Therefore, the increase in *A.muciniphila* in MS patients was suggested to represent an endogenous protective mechanism [250]. These results suggest that although present in patients affected by neurodegenerative disease, *A.muciniphila* may be involved in a generic endogenous mechanism to protect the host, which can be induced by CRL treatment as shown in this study.

Moreover, *Anaerostipes* was higher in the treatment group at 30 and 60 days and appeared to be associated with CRL treatment. The *Anaerostipes* genus is another bacterial taxa thought to be beneficial in humans as it contains many butyrate-producing species including *A.rhamnosivorans* and *A.butyraticus* [251-253].

To investigate the impact of CRL supplementation, not only over time but also directly in the gastrointestinal environment, the microbial taxa differences in cecal content were analysed. The results implied that the enzyme supplement changed the microbial composition and sustained the effects long after the supplementation had stopped (day 60). The data analysis of the fecal samples supports this hypothesis, although no differences were detected in α-diversity between treated and control animals at different time-points. Moreover, higher α-diversity between treated and control animals in the cecum was observed, which is generally associated with

outcomes advantageous to health [254, 255]. These results are not in accordance with the results acquired in the short-term study. However, in the short-term study, the microbiota might have been still in the process of reorganizing and adapting to the changing environment induced by CRL treatment, that might have been changed over time. Moreover, β-diversity in the long-term study highlighted the dissimilarity between the two groups post CRL administration that was already seen as a trend in the short-term study. When investigating the taxa differences, both species *Christensenellaceae* and *A.muciniphila* were significantly higher in treated animals. *Christensenellaceae* is another genus associated with low body mass index (BMI) and high-fat diets. Both *Christensenellaceae* and *A.muciniphila* reflect CRL's activity in the intestine and the potential health benefit obtained by increasing their levels. Both have been associated with healthy individuals protecting the host from metabolic syndrome and obesity [256, 257]. Nevertheless, we acknowledge the limitations of 16S rRNA sequencing, which includes the measurement of relative rather than absolute abundance of bacteria and that bacterial taxonomy mostly remain unidentified on the species level [258]. In addition, the analysis of the datasets is biased due to the inherent variation of PCR amplifications, which is used during sample preparation for 16S rRNA sequencing. Therefore, future studies could use deep sequencing strategies such as shallow shot-gun sequencing to enhance identification on the species level and *de novo* assembly to improve ASV identification.

In summary, the investigation of CRL's treatment effect in healthy Wt mice showed that CRL could be orally administered and was capable of evoking gut microbiota and metabolite alterations without harming the gut environment. This supported hypothesis (1) and laid the foundation for the subsequent investigation of hypothesis (2) and (3).

Chapter III: The impact of orally administered CRL on the gut, periphery and brain pathology of APP/PS1 mice

3.1 Introduction

Despite an abundance of research identifying the neuropathological hallmarks of AD, so far no disease-modifying pharmaceuticals have been identified in clinical trials conducted in the past decades [54]. Since most of the failed and currently failing approaches have targeted amyloid plaques or inhibited γ-secretase activity, researchers' interest were directed towards novel targets associated with AD pathology [54]. The gut microbiome was regarded a novel research prospect due to its association with disease pathologies of neurodegenerative diseases including AD [259]. In both murine models and clinical studies of AD patients, gut dysbiosis has been observed denoted by a decrease in the phyla *Firmicutes* and *Actinobacteria* and increased abundance of *Bacteroidetes* [59, 60, 260]. Furthermore, it was shown that the compositional state of the gut microbiota in a murine model of AD impacted the progression of disease pathology [139]. Consequently, dysbiosis of the gut microbiota in AD has been hypothesized to potentially contribute to disease onset and/or progression and has been suggested as potential treatment target, although it still needs to be elucidated whether this represents a trigger, facilitator or consequence of AD pathology [59, 261]. However, due to the recent findings normalization of the gut microbiota in AD has been proposed to improve levels of beneficial metabolites and bacteria in the gut and ameliorate disease pathology through transmission of beneficial signals by the gut-brain axes [59, 262]. These axes have been suggested to transmit signals from the gut into the brain and vice versa, although the precise mechanism and their contribution to host health and diseases has not yet been fully revealed [262, 263].

Targeted alteration of the gut microbiota composition can be achieved by permanent dietary changes and has been demonstrated as the most efficient strategy to enhance gut microbial

composition [216, 240]. In addition, certain diets such as the Mediterranean or ketogenic diet have been reported to benefit the gut microbial composition and microbiota-derived metabolites, which have also been associated with reduced cognitive decline, which proposes a possible link between gut and brain health [264-267]. Therefore, we investigated in this chapter the potential beneficial effects of CRL administration in a mouse model of AD, which was proposed to enhance both gut microbiota and metabolite composition by increased digestion of dietary macromolecules and consequently AD pathology (hypothesis (2)). This hypothesis was supported by the findings of Chapter II, which presented evidence that CRL supplementation altered microbiota and metabolite composition in Wt mice and by the findings of other studies which have demonstrated anti-inflammatory and anti-bacterial effects of CRL's cleavage products in the host potentially impacting AD pathology [182, 268-271].

To test our hypothesis, we examined in *Study 1* the effect of 5000 FIP/kg CRL on the gut, periphery, and brain pathology comparing a mouse model of AD (APP/PS1) to Wt mice. The dose of CRL was extrapolated from the normal human dose that is used for pancreatic insufficiency. In addition, we showed in chapter II, that administration of three different doses of CRL in the short-term study, which spanned the range of human recommended doses, did not lead to observation of adverse effects. Thus, the dose was increased to 5000 FIP/kg when compared to the previously performed long-term study and represented an extrapolated normal human dose in mice [272]. Subsequently, the fecal matter of all groups in *Study 1* were collected and transferred into antibiotic-induced microbiome-depleted (ABX) Wt mice to assess whether treatment-dependent enhancement of memory was evoked by the changes in the gut.

The findings from *Study 1* supported the potential of CRL to alter AD pathology by normalizing gut microbial composition and unsaturated fatty acid levels in plasma. Furthermore, we determined enhanced cognition and reduced disease pathology post treatment. Finally, we

showed in *Study 2* that the treatment-dependent enhanced cognitive function of treated APP/PS1 animals was transferable into ABX Wt mice of *Study 2* via FMTs.

3.2 Materials and methods

3.2.1: Animal models

Animals were kept in the AAALAC accredited vivarium of the Roskamp Institute. Experiments with mice were reviewed and approved by the IACUC of the Roskamp Institute before implementation and conducted in compliance with the National Institutes of Health Guidelines for the Care and Use of Laboratory Animals. The design of both animal studies and their connection have been visualized in a study overview figure (supplementary figure 3.1.1). Wt and APP/PS1 mice for *Study 1 (CRL treatment study)* were obtained from in-house breeding. Wt mice for the *Study 2: FMT study* were also obtained from in-house breeding. Mice were maintained on a 12 h/12 h light/dark cycle and received food and water ad-libitum. Mice were weighed and monitored throughout and before procedures.

3.2.2: *Study 1*: CRL treatment study

Male and female Wt or APP/PS1 mice (8 months of age, n = 12-15/group) were obtained from an internal breeding protocol, group housed and randomly subdivided into CRL treated and untreated groups. At the selected timepoint, mice were hypothesized to be in an earlier stage of the disease, where patients might recognize changes due the progressing neuroinflammation and amyloid plaque deposition that would make them report to their physicians and therefore, enable treatment. Mice received 5000 FIP/kg body weight CRL in drinking water for 2 months, or regular water. Since we did not observe any adverse effects in Chapter II for a low human dose of CRL, we decided to increase the dose in this chapter to the recommended normal dose for cystic fibrosis patients. CRL has been shown to be stable in water for up to 7 days and hence, water, treated or untreated, was changed twice a week [273]. Four weeks before the start of

Study 1, nesting and bedding materials were exchanged between all groups and throughout the study within groups twice a week to normalize endogenous gut microbial variance and to prevent cage effects. Four groups were assessed in *Study 1* (APP/PS1 n= 12, APP/PS1+CRL n=12, Wt n= 13, Wt+CRL n= 15). Fecal samples were collected at 0, 4, and 8 weeks of treatment for microbiome analysis and three times per week during treatment week 5 to 8 for the FMTs in *Study 2,* which were maintain as life stocks until used for fecal matter transplants (s.3.2.3). In the last two weeks of treatment, mice were trained and tested for spatial learning and memory in the Barnes maze. On the last day of treatment, gut integrity was assessed (see 3.2.4). At 10 months of age, mice were anaesthetized with isoflurane (3% in 1.5 L/min O_2; Patterson Veterinary, Greeley, CO) delivered to an induction chamber via a calibrated vaporizer equipped with a waste-gas scavenger device. Once deeply anaesthetized mice were humanely euthanized by cardiac puncture-induced exsanguination and subsequently perfused with phosphate buffered saline (PBS) in accordance with the approved IACUC protocol. Subsequently, the right hemispheres of the brain were fixed in 4% PFA (Sigma, St. Louis, MO) for 24h for immunohistochemical analysis. The left hemisphere of the brain, small intestine, cecum, colon and plasma were collected and immediately flash frozen in liquid nitrogen and stored at -80ºC.

3.2.3: *Study 2*: FMT study

For the fecal matter transplants, fecal samples were immediately homogenized 1:5 (w/V) in 0.9 % sodium chloride (Sigma, St. Louis, MO) solution containing 10% glycerol (Sigma, St. Louis, MO) to maintain life stocks by stabilizing fecal bacteria during storage and shorten oxygen exposure [274]. Before usage, all samples of the same group were flash thawed in a 37 ºC water bath and combined [275]. The fecal pool of each group was strained through a 40 µM nylon filter (Fisher Scientific, Waltham, MA) by centrifugation at 350 g until a viscous layer formed. The cell density of the flow through was measured in a cell counter (APP/PS1: 6.74 x 10^6/50 µL; APP/PS1+CRL: 5.04 x 10^6/50 µL; Wt: 7.47 x 10^6/50 µL; Wt+CRL: 8.68 x 10^6/50 µL) and

adjusted to 5 x 10^6 cells/50µL. Samples were divided in 700 µL aliquots, flash frozen in liquid nitrogen and stored at -80 ºC and used for the FMT treatment described below.

Female and male Wt mice (n=72, aged 13-14 weeks) were randomly subdivided into 6 groups with 12 mice per group (Sham, ABX, FMT: APP/PS1, FMT: APP/PS1+CRL, FMT: Wt, FMT: Wt+CRL) and group housed. Age was not considered as an influencing parameter since the cognitive impairment was induced through the antibiotics, which justified the use of younger mice. The bedding and nesting materials were exchanged between all groups four weeks prior to the study as well as within groups twice a week throughout the study to prevent cage effects. Briefly, the strategy used was adapted from Zarrinpar et al., Wrzosek et al. and Kang et al. [168, 276, 277]. Mice were treated with an antibiotic cocktail (Neomycin:Ampicillin:Metronidazole:Vancomycin (Sigma, St. Louis, MO) in 1:1:1:0.25 ratio of 200 mg/kg in drinking water containing 2 % sucrose, [168, 276]) – or sucrose only for controls – for two weeks. Water was changed twice a week. In addition, mice received 100 µg Amphotericin B (Sigma, St. Louis, MO) in 5 % DMSO (Sigma, St. Louis, MO) or 5 % DMSO (Sham) twice a week in water via oral gavage (20 G, 38 mm, 2 mm tip, straight; GavageNeedle.com, Phoenix, AZ) to prevent fungal overgrowth in depleted gut microbial environment [276]. After antibiotic treatment on day 15, mice were fasted for 1h (water and food) followed by 4 oral gavage administrations of 200 µL of 400 g/L Macrogol 4000 (Sigma, St. Louis, MO) 20 min apart or water for controls (Sham) to further remove gut microbiota and remove residual antibiotics before FMT [168, 277]. Subsequently, all mice were fasted for 4 h. Finally, mice received the first FMT with 5.00 x 10^6 cells in 50 µL per fecal matter transplant or 10 % glycerol in 0.9 % NaCl (Sham, ABX) via oral gavage [275, 278]. The three subsequent gavages were administered once weekly thereafter. One week after the last FMT, mice were trained and tested for Barnes Maze to determine the effect of FMTs on learning and memory. After behavioral testing, animals were anaesthetized with isoflurane (3% in 1.5 L/min O_2;

Patterson Veterinary, Greeley, CO) delivered to an induction chamber via a calibrated vaporizer equipped with a waste-gas scavenger device. Once deeply anaesthetized mice were humanely euthanized by cardiac puncture-induced exsanguination and subsequently perfused with phosphate buffered saline (PBS) in accordance with the approved IACUC protocol. Small intestine, cecum and colon were collected for 16S sequencing analysis.

3.2.4: Gut integrity

Prior to euthanasia, mice (APP/PS1 n= 6, APP/PS1+CRL n=5, Wt n= 3 and Wt+CRL n= 3 from *Study 1*) were fasted (food and water) for 5 h. Next, 4 kDa fluorescein isothiocyanate (FITC)-dextran (0.6 mg/g body weight, Sigma, St. Louis, MO) was orally administered via oral gavage. 60 min later mice were humanely euthanized. Following euthanasia, plasma was collected, flash frozen in liquid nitrogen, and then stored at -80 °C. For analysis plasma samples were diluted 1:5 in PBS pH 7.4. 100 µL of water and 50 µL of sample – or standard (0 – 40 µg/mL 4 kDa FITC-dextran) – were added to a black 96-well µ-clear bottom plate (Greiner Bio-One, Monroe, NC). Fluorescence was immediately measured at 485/528 nm and FITC dextran concentration was examined in each sample. Data was analysed with 2-way ANOVA and Tukey multiple comparisons correction and plotted in GraphPad Prism 8 (GraphPad, San Diego, CA).

3.2.5: Microbiome analysis

DNA (n=6/group for *Study 1* and for *Study 2*) was extracted from feces (20−100 mg/pellet) and cecum (30 mg) samples using the Fast DNA stool mini kit (Qiagen, Germantown, MD) according to the manufacturer's protocol. Volumes were adjusted to account for lower sample weight. DNA extracts were analysed by V3-V4 region 16S rRNA gene amplicon sequencing using the Illumina MiSeq sequencing platform (Illumina, San Diego, CA) in collaboration with Prof. Dr. Klatt, University of Minnesota, following the Earth Microbiome Project protocols (http://press.igsb.anl.gov/earthmicrobiome/protocols-and-standards/16s/) and our recent publication [234]. In addition, the MicrobiomeAnalyst interface

(https://www.microbiomeanalyst.ca) was used to identify differentially abundant microbial genera with the Linear discriminant analysis Effect Size (LEfSe) application [279]. Data was plotted in GraphPad Prism 8 (GraphPad, San Diego, CA) and β-diversity plots were acquired in Qiime2 using the Emperor suite [280].

3.2.6: Pro-inflammatory cytokine panel

Cortex and plasma cytokine levels (n=6/group for *Study 1*) were analysed with the V-PLEX Plus Proinflammatory Pane1 Mouse Kit (MSD, Rockville, MD) according to the manufacturer's protocol. Plasma and cortex lysate were diluted 1:2 in Diluent 41, added in duplicates and incubated over night at 4°C. Subsequently cortex cytokines were normalized to protein content of lysates, which were determined with by bicinchoninic protein assay (ThermoFisher, Waltham, MA) analysis. Data was plotted and analysed via 2-way ANOVA and Tukey correction in GraphPad Prism 8 (GraphPad, San Diego, CA).

3.2.7: Cecum metabolomics

Cecal metabolites (n=4/group for *Study 1*) were investigated by gas chromatography mass spectrometry analysis. 50 mg of cecum were mixed with 50 µL internal standard mix (10 µg/mL 6,6-D2-glucose, 300 µg/mL D6-γ-aminobutyric acid (all from Sigma, St. Louis, MO); 20 µg/mL 2,2,4,4-D4-citric acid, 10 µg/mL 2,3-D2-fumaric acid, 50 µg/mL U-13C-α-ketoglutaric acid, 50 µg/mL 13C3-malonic acid, 500 µg/mL 3,3,3-D3-lactate, 100 µg/mL 13C3-pyruvate, 10 µg/mL D4-succinic acid, 5 µg/mL D5-phenylalanine, 200 µg/mL 2,3-13C-phosphoenol pyruvate, 100 µg/mL 2,4,4-D3-glutamic acid (all from Cambridge Isotope Laboratories, Tewksbury, MA); 2.5 µg/mL D4-β-hydroxybutyric acid (Cayman Chemicals, Ann Arbor, MI), 20 µg/mL D27-myristic acid (Indofine Chemical Company, Somerville, NJ). Cecal content (30 mg) was homogenized in 50 µL PBS. Samples were extracted by protein precipitation through sample adjustment to 80% methanol and incubation at 80 °C for 3 min (200 µL, ThermoScientific, Waltham, MA). Subsequently, samples were incubated at room temperature for 30 min. Next,

samples were methoximated with 10 µL of 40 mg/mL methoxamine hydrochloride in pyridine (Sigma, St. Louis, MO) and incubate at 30 °C for 90 min. Finally, samples were trimethylsilylated for 60 min at 40 °C by adding 50 µL of N-Methyl-(N-trimethylsilyltrifluoroacetamide) (MSTFA) and 1% chlorotrimethylsilane (TMCS, Thermo Fisher, Waltham, MA) and were subsequent incubated overnight at room temperature. Samples (100 nL: 1 µL split 1:10) were injected and analysed with a flow of 1.0246 mL/min on the Agilent 7890A (Agilent Technologies, Santa Clara, CA) GC-MS instrument using the Agilent metabolomics protocol. Samples were separated on a Rxi-5ms fused silica column (30 m x 0.25 mm, 0.25 um, Restek, Bellefonte, PA) in hexane with a temperature gradient separation: 0-5 min 80°C, 5-8 min 100°C, 8-33 min 10°C/min increase to 350°C. Quality control samples were generated by combining 5 µL of each sample, which were subsequently injected after each batch. Samples were identified with the NIST database in AMDIS (NIST, Gaithersburg, MD) and deconvoluted with XCMS [281]. Data and statistical analysis were performed in MetaboAnalyst and treatment and control groups combined for determination of treatment-specific effects [282]. Data was plotted in GraphPad Prism 8 (GraphPad, San Diego, CA).

3.2.8: Plasma metabolomics

Plasma samples (n=4/group), which were collected during the cardiac-puncture, were sent to Creative Proteomics (Shirley, NY) for sample preparation, untargeted liquid chromatography mass spectrometry analysis in both positive and negative modes, metabolite identification and pathway analysis. Data was plotted and analysed via 2-way ANOVA and Tukey correction in GraphPad Prism 8 (GraphPad, San Diego, CA).

3.2.9: Flow cytometry

Flow cytometry analysis of T lymphocytes was conducted according to the protocol of Joshi et al. [283]. In brief, 200 µL of whole blood (n=6/group for *Study 1*) were diluted 1:10 in red blood cell lysis buffer (RBC, Fisher Scientific, Waltham, MA), centrifuged, and pellet was

resuspended in 500 µL 95 % PBS and 5% fetal bovine serum (FBS). 100 µL suspensions were labeled with 0.25 µg of α-CD4-FITC antibody, 0.25 µg of α-CD8a-PE and/or 0.5 µg α-CD3-Cy7 antibody (11-0042-82, 12-0081-82 and 25-0032-80, respectively, Fisher Scientific, Waltham, MA) for 10 min, then 1 mL 95 % PBS (Thermo Fisher, Waltham, MA) and 5 % FBS (Thermo Fisher, Waltham, MA) were added to dilute samples. The flow cytometry analysis was performed using the Attune® NxT Acoustic Focusing Flow Cytometer (Thermo Fisher Scientific, Waltham, MA, USA) using Attune® NxT software version 2.7 (Thermo Fisher Scientific, Waltham, MA, USA). The population was gated, subdivided by antibody staining and quantified. Data were presented as percentage to absolute count for each channel and plotted and analysed via 2-way ANOVA and Tukey correction in GraphPad Prism 8 (GraphPad, San Diego, CA).

3.2.10: Immunohistochemistry

The collected brain hemispheres of cohort 1 (n=4/group for *Study 1*) were fixed in 4% PFA solution for 24h and subsequently dehydrated and embedded in paraffin. Brains were cut into 9 µm sections and deparaffinized followed by rehydration through Histo-Clear (Fisher Scientific, Waltham, MA) and ethanol gradient and were then treated with 0.3 % hydrogen peroxide to reduce background staining. Sections were washed in PBS and incubated in blocking serum before an overnight incubation at 4 °C in a 1:8000 dilution of GFAP antibody (Polyclonal Rabbit Anti-GFAP, DAKO, Z0334) or 1:2000 dilution of Iba1 antibody (Polyclonal Rabbit Anti-Iba1, Abcam, Cambridge, MA). Next, the sections were washed with PBS and placed in secondary antibody Vectastain Elite ABC reagent (Vector Laboratories, Inc., Burlingame, CA) for 30 min. Iba1 slides were then stained with CongoRed for 10 min to stain Aβ plaques. Then, all slides were incubated in 3,3′-diaminobenzidine (DAB) for 1-3 min. Subsequently, tissue sections were counterstained with hematoxylin, dehydrated through an ethanol gradient, cleared using Histo-Clear and were then mounted with coverslips. Once the slides were dry, images at 20x or 40x

magnification of the hippocampus and cortex were taken using an Olympus BX63 Intelligent microscope and quantified with ImageJ. Four animals per group were analyzed using four sections that were 90 μm apart were randomly chosen per animal and three pictures were randomly taken per section. Three pictures were taken per section in the cortex area spanning the hippocampus and the CA1 area of the hippocampus. Pictures were processed with ZEN 2.3 and quantified with ImageJ 1.8.0 software. Data was plotted and analysed via 2-way ANOVA and Tukey correction in GraphPad Prism 8 (GraphPad, San Diego, CA).

3.2.11: Barnes maze

To analyse memory and spatial learning the Barnes maze was used with 18 equally spaced holes around the outer perimeter of the circular maze (n=11-15 mice/group for *Study 1*; n=11-12 mice/group for *Study 2*). The target hole had a box positioned directly beneath it that allowed the mice to exit the maze. Distinct visual cues were positioned on each of the four walls of the room. Mice were trained for 4 days (3 min/trial/day), where animals learned to use the cues on the wall to locate the target hole and escape the maze, which was achieved when the mouse entered the target box positioned under the target hole. On day 5, the target box was removed in order to test for learning and spatial memory in a 90-second probe trial. Each trial was tracked and recorded using EthoVision XT 14 software. Data plotting and statistical analysis was performed in GraphPad Prism 8 (GraphPad, San Diego, CA) with 3-way ANOVA testing for acquisition and one- or two-way ANOVA dependent on the respective parameter on the probe day with post-hoc multiple comparisons.

3.2.12: Transcriptomics

Cortex (n=4/group for *Study 1*) was separated from one frozen hemisphere and immediately transferred into 1mL of TRIzol (Fisher Scientific, Waltham, MA) under RNase free conditions. Samples were disrupted by ultrasonication. One hundred μL of 1-bromo-3-cholorpropane reagent (Sigma, St. Louis, MO) were subsequently added and samples mixed and centrifuged at

12000 g for 15 min. Finally, RNA was precipitated by addition of 500 µL ice-cold isopropanol and washed with 75% ethanol in DEPC water (Fisher Scientific, Waltham, MA). The air-dried pellet was resuspended in DEPC water and RNA concentration measured at Cytation 3 (BioTek, Winooski, VT). At least 500 ng RNA was subsequently sent to GENEWIZ LLC (South Plainfield, NJ), for sample processing and total RNA sequencing (20-30 million reads). The sequencing data was analysed using the following applications from the Galaxy platform [284]: FastQC, MultiQC [285], Trimmomatic [286], HiSAT2 [287], MarkDuplicates, Feature Counts [288], Column Join on Collections, annotateMyIDs, edgeR [289]. These pipelines allowed to remove artefacts, identify genes and normalize the datasets. Gene enrichment analysis was performed with EnrichR [290, 291]. Data was plotted and analysed via 2-way ANOVA and false discovery rate (FDR) correction in GraphPad Prism 8 (GraphPad, San Diego, CA).

3.2.13: Multi-omics analysis

Multi-omics analysis was performed according to the Liu et al. protocol [292]. Briefly, a repeated double cross validation random forest (rdCV-RF) analysis method was applied with an inner tuning and outer testing loop of 100 repetitions and subsequent cross-validation with 1000 permutations [293, 294]. This allowed the assessment of the quality of each of the datasets by predicting the group association in each sample and comparing the theoretical assignment with the experimental assigned group. This was followed by Data Integration Analysis for Biomarker discovery using a latent component method for Omics (DIABLO) in the R package mixOmics [295, 296], which was employed for multi-Omics integration to determine variable correlation throughout the three datasets and within the assessed significant parameter of all three datasets.

3.3 Results

To investigate the underlying hypothesis that the CRL treatment-dependent gut microbial and metabolic changes may ameliorate AD-like pathology, the investigation of *Study 1* was

subdivided into three analysis sections: gut, peripheral, and brain-related changes. In addition, ABX mice of *Study 2* received FMTs from treated and untreated APP/PS1 and Wt animals of *Study1* to analyze the consequences of the treatment-dependent gut alterations on memory in non-transgenic mice. No differences in water consumption and animal weight were determined for both studies.

3.3.1: Gut alterations

In *Study 1,* mice of both genotypes were treated for 2 months with 5000 *Fédération Internationale Pharmaceutique* (FIP)/kg CRL or regular water, which was extended when compared to with the study design of chapter II to overcome the effects driven by the genetic modification in this mouse model . No differences in water consumption and animal weight were determined throughout the study. First, we examined the hypothesis that the most prominent changes in response to treatment would be observed in the gut environment where the administered enzyme performed its catalytic reaction (figure 3.1).

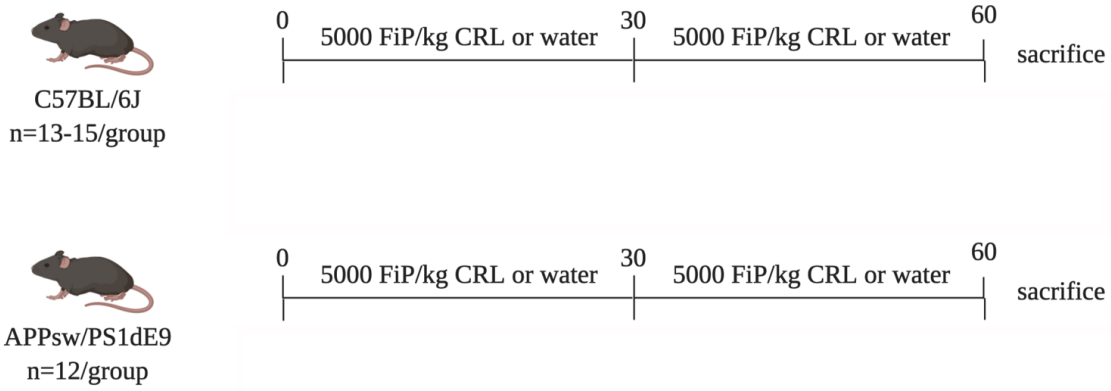

Figure 3.1: Study design.
Wt (n=13-15, 8 months of age) and APP/PS1 (n=12, 8 months of age) received 5000 FIP/kg CRL for two consecutive months or regular water before sacrifice.

.

Accordingly, the fecal microbiota, the gut metabolome, as well as gut integrity (due to the administration of a higher dose) in the gut post treatment were investigated and compared to untreated age-matched controls. This allowed the assessment of CRL treatment effects on the immediate environment of the gut, and at the same time the determination of whether the gut

homeostasis was adversely affected by CRL treatment. No changes in α-diversity were observed between groups after 2 months of treatment in the fecal microbiota (figure 3.2A), which was consistent across the cecal (2 months of treatment, figure 3.2B) and longitudinal fecal data (0, 1 and 2 months of treatment; figure 3.2C) between Wt and APP/PS1 (genotype-dependent) as well as in treated and untreated animals (treatment-dependent).

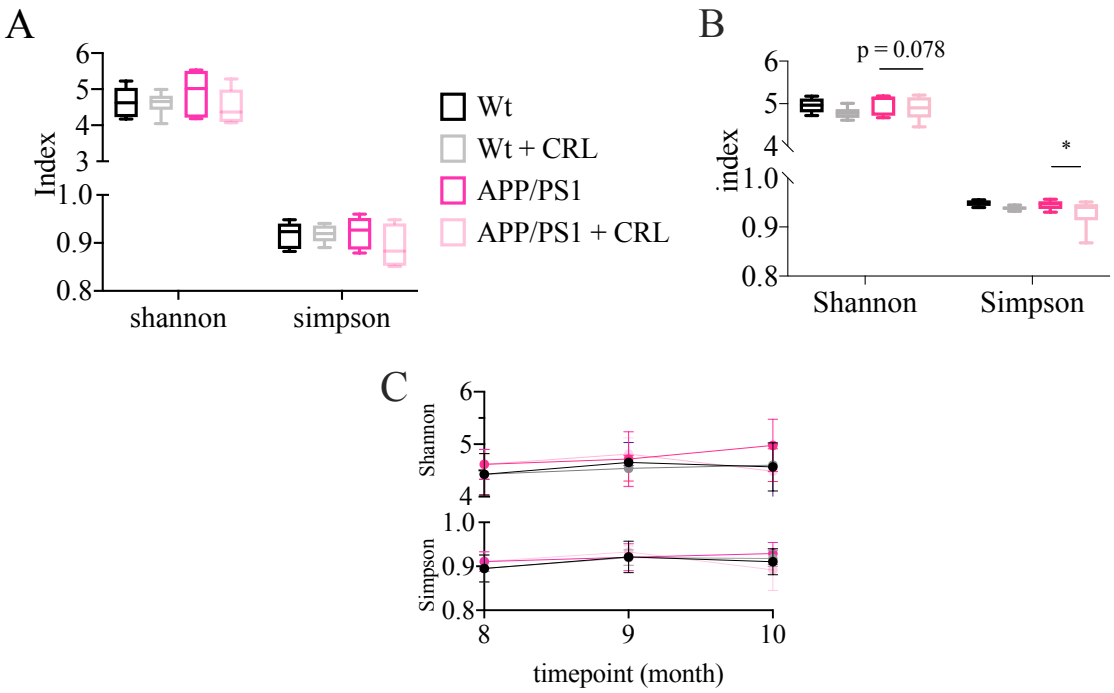

Figure 3.2: CRL treatment effect on α-diversity in APP/PS1 mice compared to Wt mice.
*A. α-diversity analysis in fecal matter post 2 month of treatment analysed by Shannon and Simpson index. B. α-diversity in cecal matter post 2 months of treatment measured by Shannon-index and Simpson-index C. Longitudinal α-diversity of fecal matter post treatment from 0 to 2 months. Significance of α-diversity was determined by Kruskal-Wallis H-test. Significance: * p<0.05, ** p<0.01, *** p<0.001.*

By contrast, β-diversity showed genotype-dependent and treatment-dependent dissimilarity in both fecal (p = 0.001 and p = 0.031, respectively, figure 3.3A) and cecal matter (p = 0.001 and p = 0.017, respectively, figure 3.3B) post 2 months of treatment, although genotype effects were more pronounced. When investigating longitudinal changes of fecal β-diversity (0, 1 and 2 months of treatment), dissimilarities were observed between all groups (figure 3.3C,D,E). However, changes were most pronounced between genotypes (p = 0.001, figure 3.3C) and

treatment groups (APP/PS1: p = 0.001; Wt: p = 0.017, figure 3.3D,E) suggesting an impact of progressing disease pathology but also a treatment effect.

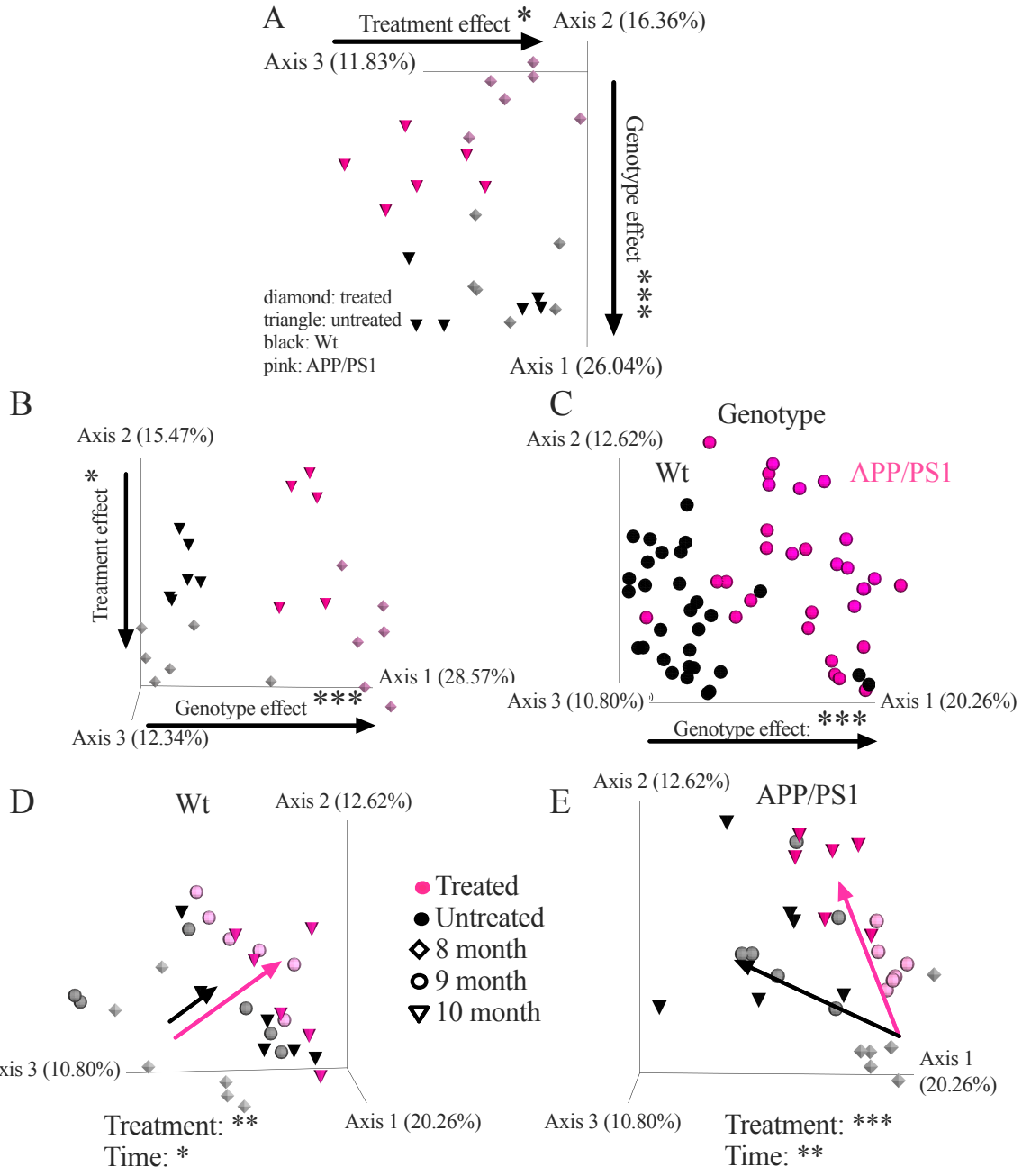

Figure 3.3: CRL treatment effect on β-diversity in APP/PS1 mice compared to Wt mice.
*A. β-diversity analysis by Bray-Curtis dissimilarity of fecal matter collected after 2 months of treatment. B. Cecal β-diversity post 2 months of treatment measured by Bray-Curtis dissimilarity. C. Longitudinal β-diversity of fecal matter between genotypes comprising animals from 0 to 2 months of treatment. D. Longitudinal β-diversity of fecal matter between collected time-points (0, 1 and 2 month) within APP/PS1 or Wt mice. Data was displayed as Principle Coordinate analysis plots. Significance of Bray-Curtis distance was determined by PERMANOVA. Significance: * p<0.05, ** p<0.01, *** p<0.001.*

Furthermore, taxonomic summaries of fecal samples on the phyla level after 2 months of treatment indicated differences between untreated Wt and APP/PS1 animals while the fecal microbiota of treated APP/PS1 was reshaped towards Wt taxa composition (figure 3.4). In addition, 2 months of CRL treatment increased *Proteobacteria* levels in both genotypes but appeared to be more pronounced in treated Wt mice, which was determined in fecal samples (figure 3.4).

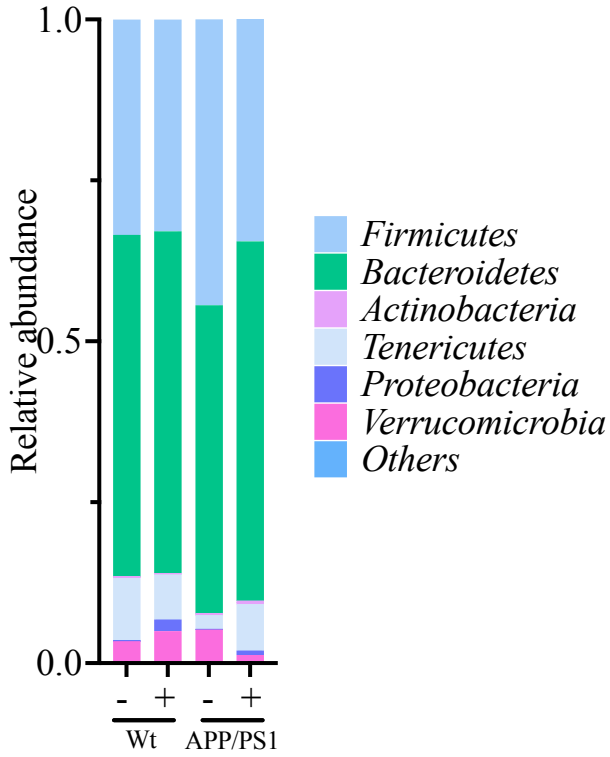

Figure 3.4: CRL treatment effect on fecal taxonomy post 2 month of treatment in APP/PS1 compared to Wt mice. Taxonomy was assigned by data alignment with the Greengenes database.

Finally, LEfSe analysis was applied in fecal samples of APP/PS1 mice due to their more pronounced changes after 2 months of treatment, which enabled identification of features discriminating between the sample groups. We found a significant increase in the abundance of two bacterial species from the genera of *Clostridiales vadin BB60 group* as well as *Acetatifactor*, which suggested treatment-dependent compositional shifts in the microbial communities (figure 3.5). In addition, six bacterial taxa were reduced in fecal samples with CRL treatment (two

unspecified *Bacteroidales*, *Ruminiclostridium* 5, *Ruminiclostridium* 9, *Oscillibacter* and *Eubacterium xylanophilum*), but they did not reach significance after FDR correction (data not shown). Next, we examined by gas-chromatography mass-spectrometry whether the fecal microbial shifts were associated with alteration in the cecal gut metabolome after 2 months of treatment. Out of the three identified genera in treated APP/PS1 mice, the *Acetatifactor* genus (which has been discovered in an obese mouse) was hypothesized to have occurred in response to lipase-dependent fatty acid release and other potential alterations of the gut metabolome due to its association to high-fat diets (figure 3.5, [297]).

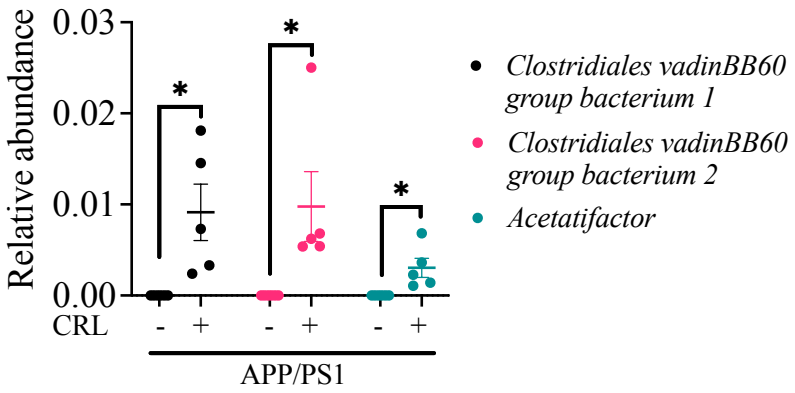

Figure 3.5: Biomarker identification in APP/PS1 mice post CRL treatment.
*Biomarker identification on genus level to identify significant genera driving microbial distinguishing APP/PS1 treated vs. untreated animals. Biomarkers were identified using 2-way ANOVA and FDR correction post-hoc. Significance: *p<0.05.*

When examining the metabolome, 5-hydroxytryptophan (fold change (FC) = 0.280, p_{FDR} = 0.071), allocholic acid (FC = 0.498, p_{FDR} = 0.065) and phenylalanine (FC = 0.522, p_{FDR} = 0.071) were significantly decreased, while malic acid (FC = 1.988, p_{FDR} = 0.018), ethanolamine (FC = 1.732, p_{FDR} = 0.017), linoleic acid (FC = 1.690, p_{FDR} = 0.052), oleic acid (FC = 1.650, p_{FDR} = 0.029) and glycerol (FC = 3.393, p_{FDR} = 0.017) were significantly increased (figure 3.6). The associated metabolome pathway analysis further identified numerous pathways associated with unsaturated fatty acids and lipid metabolism supporting our hypothesis that oral administration of exogenous CRL enhances fatty acid release in the gut lumen of APP/PS1 mice (figure 3.6B).

A

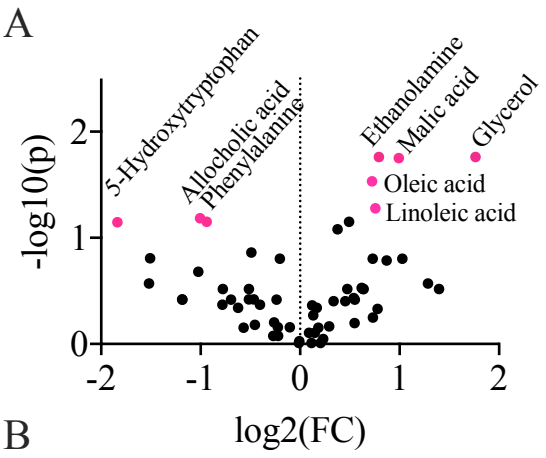

B

Pathway	Overlap	Raw p	-log10(p)	FDR	Impact
Glycerophospholipid	1/36	0.0006	3.2545	0.0256	0.0132
Linoleic acid	1/5	0.0015	2.8175	0.0284	1
Glycerolipid	2/16	0.0019	2.7151	0.0284	0.3302
FA elongation	1/39	0.0049	2.3072	0.0284	0
FA degradation	1/39	0.0049	2.3072	0.0284	0
Biosynthesis of UFAs	4/36	0.0087	2.0592	0.0401	0
FA biosynthesis	2/47	0.0191	1.7202	0.0548	0.0147

Figure 3.6: Gut metabolomic changes through CRL treatment in APP/PS1 mice.
A. Metabolomics analysis of cecal matter of APP/PS1 groups to determine treatment specific differences indicated in red if significant. B. Pathway analysis of identified metabolites to determine key pathways activated through lipase administration. Cecal metabolomics was analysed and FDR corrected.

Finally, because we used a higher dose than in Chapter II and since we observed elevated levels of *Proteobacteria* post treatment, we examined gut barrier integrity in all groups (figure 3.7). No differences between treated and untreated animals or APP/PS1 and Wt animals were observed. Therefore, we concluded that the gut barrier was functional.

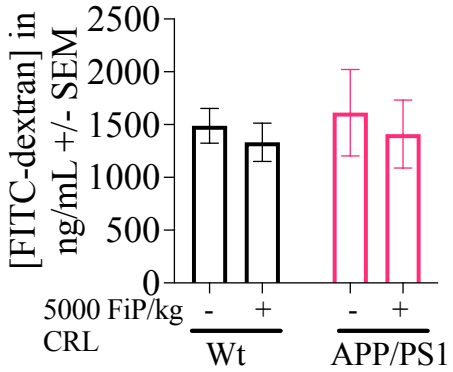

Figure 3.7: Gut integrity of treated and untreated APP/PS1 and Wt mice.
*Gut integrity analysis by transition measurement of oral administered FITC-dextran dye from the gut into plasma. Gut integrity was tested using 2-way ANOVA. Significance: *p<0.05, **p<0.01.*

The gut analysis supported our hypothesis that CRL treatment in the gut could induce changes in the gut environment with potential benefits to the host without affecting the gut barrier integrity. These results were in accordance with the findings described in Chapter II.

3.3.2: Periphery

Subsequently, we investigated whether the identified alterations in the gut were reflected in the host's peripheral circulation since the metabolic and immunological axis of the gut-brain axes have been shown to be in direct exchange with the gut lumen [108]. First, immune cell populations (T-helper cells: CD3+CD4+ and cytotoxic T-cells: CD3+CD8+) were examined by flow cytometry in all four groups to determine positive or negative consequences of CRL administration, which represented the main responders to metabolic and microbial changes in the gut environment (figure 3.8A). While no difference was detected between untreated Wt and APP/PS1 mice, a trend for decreased CD3+CD4+ and CD3+CD8+ populations was observed in treated APP/PS1 mice compared to untreated animals. But since the ratio was unaffected by treatment compared to control groups, we suggested that there was no treatment-dependent effect (figure 3.8A). Furthermore, plasma cytokine levels were measured to evaluate treatment-dependent activity changes of immune cells (figure 3.8B). Although some cytokines showed treatment-dependent trends, the results had negligible biological relevance due to the low concentrations, which was evident when compared to levels in another AD model and AD patients [298]. Hence, the immunological axis was excluded from further investigations since no treatment effect was detected at this point, although we acknowledge that functional or more detailed analysis might reveal new insights.

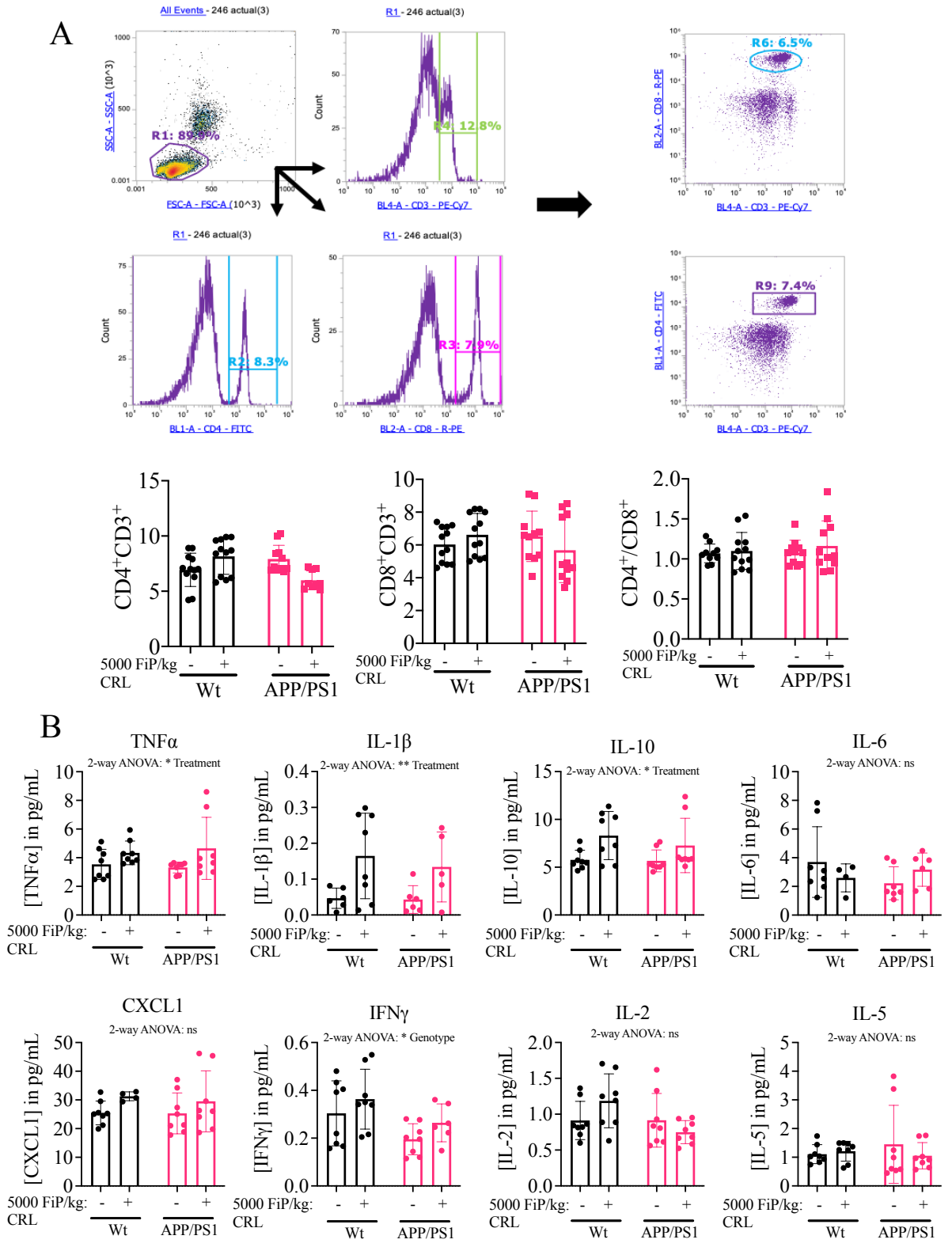

Figure 3.8: Treatment effect of CRL on imune cell populations and peripheral cytokine levels. A. Quantification of immune cell population through flow cytometry. No difference was observed in CD4+CD3+, CD8+CD3+ and their ratio, respectively. B. Peripheral inflammation measured by plasma cytokine and chemokine levels. No biologically-relevant significant change in pro-inflammatory and anti-inflammatory cytokine and chemokine levels could be determined suggesting overall low levels and independence of immunological responses from the treatment strategy. Significance was assessed by 2-way ANOVA and post-hoc Tukey correction. Significance: ns p>0.1.

Next, the metabolic axis was analysed to determine the treatment-dependent effects in plasma by untargeted metabolomics comparing treated and untreated animals. The pathway analysis revealed, for both genotypes, significant treatment-dependent changes in pathways associated with unsaturated fatty acids, which was expected due to administration of a lipase that hydrolyses lipids (figure 3.9A).

To ascertain the direction of the identified alterations, the data was sub-grouped in total saturated (SFA) and unsaturated fatty acids (UFA) to assess the treatment effect on the different fatty acid populations (figure 3.9B). While no significant genotype-dependent and treatment-dependent effects in SFAs and UFAs-to-SFAs ratio were observed, the results of the pathway analysis showed significant increase in UFA levels in untreated APP/PS1 mice compared to treated APP/PS1 mice ($p = 0.001$, figure 3.9B). Further subgrouping of UFAs in ω-3 and ω-6 fatty acids displayed the same treatment-dependent trend in both sub-groups (ω-3: $p = 0.0008$; ω-6: $p = 0.021$, figure 9C), although the effect was more pronounced in ω-3 fatty acids.

A

Pairwise comparison	Pathway name	p value
Wt+CRL vs. Wt	Linoleic acid metabolism	0.009934
	alpha-Linolenic acid metabolism	0.02569
	Arachidonic acid metabolism	0.070058
	Glycerophospholipid metabolism	0.070058
APP/PS1+CRL vs. APP/PS1	alpha-Linolenic acid metabolism	0.001411
	Biosynthesis of unsaturated fatty acids	0.010823

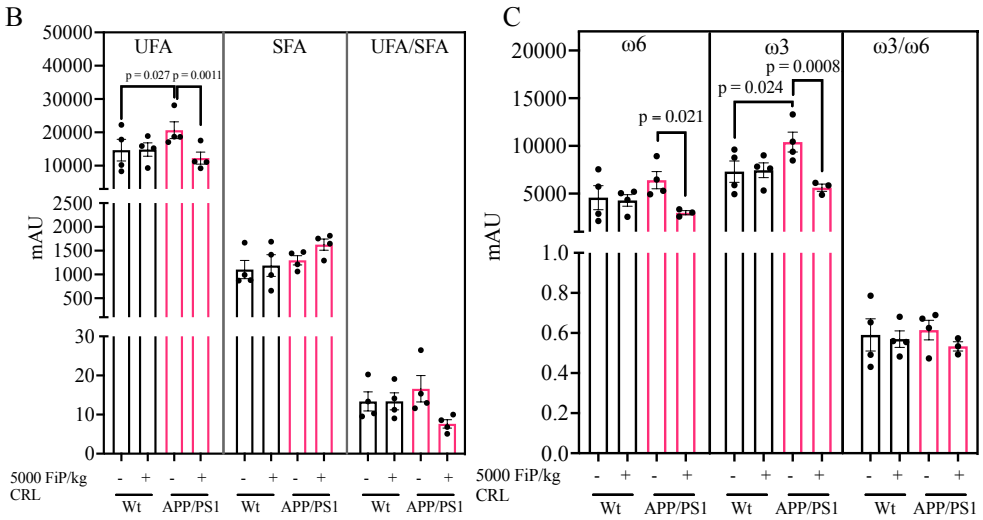

Figure 3.9: Treatment effect of CRL on peripheral metabolite composition.
A. Pathway analysis of untargeted plasma metabolomics data indicating significant changes in UFA and glycerophospholipid metabolism. B. Investigation of subclasses of UFA, SFA and UFA/SFA revealed an UFA

*specific elevation in APP/PS1 mice and reduction post treatment. Significance was assessed by 2-way ANOVA and post-hoc Tukey correction. Significance: *p<0.05, **p<0.01, ***p<0.001.*

Finally, these results warranted the subsequent analysis of specific unsaturated fatty acid levels and their downstream products. Both ω-3 but primarily ω-6 fatty acids showed significant reduction of the associated metabolites in treated APP/PS1 mice in comparison to untreated APP/PS1 levels including linoleic ($FC_{APP/PS1}$ = 0.651; p = 0.0002; figure 3.10A), arachidonic ($FC_{APP/PS1}$ = 0.618; p = 0.0001; figure 3.10A) and docosahexaenoic acid ($FC_{APP/PS1}$ = 0.569; p < 0.0001; figure 3.10A). Finally, it was examined whether alterations in lipid transport favored the peripheral differences of UFA in APP/PS1 mice. The plasma levels of high-density lipoprotein (HDL) and very-low-density lipoprotein/low-density lipoprotein (VLDL/LDL) cholesterol plasma levels were assessed (figure 3.10B) but did not show differences for total cholesterol and cholesterol ester levels. However, when separating HDL from VLDL/LDL fractions treatment-dependent differences were observed, which were significantly elevated for VLDL/LDL cholesterol and cholesterol ester levels post treatment (cholesterol: FC = 1.459, p = 0.031; cholesterol ester: FC = 1.529, p = 0.031; figure 3.10B).

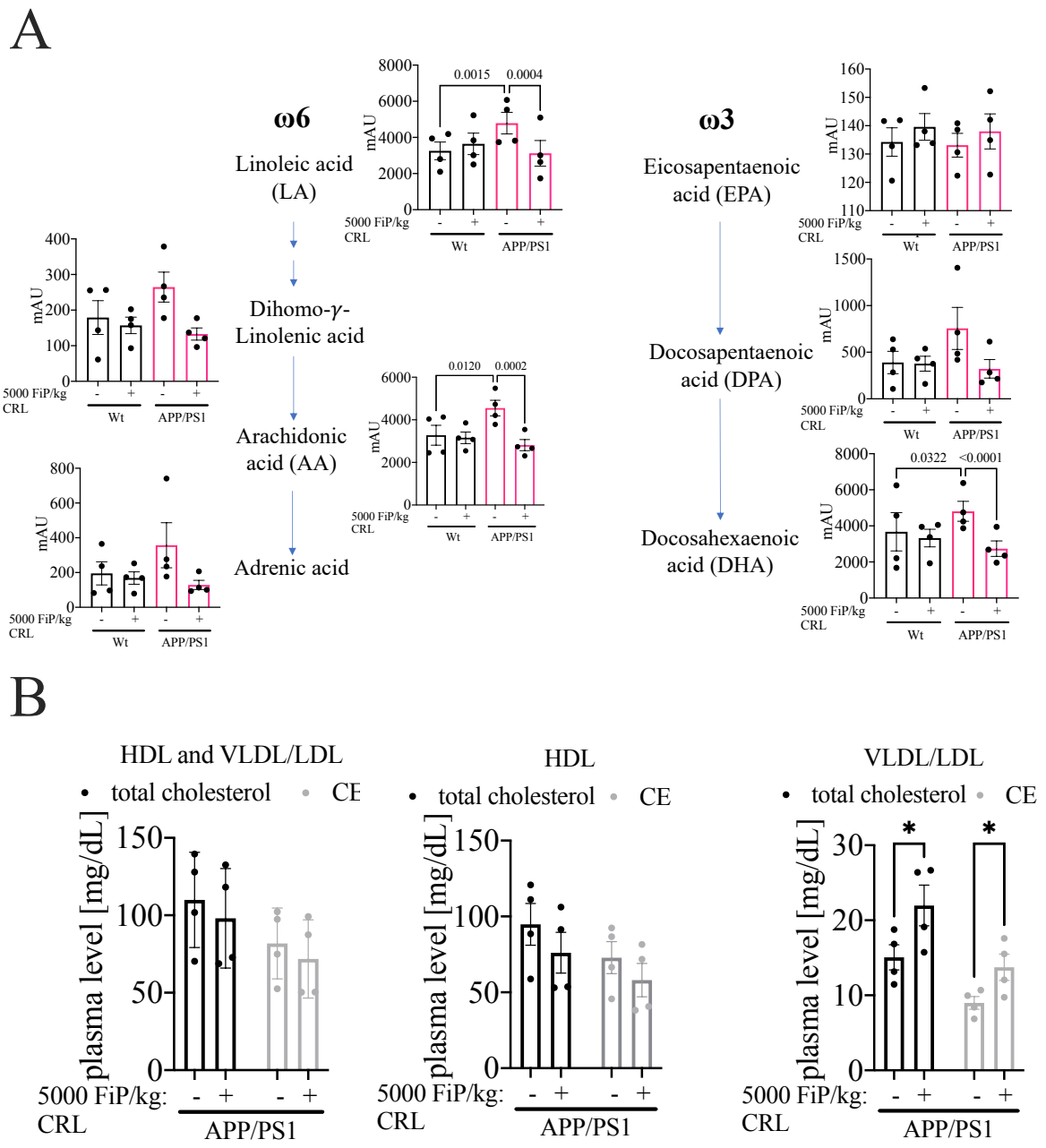

Figure 3.10: Treatment effect of CRL on ω-3 and ω-6 fatty acid levels and lipid transport.
*A. ω-3 and ω-6 fatty acid levels measured in plasma. All subtypes showed significant or trending reduction of UFA level post CRL treatment in APP/PS1 mice. B. HDL and VLDL/LDL cholesterol and cholesterol esters to analyse CRL's effect on lipid transport. VLDL/LDL cholesterol and cholesterol ester fraction were both significantly increased. Significance was assessed by 2-way ANOVA and post-hoc Tukey correction. Significance: *p<0.05, **p<0.01, ***p<0.001.*

In summary, we showed that CRL treatment altered the microbial β-diversity in fecal and cecal specimen and elevated two *Clostridiales vadin BB60* genera as well as *Acetatifactor* abundance. Furthermore, enhanced UFA release that may have resulted in alteration of the gut metabolome

was identified, which resulted in normalization of plasma UFA levels in APP/PS1 treated animals and increased VLDL/LDL cholesterol and cholesterol esters. Hence, the treatment-dependent effects on AD-like pathology in the brain were investigated with focus on the APP/PS1 mice, where lipid metabolism has been shown to be disturbed and treatment-dependent differences in the gut and periphery were more pronounced [299].

3.3.3: Brain

Next, we assessed how CRL treatment impacted short-term memory and spatial learning (Barnes maze), neuroinflammation (GFAP and Iba1/CongoRed staining), and gene expression (RNAseq). The Barnes maze acquisition trials mostly showed significant differences between untreated Wt and APP/PS1 animals and trends in treatment-dependent improvements suggested enhancement of learning in treated animals (figure 3.11A, supplementary figure 3.1.2B). However, during the probe trial significant genotype-dependent differences for frequency to find the target hole and a trend for latency to find the target hole were shown (latency: $p = 0.114$; frequency: $p = 0.043$; figure 3.11B, supplementary figure 3.1.2A). Moreover, a significant improvement in latency to find the target hole and a trend for improvement in frequency of target hole investigations in treated APP/PS1 mice was identified when compared to untreated littermates (latency: $p = 0.025$; frequency: $p = 0.478$; figure 3.11B, supplementary figure 3.1.2A). CRL treated Wt mice only showed a trend for improvement when compared to untreated Wt mice (latency: $p = 0.158$; frequency: $p = 0.325$; figure 3.11B, supplementary figure 3.1.2A/B). In addition, untreated APP/PS1 mice exhibited decreased velocity results in both acquisition and probe days, which was normalized in treated APP/PS1 mice (velocity: $p = 0.045$, figure 3.11A/B).

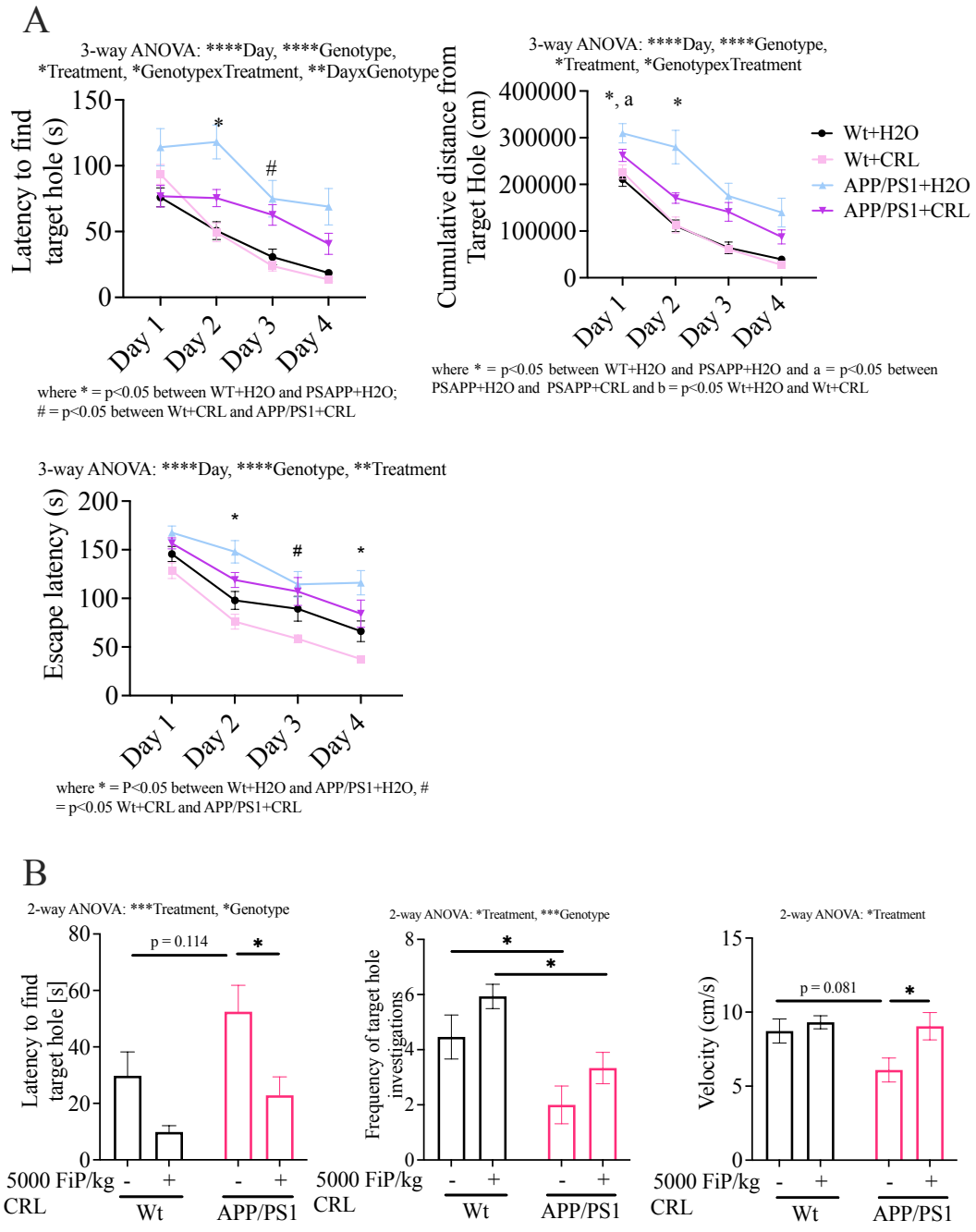

Figure 3.11: CRL treatment effect on memory and learning assessed in the Barnes maze.
*A. The acquisition data suggested trends for improved learning in trested APP/PS1 mice. B. The probe trial showed a significant improvement in memory and learning for APP/PS1 treated mice and a trend for Wt mice. Significance was determined by 1- or 2-way ANOVA and post-hoc Tukey analysis for probe trial, dependent on the respective parameter, while acquisition data was analysed with 3-way ANOVA and post-hoc Tukey analysis. Significance: *p<0.05.*

The reduction in velocity was attributed to diminished exploratory behavior evident through investigation phases, which alternated with immobile phases. In addition, the primary data showed that the untreated APP/PS1 mice were exploring similar to untreated wildtype mice

during the probe trial, which confirmed that they explored the maze although not as targeted. In summary, CRL treated APP/PS1 animals exhibited improvement in memory and learning but also velocity in addition to the beneficial effects assessed in the gut and the periphery.

Next, we examined whether improvement of cognition was associated with decreased neuroinflammation and amyloid plaques. The treatment-dependent impact on microgliosis and astrocytosis by GFAP and Iba1/CongoRed staining in cortex and hippocampus were analysed (figure 3.12). Increased GFAP expression is a marker of reactive astrocytes, while Iba1 upregulation indicates an increase in activation of microglia. While no differences were detected between treated and untreated Wt mice, a genotype-dependent difference in the cortex was determined between Wt and APP/PS1 animals as expected (GFAP: $p < 0.0001$; Iba1: $p < 0.0001$; figure 3.12). Furthermore, a significant reduction of GFAP as well as Iba1 staining in the cerebral cortex were observed in treated APP/PS1 mice (GFAP: $p < 0.0001$; Iba1: $p = 0.0094$; figure 3.12). In the hippocampus, neuroinflammation (% reactive area) was significantly different between Wt and APP/PS1 animals (GFAP: $p < 0.0001$; Iba1: $p < 0.0001$; figure 3.12), while no differences were identified for GFAP and Iba1 immunoreactivity in untreated and treated Wt animals. In untreated and treated APP/PS1 animals, significant differences were observed in hippocampal tissue (GFAP: $p = 0.0003$; Iba1: $p = 0.056$; figure 3.12), but these differences were less pronounced when compared to the differences observed in cortical tissue.

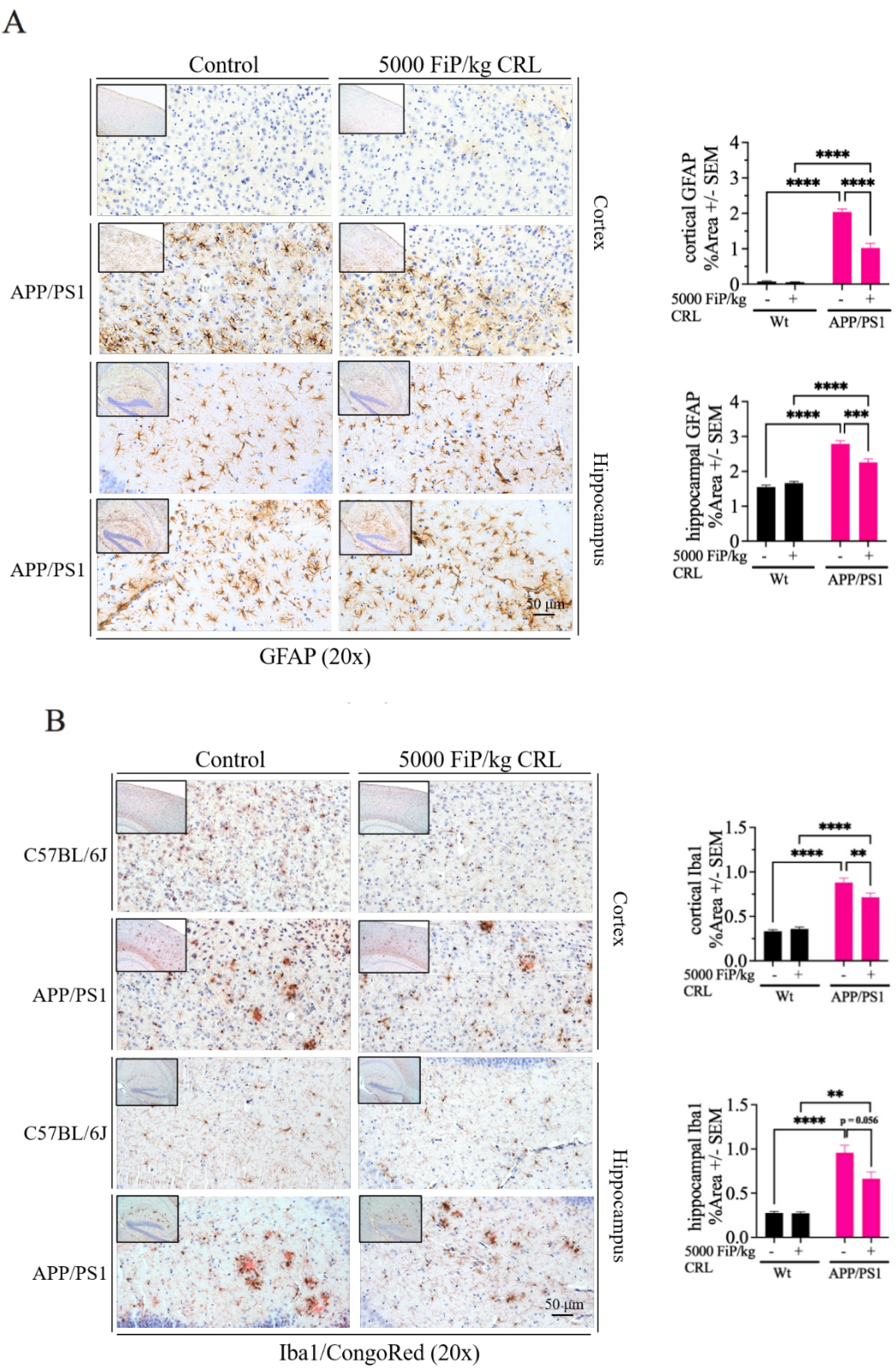

Figure 3.12: CRL treatment effect on neuroinflammation.
A. Imunohistochemical analysis of GFAP staining in cortical S1 and hippocampal areas in APP/PS1 and Wt mice (20x magnification: four animals per group, four slides per animal, three images per slide). B. Analysis of treatment effect on microgliosis in APP/PS1 and Wt analysed by quantitation of Iba1 staining. Slides were co-stained with CongoRed to visualize amyloid plaques in the brain. Four brain sections per animal were analysed and three

*images per section taken. While hippocampal areas were located in the CA1 region, the analysed cortical area was spanning the hippocampal area. Fiji's ImageJ software was used to color deconvolute images and quantify tissue staining. 2-way ANOVA and Tukey corretion were further applied for immunohistochemical results. Significance: *p<0.05, **p<0.01, ***p<0.001.*

In addition, no differences were found in the ratio of Iba1 stained microglia counts surrounding amyloid plaques to the area of the respective CongoRed stained amyloid plaques in the cerebral cortex when comparing treated and untreated APP/PS1 mice (figure 3.13). In contrast, the ratio of microglia counts-to-proximal amyloid plaque area in the hippocampus of APP/PS1 animals revealed a significant reduction in treated animals (p = 0.015; figure 3.13).

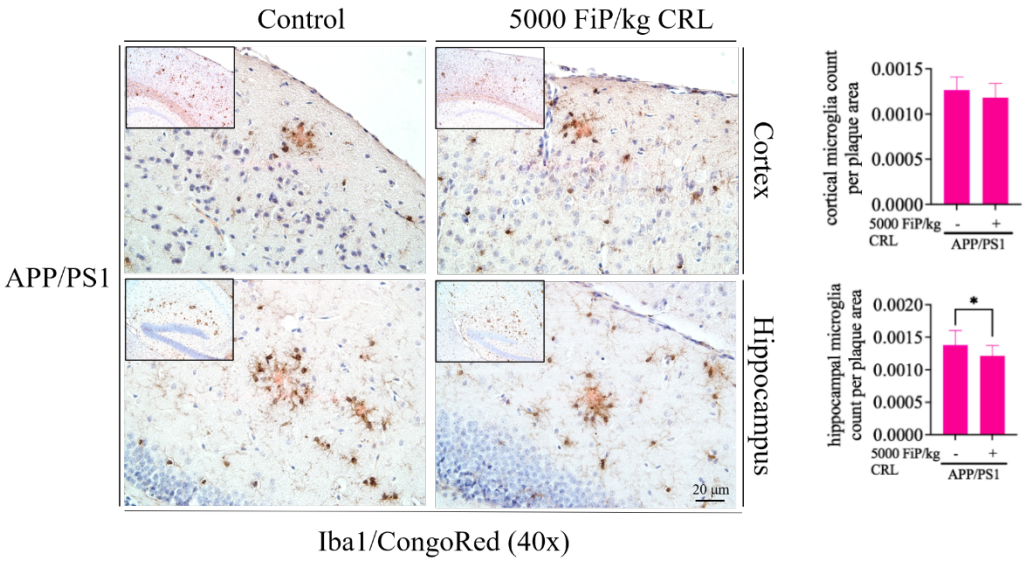

Figure 3.13: CRL treatment effect on amyloidosis.
*Assessment of amyloid plaque size to associated microglia counts to determine changes in inflammatory response and plaque burden (40x magnification: four animals per group, four slides per animal, six images per slide). 2-way ANOVA and Tukey corretion were further applied for immunohistochemical results. Significance: *p<0.05, **p<0.01, ***p<0.001*

This suggested less microglia surrounding amyloid plaques in the hippocampus of these animals and therefore, reduced neuroinflammation. Due to the stronger impact of treatment on microgliosis and astrocytosis in cortical tissue, the treatment-dependent effect on cortical cytokine and chemokine levels and transcriptome were measured. IL-1β and TNFα showed significant differences, but the results had no biological relevance due to the absolute low levels

of cytokines and chemokines (figure 3.14). Nevertheless, isolating and enriching glia might have improved this analysis and could be considered in future experiments.

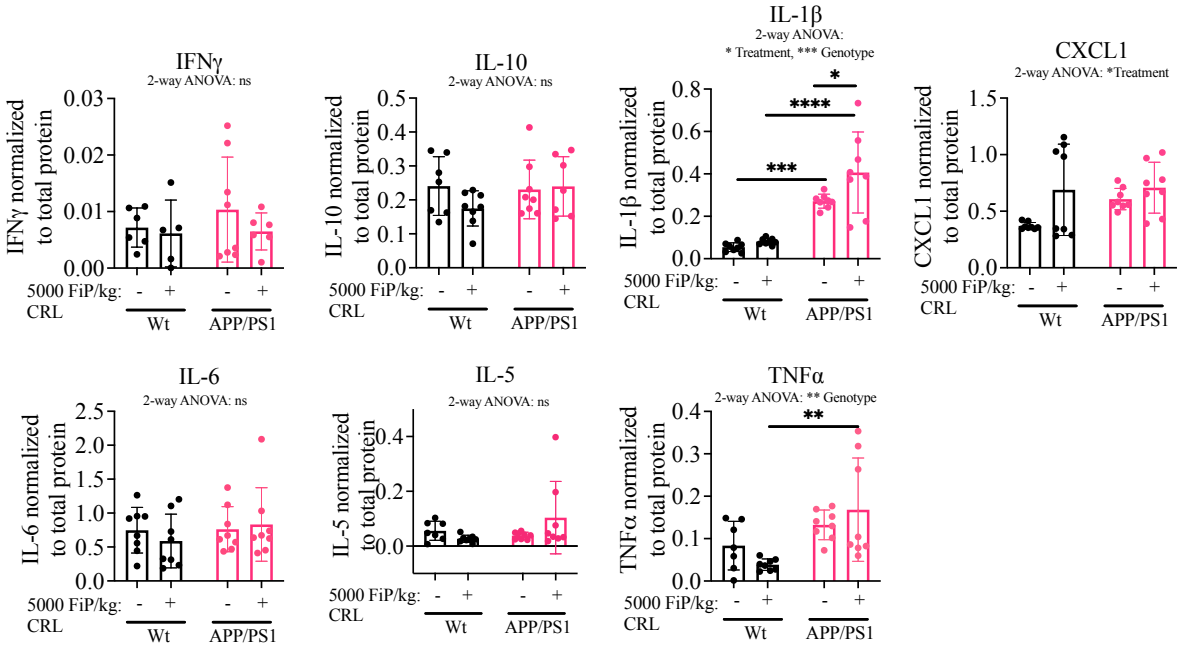

Figure 3.14: CRL treatment effect on cortical cytokine expression.
*Plasma cytokine and chemokine levels in whole cortical tissue. Significance was assessed by 2-way ANOVA and post-hoc Tukey correction. Significance: ns p>0.1, *p<0.05, **p<0.01, ***p<0.001.*

The total RNA expression of whole cortical tissue did not show significantly differential expressed transcripts after FDR-correction of pairwise comparisons in EdgeR of APP/PS1 treatment groups when compared to untreated littermates (data not shown). However, a focused hypothesis-driven analysis (gene enrichment) was subsequently conducted comparing treated and untreated APP/PS1 mice (figure 3.15). Enrichment analysis revealed three significantly altered pathways: endocytosis, lysosome and glycerophospholipid metabolism ($p = 0.032$, $p = 0.048$ and $p = 0.051$, respectively; figure 3.15A). As endocytosis and lysosomal activity are particularly associated with glial cells, the dataset was reanalysed for specific brain cell markers to determine whether these cell populations' activation states were altered in accordance with our previous findings. The markers examined were: Aldh1l1, Atp1b2, Aqp4, Sox9, Slc4a4, Mlc1, GFAP (astrocytes); Cx3cr1, P2ry12, TMEM119, Aif1, Olfml3, Ccl3, Itgam (microglia); stmn2, Rbfox3, syt1, syn1 (neurons); Pecam1, Tie1 (Endothelia) and Nfasc, Kndc1

(Oligodendroglia). Analysis of this subset revealed significant treatment effects after FDR correction and revealed microglial cell markers TMEM119, Aif1, Olfml3 and Ccl3 and astrocyte marker GFAP to be differentially expressed in treated APP/PS1 mice (p_{FDR} = 0.046, p_{FDR} = 0.036, p_{FDR} = 0.005, p_{FDR} = 0.010 and p_{FDR} = 0.002, respectively; figure 3.15B). Together these results further support the behavioral and immunohistochemical analysis suggesting a treatment-effect in APP/PS1 mice.

A

Term	Overlap	Adjusted p value	Odds ratio	Combined score
Endocytosis	42/269	0.0321	1.9919	18.1129
Lysosome	23/124	0.0481	2.4410	19.5219
Glycerophospholipid metabolism	19/97	0.0507	2.6082	19.6628

B

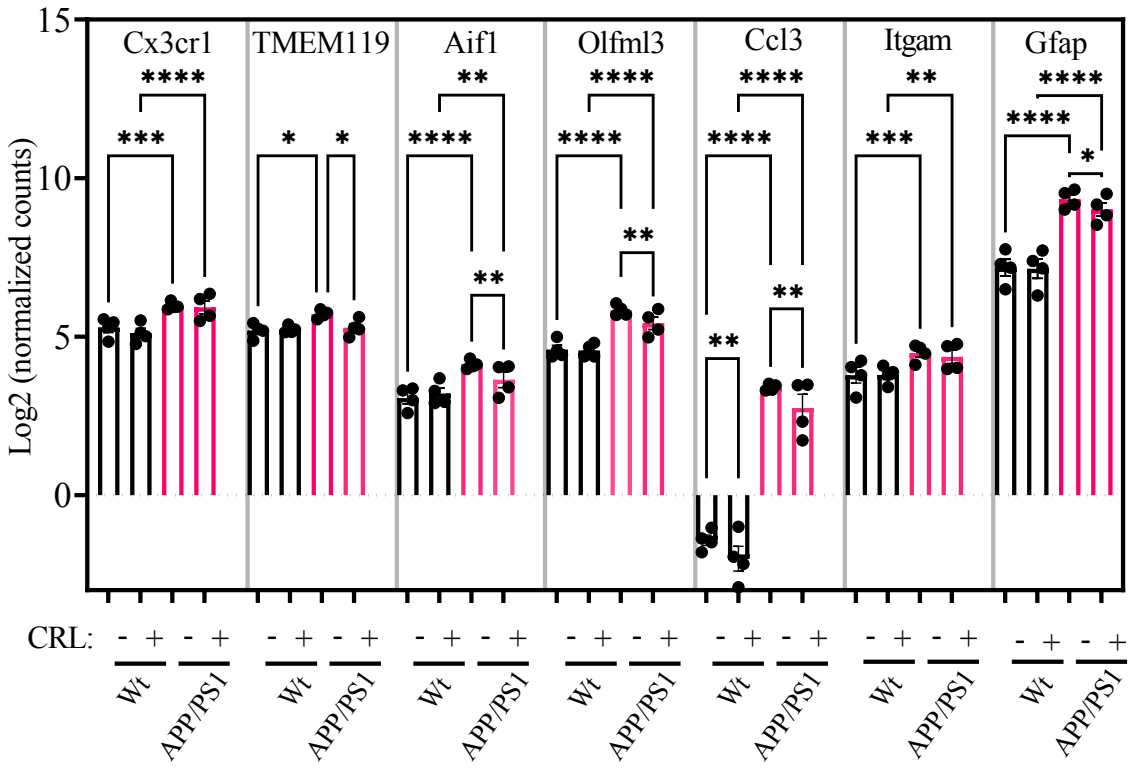

Figure 3.15: CRL treatment effect on cortical transcripts.
*A. Enrichment analysis of significant uncorrected cortical transcriptomics data suggesting microglia and astrocyte activty being altered as well as glycerophospholipid metabolism. B. Transcriptomics analysis of brain cell markers of whole cortical tissue revealing treatment-dependent changes in microglia-specific genes in APP/PS1 mice. Statistical analysis was conducted with 2-way ANOVA and FDR correction for transcriptomics analysis. Significance: *p<0.05, **p<0.01, ***p<0.001, ****p<0.001.*

3.3.4: Multi-omics integration

A total of three Omics datasets including metagenomics (fecal 16S rRNA), metabolomics (plasma untargeted metabolomics) and transcriptomics (cortical RNAseq) were integrated to understand the observed treatment effects in APP/PS1 mice. The focus of our integrated omics analysis was guided by the significant variables determined in the gut metagenomics, plasma metabolomics and cortical transcriptomics datasets described above. To assess the variables' dependencies and strength in relation to treatment, a rdCV-RF was applied to prevent statistical overfitting when correlating the significant parameters of the three omics datasets as described by Liu et al. (figure 3.16) [292, 294]. The rdCV-RF analysis revealed that 100 % (determined by division of misclassified parameters and total number of parameters) of ASVs, 75 % of metabolites and 20 % for transcripts were correctly classified suggesting strength for determined ASVs and metabolites and weakness of the transcriptomics parameters (figure 3.16). This was further emphasized by the under the curve (AUC) values, which were used to evaluate model performance post rdCV-RF analysis. ASVs and metabolite datasets indicated an AUC, which was used to additionally evaluate quality of the datasets, of 0.8 to 1 suggesting good model performance, while the transcriptomics dataset only reached 0.62 suggesting weak performance.

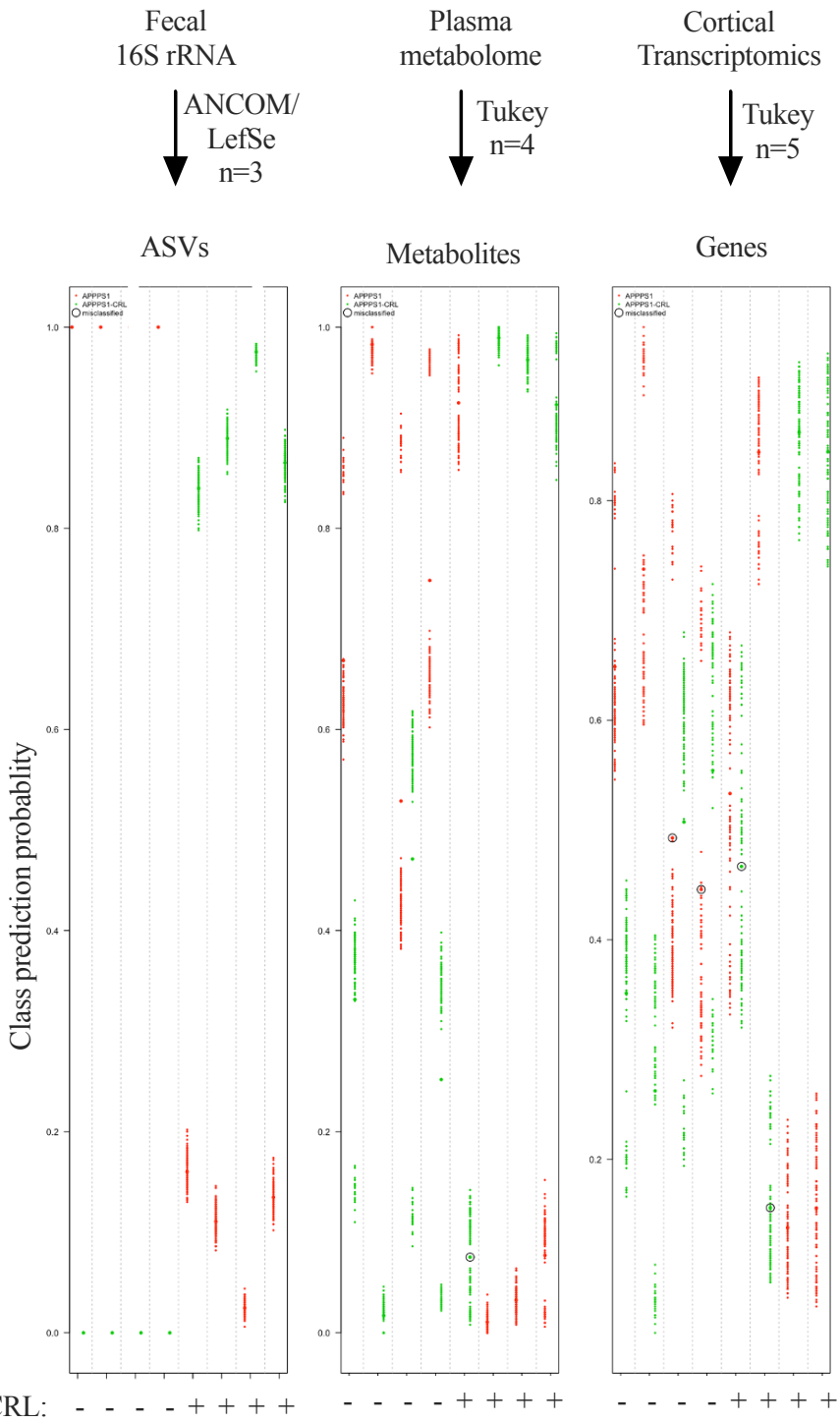

Figure 3.16: Multi-omics cross-validation via rdCV-RF analysis.
rdCV-RF analysis displayed as swim lane plot. Each swim lane displays one sample. For each parameter the algorithm predicts the class of the sample (200 double cross validations) and evaluates whether parameters have been correctly assigned. Circled points indicate misclassified components. Each plot represents the significant parameters of one of the three omics datasets (ASVs, metabolites and transcripts).

When determining the correlation between the three datasets, the greatest correlation was observed between ASV and metabolite components, while metabolite and cortical gene

components showed the weakest interaction (figure 3.17A). The correlation between variables was determined by using the DIABLO method (correlation cut-off of 0.95), which revealed two separated correlated pathways: (1) *Clostridiales vadin BB60 group uncultured bacterium 2* showed significant negative correlations with linoleic, arachidonic and docosahexaenoic acid and mRNA associated with microglial gene expression; while (2) *Acetatifactor* was negatively correlated with GFAP and oleic acid (figure 3.17B). While the negative correlation between these bacterial species and free fatty acids has not been reported yet, the interpretation of correlations to RNA transcripts must be further validated by investigating transcriptomic analysis of isolated cortical microglia or astrocyte cell populations.

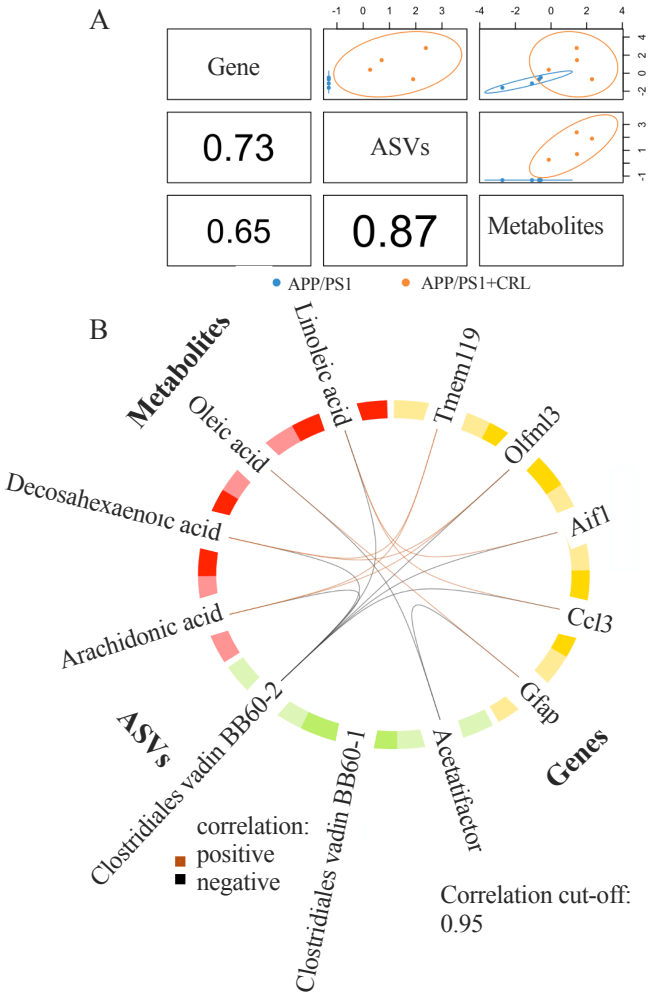

Figure 3.17: Multi-omics integration via DIABLO mixOmics analysis.
A. Component correlation of each of the three datasets determined by DIABLO analysis, which maximized the correlated information. B. Variable correlation displayed in Circos plot with correlation cut-off of 0.95. Two separate pathways were identified. Positive correlation (brown), negative correlation (black).

In summary, CRL treatment altered the gut metabolome and microbial composition. These alterations were transmitted into the host organism normalizing peripheral UFA levels and increasing fatty acid transport, while reducing AD-like pathology and improving aberrant behavior.

3.3.5: FMT study

To categorially establish that the observed changes of AD-like pathology in APP/PS1 mice from *Study 1* were primarily driven by the gut-induced changes through CRL treatment; fecal samples of all groups of *Study 1* were collected between treatment week 5 and 8, and stored for fecal matter transplants (s. 3.2.3). Then, in *Study 2* the gut microbiome of healthy 13 to 14 weeks old Wt mice was disturbed by administration of an antibiotic cocktail for 14 days (ABX); then subsequently at day 15 cleansed from further microbes and residual antibiotics via Macrogol 4000 administration (PEG, figure 3.18A). This enabled the subsequent transfer of fecal matter from *Study 1* into the ABX animals of *Study 2* (figure 3.18). No differences in water consumption and animal weight were determined. The α-diversity index (observed ASVs) from fecal samples at day 42 (post ABX, PEG and FMT) showed that animals receiving FMTs from Wt animals (untreated) and APP/PS1 animals (treated and untreated) exhibited comparable ASVs when compared to the Sham group (figure 3.18B). In contrast, the ABX group which did not receive FMTs showed a reduction of 30 to 40 % observed ASV levels even after 4 weeks of discontinuation of antibiotic cocktail administration, which suggested successful disturbance of the gut microbiota post ABX (figure 3.18B). In addition, animals receiving FMTs from CRL treated Wt donors exhibited unexpectedly low α-diversity, which will be discussed later.

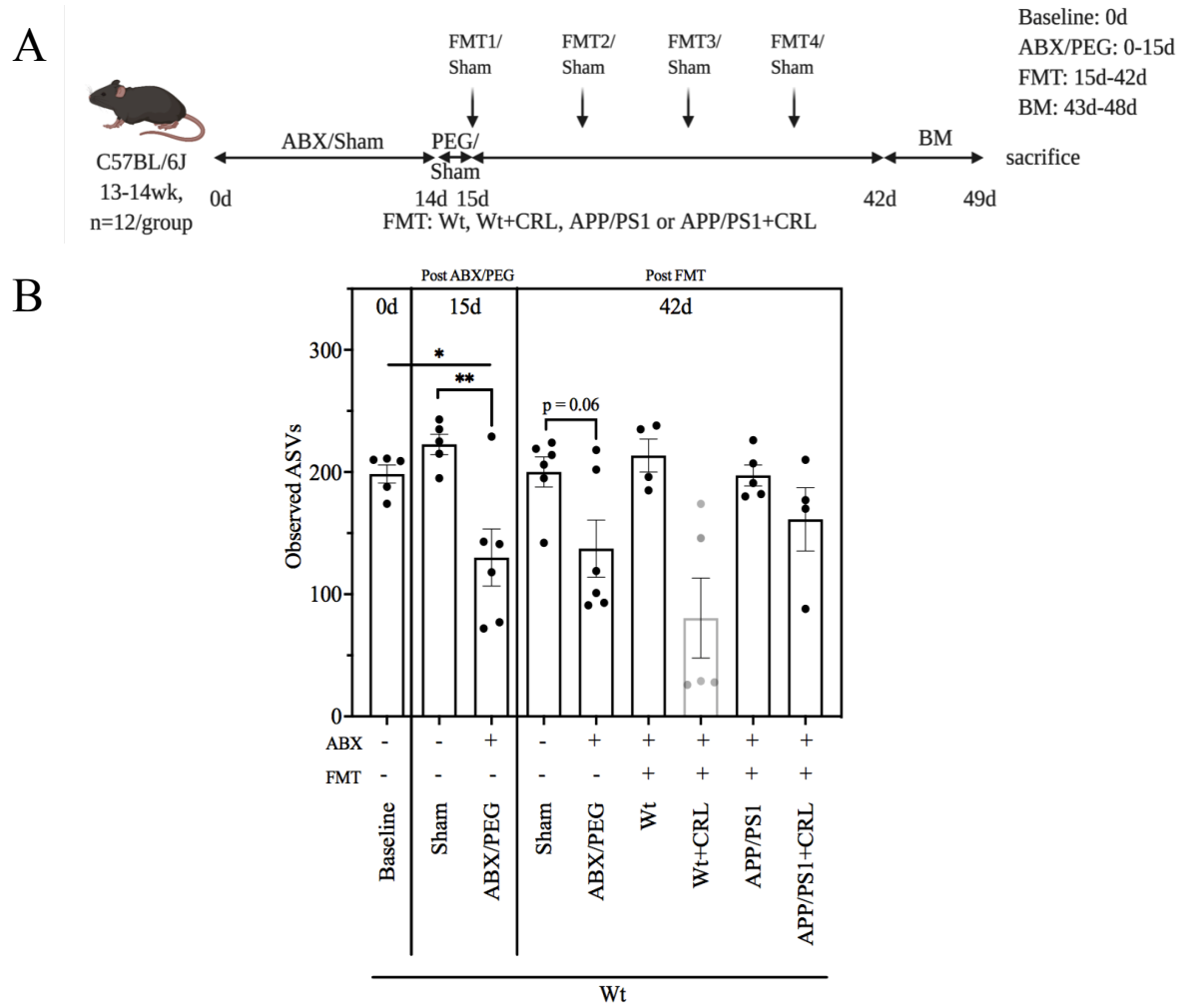

Figure 3.18: Transfer of treatment-dependent benefits into antibiotic-depleted Wt mice via FMTs.
*A. Experimental design of Study 2. B. α-diversity measured as observed ASVs indicated depletion post antibiotic-depletion and bowel cleanse and reshaping post FMT. Significance was tested by Kruskal-Wallis H test and pairwise comparisons (A). Significance: *p<0.05, **p<0.01, ***<0.001.*

When comparing differences in fecal β-diversity, Sham animals at 0, 15 and 42 days co-located, while ABX/PEG groups on day 14 and 15 showed a significant dimensional separation of the Bray-Curtis distance from the Sham group. This further confirms the induced dysbiosis post antibiotic cocktail and PEG administration (figure 3.19). In addition, after 42 days, mice receiving antibiotics only (ABX) or FMT from treated Wt mice (Wt+CRL) post antibiotic administration were still separated from the Sham group, while mice receiving fecal matter from APP/PS1, APP/PS1+CRL and Wt mice shifted towards the Sham groups suggesting partial recovery of these groups.

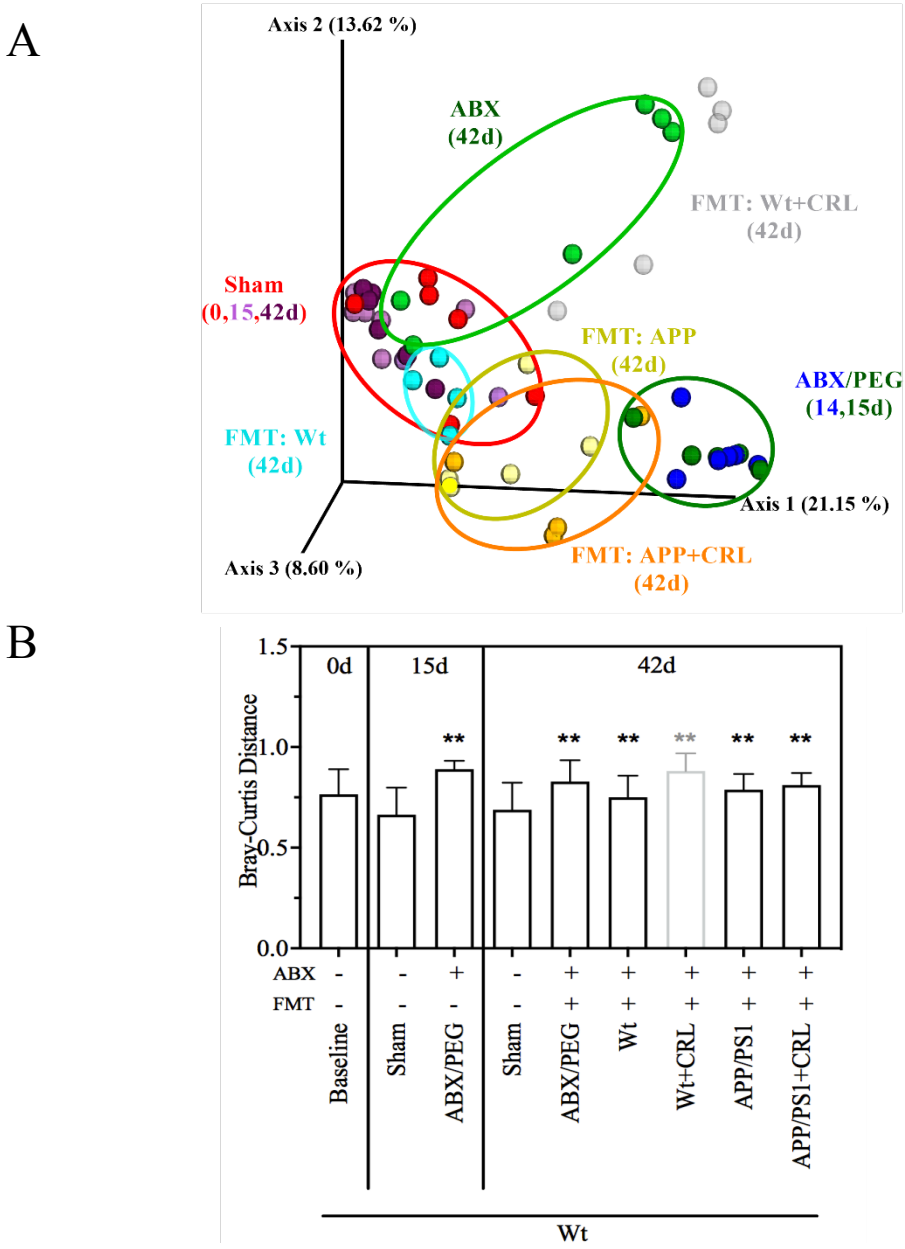

*Figure 3.19: Effect of FMTs from treated and untreated APP/PS1 and Wt mice on β-diversity of ABX Wt mice. A. Principle Coordinate analysis plot of β-diversity measured by Bray-Curtis distances. While Sham groups co-located as well as an antibiotic cocktail and PEG, samples receiving FMTs were distinct but located separately. ABX without FMT recovered partly. For analysis the group receiving Wt+CRL FMT showed abnormal α- and β-diversity and was displayed fainted throughout this study, although it did not have an impact on behavior. B. PERMANOVA analysis of Bray-Curtis distances determining significant differences between Sham and all other groups. Significance: *p<0.05, **p<0.01, ***p<0.001.*

However, animals receiving FMTs from CRL-treated Wt mice showed in addition to the abnormal α- and β-diversity scores, phyla levels, enlarged ceca and an abnormal increase in δ-Proteobacteria (figure 3.18, 3.19, 3.20). This suggested either a potential introduction of an

infection during FMT or that the administered antibiotics allowed the spread of this bacterium, which would have been suppressed in a healthy gut environment.

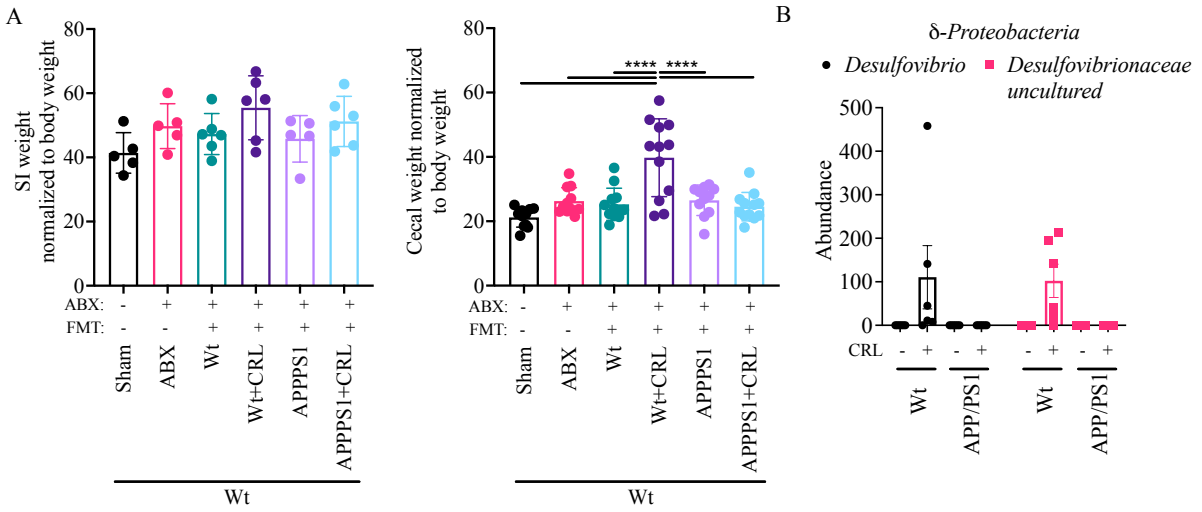

Figure 3.20: Infection in ABX Wt mice receiving FMTs from Wt+CRL donor mice.
*A. Cecal and SI weight of each group in Study 2. B. ANCOM analysis of animals from Study 1 revealing Desulfovibrio increase in Wt+CRL donors. Significance was assessed by 2-way ANOVA and post-hoc Tukey correction Significance: *p<0.05, **p<0.01, ***p<0.001.*

Consequently, this group was excluded and labelled by light grey data points/bars in the microbial analysis (figure 3.18, 3.19, 3.21). Subsequently, taxonomy on the phyla level was analysed for all groups (figure 3.21, supplementary figure 3.1.3A). ABX Wt mice, which did not receive FMTs, showed decreased *Bacteroidetes, Tenericutes*, *Actinobacteria* and increased *Firmicutes, Verrucomicrobia* abundance when compared to Sham animals (figure 3.21). The most prominent difference between ABX, Wt+CRL and APP/PS1 compared to the other groups was the increased abundance of *Verrucomicrobia* and *Firmicutes*, and decreased *Bacteroidetes* (figure 3.21). When comparing donor and recipient fecal material, no major differences between phyla were determined except for the excluded group, which received FMTs from Wt+CRL donors suggesting that the infection was introduced during transfer and establishment and was not originating from an infection in donor animals (supplementary figure 3.1.3A).

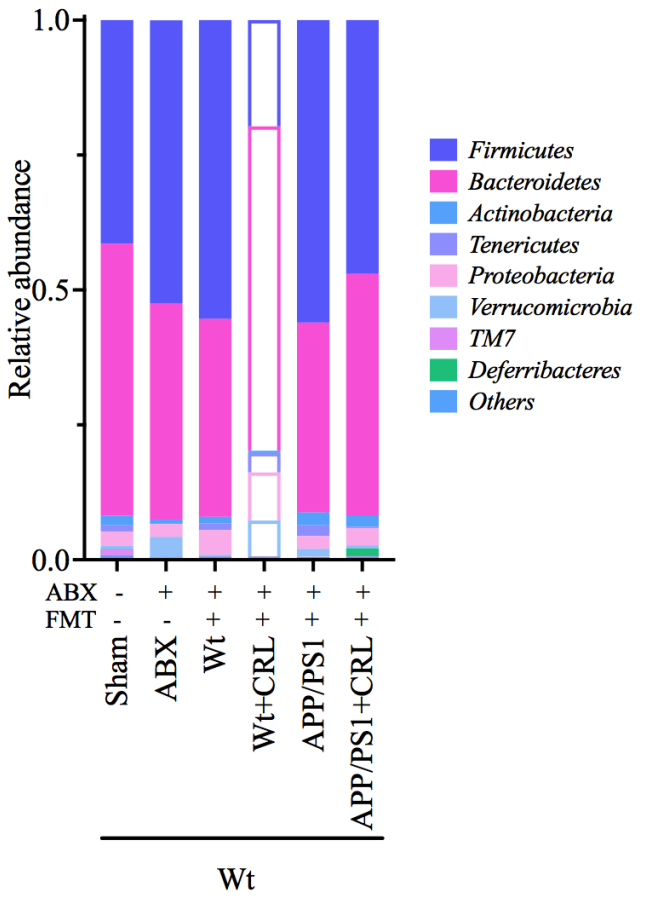

Figure 3.21: Effect of FMTs from treated and untreated APP/PS1 and Wt mice on taxonomy of ABX Wt mice. Taxonomic analysis of phyla level in fecal samples post FMT. Taxonomy was assigned by alignment with the Greengenes database. No major differences except in animals receiving Wt+CRL were found between groups.

After microbial depletion and recolonization, the respective microbiota were analysed in relation to cognitive performance, since antibiotic treatment and the associated dysbiosis have been reported to inhibit learning and long-term memory [300]. All groups were normalized to Sham and compared to the ABX group. Of note, none of the groups showed overt differences during acquisition trials in the Barnes maze (figure 3.22A, supplementary figure 3.1.3C). However, during the probe trial antibiotic-depleted Wt mice receiving FMT's from untreated APP/PS1 mice showed impaired memory (APP/PS1; frequency: 68.33 %, p = 0.919; latency: 140.96 %, p = 0.661; figure 3.22B, supplementary figure 3.1.5D/E) similar to antibiotic-depleted mice not receiving FMT (ABX; frequency: 55 %; latency: 136.77 %; figure 3.22B, supplementary figure 3.1.3B/C), while mice receiving FMT from CRL treated APP/PS1 mice exhibited a trend for improvement (APP/PS1+CRL; frequency: 100 %, p = 0.116; latency: 60.24

%, p = 0.257; figure 3.22B, supplementary figure 3.1.3B/C) similar to mice receiving fecal matter from untreated or treated Wt mice (Wt; frequency: 108.47 %, p = 0.041; latency: 58.83 %, p = 0.067; Wt+CRL; frequency: 108.47 %, p = 0.041; latency: 35.71 %, p = 0.022; figure 3.22B, supplementary figure 3.1.3B/C).

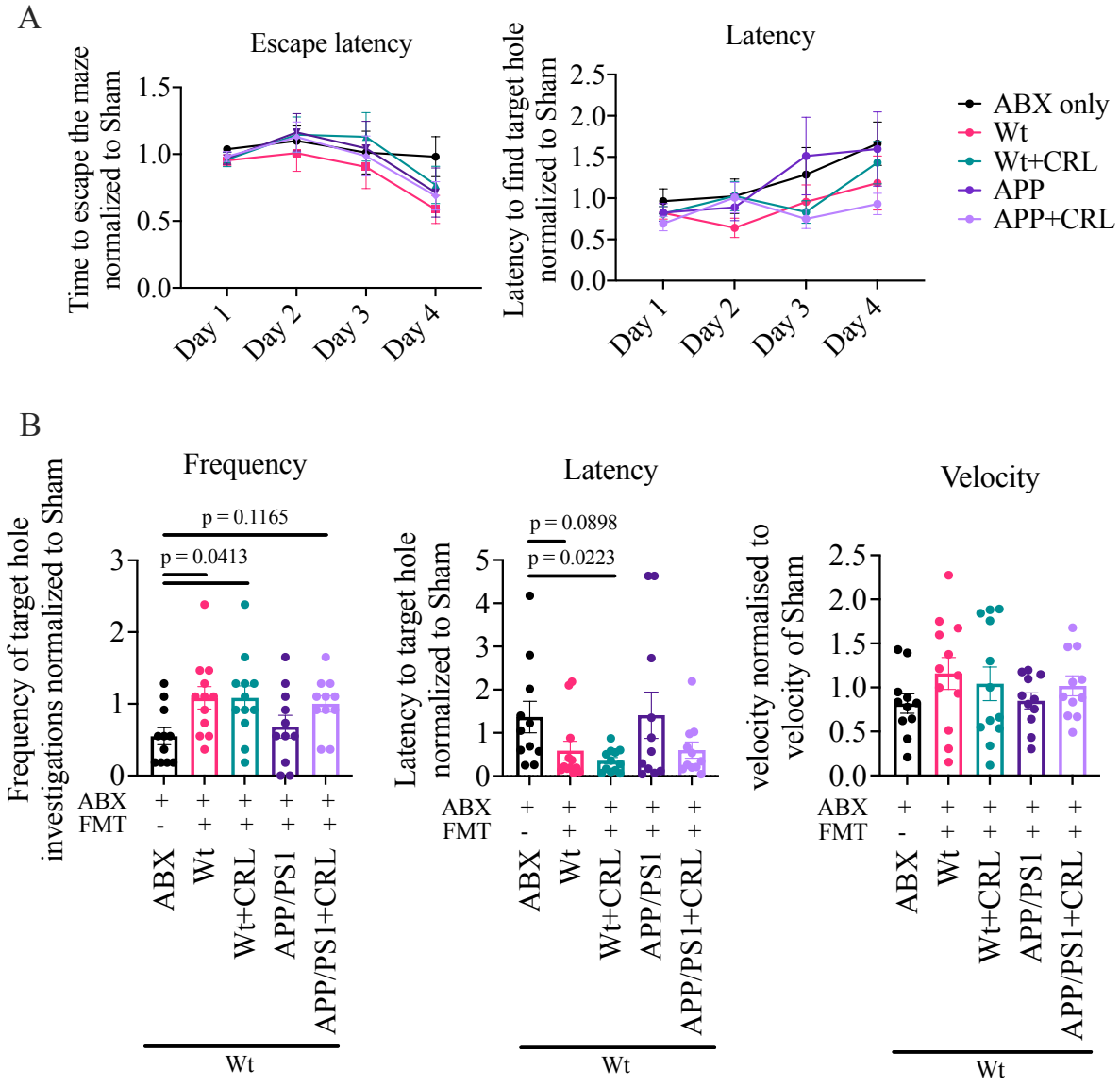

*Figure 3.22: Barnes maze experiment to examine differences in memory and learning post ABX and FMTs. All groups were normalized to Sham animals to reduce complexity of the analysis. A. Analysis did not show any differences between groups during the acquisition trials. B. Analysis of the probe data revealed that antibiotic depleted Wt mice receiving none or FMT from untreated APP/PS1 mice performed worse than Sham animals, while animals receiving FMT from Wt or treated APP/PS1 showed improved or similar performance when compared to Sham groups despite prior ABX treatment. Significance was determined as in prior experiments of the Barnes maze analysis. Groups were compared to normalized ABX animals. Significance: *p<0.05, **p<0.01, ***p<0.001.*

Hence, it was established that alteration of the microbial and metabolic composition by CRL treatment contributed to mitigation of AD-like pathology and normalized aberrant behavior in treated APP/PS1 mice.

3.4 Discussion

In the previous Chapter we have shown that CRL administration can lead to an altered gut microbial and metabolite composition with potential benefits to the host's health [301]. However, it is still unclear how these alterations can evoke benefits at body sites distal to the gut including the brain. Understanding the underlying mechanisms is an urgent need to determine the potential for microbiome-targeting treatment approaches in AD. Therefore, *Study 1* aimed to expand the results acquired in Chapter II by examining CRL's treatment-dependent alterations of gut microbiota and metabolite composition in APP/PS1 mice, and furthermore, their effects on periphery and AD pathology. In addition, we examined in *Study 2* whether those evoked beneficial changes could be transferred via FMT.

In *Study 1*, animals were treated with CRL at 8 months of age, which reflected a time-point in the disease progression where individuals might self-observe alterations of cognitive functions and report to their physicians. Hence, the selected start of treatment represents a relevant time-point for AD patients. The investigation CRL treatment altered the microbial and metabolic composition in the gut without affecting gut barrier integrity, which supported the results of Chapter II. The selected CRL dose in this study was determined by translation of an approved normal human dose, which can be administered continuously in patients with cystic fibrosis or pancreatic insufficiency. Three biomarkers distinguishing CRL treated from untreated APP/PS1 mice were observed: two *Clostridiales vadin BB60 uncultured genera* and *Acetatifactor*, while the cecal metabolomics analysis showed elevated fatty acid release upon treatment. *Acetatifactor* which was discovered in an obese mouse, has been reported to occur in response

to high-fat diets further supporting CRL's activity in the gut [297, 302]. This genus has been suggested to counteract some of the harmful effects of high-fat diets such as liver dysfunction and disturbance of glucose and insulin metabolism by stimulating GLP-1 secretion, although the precise mechanism is unknown [303, 304]. The increased abundance of *Acetatifactor* might have, therefore, supported functionality of these pathways, which are known to be disturbed in APP/PS1 mice and AD patients prior to onset of AD pathology[305-307]. Furthermore, we hypothesized that this might have reduced severity of AD pathology in treated animals. The genus Clostridiales vadin BB60 was less explored but had been associated with homovanillic acid and 5-hydroxyindole acetic acid levels in the brain stem [308]. Hence, the increased abundance of all three genera might suggest increased communication between the gut and the brain via the gut-brain axes. In addition, an increase in *Proteobacteria* levels, a phylum including numerous pathogens, was identified in both genotypes post-CRL treatment, which suggested a need for further investigations such as optimization of treatment length and dosage. Next, peripheral and brain alterations were investigated in this study to assess whether the treatment-dependent changes were propagated beyond the gut affecting AD-like pathology. While the immunological axis was shown to be treatment-independent, the metabolic axis revealed treatment-dependent changes in certain UFA levels, which were elevated on average by 65 % in untreated APP/PS1 mice but were mitigated in treated APP/PS1 mice. Elevation of ω-3 fatty acids levels in particular have been shown to evoke anti-inflammatory effects and might have been an endogenous mechanism to counteract progressing pathology in APP/PS1 mice [309]. Hence, one might hypothesize that reduction of ω-3 fatty acids levels might harm the host and facilitate progression of the disease post CRL treatment [310]. However, these mice exhibited ameliorated brain pathology suggesting a benefit through the peripheral normalization of UFA levels. To explain these results, we hypothesize that increased peripheral UFA might have been induced by increased lipolysis and/or reduced liver metabolism in untreated APP/PS1

mice rather than an endogenous protective mechanism. This hypothesis is supported by a study showing that insulin resistance can enhance lipolysis, which has been associated with Alzheimer's disease pathology, while glucose sensitivity was shown to be reduced in the APP/PS1 mouse model [305, 311]. The identified chronic increase of peripheral ω-6 fatty acid levels could have, therefore, resulted in increased brain levels, which has been demonstrated to enhance lipid peroxidation, ROS formation and neuronal damage, when present in neurons [312]. To prevent damage, neurons can subsequently transmit excess fatty acids to astrocytes by lipoprotein-like particle formation, which reduces intracellular oxidative stress [313]. This could lead to increased β-oxidation in astrocytes increasing their metabolic energy generation, but it has been shown, for instance in Huntington's disease (HD), that long-lasting mitochondrial β-oxidation in astrocytes led to increased ROS production and neuronal damage [313-315]. Hence, the treatment-dependent reduction of ω3- and ω6-fatty acids in the present study might have therefore contributed to the observed amelioration of brain pathology, which needs to be investigated in future studies considering insulin resistance, liver metabolism and reactive oxygen species in the brain.

The subsequent treatment-dependent reduction of astrocytosis and microgliosis further supports this hypothesis. The pronounced reduction of astrocytosis suggested that astrocytes might have been more susceptible to treatment further emphasizing the potential role of unsaturated fatty acids and their impact on AD-like pathology in APP/PS1 mice. Interestingly, it has been reported that defective lipid metabolism of astrocytes is reversed by a high-fat diet in sterol regulatory element-binding protein (SREBP) cleavage-activating protein (SCAP) knock-out mice, thus, counteracting neurological deficits [316]. Based on the microbial and metabolic results of this study, we propose that CRL treatment might have created a similar environment affecting neuroinflammation and enhancing cognitive performance as determined in the Barnes maze. Rebalancing of astrocyte's activation state can prevent neuronal damage and restore their

neurosupportive functions and therefore, might have contributed to the improvement of memory [317].

Finally, to identify potential drivers of the observed effects and the associated pathways, we conducted a transcriptomics analysis of the cortex. No significant differences post FDR correction were found. When applying gene enrichment analysis on the significant transcripts prior to FDR correction, endocytosis, lysosomal degradation and glycerophospholipid metabolism were identified as significant pathways. Endocytosis and lysosomal degradation are important protective mechanisms of microglial and astrocyte neuroimmune activity, which further supports the findings from the immunohistochemistry analysis. Glycerophospholipid metabolism was associated with the peripheral results of altered lipid metabolism supporting the findings in the gut and periphery. Based on these findings, cell-specific brain markers were selected in the dataset for reanalysis. The sub-group revealed gene expression differences of mostly microglial genes, which were significantly reduced post-treatment, while astrocyte-specific genes did not show genotype- or treatment-dependent differences except for GFAP. In future studies, transcriptomics analysis of isolated cell populations such as microglia or astrocytes of both cortex and hippocampus should be applied to prevent transcript dilution. This will enable stronger conclusions through comparison of differential gene expression in specific cell populations of the brain. This shortfall was further emphasized in the multi-omics integration analysis, which exposed the transcriptomics dataset's weak performance, while highlighting the central role of the determined ASVs and metabolites in the treatment-dependent effects.

In summary, CRL administration in the gut might have reduced AD-like pathology by increased release of a variety of fatty acids, which altered the gut microbiota and metabolome and rebalanced energy metabolism. The identified genera have not been investigated for their lipid metabolism, but analysis of their genetic material could reveal potential function that allows

them to process free fatty acids or providing them an advantage in the CRL treated environment. Nevertheless, this need to be further investigated in future studies. Consequently, the induced gut changes (microbial and metabolomic) might have led to normalization of peripheral fatty acid levels by enhancing liver homeostasis and thereby lipid transport. Consequently, this might have rebalanced the fatty acid composition in the brain and reduced oxidative stress in neurons, which resulted in reprogramming of astrocytes and microglia enhancing neuronal activity and brain performance.

As an alternative hypothesis, we proposed that UFA level reduction represented a consequence of treatment-dependent amelioration of brain pathology. Hence, microbial and metabolic alterations in the gut might have propagated through a different axis to the brain - such as the neuronal axis. The treatment-dependent increase in cecal indole derivatives or unidentified (due to limitation of untargeted metabolomics analysis) compounds such as short-chain fatty acids might have activated enteric vagal signaling. Enteric vagal afferents project into the nucleus tractus solitarius and dorsal motor nucleus, which can signal via dopaminergic or serotonergic neurons in different areas of the brain such as the hippocampus and cortex [318-320]. As a consequence, astrocytes and microglia might have been reprogrammed into the anti-inflammatory subtype induced by neuronal signaling or respective metabolites travelling to the brain via the vagal route [321, 322]. The reduction of neuroinflammation might have in turn recovered lipid transport and normalized peripheral levels of ω3- and ω6-fatty acids in APP/PS1 mice.

To finally test whether the beneficial treatment-dependent changes in the gut caused the reduction in AD-like pathology, we investigated whether these beneficial changes were transferable, which represented the foundation of both of our study hypotheses. Therefore, ABX Wt mice of *Study 2* received FMTs of each of the groups of *Study 1*. Wt mice receiving FMT's from treated APP/PS1 mice exhibited improved memory when compared to ABX mice without

FMT or mice receiving FMT from untreated APP/PS1 mice. This supported the study's hypothesis that CRL treatment could recover a healthy gut environment, which subsequently ameliorated AD-like pathology in APP/PS1 mice.

In conclusion, these findings denote the potential of CRL treatment to reduce AD pathology by altering gut microbial and metabolite composition, which supported the hypothesis of this and the previous study. While some unknowns remain, this series of studies may have presented a strategy to target and treat AD pathology but also pathology of other neurodegenerative diseases due to their common association with ageing and inflammation.

Chapter IV: *In silico* and *in vitro* identification of novel, natural allosteric inhibitors and enhancers of CRL activity

4.1 Introduction

The investigations in Chapter II and III showed that orally administered CRL is active in the gastrointestinal tract and alters the gut microbial and metabolite composition, benefitting the host. Therefore, we hypothesized that a PAM of CRL's activity has the potential to enhance CRL's observed beneficial effects from (hypothesis (3)). Furthermore, it was proposed that the PAM itself might entail beneficial functions by targeting endogenous lipases in the gut.

In industrial processes, activity enhancement of CRL has been used to increase the enzyme's stability or efficacy by stabilizing the exposed hydrophobic areas in the enzymatic active conformation of CRL [323-326]. While these approaches applied inexpensive strategies to enhance CRL activity such as immobilization, hydrophobic organic solvents, or emulsions, they are often not applicable for human use due to toxicity. Therefore, allosteric enhancement represents a more specific and efficient approach to enhance enzyme activity without the issue of toxicity. In addition, the assembled compound libraries contained only natural products to avoid potential toxicity, which is more often encountered with chemical substances.

The enzymatic reaction of CRL is initiated through movement of the helical loop structure, which covers the active center of the enzyme. Upon opening, the substrate can bind to the catalytic center, while its hydrophobic hydrocarbon chain is stabilized in the tunnel during the enzymatic reaction. Hence, it was proposed that stabilization of CRL's open conformation through binding of an allosteric modulator results in enhanced CRL activity due to potentially slower closure or extended opening of the lid. To test this hypothesis, a combined approach of an *in silico* workflow (Schrodinger Software: Glide suite) with a published X-ray

crystallography structure of CRL's open conformation (PDB: 1CRL), was used to predict allosteric sites and modulators of CRL that might stabilize the open conformation [208-210]. Finally, a miniaturized in-house developed CRL activity assay was used for PAM characterization and subsequent assessment of enhancer concentration for *in vivo* administration and the enhancement effect on an endogenous lipase to subsequently investigate hypothesis (3). Although the *in silico* and *in vitro* analysis resulted in characterization of three natural PAMs of CRL activity, the PAMs could not satisfy the criteria to be applied *in vivo* to test hypothesis (3).

4.2 Materials and methods

4.2.1: Library preparation

2D structures of natural products were downloaded from the ZINC 12 database (Zbc: Biogenic compounds: primary and secondary metabolites; Zbc Lead: biogenic lead-like compounds, Zbc Drugs: biogenic drug-like compounds; Zbc frags: biogenic fragment-like compounds, [327]), InterBioScreen's database (natural compounds) and AnalytiCon's database for natural products (FRGx, MEGx) and approximately 200,000 total compounds were analysed. Sdf-files were subdivided with a maximum of 25,000 compounds per file with an in-house Python script (supplementary figure 4.1.1). 3D structures for each compound were calculated with the LigPrep application (Schrodinger, version 2017-4, New York, NY) and included angle restriction, assignment of charges and compound desalting. Simultaneously, tautomers and enantiomers for ligands with a chiral flag of 0 and possible states were generated at pH 7 ± 2 with up to 10 combinations per ligand.

4.2.2: Enzyme preparation

A crystal structure of CRL's isoform CRL1 (PDB: 1CRL) was prepared with the Protein Preparation Wizard in the Schrodinger software (version 2017-4, New York, NY). Flexible loops and missing sidechains were filled in with the Schrodinger software component Prime

(version 2017-4, New York, NY) by applying homology modeling and fold recognition. Waters beyond 5 Å were removed and missing hydrogens were added. Optimal conformation of proline, serine, and threonine were determined to further reduce restraints. Rotational and dihedral angles were optimized for each amino acid, including side chains. Disulfide bridges were formed, and het states were generated using Schrodinger's software component Epik (Schrodinger, version 2017-4, New York, NY), which identifies non-amino acid groups in the structure that can be selectively removed if identified as a crystallographic artifact. In addition, the termini were capped and position 399 was computationally mutated into a glycine, which both reduced restraints and enabled determination of novel allosteric sites without changing the protein's conformation. All changes were calculated at pH 7.

4.2.3: Allosteric site determination

To identify top-ranked allosteric binding sites we used SiteMap (Schrodinger, version 2017-4, New York, NY), and required at least 15 site points per hit. In addition, a standard grid was used with a more restrictive definition of hydrophobicity without consideration of shallow binding sites. From the 10 determined sites we selected three- site 2, 4 and 7 (screening site 1, 2 and 3, respectively)- due to their small and distinct nature as well as proximal location to the catalytic center. Finally, a grid was generated for each screening site using Receptor Grid Generation (Schrodinger, version 2017-4, New York, NY) with a scaling factor of 1.0 and a partial-charge cutoff of 0.25. Rotations were allowed for Ser348, Thr68 and 990NAG.

4.2.4: Ligand docking

Ligands were docked with the Ligand Docking application (Schrodinger, version 2017-4, New York, NY) in standard precision mode. Ligands with more than 500 atoms and more than 100 rotatable groups were excluded from docking. Van der Waals radii were scaled with a factor of 0.8, while the partial charge cutoff was 0.15. Nitrogen inversions and ring conformations were sampled. Bias samples of torsions for amides were penalized for non-polar conformations, while

Epik state penalties were considered in docking score. The resulting ligands were additionally docked in extra precision mode if standard precision docking scores were below -5. Finally, post-docking minimization was executed, creating a maximum of 5 poses per ligand.

4.2.5: Enzyme activity assay

Standards and samples were measured in triplicates in a black, μ-clear bottom 96-well plate. Dilutions and blanks were prepared with 0.1 M phosphate buffer pH 7 (0.0578 M sodium phosphate dibasic heptahydrate and 0.0422 M sodium phosphate monobasic monohydrate (Sigma, St. Louis, MO)). The standard curve was prepared with a 400 μM stock of 4-methylumbelliferone (4-MU, Sigma, St. Louis, MO) in DMSO and 0.1 M phosphate buffer (pH 7.0) with a range of 7.813 μM to 500 μM (final: 1.95 to 62.5 μM). 50 μL buffer and 50 μL of standard solution was added to respective standard wells, while 100 μL buffer were added to the blank wells. 50 μL of CRL at 10 ng/mL (final concentration: 3.3 ng/mL, Enzymedica, Venice, FL) for 4-MUB (Sigma, St. Louis, MO) or 50 ng/mL CRL (final concentration 16.6 ng/mL, Enzymedica, Venice, FL) for 4-MU palmitate (4-MUP, Cayman Chemicals, Ann Arbor, MI) and 50 μL of buffer or modulator (see supplementary table 4.3.1) were added to the respective sample wells. A 10 mM stock of 4-MUB and 10 mM stock of 4-MUP were prepared in DMSO and diluted in buffer (4-MUB) or buffer and 0.006% SDS (w/V) and were incubated at 37°C (4-MUP) to a concentration of 0.25 mM. 50 μL of 4-MUB and 150 μL of 4-MUP were added to each well. The 96-well plate was incubated at 37°C for 25 min. The reaction was stopped with 50 μL of 10% o-phosphoric acid (Fisher Scientific, Waltham, MA) in MilliQ water for 4-MUB and 10 μL for 4-MUP. The fluorescence was immediately measured with the BioTek Cytation 3 system at λ=326/472 with a gain of 72.

4.2.6: Validation of enzyme activity assay

Blank and standards were diluted and prepared as described in the enzyme activity section 2.2. Samples were run in triplicates containing CRL in buffer, CRL with 200 μM 4-MU (final: 50 μM 4-MU) and CRL with 12.5 μM 4-MU (final: 3.125 μM 4-MU). The experiment was executed over three consecutive days to determine intra- and inter-day CV for all three samples as well as intra- and inter-day precision for both spiked reactions.

4.2.7: Temperature and pH stability of enzyme activity assay

Robustness of the assay conditions were tested by performing the assay at different temperature or pH conditions according to the protocol in section 4.2.5. *Temperature*: The standard curve was prepared in triplicates and several plates incubated at different temperatures including enzyme plus substrate and blank samples in triplicates for each temperature point (4℃, 15℃, 25℃, 28℃, 37℃, 45℃). Each sample was corrected for their individual blank at the respective temperature. *pH*: Sample containing the enzyme plus substrate and blank were also ran in duplicates for each pH. Reaction conditions were otherwise maintained as described above in the assay protocol.

4.2.8: EC50 and IC50

The determination of EC50 and IC50 was performed following methods described in 4.2.5 [273]. In summary, a standard curve from 0.3 to 20 μM 4-MU was used to translate relative fluorescence units (RFU) into concentrations. Concentration ranges reflecting the whole IC50 or EC50 curve were determined and selected to most accurately determine IC/EC50 values. The modulator dilutions were combined with 6 ng/mL CRL and 250 μM 4-MUB in triplicates in a black μ-clear 96-well plate. The reaction was incubated for 25 min at 37°C. Each modulator concentration was performed in triplicate and repeated three times in separate experiments. The reaction was stopped with 10% o-phosphoric acid and fluorescence immediately measured with the BioTek Cytation 3 system at $\lambda = 326/472$ with a gain of 72. RFUs were converted to

concentrations and normalized to CRL's activity without any modulator. Calculations of the IC50 and EC50 were performed with the Prism8 software.

4.2.9: Michaelis-Menten kinetics

A standard curve from 0.3 to 20 μM 4-Methylumbelliferone was used to translate RFUs into concentrations. For each modulator, two concentrations close to the IC50 or EC50 were used compared to the reaction without modulator addition to determine changes in Michaelis-Menten constant (Km) and maximal velocity (Vmax). The modulators were combined with 6 ng/mL CRL with varying 4-Methylumbeliferryl butyrate concentrations from 7.8 μM to 1 mM. The reaction was performed at 37°C and stopped with 10% o-phosphoric acid at 1, 5, 10, 15, 20, 30, and 45 min. RFUs were immediately measured with the BioTek Cytation 3 system at $\lambda = 326/472$ with a gain of 72.

Km and Vmax were determined by measuring eight different substrate concentrations at six time points. Each concentration at each time point had a separate blank. The plot of time vs. concentration of fluorescent dye for each substrate concentration determined initial velocity (V0, slope of linear graph). V0 values were subsequently plotted against the substrate concentration based on the Michaelis-Menten plot to calculate Km and Vmax.

$$V0 = \frac{Vmax}{Km + [S]} \qquad (1)$$

Km: Michaelis-Menten constant; Vmax: maximal velocity; V0: initial velocity; [S]: substrate concentration

Statistical analyses were performed for determination of Km and Vmax using GraphPad Prism 8.

4.2.10: Biolayer-interferometry (BLI)

K_D determination by BLI. 1mL CRL in PBS (10 mg/mL) was biotinylated with 200 nmol of EZ-link Sulfo-NHS-Biotin (ThermoScientific, Waltham, MA) for 2h at 4ºC and stored at -20°C. Superstreptavidin-sensors (SSA, ForteBio, San Jose, CA) were rehydrated for 10 min in PBS and loaded for 30 min in 200 μL of diluted biotinylated CRL (1 mg/mL) using the Octet RED96e platform (ForteBio, San Jose, CA). Before the association step, sensors were washed in PBS and a baseline was established. During the association step, a range of concentrations for each of the allosteric modulators of CRL were tested for 30s, which was sufficient to reach the equilibrium binding signal. The range of concentrations was overlapping with the determined EC50 and IC50 curves of each compounds (cynaroside: 1000 μM – 31.25 μM; rutin: 2000 μM – 62.5 μM, NP-008496: 2000 μM – 62.5 μM, 1-deoxynojirimycin: 5 mM – 0.15 mM, quinic acid: 20 mM – 0.625 mM). The subsequent dissociation was executed for 60 seconds to allow complete dissociation of the allosteric modulators from the enzyme. Finally, K_Ds for each compound were determined. All binding experiments were performed in quadruplicate using 4 different sensors for each compound.

4.3 Results

4.3.1: Computational screening

The *in silico* screening was performed with approximately 200,000 compounds from three free online databases (ZINC, AnalytiCon and InterBioScreen). Before the docking approach, CRL's X-ray and ligand structures were optimized and allosteric sites determined. Only three of the ten predicted sites showed the required properties: small, distinct, and deep in the open conformation (figure 4.1). It was hypothesized that binding of screening sites 1 and 3, which are both positioned in front of one of the sites of the loop on the surface beneath, would retain the open conformation by blocking the transition back from the open into the closed conformation,

hence enabling discovery of modulators altering the enzyme's activity. Similarly, modulators of screening site 2, which is located in-between the loop and the surface behind the loop, were hypothesized to form secondary bonds in this location, thereby stabilizing and retaining the open conformation and modulating the enzyme's activity.

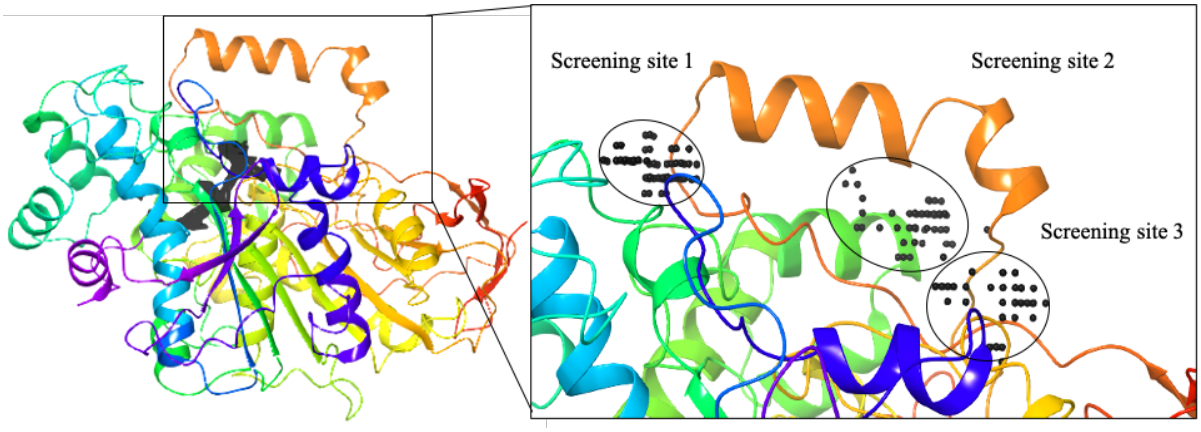

Figure 4.1: Structure of CRL 1 in the open conformation (PDB: CRL1).
The flexible loop domain is highlighted in orange. The loop determines the enzyme's state converting the active into the inactive state and vice versa. Black dots are site points describing the potential allosteric site. These points are positioned 1Å apart and have no overlap with the protein atoms. Also, each of them has sufficient van der Waals interaction energy with the protein. To define a site, each group of site points must contain at least 15 (black circles) to be identified as an allosteric binding site. The selected screening sites 1 and 3 are located on the protein's surface beneath each side of the flexible loop. Site 2 is located in-between the two helices of the loop and the surface behind.

After selection of the predicted allosteric sites, grid generation, and ligand docking the number of resulting compounds with modulator potential was reduced to 1,101 compounds for screening site 1, 594 for screening site 2 and 898 compounds for screening site 3. Furthermore, replicates were removed with the Canvas application and the compounds' natural origin and availability were determined, which reduced the number further to a total of 132 natural products. 53 of those compounds were selected for the subsequent *in vitro* characterization based on cost and prompt availability (supplementary table 4.3.1).

The docking compound assigned to tropolone shows a tropolone derivative with an additional hydroxide group (figure 4.2). However, the displayed structure was not readily available, which led to the selection of tropolone for *in vitro* assessment due to availability and the high structural similarity. It was hypothesized that absence of the hydroxide group would cause the loss of one

hydrogen bond but would still enable the fit predicted by Schrodinger, although the docking score changed to -3.314. For the subsequently developed *in vitro* assay tropolone was selected as proof of concept approach to assess tropolone's effect on CRL activity and to test the assay's performance.

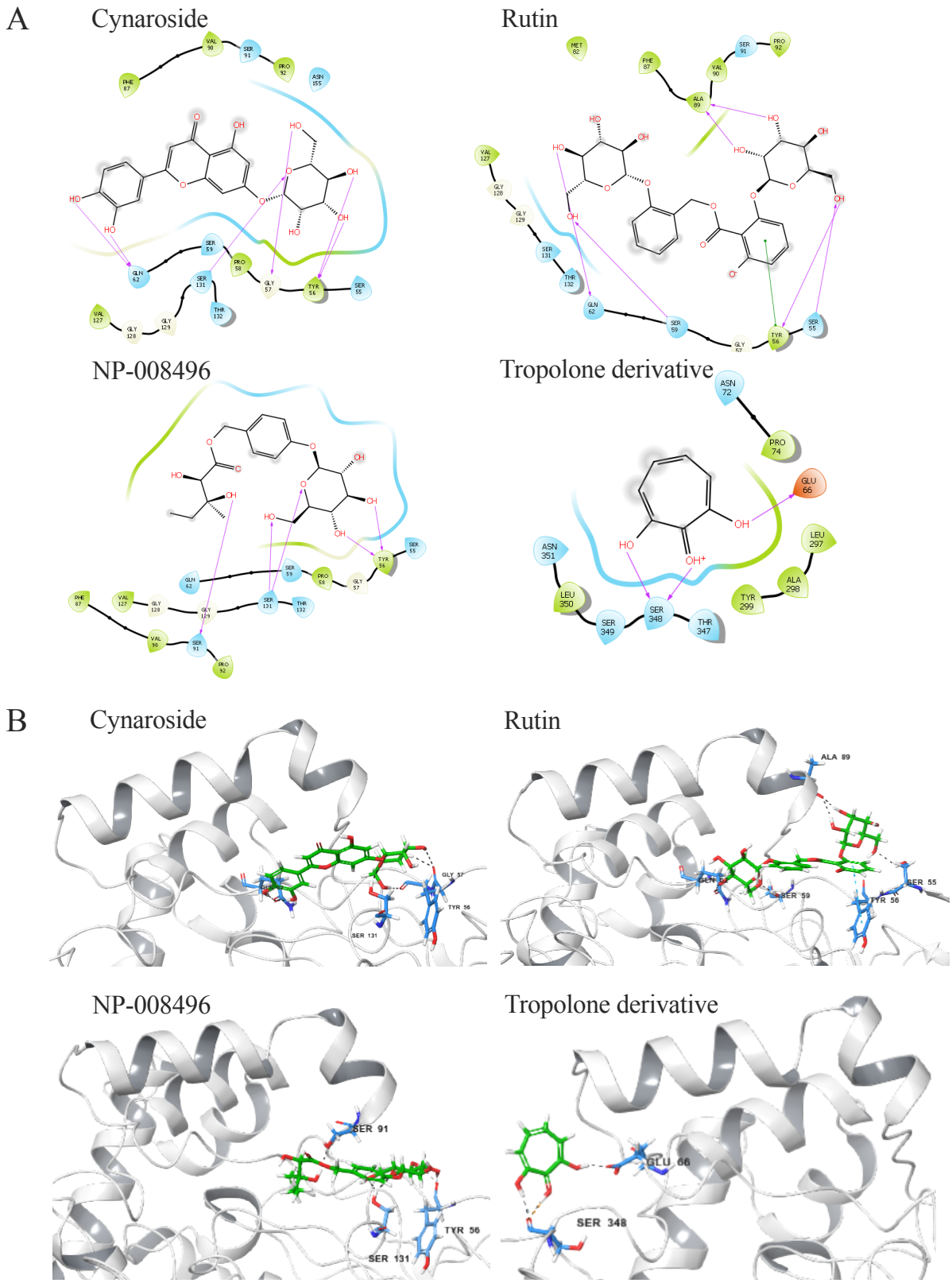

Figure 4.2: Allosteric modulators of CRL determined by in silico screening with the Schrodinger software suite. Two-dimensional depiction of the four allosteric modulators cynaroside, rutin, NP-008496 and tropolone derivative determined in this publication and their interactions points in the allosteric sites of CRL. B. Three dimensional illustration of the four allosteric modulators bound to the interaction sites determined on CRL's surface in the open conformation. Tropolone derivative was determined to bind to screening site 1 (XP Score: -5.603), while rutin, cynaroside and NP-008496 were determined to bind to screening site 3 (XP Score: 8.216, -8.818, -8.931, respectively).

4.3.2: Enzyme activity assay development

Starting with Dairaku et al.'s proposed protocol for the human lysosomal acid lipase [328] we developed an enzyme activity assay, which is applicable for two types of lipase specificities: short-chain fatty acid (butyrate) and long-chain fatty acids (palmitate). Both could be solubilized in an aqueous environment and represent preferred targets of CRL. The selected substrates (4-MUB and 4-MUP) comprise these fatty acids connected to the fluorescent dye 4-MU via an ester bond, respectively. 4-MU emits fluorescence upon hydrolysis of the ester bond and excitation at the corresponding wavelength. While 4-MUB is stable in phosphate buffer (pH 7.0), 4-MUP requires SDS to stabilize the hydrophobic longer-chain fatty acid palmitate in aqueous solution (37°C). To translate the subsequent fluorescence emitted by 4-MU after CRL hydrolysis of the substrate into concentration units; a seven-point standard curve of defined 4-MU concentrations was included ranging from 1.563 to 62.5 µM diluted in assay buffer. The curve (figure 4.3A) is linear within the defined range (figure 4.3B) and was analysed with a linear regression fit. The standard curve allows the translation of RFUs into concentration (µM) within the lower limit of quantification (LLOQ) of 0.5 µM 4-MU and the upper limit of quantification (ULOQ) of 62.5 µM.

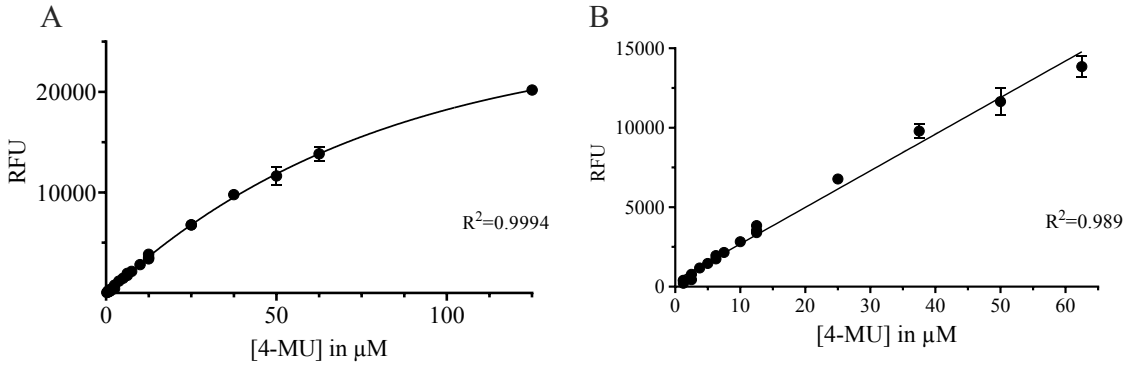

Figure 4.3: 4-MU standard curve.
Plot of several 4-MU concentrations (0.125 – 125 µM) to determine the shape of the standard curve. The sigmoidal shape was analysed with a 4-parameter logistic fit. B. The linear range for the standard curve was determined between the LLOQ and ULOQ, which is in the linear range at concentrations ranging from 0.5 – 625.5 µM.

Subsequently, several parameters were adjusted separately for both substrates. While the concentration of the substrate was constant in both assays (250 µM), the concentration of the enzyme was adjusted to account for SDS's inhibitory effect on CRL (figure 4.4). Therefore, the 4-MUP assay required 10 ng/mL, while the 4-MUB assay's concentration needed to be reduced to 3.3 ng/mL CRL.

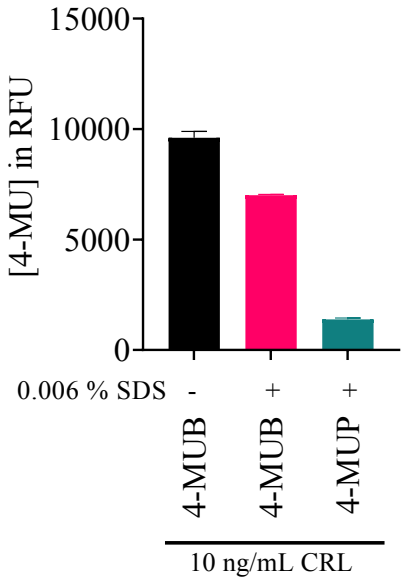

Figure 4.4: Comparison of substrates 4-MUB and 4-MUP and the impact of SDS on enzyme activity.
All data points were obtained by equalizing the assays conditions. The enzyme concentration was set to 3.3 ng/mL in 50 µL PB, while the substrate and stop reagent volume was 50 µL for both. This experiment indicates the CRL's specificity difference between the two substrates 4-MUP and 4-MUB. In addition, it was demonstrated that CRL activity was affected by SDS addition.

Furthermore, it was determined that 10 µL and 50 µL of 10% o-phosphoric acid was sufficient to completely stop the reaction for 4-MUB and 4-MUP, respectively (figure 4.5).

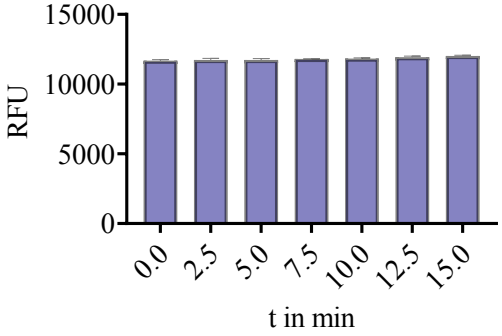

Figure 4.5: Stability of 4-MU after addition of 10% phosphoric acid to reaction.
The increase of fluorescence was less than 3% 20 min after the stop reagent was added. The fluorescence is therefore considered stable for 20 min after stop reagent addition.

Moreover, the accuracy and precision for each substrate was evaluated separately over three-days, (table 4.1), which confirmed reproducibility and comparability of measurements within the assay and between days.

Table 4.1: Validation of the enzyme activity assay for both substrates 4-MUB (A) and 4-MUP (B). Samples were measured in triplicates each day allowing determination of precision (Intra-Day and Inter-Day CV%) and accuracy (%) for the validation.

A

Analytes	**Concentration (µM)**	**Precision (CV) (%)**		**Accuracy (%)**
(Substrate: 4-MUB)	**(n=3)**	**Intra-Day (n=3)**	**Inter-Day (n=3)**	**(n=3)**
QC1[a]	12.8 ± 0.6	0.5 - 6.5	4.6	
QC2[b]	16.7 ± 1.2	1.3 - 3.3	6.9	0.7%
QC3[c]	74.2 ± 3.2	0.9 - 2.6	4.4	1.7%

B

Analytes	**Concentration (µM)**	**Precision (CV) (%)**		**Accuracy (%)**
(Substrate: 4-MUP)	**(n=3)**	**Intra-Day (n=3)**	**Inter-Day (n=3)**	**(n=3)**
QC1[a]	6.5 ± 0.4	0.9 – 2.2	5.6	
QC2[b]	9.8 ± 0.6	0.6 – 4.2	6.0	2.0%
QC3[c]	56.8 ± 1.9	0.8 - 2.6	3.4	0.6%

[a]*QC1: CRL and substrate*
[b]*QC2: CRL, substrate and a low spike of 4-MU (3.13 µM)*
[c]*QC3: CRL, substrate and a high spike of 4-MU (50 µM)*

4.3.3: Assay robustness

Although the assay was validated for both substrates, our data showed superior aqueous solubility of the substrate 4-MUB as compared to 4-MUP due to the shorter hydrocarbon chain. The addition of SDS for 4-MUP stabilization reduced the enzyme's activity (figure 4.4). Thus, we focused on the substrate 4-MUB for further determination of validation parameters to avoid interference with the enzyme's activity. Subsequently, we investigated the assay performance with 4-MUB at different temperatures (figure 4.6A) and pHs (figure 4.6B).

Five different temperatures, 4, 15, 28, 37 and 45°C were tested. Our data indicated that the enzyme is temperature sensitive and most active between 37-45°C as the optimal temperature for the enzyme activity (figure 4.6A). However, 37°C was maintained for further experiments as it represents physiological conditions. The investigation of the reaction's efficiency at six

different buffer pH revealed stability of the enzyme's activity in a wide pH range, which can vary in the gut of mice between 3.5-4 (stomach) to 6.5-7.5 (intestine, figure 4.6B).

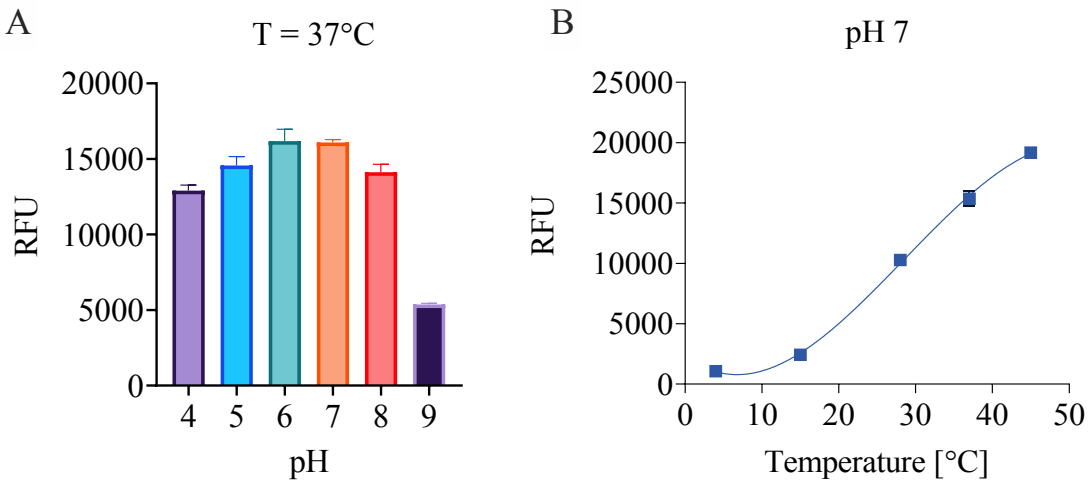

Figure 4.6: Determination of assay robustness by alteration of pH and temperature.
A. Temperature variation (4 – 45°C) of the activity assay with constant buffer pH at 7. B. Buffer pH variation (pH 4 – 9) in the activity assay with constant reaction temperature at 37°C.

The instability at pH 8 was identified as autocatalysis of the substrate, which is characteristic for ester bonds under basic conditions and makes the reaction independent of the enzyme's activity. Therefore, the selected reaction conditions were approximated to physiological conditions at pH 7 since they show robustness and optimal reaction requirements.

4.3.4: Proof of concept: characterization of tropolone

Subsequently, we used the *in vitro* assay to verify the allosteric modulator potential of tropolone to demonstrate the underlying workflow [329]. Tropolone was investigated in both developed *in vitro* assays in a concentration range of 2 µM to 10 mM with both substrates showing a concentration-dependent inhibition (figure 4.7A). We calculated the corresponding IC50 values (4-MUP: 3.75×10^{-4} M; 4-MUB: 3.95×10^{-4} M) by plotting the logarithmic tropolone concentration against the activity of CRL (%), which indicates CRL's inhibition being slightly more efficient in 4-MUP samples with a lower IC50 value (figure 4.7B).

A

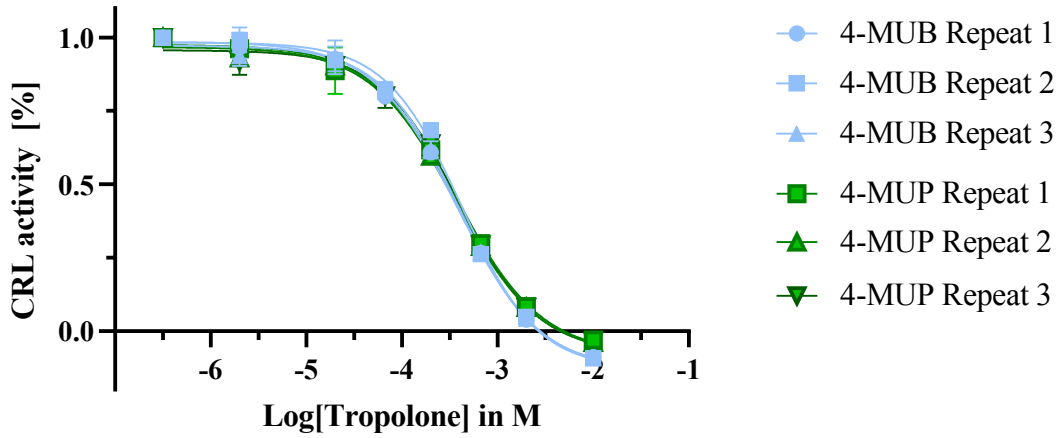

B

	Replicate	IC50 [M]	Mean(IC50) [M]	SD(IC50) [M]
4-MUB	1	3.76E-04	3.95E-04	2.19E-05
	2	4.19E-04		
	3	3.90E-04		
4-MUP	1	3.73E-04	3.75E-04	1.65E-05
	2	3.60E-04		
	3	3.93E-04		

Figure 4.7: IC50 determination of tropolone using the developed enzyme activity assay.
A. Plot of replicated IC50 curves for 4-MUP and 4-MUB with tropolone concentrations between 2 µM and 10 mM. B. Analysis of the IC50 values for both substrates. IC50 values were determined by plotting the logarithmic tropolone concentration against the percentage of CRL activity, which allows the determination of IC50 values: 4-MUP: $3.75x10^{-4}$ M; 4-MUB: $3.95x10^{-4}$ M and standard deviations of $1.65x10^{-5}$ and $2.19x10^{-5}$, respectively.

In addition, we investigated reported CRL inhibitors and their IC50 values in the developed assay to assess the assays ability to measure IC50s (figure 4.8). The reduction of CRL's assay concentration by 10-fold allowed the measurement of IC50 values of weak inhibitors. The measured IC50 values in the in-house activity assay were close to the reported IC50s of trigonelline, β-aescin and berberine (figure 4.8) [330, 331].

A

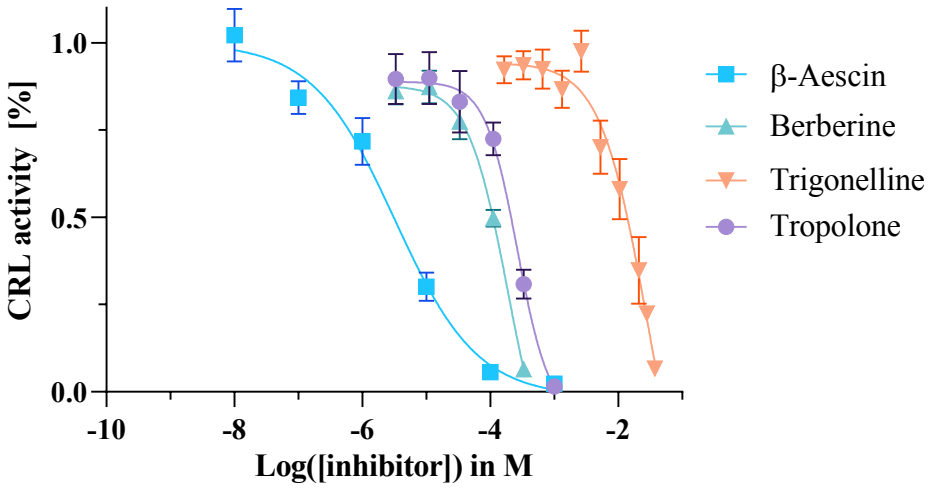

B

	IC50, measured [M]	IC50, reported [M]
β-Aescin	3.24E-06	8.00E-06
Berberine	1.87E-04	2.50E-04
Tropolone	2.65E-04	-
Trigonelline	2.85E-02	2.00E-02

Figure 4.8: IC50 of tropolone and other published inhibitors.
A. Plot of varying concentrations of β-aescin, berberine, tropolone and trigonelline, and their impact on CRL activity. Tropolone and berberine have a similar IC50 range, while β-aescin is two orders of magnitude lower and trigonelline two orders of magnitude higher. The CRL concentration in the assay was ten-fold lower, which allowed the measurement of weak inhibitors such as trigonelline. The resulting IC50s are comparable to the published IC50s, which had been determined by high-performance liquid chromatography.

Finally, we determined the kinetic parameters of the CRL extract. The in-house developed assay with the substrate 4-MUB was used and applied in 8 different concentrations over a 50-minute time span by measuring the increase of RFUs over time. The subsequent plot of initial velocity against the substrate concentration (Michaelis-Menten plot) allowed the determination of Vmax (0.54 +/- 0.03 µM/min) and Km (0.46 +/- 0.06 mM) for 4-MUB (figure 4.9). The additional analysis of Km and V_{max} after addition of tropolone in two different concentrations (100 and 400 µM), respectively, determined tropolone's mode of inhibition. While Km did not show a clear trend of decline or increase due to inhibitor addition, V_{max} decreased with increasing inhibitor concentration (figure 4.9).

A

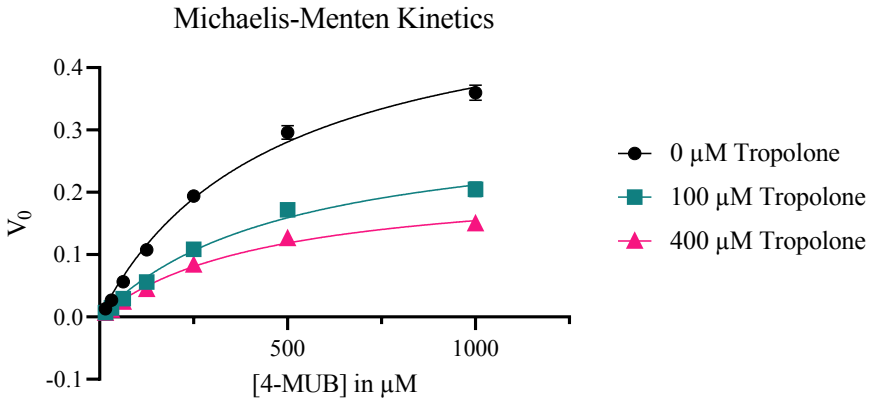

B

	Km [mM]	SD(Km) [mM]	**Vmax [µM/min]**	SD(Vmax) [µM/min]
0 µM Tropolone	**0.456**	0.059	**0.540**	0.032
100 µM Tropolone	**0.494**	0.091	**0.316**	0.028
400 µM Tropolone	**0.438**	0.069	**0.222**	0.016

Figure 4.9: Michaelis–Menten kinetics of tropolone measured by the in-house developed enzyme activity assay. 0, 100, or 400 µM tropolone were tested to measure the inhibitor's impact on Vmax and Km of CRL. While Km was maintained after inhibitor addition, Vmax was decreasing with increasing inhibitor concentration. Therefore, tropolone was identified as a non-competitive inhibitor.

This experimental trend confirmed the *in-silico* analysis, which identified tropolone as an allosteric modulator of CRL and identified the inhibition as non-competitive. Furthermore, we examined the binding of CRL to trigonelline, β-aescin and tropolone using BLI (figure 4.10). β-Aescin's KD was determined to be relatively low (KD: 1.76 x 10-4 ± 3.6 x 10-5, figure 4.10) but was inconsistent with the measured IC50 value suggesting non-specific binding to CRL. By contrast, tropolone's determined KD value was consistent with its relatively low IC50 (KD: 5.7 x 10-6 ± 7.25 x 10-7, figure 4.10) indicating a more specific interaction. However, the relatively modest IC50 is consistent with tropolone's deemed mechanism of action, namely allosteric modulation. Finally, trigonelline showed relatively high KD and IC50 (KD: 1.28 x 10-3 ± 8.26 x 10-4, figure 4.10), indicating low or nonspecific interaction with CRL.

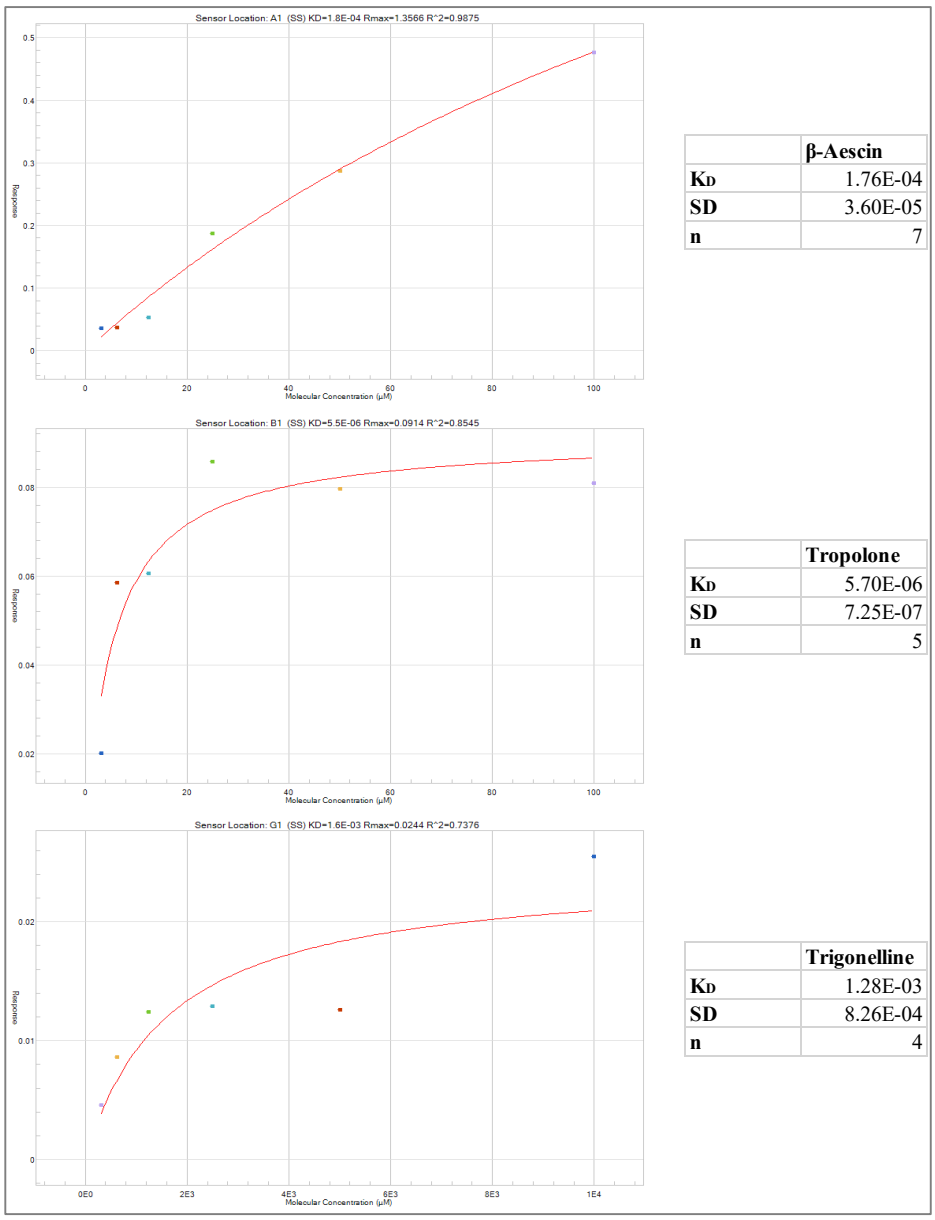

	β-Aescin
KD	1.76E-04
SD	3.60E-05
n	7

	Tropolone
KD	5.70E-06
SD	7.25E-07
n	5

	Trigonelline
KD	1.28E-03
SD	8.26E-04
n	4

Figure 4.10: KD determination of each CRL-modulator interaction assessed by BLI.
KD values and standard deviation of trigonelline, tropolone and β-aescin were determined by measuring different concentrations of modulator.

In summary, we showed that the developed enzyme activity assay can be used to identify and characterize *in silico* identified allosteric modulators of CRL.

4.3.5: IC50 and EC50

Prior to the determination of the IC50 and EC50 values of the 53 compounds selected from the *in silico* screening, we determined the concentration range, potential interaction between substrate and modulator, and the pH impact of the modulator (data not shown). Modulators,

which showed nonspecific enhancing or inhibiting activity due to pH changes or secondary interactions other than modulator-enzyme-interaction were excluded for the subsequent analysis of IC50 and EC50 values. This reduced the number of modulators to be assessed *in vitro* to 14. We found 5 inhibitors, of which tropolone (XP Score: -3.314, supplementary table 4.3.1) had been used as proof of concept for enzyme activity assay. Cynaroside and rutin (XP Scores: -8.216 and -8.818, respectively; figure 4.2, supplementary table 4.2.1) were the strongest determined inhibitors of CRL activity (IC50: 227 ± 26 µM and 446 ± 15 µM, respectively, figure 4.11A, table 4.2), and were predicted to bind to screening site 3. In addition, although less efficient, NP-000042 and NP-0201046 inhibited CRL activity with an IC50 of 582 ± 27 µM and 877 ± 77 µM, respectively (supplementary figure 4.1.2, 4.1.3A). Furthermore, 3 enhancers were discovered: NP-008496, quinic acid and 1-deoxynojirimycin. NP-008496 (XP Score: -8.931, supplementary table 4.2.1) was the most potent enhancer of CRL activity (EC50: 425 ± 18 µM, table 4.2, figure 4.10B). In addition, quinic acid as well as 1-Deoxynojirimycin were both able to enhance CRL's activity but less efficiently with an EC50 of 5911 ± 883 µM and 1226 ± 205 µM, respectively (supplementary figure 4.1.2, 4.1.3B).

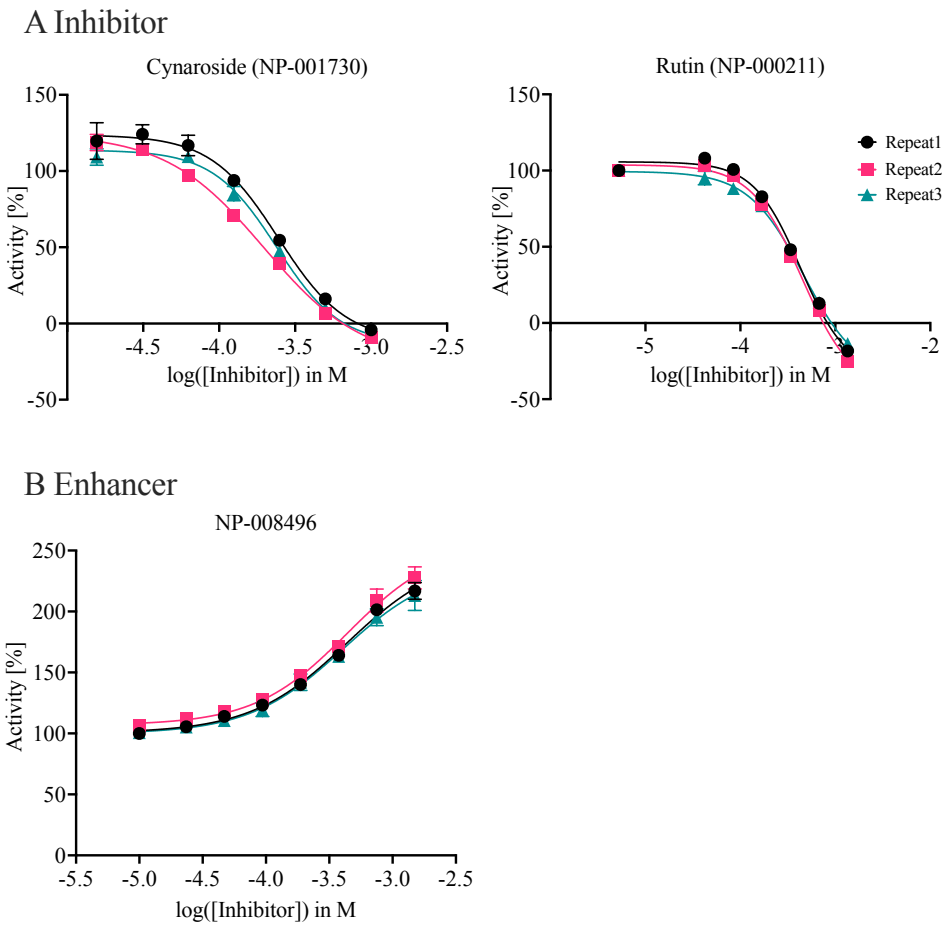

Figure 4.11: IC50 and EC50 curves to analyse the allosteric modulators' affinity to CRL.
A. IC50 curves of rutin and cynaroside, which were in silico selected compounds determined to inhibit CRL's activity. B. EC50 curve of NP-008496, which was in silico determined to modulate CRL's activity through binding of screening site 3. All values were normalized to base activity of CRL and IC50/EC50 determined in triplicates and curves were fit according to Michaelis-Menten kinetic and EC50/IC50 determined with 4-parameter fit in Prism software (table 1).

Finally, BLI was applied to determine K_Ds of each modulator-enzyme interaction to confirm the direct interaction (figure 4.12). We identified rutin, cynaroside and NP-008496 to exhibit the strongest interaction of the tested metabolites (130 µM, 570 µM, 160 µM, respectively; figure 4.12).

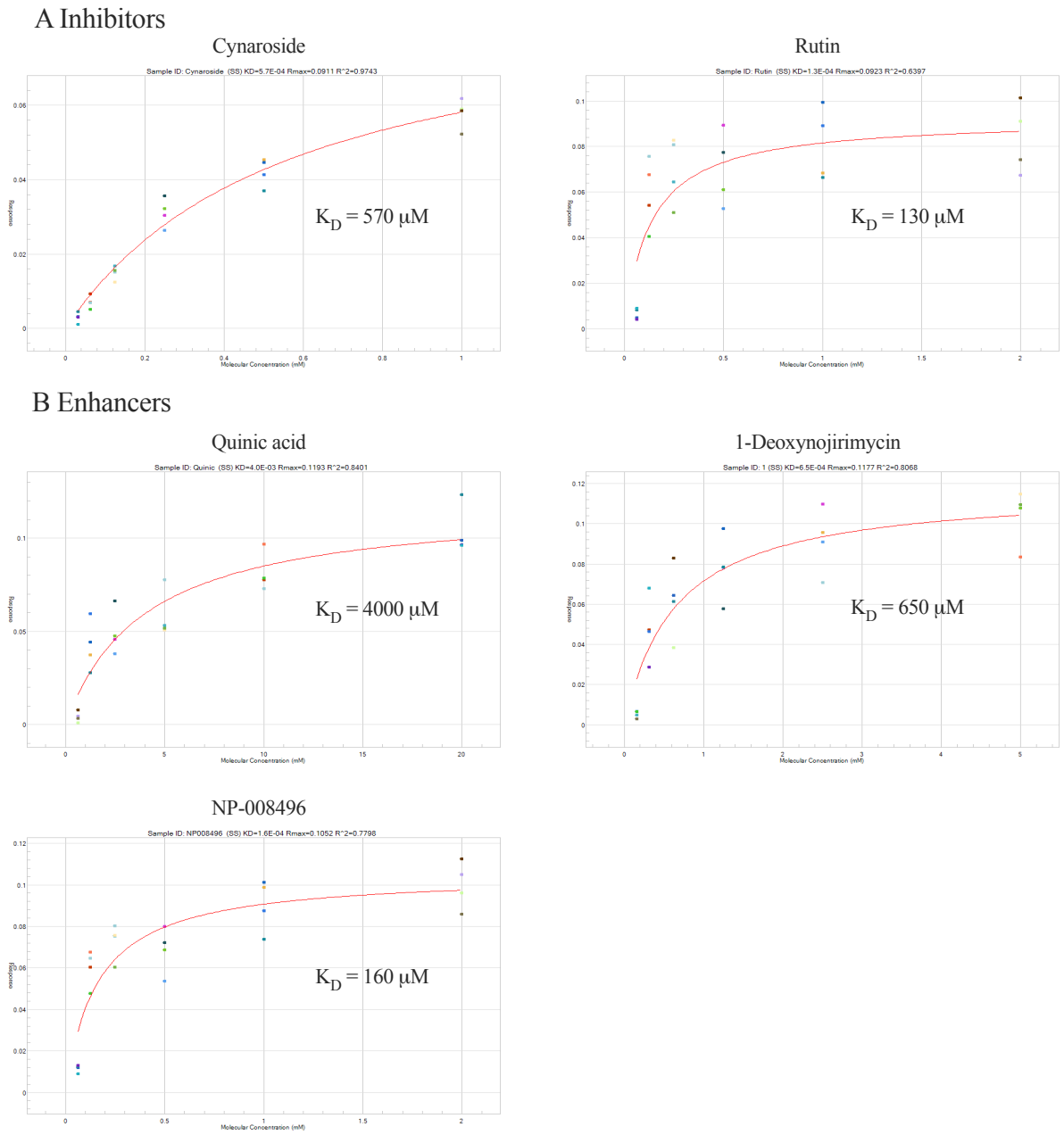

Figure 4.12: KD determination of each CRL-modulator interaction assessed by BLI.
Each modulator was measured using 6 concentrations covering the range of the EC50 and IC50 curves.

4.3.6: Michaelis – Menten kinetics

Next, Michaelis-Menten kinetic parameters were determined for rutin and cynaroside, the most potent inhibitors and NP-008496, the most potent enhancer to determine how the modulators impact CRL's activity (table 4.2).

Table 4.2: Summary of IC50/EC50 and kinetic parameters.
For rutin, cymaroside and NP-008496 half of the enzyme was applied compared to tropolone's data acquired for our previous publication. This reduced the amount of modulator needed, which were in low

amounts available, while not interfering with the characterization of the modulators. IC50 and EC50 values were determined under the same conditions reported previously by Menden et al., 2019.

	IC50/EC50 (μM)	SD (μM)	**[Modulator]** (μM)	**Km** (μM)	SEM (μM)	**Vmax** (μM/min)	SEM (μM/min)	**Reference**
Tropolone	395	22	0	456	59	0.540	0.032	4.3.4
			100	494	91	0.316	0.028	
			200	438	69	0.222	0.016	
Rutin	446	15	0	179	18	0.236	0.009	-
			200	199	26	0.106	0.004	
			400	488	90	0.086	0.008	
Cynaroside	227	26	0	245	26	0.251	0.009	-
			150	216	44	0.160	0.012	
			300	287	108	0.094	0.015	
NP-008496	425	18	0	186	8	0.298	0.005	-
			150	82	11	0.369	0.016	
			300	98	10	0.466	0.018	

These modulators had the lowest K_D, IC50 and EC50 values, which was also consistent with the predicted *in silico* docking scores for screening site 3 (supplementary table 4.2.1). Two concentrations per modulator in the range of their IC50 or EC50, respectively, were selected to describe their kinetic parameters. Rutin showed a decrease in Vmax and increase in Km suggesting mixed inhibition mimicking competitive binding, which indicates that rutin prefers binding of the unbound enzyme over the enzyme-substrate complex (figure 4.13A, 4.2). Cynaroside's mode of inhibition suggested non-competitive inhibition with decreasing Vmax and similar Km values (figure 4.13A, 4.2), although the inhibitory effect might be a result of nonspecific interactions with CRL as suggested by BLI (figure 4.12). NP-08496, the strongest determined enhancer, showed increasing Vmax which suggested that the reaction occurred at a higher rate compared to control, while decreased Km suggested a positive allosteric effect on CRL's activity as well as the lowest KD (figure 4.2, 4.12, 4.13B).

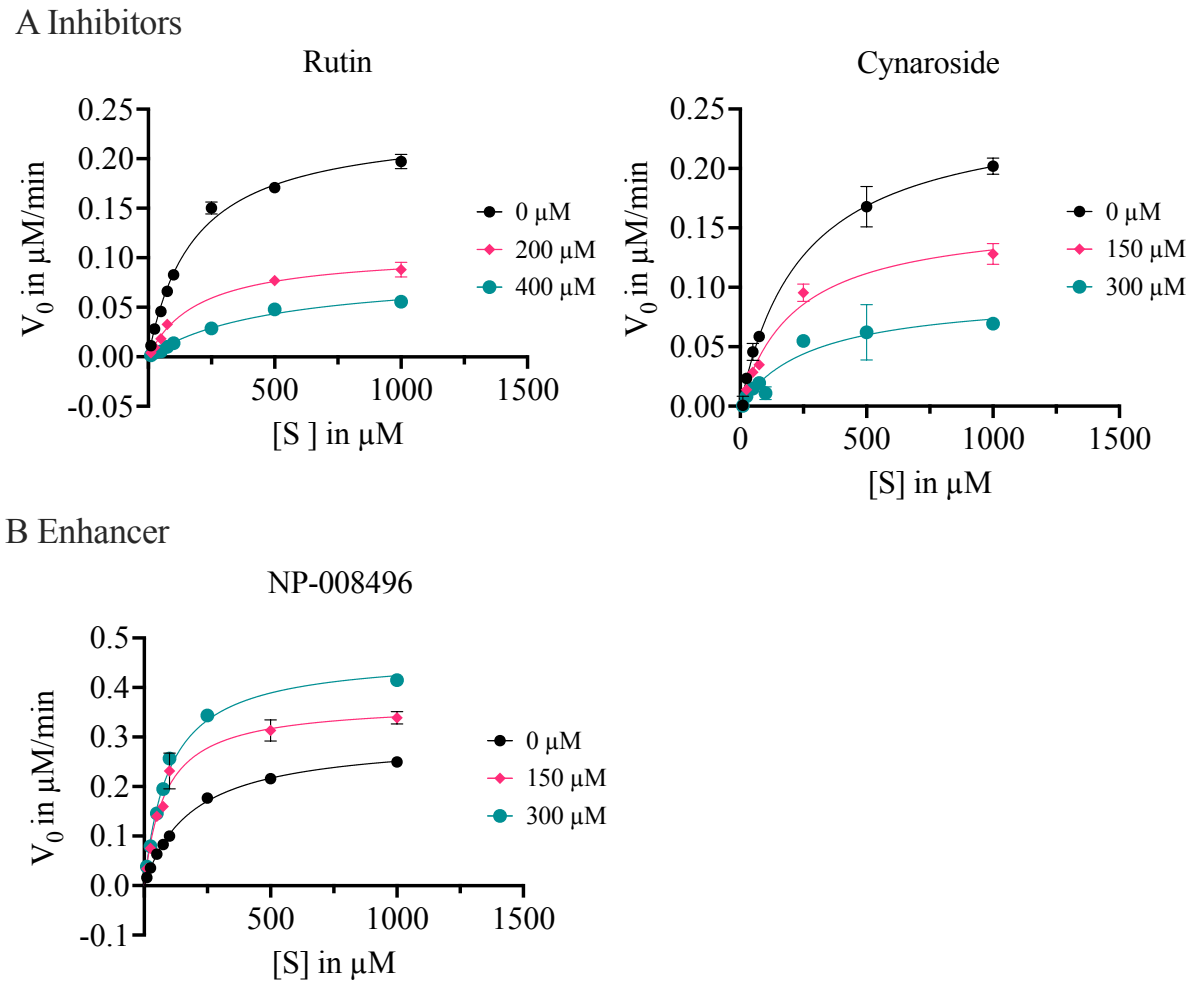

Figure 4.13: Michaelis-Menten kinetics of rutin, cynaroside and NP-008496 to determine their type of action. A. Inhibitors concentrations were selected around the determined IC50 value (table 1), respectively. B. Enhancer concentrations were selected around the determined EC50 value. Curves were fit according to Michaelis-Menten kinetic and Km and Vmax determined with Prism software (table 1).

4.3.7: Enhancer effect on other lipases

Finally, it was determined whether NP-008496's enhancing effect on CRL activity could be observed when added up to a concentration of 2 mM to 5000 FIP/kg CRL (9.1 mg/mL CRL) and triacetate (lipid substrate). No activity enhancement was measured between groups independent of enhancer addition (figure 4.14).

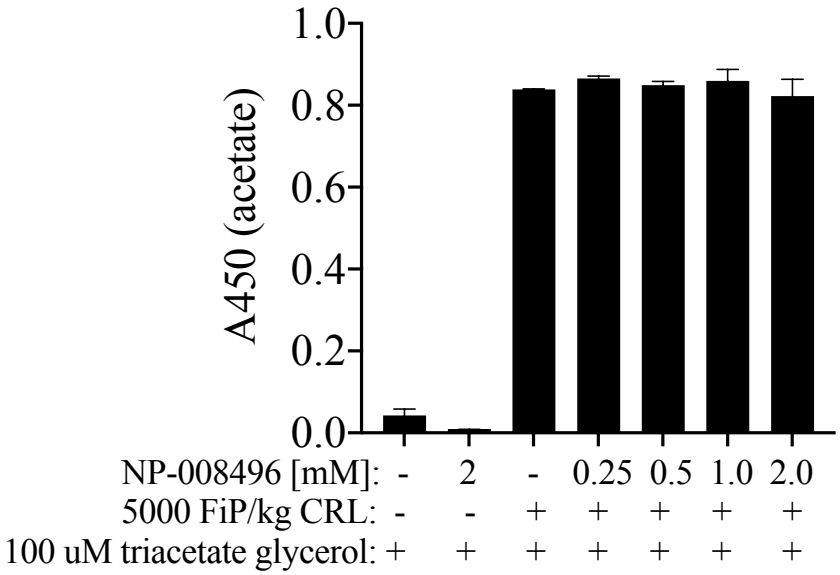

Figure 4.14: Biologically relevant dose of CRL reacting with different NP-008496 doses and glycerol triacetate. While a difference in activity was measured in control samples with and without CRL, no difference could be examined in samples including CRL with and without enhancer.

Finally, it was tested whether the enhancer could modulate the activity of other lipase species, to justify its use in animals despite the lack of enhancement at endogenous lipase concentrations as described above. Lipase activity of *Aspergillus niger, Rhizopus oryzae* and human pancreatic lipase were optimized for the assay measurement range and relative values determined to allow comparison between lipases (figure 4.15).

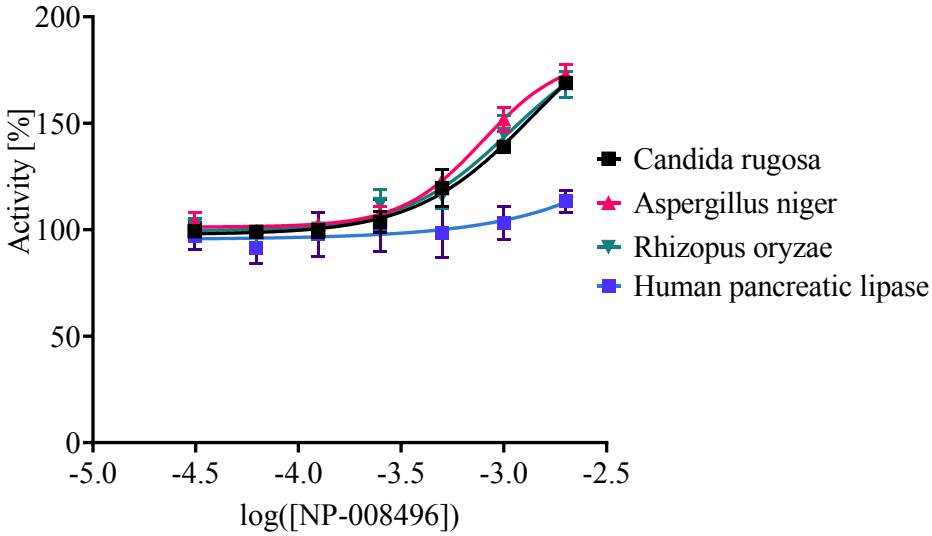

Figure 4.15: Enhancement effect of NP-008496 on CRL activity compared to other lipases.
While Aspergillus niger and Rhizopus oryzae showed comparable activity enhancement of enzyme activity compared to CRL, the human pancreatic lipase showed no change.

While the enhancer impacted the lipase activity within the lipase family of *yeast*, no effect was observed on the human pancreatic lipase. Hence, the null hypothesis that the enhancer will not have any effect on endogenous lipase activity could not be rejected.

4.4 Discussion

In Chapter IV, we applied a combined approach of computational and *in vitro* screening to identify novel, natural allosteric modulators of CRL to subsequently investigate hypothesis (3). Although our approach was based on a theoretical model predicting the probability of compound and enzyme interaction, the advances in the Schrodinger algorithm and application in numerous research studies increased the level of confidence in the results [332, 333]. For the computational modelling approach, the target enzyme underwent several modifications. However, each of these alterations was performed only after it was determined that they had minimal effects on predicted substrate catalysis. Thus, the enzyme's structure was maintained as close as possible to the natural conformation captured by X-ray crystallography. The computational screening reduced the library from 200,000 natural compounds to 53 compounds, which then needed to be assessed by the *in vitro* CRL activity assay.

Therefore, we developed and optimized a miniaturized lipase activity assay for two different substrates (4-MUB (short-chain fatty acids) and 4-MUP (long-chain fatty acids)) to account for CRL's substrate specificity. The assay conditions were validated and additionally applied to characterize tropolone, one of the *in silico* selected allosteric modulators of CRL. Although the current assay conditions were optimized to the obtained CRL extract for the discovery of allosteric modulators of CRL, the assay allowed adjustments for any enzyme's specificity as 4-MU can not only be synthesized to other fatty acids, but also to substrates of glucosidases or

phosphatases. Furthermore, the use of 4-MUB and 4-MUP demonstrated the assay's adaptability to different substrate specificities of enzymes. During the development of the assay, consideration of a reagent to stop the reaction, which differentiated this from other published assays, was pivotal for reproducibility within and between different reads [334, 335]. However, we acknowledge the limitations of the assay such as the intrinsic decrease in solubility of the hydrophobic fatty acid tail with length and the autocatalysis of the substrate in the basic pH range.

Subsequently, the assay was used to verify the impact of tropolone on CRL activity. Tropolone is a seven-carbon aromatic ring, which is a common motif in naturally occurring compounds such as β-Thujaplicin or Colchicine [336]. Although a tropolone similar structure was determined in the initial *in silico* screening, it was hypothesized that absence of the hydroxide group would still enable the fit predicted by Schrodinger- although the docking score changed to -3.314. So far, it has not been reported that tropolone can inhibit lipases, although other natural compound classes such as flavonoids, alkaloids, and saponins are known to inhibit CRL's activity with varying efficacy depending on the concentration used [330, 331]. The developed, optimized assay was applied to measure IC50s and kinetic parameters describing the tropolone-CRL interaction, which characterized tropolone as a non-competitive inhibitor. This was further investigated by BLI, which confirmed tropolone's direct interaction with CRL as a non-competitive inhibitor. Given the slight differences in the assay conditions between 4-MUB and 4-MUP, it was not possible to directly compare the results of both assays. However, each assay individually is inter-comparable between runs and samples and can be applied for high-throughput screening.

Therefore, the 53 compounds selected by *in silico* screening were tested in the assay (table 4.3.1). Out of 53 compounds, 14 appeared to impact the enzyme's function in the *in vitro* screening assay. These 14 modulators were additionally assessed for their impact on pH, the

substrate, and the fluorophore, which would have suggested unspecific interactions. This reduced the number of compounds to eight (data not shown). Out of those, tropolone and cynaroside were identified as non-competitive inhibitors, rutin as a mixed inhibitor and NP-008496 as an allosteric enhancer.

Cynaroside, the most potent non-competitive inhibitor, is a flavone present in dandelion or artichokes and has been reported to inhibit hepatic cholesterol biosynthesis. Furthermore, it has been suggested to be the active ingredient of different natural extracts- which have been applied to treat diseases such as obesity due to their ability to inhibit, for instance, fatty acid synthase (figure 4.4A) [337-339]. Based on the *in silico* screening results, we hypothesized that when cynaroside is bound to screening site 3, the free, unbound portion of cynaroside's structure would reach over the tunnel entrance, thus inhibiting the substrate from entering or exiting the catalytic site (figure 2). However, as BLI showed unspecific effects of cynaroside on CRL activity suggesting irreversible unfolding of the protein, cynaroside's mode of action might be less specific than determined.

Rutin's unbound substructure seemed to reach over the tunnel entrance as well when bound to screening site 3 suggesting the same mechanism as cynaroside's binding, but with a specific interaction in the BLI assay. Rutin is a flavonoid derived from plants such as buckwheat or eucalyptus and was shown to inhibit CRL's activity through mixed inhibition (figure 4.4A). Additionally, rutin's mode of inhibition suggested that rutin did not bind the enzyme with high efficacy when a substrate was bound to the catalytic center and tunnel region. Interestingly, rutin has been reported to inhibit human pancreatic lipase, and hence, might suggest that the inhibitors and enhancers of this allosteric site are applicable for other lipases [340].

Next, we predicted that NP-008496 would bind to screening site 3 with its glycosyl group, similar to cynaroside and rutin, and also reach with its unbound substructure over to the catalytic center. We determined *in vitro* that NP-008496 enhanced CRL's activity. NP-008496 is derived

from pumpkin with a substructure similar to arbutin. We hypothesized that the 2,3-dihydroxy-3-methylpentanoate group might orientate the substrate into position, therefore enhancing CRL's activity and efficiency, while rutin's and cynaroside's 6-membered rings would inhibit binding and release of the substrate, thus inhibiting the enzyme's activity. Of particular importance was the prediction that NP-008496 would form a secondary bond to Ser91, an amino acid of the loop region, which could maintain the open conformation. This supports our initial hypothesis that formation of secondary bonds with the loop will maintain the open conformation and thus, will increase the enzyme's activity.

In conclusion, this study resulted in the proposition of a potential generic allosteric site to inhibit and enhance CRL's activity. The three modulators rutin, cymaroside, and NP-008496 have a glycoside group, which anchors their structures on the enzyme's surface, while the unbound sub-structures of each modulator determined whether enhancement or inhibition of the enzyme's activity was achieved.

Finally, we tested NP-008496 potential to enhance 5000 FIP/kg CRL activity *ex vivo*. No dose-dependent activity enhancement effect or an enhancement effect on an endogenous human lipase was observed within the tested range. Furthermore, other lipase species did not exhibit significant lower EC50s, which resulted in the suggestion to use a higher dose to enhance the enzyme activity. Therefore, to estimate the required dose, we extrapolated from the EC50 determination, the theoretical concentration of NP-008496 to enhance 5000 FIP/kg CRL by 50 %. The calculation revealed a required concentration of 0.5 M of NP-008496, which raised concerns about tolerability and specificity in mice. In addition, NP-008496 could not obtained in the required amounts in a time- and cost-effective matter to conduct an animal study. Hence, hypothesis (3), which aimed to determine the effect of NP-008496 *in vivo*, could not be tested. Nevertheless, optimization of the enzyme-modulator interaction through structure-activity

relationship of the identified structures is warranted to allow analysis of hypothesis (3) in a future study.

Chapter V: Discussion

5.1 Summary of dissertation research

Dementia affects over 50 million people worldwide and has been projected to exceed 150 million cases by 2050 [341]. While researchers have explored the mechanisms behind the development of AD, the most common form of dementia, and have identified various targets for treatment in the past three decades, no disease-modifying treatment has been discovered to stop onset or progression of AD [342]. Therefore, novel strategies have been suggested to enhance selection, treatment approaches, and understanding of AD's mechanisms. The gut microbiome represents one such area of active research, which has been shown in recent studies of neurodegenerative diseases to modulate neuropathology [145, 343-347]. In addition, gut dysbiosis has been observed in AD patients as well as in mouse models of AD [59, 139, 212]. It has also been demonstrated in AD mouse models that the compositional state of the gut microbiota can modulate severity despite the genetic predispositions driving AD-like pathology, which emphasized the potential role of the gut microbiota in AD pathogenesis [59, 348, 349]. Moreover, ageing, the main risk factor of AD, has been demonstrated to be associated with altered gut microbiota composition as a result of reduced gastrointestinal functions such as motility, digestive enzyme activity and nutritional supply, which highlights the pivotal connection between gut health and AD [180]. Hence, this thesis was aimed at enhancing the understanding of the role of the gut microbiome in AD through evaluation of a gut-directed treatment strategy and determining whether restoration of gut homeostasis and nutritional supply may reduce AD pathology.

The work presented in this thesis described our used approaches to test this hypothesis. We selected CRL, an exogenous lipase with a broad specificity range, for this thesis as treatment strategy. Distinct from a previous study, which investigated the effect of a supplement combining multiple enzyme classes in one product (Pancrealipase), we focused on one enzyme to assess the specific effects and mechanisms [180]. CRL has the potential to release beneficial metabolites that could be directly absorbed by the host such as UFA or used by the gut microbiota to metabolize these compounds into molecules with anti-inflammatory or anti-microbial properties further benefitting the host [269, 350].

First, we presented in this thesis the findings of the CRL treatment study in Wt mice, which assessed efficient delivery of active CRL into the gastrointestinal tract and CRL's treatment effects on the gut environment (Chapter II). After we showed CRL's composition and stability in drinking water, we examined the activity of orally administered CRL throughout the digestive tract since it was proposed that the administration of unprotected enzyme might be inactivated by the acidity of the stomach or protease activity in the gut [351]. Administration of biotinylated CRL revealed that CRL was active in the content of each of the intestinal sub-units. In addition, we observed treatment-dependent elevation of FFA levels in the SI and cecum, which confirmed what has been observed in human administrations [352, 353]. This confirmed that the selected administration route was efficient in delivering CRL in an active state into the gastrointestinal tract of mice. Hence, mice received CRL in their drinking water in the subsequent *in vivo* studies.

Next, we demonstrated that exogenously administered CRL induced short- and long-term biological changes in the gut environment. Administration of CRL resulted in differences of β-diversity indices and promotion of species in the short- and long-term that are associated with beneficial effects such as direct or indirect butyrate production (*Allobaculum, Christensenellaceae, Bifidobacterium pseudolongum*) or gut health (*Akkermansia muciniphila*)

[249, 354, 355]. Furthermore, the changes in fecal and cecal diversity and taxonomy persisted even after 30 days of discontinued treatment, which emphasized CRL's effect on gut microbial composition. Between sample sites, administered CRL concentrations and time-points, we did observe unexpected variation and no dose-dependency, but we concluded that the variations have been caused by the varying environmental conditions dependent on the CRL concentration used. For instance, we revealed a dose-dependent trend for decreasing acetic acid levels in the short-term study. Acetic acid has been reported to possess pivotal functions to the host such as enhancing energy metabolism and butyrate production, which can alter the gut microbial composition dependent on its concentration in the gut [356]. Furthermore, it has been demonstrated that reorganization of the gut microbiota in response to dietary change can be a lengthy process, if the diet remains mostly unchanged and the gut microbiome is in balance and resilient [357]. Hence, the dose-dependent reduction of acetate levels might have occurred due to reorganization of the gut microbiota, which differed dependent on the administered CRL concentration, treatment length and sampling location, respectively.

In conclusion, we demonstrated that CRL could be delivered in an active state to the gastrointestinal tract via drinking water, which impacted biological pathways that resulted in beneficial effects on the gut environment, all of which supported hypothesis (1) and the subsequent investigation of hypothesis (2).

Subsequently, we examined the long-term effects of CRL administration on AD-like pathology in APP/PS1 mice and how the treatment effects in the gut were transmitted into the host's circulatory system and the brain. We showed that CRL treatment altered the host's gut environment by increasing the levels of metabolites associated with unsaturated fatty acid pathways and changing the abundance of two species of the *Clostridiales vadin BB60* genera and *Acetatifactor*. This supported our previous findings and other reports from human and

animal studies where exogenous lipase was administered, which have suggested that lipase treatment increases fatty acid levels and enhances beneficial bacteria, which benefit from the metabolic changes in the gut [180, 352, 353]. Furthermore, we demonstrated that CRL treatment normalized peripheral levels of unsaturated fatty acids and increased VLDL/LDL cholesterol and cholesterol ester levels in treated APP/PS1 mice. A study of patients with probable AD reported reduced VLDL/LDL cholesterol levels in these patients supporting our finding and emphasizing the potential treatment mechanism of CRL [358]. In addition, a lipase containing PERT has been reported to normalize lipid and cholesterol levels and transport in patients with cystic fibrosis, supporting the idea that CRL administration might benefit lipid and cholesterol metabolism [359, 360]. Also, increased levels of peripheral FFAs - as observed in untreated APP/PS1 animals - have been shown to reduce BBB integrity and enhance neuroinflammation, which could promote progression of AD pathology [361]. However, while we reported increased UFA levels in APP/PS1 mice, levels in AD patients have been shown to be decreased [362]. Hence, a more extensive analysis of lipid profiles should be performed to confirm the changes in this lipid subclass as well as a longitudinal study of peripheral fatty acid to understand whether our observation was based on a disease-relevant mechanism at a specific time-point in the disease progression or whether this represented a specific occurrence in the selected mouse model. Furthermore, the lipid levels in the cortex and hippocampus should be investigated to assess, whether the peripheral levels are transmitted into the brain.

The observed treatment-dependent alterations in the gut and periphery further extended into the brain, where we examined significant improvement of long-term spatial memory APP/PS1 mice accompanied by reduced cortical and hippocampal microgliosis and astrogliosis post CRL treatment. Reactive astroglia and microglia populations have been reported to contribute to synaptic loss in cortical and hippocampal tissue and cognitive decline [363-366]. CRL treatment might have therefore impacted the glial activation state, which consequently ameliorated AD-

like pathology. Since these changes were shown to be more pronounced in cortical tissue, a cortical transcriptomic analysis was investigated, but did not yield in identification of differentially expressed genes. However, enrichment analysis of a subset of brain cell-specific markers showed that microglial and astrocyte cell-specific markers of the brain were significantly altered following CRL treatment. The reduction in astrocyte marker GFAP suggested a potential reduction in reactive astroglia, while microglia marker TMEM119 (homeostatic marker), Aif1 (activated microglia), Ccl3 (inflammatory marker) and Olfmfl3 indicated a reduction of the reactive microglia population in the cortex [363, 367-370]. The subsequent cross-validation (rdCV-RF) and multi-omics integration (DIABLO) of the three datasets (gut microbiota, plasma metabolome and cortical transcriptome) supported our findings and emphasized the strong link between the gut microbiota and peripheral metabolome. This finding is consistent with several reports describing the gut microbiome's contribution to peripheral metabolite levels through digestion of lipids, carbohydrates and proteins [221]. The associated digestion products and metabolites can be directly absorbed by the host inducing beneficial but also harmful effects depending on the respective metabolite such as UFA derivatives, SCFA, monosaccharides, indole-SCFAs and phenolic compounds [205, 221]. Furthermore, the associations between the gut microbiota composition and host gene expression has been reported in multiple studies of model organisms and humans [371]. Nevertheless, our transcriptional dataset of whole cortical tissue was identified as weak due to the selected experimental design. Consequently, we suggested to investigate isolated cell populations to avoid signal dilution, which was suspected to have caused the low quality of the acquired dataset.

Finally, we validated through a FMT study that CRL's treatment effects in the gut were responsible for the beneficial effects observed in the brain of APP/PS1 mice. Antibiotic-depleted Wt mice receiving FMTs from CRL treated APP/PS1 and Wt as well as untreated Wt animals

showed improved memory when compared to antibiotic-depleted mice not receiving FMTs or FMTs from untreated APP/PS1 mice. Similarly, two studies have shown that GF APP/PS1 animals exhibit a drastic reduction in Aβ pathology and subsequently upon recolonization with fecal matter from Wt mice, a reduction in Aβ pathology compared to conventionally raised APP/PS1 mice [59, 139]. This suggests that the gut microbiota composition is important in determining the severity of AD-like pathology and supports our hypothesis that the observed treatment-dependent changes in the gut improved AD-like neuropathology.

As described in the introduction, no disease-modifying treatments are available to stop or slow the progression of AD pathology due to continuous failure of clinical trials to meet their primary endpoints [54]. Consequently, novel treatment strategies are needed and have been considered such as modulation of the gut microbiota composition by dietary changes [372]. This has been supported by numerous discoveries revealing the pivotal connection and modulating capacity between gut and brain functions and suggests that the gut microbiota might be critical for AD development and progression [129, 343, 373]. In this thesis, we presented the therapeutic potential of oral CRL administration in modulating nutritional availability in the gut and as a consequence improving gut microbiota composition and AD-like pathology. While the presented results in this thesis showed changes and normalization in regard to gut and peripheral parameters, the investigated neuropathological parameters (behavior and neuroinflammation) showed improvement but were still elevated compared to Wt controls. Therefore, we suggested that combined administration of a PAM of CRL activity with CRL might enhance the assessed treatment effects (hypothesis (3)).

To test this hypothesis, the *in silico* allosteric modulator screening was integrated with the developed miniaturized *in vitro* assay to identify PAMs of CRL activity. About 200, 000 natural compounds were composed in libraries and fitted in each of the three *in silico* selected allosteric

sites on CRL's surface. The library was reduced to 132 compounds due to duplicate removal, and availability limitations. 53 of these compounds were readily available and tested in the *in vitro* screening assay, which was optimized for CRL's substrate specificity and reaction conditions in the gut [186, 374]. While CRL was reported to have a preference for medium to long-chain fatty acids, we selected a butyrate conjugate due to solubility issues with longer-chain fatty acids [186]. Furthermore, we established 37ºC as reaction temperature and 7 for the reaction pH. Although the average pH of the mouse gastrointestinal tract is 6, pH 7 was selected based on the average pH in the human gastrointestinal tract, which represented the intended use of this treatment in humans, if the mouse were found to be successful [374]. As proof-of-concept, the assay performance was validated using the *in silico* identified inhibitor tropolone to assess the assays' ability to identify (inhibitor, enhancer, or no effect) and characterize (IC50/EC50, Km and Vmax) allosteric modulators of CRL. Next, the *in vitro* assay was used to characterize the 53 *in silico* identified modulators, which revealed five inhibitors and three enhancers. Determination of Kd and IC50/EC50 as well as Km and Vmax values identified NP-008496 as the strongest PAM.

However, subsequent investigation of the enhancer's effect on CRL activity at the *in vivo* administered dose (5000 FIP/kg) of Chapter III did not reveal an activity enhancing effect. Hence, we extrapolated from the EC50 assessment of Chapter IV the theoretical needed enhancer concentration to achieve 50 percent of CRL activity enhancement at a dose of 5000 FIP/kg CRL. The theoretical calculation suggested a required concentration of 500 µM of NP-008496, which was not available and additionally raised concerns about specificity and tolerability of the enhancer when administered in mice. Finally, we investigated whether the PAM enhanced endogenous lipase activity. This was supported by our finding that rutin inhibited CRL activity, which has been also reported to inhibit human pancreatic lipase [375]. Since we described a common binding strategy of rutin, cymaroside and NP-008496 to CRL's

screening site 3, we suggested that a potential structural similarity between CRL and human pancreatic lipase might exist that would allow NP-008496 enhancing human pancreatic lipase. However, no enhancing effect was observed when this hypothesis was tested. In summary, the data did not justify *in vivo* testing of hypothesis (3) at this point.

5.2 Limitations and future directions

The investigations of hypothesis (1) and (2) resulted in the proposed treatment associated pathway which included enhancement of the gut environment, the periphery and brain pathology (metabolic axis) in APP/PS1 mice. Nevertheless, based on the results and selected model of AD in this thesis, as well as the fact, that we were only able to investigate certain aspects of the disease model, these studies need to be validated and expanded. For instance, the transcriptomic analysis did not lead to the expected valuable insights and was therefore suggested to be repeated by a more targeted approach, where the transcriptome of isolated cell populations such as microglia and astrocytes will be investigated. Furthermore, the observed treatment effects as well as the elevated levels of UFAs in untreated APP/PS1 mice need to be further assessed to specify whether these findings were model-specific, time-point specific, or whether a broader underlying mechanism was responsible. To perform the analyses, we suggest including other mouse models of AD such as 5xFAD or 3xTg to reproduce our findings and support the treatment hypothesis. Furthermore, the assessment in other mouse models could include other aspects of AD pathology such as tau pathology or ApoE genotype status, which were not features of the APP/PS1 mouse model used in this thesis. This could expand the investigation of CRL's treatment effects and associated pathway on other AD-relevant aspects such as Tau pathology and ApoE isoform status. The ApoE isoform status might be of special interest since the isoforms determine the efficiency of ApoE as a cholesterol transporter [376]. Indeed, cholesterol transport was shown in Chapter III to be impacted by CRL treatment in the periphery

and could potentially affect lipid homeostasis in the brain, which has been shown to be disturbed in AD [377, 378].

Time-point of administration is another important factor in enhancing translation of the treatment strategy into clinical applications. Recently, an increased number of studies have been suggesting that earlier interventions and treatments might be more successful in modulating disease pathology [379, 380]. The investigation of more than one time-point will therefore define the treatment window in which CRL administration could reduce AD pathology. The time-point in Chapter III was selected due to the suggestion that AD patients at the equivalent human time-point might self-observe memory deficits, and hence, report to their doctors to allow disease classification and treatment. Assessment of CRL administration at earlier and later time-points would aid in determining CRL's efficiency in the various stages of AD progression and its potential as preventative or late treatment strategy in AD. For instance, if the observed treatment-dependent normalization of plasma UFA levels would be the critical element for evoking CRL's beneficial effects in the brain, the time-point of treatment would need to be synchronized in the clinic with the occurrence of UFA elevation in AD patients. In conclusion, CRL's contribution to the reduction of UFA levels and AD pathology in APP/PS1 mice needs to be further examined.

A comprehensive understanding of the propagation of CRL's treatment effects will be necessary to successfully use CRL in clinical applications. The proposed additional investigations will enhance our understanding of the treatment mechanism and improve treatment efficiency. The proposed experiments are projected to: (1) establish parameters as components of the proposed treatment mechanism if findings can be replicated in other mouse models of AD; (2) exclude parameters if observations of this thesis cannot be replicated in other mouse models of AD; and (3) specify the CRL treatment window in AD progression. Hence, the probability of

encountering failure to translate this AD treatment strategy from mouse models into the clinic would be reduced.

While we did examine some treatment-dependent parameters in APP/PS1 mice, we did not cover all possible targets due to a missing specific hypothesis supporting their examination, which was required for a target to be considered for study in this thesis. However, after data analysis, some of these excluded components were shown to be potentially important in achieving the observed treatment benefits. For instance, while we did not investigate the role of the vagal axis in the propagation of treatment effects, data analysis of gut pathological changes post CRL treatment suggested a potential impact of this axis on the observed benefits. Specifically, the increase in indole derivatives (cecal metabolomics) which have been reported to modulate vagal signaling into the brain, suggested a potential contribution of the vagus nerve to treatment efficiency [381, 382]. The analysis of the whole cortical transcriptome was hypothesized to reveal a potential contribution of the vagal axis to treatment benefits and their propagation but did not reveal differentially expressed genes. We concluded that the cortical transcripts were impacted by transcript dilution through other cell types such as neurons, which was hypothesized due to the shown trends and significant changes in cell-specific markers not reaching significance in the dataset. Therefore, we suggested analysis of gene transcripts of isolated cortical but also hippocampal astrocyte and microglia populations since both tissues showed a reduction in neuroinflammation. The addition of hippocampus-derived glia might reveal further insights on how the improvement of memory was achieved in APP/PS1 mice post treatment since the hippocampus is essential for long-term memory formation [383]. This will allow assessment of treatment-dependent alterations of gene expression and identify differentially regulated signaling pathways in these cell populations. Furthermore, this will enhance the multi-omics integration analysis and potentially reveal a more detailed pathway of treatment action. Also, subdiaphragmatic vagotomy or deafferentation of vagal afferent fibers

by injection saponin-conjugated CCK into the nodose ganglia could be included as an additional approach. Sub-diaphragmatic vagotomy would support the assessment of whether the treatment-dependent benefits are still observed in the brain similar to an experiment conducted in a mouse model of PD, which have shown the gut-to-brain transmission of α-synuclein was disabled after the vagotomy was conducted [72]. Saponin-conjugated CCK can be used to determine the direction of the treatment effect by inhibiting only afferent transmission [384].

To expand the analysis of the metabolic transmission route, we propose a lipidomic analysis of the plasma of *Study 1* in Chapter II to expand the multi-omics analysis. The used untargeted metabolomic examination showed increased plasma UFA levels in untreated APP/PS1 mice but did not cover all lipid species. This lipidomic approach may reveal further details about the propagation from treatment-dependent gut alterations into the brain and enhance the proposed hypothesis describing the potential treatment pathway. In addition, the analysis could be preceded by investigating treatment-dependent alterations of lipid profiles in the brain of APP/PS1 mice, which have exhibited a disturbed cholesterol metabolism similarly to AD patients [385-387].

Furthermore, the results could be validated by oral administration of metabolites (e.g. UFA, SFA, glycerol) and microbial species (e.g. *Acetatifactor*), which were identified to be in the gut of APP/PS1 mice post CRL treatment. This would lead to determination of the drivers of the observed benefits and potentially improve the treatment strategy. Similarly, investigation of hypothesis (3) could further contribute to enhancement of the treatment strategy. Since we were not able to develop a compound to be readily used *in vivo,* structure-activity relationship (SAR) could be used to optimize the chemical structure of NP-008496 [388]. This could identify the interaction relevant sub-structures and allow chemical modification of the interaction-relevant groups to increase binding affinity of PAM to CRL's allosteric site. In addition, the list of

identified modulators could be re-assessed, and non-natural molecules could be added to enhance the library's diversity and identify new PAMs.

The three cornerstones: reproducibility, treatment time-point and treatment mechanism will enhance our understanding of the treatment strategy and its subsequent translation into the clinic. Furthermore, assessment of treatment enhancing strategies will advance the gut-related treatment strategy and potentially reveal additional opportunities to target AD pathology. However, given that gut microbiome composition and gastrointestinal tract physiology and anatomy differ significantly between mice and humans, the observations gained from this thesis need to be further validated in human subjects before these findings can be extrapolated to human use or to AD patients for clinical trials [389].

In conclusion, this series of studies highlights the potential of an exogenously administered lipase in restoring gut microbiota and metabolite composition and in ameliorating AD pathology in a mouse model of AD. The results of hypothesis (1) and (2) presented evidence in support of the main hypothesis, but the results need to be further validated to strengthen the conclusions and to facilitate translation into humans in future studies. Finally, we highlighted the critical role of the gut microbiome in brain health and potentially revealed a treatment mechanism applicable to other neurodegenerative diseases supporting progression of AD research.

References

1. Alzheimer, A., et al., *An English translation of Alzheimer's 1907 paper, "Uber eine eigenartige Erkankung der Hirnrinde".* Clin Anat, 1995. **8**(6): p. 429-31.
2. Yegambaram, M., et al., *Role of environmental contaminants in the etiology of Alzheimer's disease: a review.* Curr Alzheimer Res, 2015. **12**(2): p. 116-46.
3. Harman, D., *Alzheimer's disease pathogenesis: role of aging.* Ann N Y Acad Sci, 2006. **1067**: p. 454-60.
4. Corder, E.H., et al., *Gene dose of apolipoprotein E type 4 allele and the risk of Alzheimer's disease in late onset families.* Science, 1993. **261**(5123): p. 921-3.
5. Farrer, L.A., et al., *Effects of age, sex, and ethnicity on the association between apolipoprotein E genotype and Alzheimer disease. A meta-analysis. APOE and Alzheimer Disease Meta Analysis Consortium.* JAMA, 1997. **278**(16): p. 1349-56.
6. Strittmatter, W.J., et al., *Apolipoprotein E: high-avidity binding to beta-amyloid and increased frequency of type 4 allele in late-onset familial Alzheimer disease.* Proc Natl Acad Sci U S A, 1993. **90**(5): p. 1977-81.
7. Liao, F., H. Yoon, and J. Kim, *Apolipoprotein E metabolism and functions in brain and its role in Alzheimer's disease.* Curr Opin Lipidol, 2017. **28**(1): p. 60-67.
8. Ashford, J.W. and J.A. Mortimer, *Non-familial Alzheimer's disease is mainly due to genetic factors.* J Alzheimers Dis, 2002. **4**(3): p. 169-77.
9. Nicolas, M. and B.A. Hassan, *Amyloid precursor protein and neural development.* Development, 2014. **141**(13): p. 2543-8.
10. Shen, J. and R.J. Kelleher, 3rd, *The presenilin hypothesis of Alzheimer's disease: evidence for a loss-of-function pathogenic mechanism.* Proc Natl Acad Sci U S A, 2007. **104**(2): p. 403-9.
11. Masters, C.L., et al., *Alzheimer's disease.* Nature Reviews Disease Primers, 2015. **1**(1).
12. Smith, A.D., *Imaging the progression of Alzheimer pathology through the brain.* Proc Natl Acad Sci U S A, 2002. **99**(7): p. 4135-7.
13. Verri, M., et al., *Mitochondrial alterations, oxidative stress and neuroinflammation in Alzheimer's disease.* Int J Immunopathol Pharmacol, 2012. **25**(2): p. 345-53.
14. Brier, M.R., et al., *Tau and Abeta imaging, CSF measures, and cognition in Alzheimer's disease.* Sci Transl Med, 2016. **8**(338): p. 338ra66.
15. Simen, A.A., et al., *Cognitive dysfunction with aging and the role of inflammation.* Ther Adv Chronic Dis, 2011. **2**(3): p. 175-95.
16. Bayer, T.A., et al., *It all sticks together--the APP-related family of proteins and Alzheimer's disease.* Mol Psychiatry, 1999. **4**(6): p. 524-8.
17. Frost, G.R. and Y.M. Li, *The role of astrocytes in amyloid production and Alzheimer's disease.* Open Biol, 2017. **7**(12).
18. O'Brien, R.J. and P.C. Wong, *Amyloid precursor protein processing and Alzheimer's disease.* Annu Rev Neurosci, 2011. **34**: p. 185-204.
19. Lesne, S., et al., *A specific amyloid-beta protein assembly in the brain impairs memory.* Nature, 2006. **440**(7082): p. 352-7.
20. Walsh, D.M., et al., *Naturally secreted oligomers of amyloid beta protein potently inhibit hippocampal long-term potentiation in vivo.* Nature, 2002. **416**(6880): p. 535-9.
21. Lambert, M.P., et al., *Diffusible, nonfibrillar ligands derived from Abeta1-42 are potent central nervous system neurotoxins.* Proc Natl Acad Sci U S A, 1998. **95**(11): p. 6448-53.
22. Mullan, M., et al., *A pathogenic mutation for probable Alzheimer's disease in the APP gene at the N-terminus of beta-amyloid.* Nat Genet, 1992. **1**(5): p. 345-7.

23. Grabowski, T.J., et al., *Novel amyloid precursor protein mutation in an Iowa family with dementia and severe cerebral amyloid angiopathy.* Ann Neurol, 2001. **49**(6): p. 697-705.
24. Levy, E., et al., *Mutation of the Alzheimer's disease amyloid gene in hereditary cerebral hemorrhage, Dutch type.* Science, 1990. **248**(4959): p. 1124-6.
25. Murrell, J., et al., *A mutation in the amyloid precursor protein associated with hereditary Alzheimer's disease.* Science, 1991. **254**(5028): p. 97-9.
26. Perez-Tur, J., et al., *A mutation in Alzheimer's disease destroying a splice acceptor site in the presenilin-1 gene.* Neuroreport, 1995. **7**(1): p. 297-301.
27. Campion, D., et al., *Mutations of the presenilin I gene in families with early-onset Alzheimer's disease.* Hum Mol Genet, 1995. **4**(12): p. 2373-7.
28. Huang, Y.-r. and R.-t. Liu, *The Toxicity and Polymorphism of β-Amyloid Oligomers.* International Journal of Molecular Sciences, 2020. **21**(12).
29. Cummings, J., et al., *Alzheimer's disease drug development pipeline: 2019.* Alzheimers Dement (N Y), 2019. **5**: p. 272-293.
30. Mehta, D., et al., *Why do trials for Alzheimer's disease drugs keep failing? A discontinued drug perspective for 2010-2015.* Expert Opin Investig Drugs, 2017. **26**(6): p. 735-739.
31. Imbimbo, B.P. and M. Watling, *Investigational BACE inhibitors for the treatment of Alzheimer's disease.* Expert Opin Investig Drugs, 2019. **28**(11): p. 967-975.
32. Arboleda-Velasquez, J.F., et al., *Resistance to autosomal dominant Alzheimer's disease in an APOE3 Christchurch homozygote: a case report.* Nat Med, 2019. **25**(11): p. 1680-1683.
33. Kaufmann, S.H., *The contribution of immunology to the rational design of novel antibacterial vaccines.* Nat Rev Microbiol, 2007. **5**(7): p. 491-504.
34. Hansen, D.V., J.E. Hanson, and M. Sheng, *Microglia in Alzheimer's disease.* J Cell Biol, 2018. **217**(2): p. 459-472.
35. Verheijen, J. and K. Sleegers, *Understanding Alzheimer Disease at the Interface between Genetics and Transcriptomics.* Trends Genet, 2018. **34**(6): p. 434-447.
36. Hemonnot, A.L., et al., *Microglia in Alzheimer Disease: Well-Known Targets and New Opportunities.* Front Aging Neurosci, 2019. **11**: p. 233.
37. Kettenmann, H., et al., *Physiology of microglia.* Physiol Rev, 2011. **91**(2): p. 461-553.
38. Prinz, M. and J. Priller, *Microglia and brain macrophages in the molecular age: from origin to neuropsychiatric disease.* Nat Rev Neurosci, 2014. **15**(5): p. 300-12.
39. Schafer, D.P. and B. Stevens, *Phagocytic glial cells: sculpting synaptic circuits in the developing nervous system.* Curr Opin Neurobiol, 2013. **23**(6): p. 1034-40.
40. Stratoulias, V., et al., *Microglial subtypes: diversity within the microglial community.* EMBO J, 2019. **38**(17): p. e101997.
41. Bolos, M., J.R. Perea, and J. Avila, *Alzheimer's disease as an inflammatory disease.* Biomol Concepts, 2017. **8**(1): p. 37-43.
42. Verkhratsky, A., et al., *Astroglia dynamics in ageing and Alzheimer's disease.* Curr Opin Pharmacol, 2016. **26**: p. 74-9.
43. Navarro, V., et al., *Microglia in Alzheimer's Disease: Activated, Dysfunctional or Degenerative.* Front Aging Neurosci, 2018. **10**: p. 140.
44. Mandrekar-Colucci, S. and G.E. Landreth, *Microglia and inflammation in Alzheimer's disease.* CNS Neurol Disord Drug Targets, 2010. **9**(2): p. 156-67.
45. Acosta, C., H.D. Anderson, and C.M. Anderson, *Astrocyte dysfunction in Alzheimer disease.* J Neurosci Res, 2017. **95**(12): p. 2430-2447.
46. Sofroniew, M.V., *Molecular dissection of reactive astrogliosis and glial scar formation.* Trends Neurosci, 2009. **32**(12): p. 638-47.

47. Ingelsson, M., et al., *Early Abeta accumulation and progressive synaptic loss, gliosis, and tangle formation in AD brain.* Neurology, 2004. **62**(6): p. 925-31.
48. Serrano-Pozo, A., et al., *Reactive glia not only associates with plaques but also parallels tangles in Alzheimer's disease.* Am J Pathol, 2011. **179**(3): p. 1373-84.
49. Hsiao, K., et al., *Correlative memory deficits, Abeta elevation, and amyloid plaques in transgenic mice.* Science, 1996. **274**(5284): p. 99-102.
50. Radde, R., et al., *Abeta42-driven cerebral amyloidosis in transgenic mice reveals early and robust pathology.* EMBO Rep, 2006. **7**(9): p. 940-6.
51. Bittner, T., et al., *Amyloid plaque formation precedes dendritic spine loss.* Acta Neuropathol, 2012. **124**(6): p. 797-807.
52. Lee, S., et al., *CX3CR1 deficiency alters microglial activation and reduces beta-amyloid deposition in two Alzheimer's disease mouse models.* Am J Pathol, 2010. **177**(5): p. 2549-62.
53. Ferretti, L., et al., *Anxiety and Alzheimer's disease.* J Geriatr Psychiatry Neurol, 2001. **14**(1): p. 52-8.
54. Oxford, A.E., E.S. Stewart, and T.T. Rohn, *Clinical Trials in Alzheimer's Disease: A Hurdle in the Path of Remedy.* Int J Alzheimers Dis, 2020. **2020**: p. 5380346.
55. Kelley, B.J. and D.S. Knopman, *Alternative medicine and Alzheimer disease.* Neurologist, 2008. **14**(5): p. 299-306.
56. Scarmeas, N., et al., *Mediterranean diet and risk for Alzheimer's disease.* Ann Neurol, 2006. **59**(6): p. 912-21.
57. Radak, Z., et al., *Exercise plays a preventive role against Alzheimer's disease.* J Alzheimers Dis, 2010. **20**(3): p. 777-83.
58. Ansari, N. and F. Khodagholi, *Natural products as promising drug candidates for the treatment of Alzheimer's disease: molecular mechanism aspect.* Curr Neuropharmacol, 2013. **11**(4): p. 414-29.
59. Harach, T., et al., *Reduction of Abeta amyloid pathology in APPPS1 transgenic mice in the absence of gut microbiota.* Sci Rep, 2017. **7**: p. 41802.
60. Vogt, N.M., et al., *Gut microbiome alterations in Alzheimer's disease.* Sci Rep, 2017. **7**(1): p. 13537.
61. Rinninella, E., et al., *What is the Healthy Gut Microbiota Composition? A Changing Ecosystem across Age, Environment, Diet, and Diseases.* Microorganisms, 2019. **7**(1).
62. Mark Welch, J.L., et al., *Spatial organization of a model 15-member human gut microbiota established in gnotobiotic mice.* Proc Natl Acad Sci U S A, 2017. **114**(43): p. E9105-E9114.
63. Mark Welch, J.L., et al., *Biogeography of a human oral microbiome at the micron scale.* Proc Natl Acad Sci U S A, 2016. **113**(6): p. E791-800.
64. Bengmark, S., *Gut microbiota, immune development and function.* Pharmacol Res, 2013. **69**(1): p. 87-113.
65. Devos, D., et al., *Colonic inflammation in Parkinson's disease.* Neurobiol Dis, 2013. **50**: p. 42-8.
66. !!! INVALID CITATION !!! [75, 76].
67. Kaelberer, M.M., et al., *A gut-brain neural circuit for nutrient sensory transduction.* Science, 2018. **361**(6408).
68. Greiner, T.U. and F. Backhed, *Microbial regulation of GLP-1 and L-cell biology.* Mol Metab, 2016. **5**(9): p. 753-8.
69. Fukui, H., X. Xu, and H. Miwa, *Role of Gut Microbiota-Gut Hormone Axis in the Pathophysiology of Functional Gastrointestinal Disorders.* J Neurogastroenterol Motil, 2018. **24**(3): p. 367-386.

70. Forsythe, P., J. Bienenstock, and W.A. Kunze, *Vagal pathways for microbiome-brain-gut axis communication.* Adv Exp Med Biol, 2014. **817**: p. 115-33.
71. Bravo, J.A., et al., *Ingestion of Lactobacillus strain regulates emotional behavior and central GABA receptor expression in a mouse via the vagus nerve.* Proc Natl Acad Sci U S A, 2011. **108**(38): p. 16050-5.
72. Kim, S., et al., *Transneuronal Propagation of Pathologic alpha-Synuclein from the Gut to the Brain Models Parkinson's Disease.* Neuron, 2019. **103**(4): p. 627-641 e7.
73. Sudo, N., et al., *Postnatal microbial colonization programs the hypothalamic-pituitary-adrenal system for stress response in mice.* J Physiol, 2004. **558**(Pt 1): p. 263-75.
74. Barrett, E., et al., *gamma-Aminobutyric acid production by culturable bacteria from the human intestine.* J Appl Microbiol, 2012. **113**(2): p. 411-7.
75. Lyte, M., *Probiotics function mechanistically as delivery vehicles for neuroactive compounds: Microbial endocrinology in the design and use of probiotics.* Bioessays, 2011. **33**(8): p. 574-81.
76. Burokas, A., et al., *Microbiota regulation of the Mammalian gut-brain axis.* Adv Appl Microbiol, 2015. **91**: p. 1-62.
77. Ochoa-Reparaz, J., et al., *Gut, bugs, and brain: role of commensal bacteria in the control of central nervous system disease.* Ann Neurol, 2011. **69**(2): p. 240-7.
78. Hueston, C.M. and T. Deak, *The inflamed axis: the interaction between stress, hormones, and the expression of inflammatory-related genes within key structures comprising the hypothalamic-pituitary-adrenal axis.* Physiol Behav, 2014. **124**: p. 77-91.
79. Gaboriau-Routhiau, V., et al., *The key role of segmented filamentous bacteria in the coordinated maturation of gut helper T cell responses.* Immunity, 2009. **31**(4): p. 677-89.
80. Ivanov, II, et al., *Specific microbiota direct the differentiation of IL-17-producing T-helper cells in the mucosa of the small intestine.* Cell Host Microbe, 2008. **4**(4): p. 337-49.
81. Macpherson, A.J. and N.L. Harris, *Interactions between commensal intestinal bacteria and the immune system.* Nat Rev Immunol, 2004. **4**(6): p. 478-85.
82. Gordon, S. and F.O. Martinez, *Alternative activation of macrophages: mechanism and functions.* Immunity, 2010. **32**(5): p. 593-604.
83. Mosser, D.M. and J.P. Edwards, *Exploring the full spectrum of macrophage activation.* Nat Rev Immunol, 2008. **8**(12): p. 958-69.
84. Macpherson, A.J. and T. Uhr, *Induction of protective IgA by intestinal dendritic cells carrying commensal bacteria.* Science, 2004. **303**(5664): p. 1662-5.
85. Chaudhry, A., et al., *Interleukin-10 signaling in regulatory T cells is required for suppression of Th17 cell-mediated inflammation.* Immunity, 2011. **34**(4): p. 566-78.
86. Zeng, H. and H. Chi, *Metabolic control of regulatory T cell development and function.* Trends Immunol, 2015. **36**(1): p. 3-12.
87. Salomon, B., et al., *B7/CD28 costimulation is essential for the homeostasis of the CD4+CD25+ immunoregulatory T cells that control autoimmune diabetes.* Immunity, 2000. **12**(4): p. 431-40.
88. Tang, Q., et al., *Cutting edge: CD28 controls peripheral homeostasis of CD4+CD25+ regulatory T cells.* J Immunol, 2003. **171**(7): p. 3348-52.
89. Russler-Germain, E.V., S. Rengarajan, and C.S. Hsieh, *Antigen-specific regulatory T-cell responses to intestinal microbiota.* Mucosal Immunol, 2017. **10**(6): p. 1375-1386.

90. Zhang, Z., et al., *Demystifying the manipulation of host immunity, metabolism, and extraintestinal tumors by the gut microbiome.* Signal Transduct Target Ther, 2019. **4**: p. 41.
91. Iacob, S. and D.G. Iacob, *Infectious Threats, the Intestinal Barrier, and Its Trojan Horse: Dysbiosis.* Front Microbiol, 2019. **10**: p. 1676.
92. Genua, F., et al., *The Role of Gut Barrier Dysfunction and Microbiome Dysbiosis in Colorectal Cancer Development.* Front Oncol, 2021. **11**: p. 626349.
93. Man, A.L., et al., *Age-associated modifications of intestinal permeability and innate immunity in human small intestine.* Clin Sci (Lond), 2015. **129**(7): p. 515-27.
94. Parker, A., S. Fonseca, and S.R. Carding, *Gut microbes and metabolites as modulators of blood-brain barrier integrity and brain health.* Gut Microbes, 2019: p. 1-23.
95. Kohler, C.A., et al., *The Gut-Brain Axis, Including the Microbiome, Leaky Gut and Bacterial Translocation: Mechanisms and Pathophysiological Role in Alzheimer's Disease.* Curr Pharm Des, 2016. **22**(40): p. 6152-6166.
96. Zhao, Y., V. Jaber, and W.J. Lukiw, *Secretory Products of the Human GI Tract Microbiome and Their Potential Impact on Alzheimer's Disease (AD): Detection of Lipopolysaccharide (LPS) in AD Hippocampus.* Front Cell Infect Microbiol, 2017. **7**: p. 318.
97. Fu, S.P., et al., *Anti-inflammatory effects of BHBA in both in vivo and in vitro Parkinson's disease models are mediated by GPR109A-dependent mechanisms.* J Neuroinflammation, 2015. **12**: p. 9.
98. Park, J., et al., *Bidirectional regulatory potentials of short-chain fatty acids and their G-protein-coupled receptors in autoimmune neuroinflammation.* Sci Rep, 2019. **9**(1): p. 8837.
99. Han, A., et al., *Butyrate decreases its own oxidation in colorectal cancer cells through inhibition of histone deacetylases.* Oncotarget, 2018. **9**(43): p. 27280-27292.
100. Kimura, I., et al., *The SCFA Receptor GPR43 and Energy Metabolism.* Front Endocrinol (Lausanne), 2014. **5**: p. 85.
101. Tolhurst, G., et al., *Short-chain fatty acids stimulate glucagon-like peptide-1 secretion via the G-protein-coupled receptor FFAR2.* Diabetes, 2012. **61**(2): p. 364-71.
102. Fumagalli, M., et al., *How to reprogram microglia toward beneficial functions.* Glia, 2018. **66**(12): p. 2531-2549.
103. Tan, J., et al., *Dietary Fiber and Bacterial SCFA Enhance Oral Tolerance and Protect against Food Allergy through Diverse Cellular Pathways.* Cell Rep, 2016. **15**(12): p. 2809-24.
104. Gao, J., et al., *Impact of the Gut Microbiota on Intestinal Immunity Mediated by Tryptophan Metabolism.* Front Cell Infect Microbiol, 2018. **8**: p. 13.
105. Zhang, L.S. and S.S. Davies, *Microbial metabolism of dietary components to bioactive metabolites: opportunities for new therapeutic interventions.* Genome Med, 2016. **8**(1): p. 46.
106. Rothhammer, V., et al., *Type I interferons and microbial metabolites of tryptophan modulate astrocyte activity and central nervous system inflammation via the aryl hydrocarbon receptor.* Nat Med, 2016. **22**(6): p. 586-97.
107. Powell, D.N., et al., *Indoles from the commensal microbiota act via the AHR and IL-10 to tune the cellular composition of the colonic epithelium during aging.* Proc Natl Acad Sci U S A, 2020. **117**(35): p. 21519-21526.
108. Carabotti, M., et al., *The gut-brain axis: interactions between enteric microbiota, central and enteric nervous systems.* Ann Gastroenterol, 2015. **28**(2): p. 203-209.
109. Paone, P. and P.D. Cani, *Mucus barrier, mucins and gut microbiota: the expected slimy partners?* Gut, 2020. **69**(12): p. 2232-2243.

110. Crespo-Piazuelo, D., et al., *Characterization of bacterial microbiota compositions along the intestinal tract in pigs and their interactions and functions.* Sci Rep, 2018. **8**(1): p. 12727.
111. Okumura, R. and K. Takeda, *Roles of intestinal epithelial cells in the maintenance of gut homeostasis.* Exp Mol Med, 2017. **49**(5): p. e338.
112. Logsdon, A.F., et al., *Gut reactions: How the blood-brain barrier connects the microbiome and the brain.* Exp Biol Med (Maywood), 2018. **243**(2): p. 159-165.
113. Huuskonen, J., et al., *Regulation of microglial inflammatory response by sodium butyrate and short-chain fatty acids.* Br J Pharmacol, 2004. **141**(5): p. 874-80.
114. Garcez, M.L., et al., *Sodium Butyrate and Indole-3-propionic Acid Prevent the Increase of Cytokines and Kynurenine Levels in LPS-induced Human Primary Astrocytes.* Int J Tryptophan Res, 2020. **13**: p. 1178646920978404.
115. Negatu, D.A., et al., *Indole Propionic Acid, an Unusual Antibiotic Produced by the Gut Microbiota, With Anti-inflammatory and Antioxidant Properties.* Front Microbiol, 2020. **11**: p. 575586.
116. Wang, Y., et al., *The Gut-Microglia Connection: Implications for Central Nervous System Diseases.* Front Immunol, 2018. **9**: p. 2325.
117. Song, L., et al., *NLRP3 Inflammasome in Neurological Diseases, from Functions to Therapies.* Front Cell Neurosci, 2017. **11**: p. 63.
118. Rahman, M., et al., *The beta-hydroxybutyrate receptor HCA2 activates a neuroprotective subset of macrophages.* Nat Commun, 2014. **5**: p. 3944.
119. Wheeler, M.A., V. Rothhammer, and F.J. Quintana, *Control of immune-mediated pathology via the aryl hydrocarbon receptor.* J Biol Chem, 2017. **292**(30): p. 12383-12389.
120. Lee, H.U., et al., *Host-microbiome interactions: the aryl hydrocarbon receptor and the central nervous system.* J Mol Med (Berl), 2017. **95**(1): p. 29-39.
121. Ronaldson, P.T. and T.P. Davis, *Blood-brain barrier integrity and glial support: mechanisms that can be targeted for novel therapeutic approaches in stroke.* Curr Pharm Des, 2012. **18**(25): p. 3624-44.
122. Lecuyer, M.A., H. Kebir, and A. Prat, *Glial influences on BBB functions and molecular players in immune cell trafficking.* Biochim Biophys Acta, 2016. **1862**(3): p. 472-82.
123. Hill-Burns, E.M., et al., *Parkinson's disease and Parkinson's disease medications have distinct signatures of the gut microbiome.* Mov Disord, 2017. **32**(5): p. 739-749.
124. Strati, F., et al., *New evidences on the altered gut microbiota in autism spectrum disorders.* Microbiome, 2017. **5**(1): p. 24.
125. Lane, E.R., T.L. Zisman, and D.L. Suskind, *The microbiota in inflammatory bowel disease: current and therapeutic insights.* J Inflamm Res, 2017. **10**: p. 63-73.
126. Dinan, T.G. and J.F. Cryan, *Gut instincts: microbiota as a key regulator of brain development, ageing and neurodegeneration.* J Physiol, 2017. **595**(2): p. 489-503.
127. Walker, K.A., *Inflammation and neurodegeneration: chronicity matters.* Aging (Albany NY), 2018. **11**(1): p. 3-4.
128. Sampson, T.R., et al., *Gut Microbiota Regulate Motor Deficits and Neuroinflammation in a Model of Parkinson's Disease.* Cell, 2016. **167**(6): p. 1469-1480 e12.
129. Kowalski, K. and A. Mulak, *Brain-Gut-Microbiota Axis in Alzheimer's Disease.* J Neurogastroenterol Motil, 2019. **25**(1): p. 48-60.
130. Coretti, L., et al., *Gut Microbiota Features in Young Children With Autism Spectrum Disorders.* Front Microbiol, 2018. **9**: p. 3146.
131. Coretti, L., et al., *Corrigendum: Gut Microbiota Features in Young Children With Autism Spectrum Disorders.* Front Microbiol, 2019. **10**: p. 920.

132. Kang, D.W., et al., *Long-term benefit of Microbiota Transfer Therapy on autism symptoms and gut microbiota.* Sci Rep, 2019. **9**(1): p. 5821.
133. Yong, S.J., et al., *Antidepressive Mechanisms of Probiotics and Their Therapeutic Potential.* Front Neurosci, 2019. **13**: p. 1361.
134. Bellou, V., et al., *Systematic evaluation of the associations between environmental risk factors and dementia: An umbrella review of systematic reviews and meta-analyses.* Alzheimers Dement, 2017. **13**(4): p. 406-418.
135. Iber, F.L., P.A. Murphy, and E.S. Connor, *Age-related changes in the gastrointestinal system. Effects on drug therapy.* Drugs Aging, 1994. **5**(1): p. 34-48.
136. Xia, X., et al., *Aging and Alzheimer's disease: Comparison and associations from molecular to system level.* Aging Cell, 2018. **17**(5): p. e12802.
137. Goldberg, E.L. and V.D. Dixit, *Drivers of age-related inflammation and strategies for healthspan extension.* Immunol Rev, 2015. **265**(1): p. 63-74.
138. Thevaranjan, N., et al., *Age-Associated Microbial Dysbiosis Promotes Intestinal Permeability, Systemic Inflammation, and Macrophage Dysfunction.* Cell Host Microbe, 2018. **23**(4): p. 570.
139. Sun, J., et al., *Fecal microbiota transplantation alleviated Alzheimer's disease-like pathogenesis in APP/PS1 transgenic mice.* Transl Psychiatry, 2019. **9**(1): p. 189.
140. D'Amato, A., et al., *Faecal microbiota transplant from aged donor mice affects spatial learning and memory via modulating hippocampal synaptic plasticity- and neurotransmission-related proteins in young recipients.* Microbiome, 2020. **8**(1): p. 140.
141. Bonotis, K., et al., *Systemic immune aberrations in Alzheimer's disease patients.* J Neuroimmunol, 2008. **193**(1-2): p. 183-7.
142. Walker, K.A., et al., *The association of mid-to late-life systemic inflammation with white matter structure in older adults: The Atherosclerosis Risk in Communities Study.* Neurobiol Aging, 2018. **68**: p. 26-33.
143. Bowman, G.L., et al., *Blood-brain barrier impairment in Alzheimer disease: stability and functional significance.* Neurology, 2007. **68**(21): p. 1809-14.
144. Zhao, Y., et al., *Microbiome-Derived Lipopolysaccharide Enriched in the Perinuclear Region of Alzheimer's Disease Brain.* Front Immunol, 2017. **8**: p. 1064.
145. Jiang, C., et al., *The Gut Microbiota and Alzheimer's Disease.* J Alzheimers Dis, 2017. **58**(1): p. 1-15.
146. Gong, D., et al., *Involvement of Reduced Microbial Diversity in Inflammatory Bowel Disease.* Gastroenterol Res Pract, 2016. **2016**: p. 6951091.
147. Kano, O., et al., *Domperidone effective in preventing rivastigmine-related gastrointestinal disturbances in patients with Alzheimer's disease.* Neuropsychiatr Dis Treat, 2013. **9**: p. 1411-5.
148. Nikolova, V., et al., *Gut feeling: randomized controlled trials of probiotics for the treatment of clinical depression: Systematic review and meta-analysis.* Ther Adv Psychopharmacol, 2019. **9**: p. 2045125319859963.
149. Genedi, M., et al., *Dysregulation of the gut-brain axis in schizophrenia and bipolar disorder: probiotic supplementation as a supportive treatment in psychiatric disorders.* Curr Opin Psychiatry, 2019. **32**(3): p. 185-195.
150. Roberfroid, M.B. and N.M. Delzenne, *Dietary fructans.* Annu Rev Nutr, 1998. **18**: p. 117-43.
151. Lecerf, J.M., et al., *Xylo-oligosaccharide (XOS) in combination with inulin modulates both the intestinal environment and immune status in healthy subjects, while XOS alone only shows prebiotic properties.* Br J Nutr, 2012. **108**(10): p. 1847-58.

152. Ramirez-Farias, C., et al., *Effect of inulin on the human gut microbiota: stimulation of Bifidobacterium adolescentis and Faecalibacterium prausnitzii.* Br J Nutr, 2009. **101**(4): p. 541-50.
153. Davis, L.M., et al., *Barcoded pyrosequencing reveals that consumption of galactooligosaccharides results in a highly specific bifidogenic response in humans.* PLoS One, 2011. **6**(9): p. e25200.
154. Ashraf, R. and N.P. Shah, *Immune system stimulation by probiotic microorganisms.* Crit Rev Food Sci Nutr, 2014. **54**(7): p. 938-56.
155. Boger, M.C.L., A. Lammerts van Bueren, and L. Dijkhuizen, *Cross-Feeding among Probiotic Bacterial Strains on Prebiotic Inulin Involves the Extracellular exo-Inulinase of Lactobacillus paracasei Strain W20.* Appl Environ Microbiol, 2018. **84**(21).
156. Soto, A., et al., *Lactobacilli and bifidobacteria in human breast milk: influence of antibiotherapy and other host and clinical factors.* J Pediatr Gastroenterol Nutr, 2014. **59**(1): p. 78-88.
157. Spacova, I., et al., *Future of Probiotics and Prebiotics and the Implications for Early Career Researchers.* Front Microbiol, 2020. **11**: p. 1400.
158. Ma, C., et al., *The gut microbiome stability is altered by probiotic ingestion and improved by the continuous supplementation of galactooligosaccharide.* Gut Microbes, 2020. **12**(1): p. 1785252.
159. Biagioli, M., et al., *Divergent Effectiveness of Multispecies Probiotic Preparations on Intestinal Microbiota Structure Depends on Metabolic Properties.* Nutrients, 2019. **11**(2).
160. Rehman, A., et al., *Effects of probiotics and antibiotics on the intestinal homeostasis in a computer controlled model of the large intestine.* BMC Microbiology, 2012. **12**(1).
161. Blaabjerg, S., D.M. Artzi, and R. Aabenhus, *Probiotics for the Prevention of Antibiotic-Associated Diarrhea in Outpatients-A Systematic Review and Meta-Analysis.* Antibiotics (Basel), 2017. **6**(4).
162. Looft, T. and H.K. Allen, *Collateral effects of antibiotics on mammalian gut microbiomes.* Gut Microbes, 2012. **3**(5): p. 463-7.
163. Nitzan, O., et al., *Role of antibiotics for treatment of inflammatory bowel disease.* World J Gastroenterol, 2016. **22**(3): p. 1078-87.
164. Kuhn, M., et al., *Long term antibiotic therapy may be an effective treatment for children co-morbid with Lyme disease and autism spectrum disorder.* Med Hypotheses, 2012. **78**(5): p. 606-15.
165. Kapel, N., et al., *Practical implementation of faecal transplantation.* Clin Microbiol Infect, 2014. **20**(11): p. 1098-105.
166. Brandt, L.J., *Fecal transplantation for the treatment of Clostridium difficile infection.* Gastroenterol Hepatol (N Y), 2012. **8**(3): p. 191-4.
167. Wilson, B.C., et al., *The Super-Donor Phenomenon in Fecal Microbiota Transplantation.* Front Cell Infect Microbiol, 2019. **9**: p. 2.
168. Kang, D.W., et al., *Microbiota Transfer Therapy alters gut ecosystem and improves gastrointestinal and autism symptoms: an open-label study.* Microbiome, 2017. **5**(1): p. 10.
169. Somaraju, U.R. and A. Solis-Moya, *Pancreatic enzyme replacement therapy for people with cystic fibrosis.* Cochrane Database Syst Rev, 2014(10): p. CD008227.
170. Fieker, A., J. Philpott, and M. Armand, *Enzyme replacement therapy for pancreatic insufficiency: present and future.* Clin Exp Gastroenterol, 2011. **4**: p. 55-73.

171. Calvo-Lerma, J., et al., *Association between faecal pH and fat absorption in children with cystic fibrosis on a controlled diet and enzyme supplements dose.* Pediatr Res, 2021. **89**(1): p. 205-210.
172. Gallagher, P. and D. O'Mahony, *Constipation in old age.* Best Pract Res Clin Gastroenterol, 2009. **23**(6): p. 875-87.
173. Remond, D., et al., *Understanding the gastrointestinal tract of the elderly to develop dietary solutions that prevent malnutrition.* Oncotarget, 2015. **6**(16): p. 13858-98.
174. Drozdowski, L. and A.B. Thomson, *Aging and the intestine.* World J Gastroenterol, 2006. **12**(47): p. 7578-84.
175. Ohkusa, T., et al., *Gut Microbiota and Chronic Constipation: A Review and Update.* Front Med (Lausanne), 2019. **6**: p. 19.
176. Zhuang, X., et al., *Fecal Microbiota Alterations Associated With Diarrhea-Predominant Irritable Bowel Syndrome.* Front Microbiol, 2018. **9**: p. 1600.
177. Di Paolo, G. and T.W. Kim, *Linking lipids to Alzheimer's disease: cholesterol and beyond.* Nat Rev Neurosci, 2011. **12**(5): p. 284-96.
178. Calsolaro, V. and P. Edison, *Alterations in Glucose Metabolism in Alzheimer's Disease.* Recent Pat Endocr Metab Immune Drug Discov, 2016. **10**(1): p. 31-39.
179. Barupal, D.K., et al., *Sets of coregulated serum lipids are associated with Alzheimer's disease pathophysiology.* Alzheimers Dement (Amst), 2019. **11**: p. 619-627.
180. Nishiyama, H., et al., *Supplementation of pancreatic digestive enzymes alters the composition of intestinal microbiota in mice.* Biochem Biophys Res Commun, 2018. **495**(1): p. 273-279.
181. Chung, H.J., et al., *Intestinal removal of free fatty acids from hosts by Lactobacilli for the treatment of obesity.* FEBS Open Bio, 2016. **6**(1): p. 64-76.
182. Cleusix, V., et al., *Glycerol induces reuterin production and decreases Escherichia coli population in an in vitro model of colonic fermentation with immobilized human feces.* FEMS Microbiol Ecol, 2008. **63**(1): p. 56-64.
183. Kim, J. and P. Sudbery, *Candida albicans, a major human fungal pathogen.* J Microbiol, 2011. **49**(2): p. 171-7.
184. Treichel, H., Oliveira, D., Mazutti, M.A., Luccio, M., Oliveira J.V. *A review on microbial lipases production.* [Journal] 2010.
185. Barriuso, J., et al., *Structural traits and catalytic versatility of the lipases from the Candida rugosa-like family: A review.* Biotechnol Adv, 2016. **34**(5): p. 874-885.
186. Benjamin, S. and A. Pandey, *Candida rugosa lipases: molecular biology and versatility in biotechnology.* Yeast, 1998. **14**(12): p. 1069-87.
187. Mine, Y., et al., *Enhanced enzyme activity and enantioselectivity of lipases in organic solvents by crown ethers and cyclodextrins.* J Biosci Bioeng, 2003. **95**(5): p. 441-7.
188. Carvalho, A.C., et al., *Recent Advances in Lipase-Mediated Preparation of Pharmaceuticals and Their Intermediates.* Int J Mol Sci, 2015. **16**(12): p. 29682-716.
189. Zehani, N., et al., *Highly sensitive electrochemical biosensor for bisphenol A detection based on a diazonium-functionalized boron-doped diamond electrode modified with a multi-walled carbon nanotube-tyrosinase hybrid film.* Biosens Bioelectron, 2015. **74**: p. 830-5.
190. Lee, G.C., et al., *Analysis of the gene family encoding lipases in Candida rugosa by competitive reverse transcription-PCR.* Appl Environ Microbiol, 1999. **65**(9): p. 3888-95.
191. Grochulski, P., et al., *Two conformational states of Candida rugosa lipase.* Protein Sci, 1994. **3**(1): p. 82-91.
192. Akoh, C.C., G.C. Lee, and J.F. Shaw, *Protein engineering and applications of Candida rugosa lipase isoforms.* Lipids, 2004. **39**(6): p. 513-26.

193. Schmitt, J., et al., *Blocking the tunnel: engineering of Candida rugosa lipase mutants with short chain length specificity.* Protein Eng, 2002. **15**(7): p. 595-601.
194. Brocca, S., et al., *Sequence of the lid affects activity and specificity of Candida rugosa lipase isoenzymes.* Protein Sci, 2003. **12**(10): p. 2312-9.
195. Khan, F.I., et al., *The Lid Domain in Lipases: Structural and Functional Determinant of Enzymatic Properties.* Front Bioeng Biotechnol, 2017. **5**: p. 16.
196. Xu, M.-H., et al., *Immobilization of lipase fromCandida rugosaand its application for the synthesis of biodiesel in a two-step process.* Asia-Pacific Journal of Chemical Engineering, 2016. **11**(6): p. 910-917.
197. Herbst, D., S. Peper, and B. Niemeyer, *Enzyme catalysis in organic solvents: influence of water content, solvent composition and temperature on Candida rugosa lipase catalyzed transesterification.* J Biotechnol, 2012. **162**(4): p. 398-403.
198. Grochulski, P., et al., *Analogs of reaction intermediates identify a unique substrate binding site in Candida rugosa lipase.* Biochemistry, 1994. **33**(12): p. 3494-500.
199. Laguerre, M., et al., *Regioselectivity and fatty acid specificity of crude lipase extracts from Pseudozyma tsukubaensis, Geotrichum candidum,and Candida rugosa.* European Journal of Lipid Science and Technology, 2017. **119**(8).
200. Redondo, O., et al., *Comparative kinetic study of lipases A and B from Candida rugosa in the hydrolysis of lipid p-nitrophenyl esters in mixed micelles with Triton X-100.* Biochim Biophys Acta, 1995. **1243**(1): p. 15-24.
201. Pfaller, M.A., et al., *Candida rugosa, an emerging fungal pathogen with resistance to azoles: geographic and temporal trends from the ARTEMIS DISK antifungal surveillance program.* J Clin Microbiol, 2006. **44**(10): p. 3578-82.
202. Zare, A., et al., *Candida rugosa lipase immobilization on various chemically modified Chromium terephthalate MIL-101.* Journal of Molecular Liquids, 2018. **254**: p. 137-144.
203. Li, X., et al., *Improving Catalytic Performance of Candida rugosa Lipase by Chemical Modification with Polyethylene Glycol Functional Ionic Liquids.* Industrial & Engineering Chemistry Research, 2015. **54**(33): p. 8072-8079.
204. Stallings, V.A., et al., *Diagnosing malabsorption with systemic lipid profiling: pharmacokinetics of pentadecanoic acid and triheptadecanoic acid following oral administration in healthy subjects and subjects with cystic fibrosis.* Int J Clin Pharmacol Ther, 2013. **51**(4): p. 263-73.
205. Schoeler, M. and R. Caesar, *Dietary lipids, gut microbiota and lipid metabolism.* Rev Endocr Metab Disord, 2019. **20**(4): p. 461-472.
206. Cleusix, V., et al., *Inhibitory activity spectrum of reuterin produced by Lactobacillus reuteri against intestinal bacteria.* BMC Microbiol, 2007. **7**: p. 101.
207. Liang, H.F., et al., *Natural antimicrobial agent (reuterin) produced by lactobacillus reuteri for sanitization of biological tissues inoculated with pseudomonas aeruginosa.* Biotechnol Bioeng, 2003. **84**(2): p. 233-9.
208. Friesner, R.A., et al., *Glide: a new approach for rapid, accurate docking and scoring. 1. Method and assessment of docking accuracy.* J Med Chem, 2004. **47**(7): p. 1739-49.
209. Halgren, T.A., et al., *Glide: a new approach for rapid, accurate docking and scoring. 2. Enrichment factors in database screening.* J Med Chem, 2004. **47**(7): p. 1750-9.
210. Friesner, R.A., et al., *Extra precision glide: docking and scoring incorporating a model of hydrophobic enclosure for protein-ligand complexes.* J Med Chem, 2006. **49**(21): p. 6177-96.
211. Bauerl, C., et al., *Shifts in gut microbiota composition in an APP/PSS1 transgenic mouse model of Alzheimer's disease during lifespan.* Lett Appl Microbiol, 2018. **66**(6): p. 464-471.

212. Liu, P., et al., *Altered microbiomes distinguish Alzheimer's disease from amnestic mild cognitive impairment and health in a Chinese cohort.* Brain Behav Immun, 2019. **80**: p. 633-643.
213. Mezo, C., et al., *Different effects of constitutive and induced microbiota modulation on microglia in a mouse model of Alzheimer's disease.* Acta Neuropathol Commun, 2020. **8**(1): p. 119.
214. Sheflin, A.M., et al., *Linking dietary patterns with gut microbial composition and function.* Gut Microbes, 2017. **8**(2): p. 113-129.
215. Goodman, B.E., *Insights into digestion and absorption of major nutrients in humans.* Adv Physiol Educ, 2010. **34**(2): p. 44-53.
216. Conlon, M.A. and A.R. Bird, *The impact of diet and lifestyle on gut microbiota and human health.* Nutrients, 2014. **7**(1): p. 17-44.
217. Valdes, A.M., et al., *Role of the gut microbiota in nutrition and health.* BMJ, 2018. **361**: p. k2179.
218. Cheng, H.Y., et al., *Interactions Between the Gut Microbiota and the Host Innate Immune Response Against Pathogens.* Front Immunol, 2019. **10**: p. 607.
219. Martin, A.M., et al., *The Influence of the Gut Microbiome on Host Metabolism Through the Regulation of Gut Hormone Release.* Front Physiol, 2019. **10**: p. 428.
220. Agus, A., K. Clement, and H. Sokol, *Gut microbiota-derived metabolites as central regulators in metabolic disorders.* Gut, 2020.
221. Oliphant, K. and E. Allen-Vercoe, *Macronutrient metabolism by the human gut microbiome: major fermentation by-products and their impact on host health.* Microbiome, 2019. **7**(1): p. 91.
222. Cox, L.M. and H.L. Weiner, *Microbiota Signaling Pathways that Influence Neurologic Disease.* Neurotherapeutics, 2018. **15**(1): p. 135-145.
223. DeGruttola, A.K., et al., *Current Understanding of Dysbiosis in Disease in Human and Animal Models.* Inflamm Bowel Dis, 2016. **22**(5): p. 1137-50.
224. Aoun, A., F. Darwish, and N. Hamod, *The Influence of the Gut Microbiome on Obesity in Adults and the Role of Probiotics, Prebiotics, and Synbiotics for Weight Loss.* Prev Nutr Food Sci, 2020. **25**(2): p. 113-123.
225. Wallen, Z.D., et al., *Characterizing dysbiosis of gut microbiome in PD: evidence for overabundance of opportunistic pathogens.* NPJ Parkinsons Dis, 2020. **6**: p. 11.
226. Ritz, S., et al., *Gut microbiome as a response marker for pancreatic enzyme replacement therapy in a porcine model of exocrine pancreas insufficiency.* Microb Cell Fact, 2020. **19**(1): p. 221.
227. Bach Knudsen, K.E., et al., *Impact of Diet-Modulated Butyrate Production on Intestinal Barrier Function and Inflammation.* Nutrients, 2018. **10**(10).
228. Maroon, J.C. and J.W. Bost, *Omega-3 fatty acids (fish oil) as an anti-inflammatory: an alternative to nonsteroidal anti-inflammatory drugs for discogenic pain.* Surg Neurol, 2006. **65**(4): p. 326-31.
229. Mu, Q., V.J. Tavella, and X.M. Luo, *Role of Lactobacillus reuteri in Human Health and Diseases.* Front Microbiol, 2018. **9**: p. 757.
230. Martinez-Guryn, K., et al., *Small Intestine Microbiota Regulate Host Digestive and Absorptive Adaptive Responses to Dietary Lipids.* Cell Host Microbe, 2018. **23**(4): p. 458-469 e5.
231. Widyarman, A.S., et al., *The Anti-inflammatory Effects of Glycerol-supplemented Probiotic Lactobacillus reuteri on Infected Epithelial cells In vitro.* Contemp Clin Dent, 2018. **9**(2): p. 298-303.
232. Jones, S.E. and J. Versalovic, *Probiotic Lactobacillus reuteri biofilms produce antimicrobial and anti-inflammatory factors.* BMC Microbiol, 2009. **9**: p. 35.

233. Munck, A., et al., *Pancreatic enzyme replacement therapy for young cystic fibrosis patients.* J Cyst Fibros, 2009. **8**(1): p. 14-8.
234. Menden, A., et al., *Candida rugosa lipase alters the gastrointestinal environment in wild-type mice.* Biomed Pharmacother, 2020. **130**: p. 110579.
235. Belzer, C. and W.M. de Vos, *Microbes inside--from diversity to function: the case of Akkermansia.* ISME J, 2012. **6**(8): p. 1449-58.
236. Li, S., et al., *Lactobacillus reuteri improves gut barrier function and affects diurnal variation of the gut microbiota in mice fed a high-fat diet.* Food Funct, 2019. **10**(8): p. 4705-4715.
237. de Oliveira, U.M.F., et al., *Effect of the Presence of Surfactants and Immobilization Conditions on Catalysts' Properties of Rhizomucor miehei Lipase onto Chitosan.* Appl Biochem Biotechnol, 2018. **184**(4): p. 1263-1285.
238. Menden, A.H., Davane; Broedlow, Courtney Ann; Darcey, Teresa; Crawford, Fiona; Klatt, Nichole; Crynen, Stefan; Mullan, Michael; Ait-Ghezala, Ghania, *Datasets for: Lipase supplement alters the gastrointestinal environment in wild-type mice.* Mendeley Data, 2020. **V1**.
239. Hill, T.C., et al., *Using ecological diversity measures with bacterial communities.* FEMS Microbiol Ecol, 2003. **43**(1): p. 1-11.
240. Singh, R.K., et al., *Influence of diet on the gut microbiome and implications for human health.* J Transl Med, 2017. **15**(1): p. 73.
241. Leeming, E.R., et al., *Effect of Diet on the Gut Microbiota: Rethinking Intervention Duration.* Nutrients, 2019. **11**(12).
242. McConnell, E.L., A.W. Basit, and S. Murdan, *Measurements of rat and mouse gastrointestinal pH, fluid and lymphoid tissue, and implications for in-vivo experiments.* J Pharm Pharmacol, 2008. **60**(1): p. 63-70.
243. Centanni, M., et al., *Bifidobacterium pseudolongum in the Ceca of Rats Fed Hi-Maize Starch Has Characteristics of a Keystone Species in Bifidobacterial Blooms.* Appl Environ Microbiol, 2018. **84**(15).
244. Mangin, I., et al., *Oral administration of viable Bifidobacterium pseudolongum strain Patronus modified colonic microbiota and increased mucus layer thickness in rat.* FEMS Microbiol Ecol, 2018. **94**(11).
245. Daniel, H., et al., *High-fat diet alters gut microbiota physiology in mice.* ISME J, 2014. **8**(2): p. 295-308.
246. Peters, B.A., et al., *A taxonomic signature of obesity in a large study of American adults.* Sci Rep, 2018. **8**(1): p. 9749.
247. Ravussin, Y., et al., *Responses of gut microbiota to diet composition and weight loss in lean and obese mice.* Obesity (Silver Spring), 2012. **20**(4): p. 738-47.
248. Cani, P.D. and W.M. de Vos, *Next-Generation Beneficial Microbes: The Case of Akkermansia muciniphila.* Front Microbiol, 2017. **8**: p. 1765.
249. Goodrich, J.K., et al., *Human genetics shape the gut microbiome.* Cell, 2014. **159**(4): p. 789-99.
250. Liu, S., et al., *Oral Administration of miR-30d from Feces of MS Patients Suppresses MS-like Symptoms in Mice by Expanding Akkermansia muciniphila.* Cell Host Microbe, 2019. **26**(6): p. 779-794 e8.
251. Schwiertz, A., et al., *Anaerostipes caccae gen. nov., sp. nov., a new saccharolytic, acetate-utilising, butyrate-producing bacterium from human faeces.* Syst Appl Microbiol, 2002. **25**(1): p. 46-51.
252. Bui, T.P.N., W.M. de Vos, and C.M. Plugge, *Anaerostipes rhamnosivorans sp. nov., a human intestinal, butyrate-forming bacterium.* Int J Syst Evol Microbiol, 2014. **64**(Pt 3): p. 787-793.

253. Eeckhaut, V., et al., *Anaerostipes butyraticus sp. nov., an anaerobic, butyrate-producing bacterium from Clostridium cluster XIVa isolated from broiler chicken caecal content, and emended description of the genus Anaerostipes.* Int J Syst Evol Microbiol, 2010. **60**(Pt 5): p. 1108-1112.
254. Human Microbiome Project, C., *Structure, function and diversity of the healthy human microbiome.* Nature, 2012. **486**(7402): p. 207-14.
255. Lozupone, C.A., et al., *Diversity, stability and resilience of the human gut microbiota.* Nature, 2012. **489**(7415): p. 220-30.
256. Tavella, T., et al., *Elevated gut microbiome abundance of Christensenellaceae, Porphyromonadaceae and Rikenellaceae is associated with reduced visceral adipose tissue and healthier metabolic profile in Italian elderly.* Gut Microbes, 2021. **13**(1): p. 1-19.
257. Xu, Y., et al., *Function of Akkermansia muciniphila in Obesity: Interactions With Lipid Metabolism, Immune Response and Gut Systems.* Front Microbiol, 2020. **11**: p. 219.
258. Jo, J.H., E.A. Kennedy, and H.H. Kong, *Research Techniques Made Simple: Bacterial 16S Ribosomal RNA Gene Sequencing in Cutaneous Research.* J Invest Dermatol, 2016. **136**(3): p. e23-e27.
259. Spielman, L.J., D.L. Gibson, and A. Klegeris, *Unhealthy gut, unhealthy brain: The role of the intestinal microbiota in neurodegenerative diseases.* Neurochem Int, 2018. **120**: p. 149-163.
260. Brandscheid, C., et al., *Altered Gut Microbiome Composition and Tryptic Activity of the 5xFAD Alzheimer's Mouse Model.* J Alzheimers Dis, 2017. **56**(2): p. 775-788.
261. Liu, S., et al., *Gut Microbiota and Dysbiosis in Alzheimer's Disease: Implications for Pathogenesis and Treatment.* Mol Neurobiol, 2020. **57**(12): p. 5026-5043.
262. Cryan, J.F., et al., *The Microbiota-Gut-Brain Axis.* Physiol Rev, 2019. **99**(4): p. 1877-2013.
263. Long-Smith, C., et al., *Microbiota-Gut-Brain Axis: New Therapeutic Opportunities.* Annu Rev Pharmacol Toxicol, 2020. **60**: p. 477-502.
264. Ghosh, T.S., et al., *Mediterranean diet intervention alters the gut microbiome in older people reducing frailty and improving health status: the NU-AGE 1-year dietary intervention across five European countries.* Gut, 2020. **69**(7): p. 1218-1228.
265. Ang, Q.Y., et al., *Ketogenic Diets Alter the Gut Microbiome Resulting in Decreased Intestinal Th17 Cells.* Cell, 2020. **181**(6): p. 1263-1275 e16.
266. Morrill, S.J. and K.J. Gibas, *Ketogenic diet rescues cognition in ApoE4+ patient with mild Alzheimer's disease: A case study.* Diabetes Metab Syndr, 2019. **13**(2): p. 1187-1191.
267. Rusek, M., et al., *Ketogenic Diet in Alzheimer's Disease.* Int J Mol Sci, 2019. **20**(16).
268. Engels, C., et al., *Acrolein contributes strongly to antimicrobial and heterocyclic amine transformation activities of reuterin.* Sci Rep, 2016. **6**: p. 36246.
269. Zhang, J., et al., *Gut Microbial Glycerol Metabolism as an Endogenous Acrolein Source.* mBio, 2018. **9**(1).
270. Vinolo, M.A., et al., *Regulation of inflammation by short chain fatty acids.* Nutrients, 2011. **3**(10): p. 858-76.
271. Natto, Z.S., et al., *Omega-3 Fatty Acids Effects on Inflammatory Biomarkers and Lipid Profiles among Diabetic and Cardiovascular Disease Patients: A Systematic Review and Meta-Analysis.* Sci Rep, 2019. **9**(1): p. 18867.
272. Trapnell, B.C., et al., *Efficacy and safety of Creon 24,000 in subjects with exocrine pancreatic insufficiency due to cystic fibrosis.* J Cyst Fibros, 2009. **8**(6): p. 370-7.

273. Menden, A., et al., *A fast, miniaturised in-vitro assay developed for quantification of lipase enzyme activity.* J Enzyme Inhib Med Chem, 2019. **34**(1): p. 1474-1480.
274. Cammarota, G., et al., *European consensus conference on faecal microbiota transplantation in clinical practice.* Gut, 2017. **66**(4): p. 569-580.
275. Hu, J., et al., *Standardized Preparation for Fecal Microbiota Transplantation in Pigs.* Front Microbiol, 2018. **9**: p. 1328.
276. Zarrinpar, A., et al., *Antibiotic-induced microbiome depletion alters metabolic homeostasis by affecting gut signaling and colonic metabolism.* Nat Commun, 2018. **9**(1): p. 2872.
277. Wrzosek, L., et al., *Transplantation of human microbiota into conventional mice durably reshapes the gut microbiota.* Sci Rep, 2018. **8**(1): p. 6854.
278. Lee, C.H., et al., *Frozen vs Fresh Fecal Microbiota Transplantation and Clinical Resolution of Diarrhea in Patients With Recurrent Clostridium difficile Infection: A Randomized Clinical Trial.* JAMA, 2016. **315**(2): p. 142-9.
279. Dhariwal, A., et al., *MicrobiomeAnalyst: a web-based tool for comprehensive statistical, visual and meta-analysis of microbiome data.* Nucleic Acids Res, 2017. **45**(W1): p. W180-W188.
280. Caporaso, J.G., et al., *QIIME allows analysis of high-throughput community sequencing data.* Nat Methods, 2010. **7**(5): p. 335-6.
281. Smith, C.A., et al., *XCMS: processing mass spectrometry data for metabolite profiling using nonlinear peak alignment, matching, and identification.* Anal Chem, 2006. **78**(3): p. 779-87.
282. Chong, J. and J. Xia, *Using MetaboAnalyst 4.0 for Metabolomics Data Analysis, Interpretation, and Integration with Other Omics Data.* Methods Mol Biol, 2020. **2104**: p. 337-360.
283. Joshi, U., et al., *A permethrin metabolite is associated with adaptive immune responses in Gulf War Illness.* Brain Behav Immun, 2019. **81**: p. 545-559.
284. Afgan, E., et al., *The Galaxy platform for accessible, reproducible and collaborative biomedical analyses: 2018 update.* Nucleic Acids Res, 2018. **46**(W1): p. W537-W544.
285. Ewels, P., et al., *MultiQC: summarize analysis results for multiple tools and samples in a single report.* Bioinformatics, 2016. **32**(19): p. 3047-8.
286. Bolger, A.M., M. Lohse, and B. Usadel, *Trimmomatic: a flexible trimmer for Illumina sequence data.* Bioinformatics, 2014. **30**(15): p. 2114-20.
287. Kim, D., B. Langmead, and S.L. Salzberg, *HISAT: a fast spliced aligner with low memory requirements.* Nat Methods, 2015. **12**(4): p. 357-60.
288. Liao, Y., G.K. Smyth, and W. Shi, *featureCounts: an efficient general purpose program for assigning sequence reads to genomic features.* Bioinformatics, 2014. **30**(7): p. 923-30.
289. Robinson, M.D., D.J. McCarthy, and G.K. Smyth, *edgeR: a Bioconductor package for differential expression analysis of digital gene expression data.* Bioinformatics, 2010. **26**(1): p. 139-40.
290. Chen, E.Y., et al., *Enrichr: interactive and collaborative HTML5 gene list enrichment analysis tool.* BMC Bioinformatics, 2013. **14**: p. 128.
291. Kuleshov, M.V., et al., *Enrichr: a comprehensive gene set enrichment analysis web server 2016 update.* Nucleic Acids Res, 2016. **44**(W1): p. W90-7.
292. Liu, Z., et al., *Gut microbiota mediates intermittent-fasting alleviation of diabetes-induced cognitive impairment.* Nat Commun, 2020. **11**(1): p. 855.
293. Filzmoser, P., B. Liebmann, and K. Varmuza, *Repeated double cross validation.* Journal of Chemometrics, 2009. **23**(4): p. 160-171.

294. Shi, L., et al., *Variable selection and validation in multivariate modelling.* Bioinformatics, 2019. **35**(6): p. 972-980.
295. Singh, A., et al., *DIABLO: an integrative approach for identifying key molecular drivers from multi-omics assays.* Bioinformatics, 2019. **35**(17): p. 3055-3062.
296. Rohart, F., et al., *mixOmics: An R package for 'omics feature selection and multiple data integration.* PLoS Comput Biol, 2017. **13**(11): p. e1005752.
297. Pfeiffer, N., et al., *Acetatifactor muris gen. nov., sp. nov., a novel bacterium isolated from the intestine of an obese mouse.* Arch Microbiol, 2012. **194**(11): p. 901-7.
298. Baulch, J.E., et al., *Immune and Inflammatory Determinants Underlying Alzheimer's Disease Pathology.* J Neuroimmune Pharmacol, 2020. **15**(4): p. 852-862.
299. Zhang, X., et al., *Untargeted lipidomics reveals progression of early Alzheimer's disease in APP/PS1 transgenic mice.* Sci Rep, 2020. **10**(1): p. 14509.
300. Frohlich, E.E., et al., *Cognitive impairment by antibiotic-induced gut dysbiosis: Analysis of gut microbiota-brain communication.* Brain Behav Immun, 2016. **56**: p. 140-55.
301. Zhu, S., et al., *The progress of gut microbiome research related to brain disorders.* J Neuroinflammation, 2020. **17**(1): p. 25.
302. Li, L.L., et al., *Inulin with different degrees of polymerization protects against diet-induced endotoxemia and inflammation in association with gut microbiota regulation in mice.* Sci Rep, 2020. **10**(1): p. 978.
303. Kim, J., et al., *Codium fragile Ameliorates High-Fat Diet-Induced Metabolism by Modulating the Gut Microbiota in Mice.* Nutrients, 2020. **12**(6).
304. Wang, X., J. Xia, and C. Jiang, *Role of gut microbiota in the development of non-alcoholic fatty liver disease.* Liver Research, 2019. **3**(1): p. 25-30.
305. Macklin, L., et al., *Glucose tolerance and insulin sensitivity are impaired in APP/PS1 transgenic mice prior to amyloid plaque pathogenesis and cognitive decline.* Exp Gerontol, 2017. **88**: p. 9-18.
306. Mosconi, L., *Glucose metabolism in normal aging and Alzheimer's disease: Methodological and physiological considerations for PET studies.* Clin Transl Imaging, 2013. **1**(4).
307. Lee, H.J., et al., *Diabetes and Alzheimer's Disease: Mechanisms and Nutritional Aspects.* Clin Nutr Res, 2018. **7**(4): p. 229-240.
308. O'Connor, K.M., et al., *Manipulation of gut microbiota blunts the ventilatory response to hypercapnia in adult rats.* EBioMedicine, 2019. **44**: p. 618-638.
309. Cole, G.M., Q.L. Ma, and S.A. Frautschy, *Dietary fatty acids and the aging brain.* Nutr Rev, 2010. **68 Suppl 2**: p. S102-11.
310. Yehuda, S., et al., *The role of polyunsaturated fatty acids in restoring the aging neuronal membrane.* Neurobiol Aging, 2002. **23**(5): p. 843-53.
311. Saponaro, C., et al., *The Subtle Balance between Lipolysis and Lipogenesis: A Critical Point in Metabolic Homeostasis.* Nutrients, 2015. **7**(11): p. 9453-74.
312. Patterson, E., et al., *Health implications of high dietary omega-6 polyunsaturated Fatty acids.* J Nutr Metab, 2012. **2012**: p. 539426.
313. Ioannou, M.S., et al., *Neuron-Astrocyte Metabolic Coupling Protects against Activity-Induced Fatty Acid Toxicity.* Cell, 2019. **177**(6): p. 1522-1535 e14.
314. Polyzos, A.A., et al., *Metabolic Reprogramming in Astrocytes Distinguishes Region-Specific Neuronal Susceptibility in Huntington Mice.* Cell Metab, 2019. **29**(6): p. 1258-1273 e11.
315. DiNicolantonio, J.J. and J.H. O'Keefe, *Omega-6 vegetable oils as a driver of coronary heart disease: the oxidized linoleic acid hypothesis.* Open Heart, 2018. **5**(2): p. e000898.

316. Camargo, N., et al., *High-fat diet ameliorates neurological deficits caused by defective astrocyte lipid metabolism.* FASEB J, 2012. **26**(10): p. 4302-15.
317. Kaur, D., V. Sharma, and R. Deshmukh, *Activation of microglia and astrocytes: a roadway to neuroinflammation and Alzheimer's disease.* Inflammopharmacology, 2019. **27**(4): p. 663-677.
318. Bonaz, B., T. Bazin, and S. Pellissier, *The Vagus Nerve at the Interface of the Microbiota-Gut-Brain Axis.* Front Neurosci, 2018. **12**: p. 49.
319. Manta, S., et al., *Enhancement of the function of rat serotonin and norepinephrine neurons by sustained vagus nerve stimulation.* J Psychiatry Neurosci, 2009. **34**(4): p. 272-80.
320. Childs, J.E., et al., *Vagus Nerve Stimulation as a Tool to Induce Plasticity in Pathways Relevant for Extinction Learning.* J Vis Exp, 2015(102): p. e53032.
321. Kim, H.W., et al., *3,3'-Diindolylmethane inhibits lipopolysaccharide-induced microglial hyperactivation and attenuates brain inflammation.* Toxicol Sci, 2014. **137**(1): p. 158-67.
322. Huffman, W.J., et al., *Modulation of neuroinflammation and memory dysfunction using percutaneous vagus nerve stimulation in mice.* Brain Stimul, 2019. **12**(1): p. 19-29.
323. Kahveci, D. and X. Xu, *Enhancement of activity and selectivity of Candida rugosa lipase and Candida antarctica lipase A by bioimprinting and/or immobilization for application in the selective ethanolysis of fish oil.* Biotechnol Lett, 2011. **33**(10): p. 2065-71.
324. Sri Kaja, B., et al., *Investigating Enzyme Activity of Immobilized Candida rugosa Lipase.* Journal of Food Quality, 2018. **2018**: p. 1-9.
325. Pereira, E.B., et al., *Esterification activity and stability of Candida rugosa lipase immobilized into chitosan.* Appl Biochem Biotechnol, 2002. **98-100**: p. 977-86.
326. Mozaffar, Z.W., J., *Invert emulsion as a medium for fungal liapse activity.* Journal of the American Oil Chemists' Society, 1995. **72**(11): p. 1361-1366.
327. Irwin, J.J., et al., *ZINC: a free tool to discover chemistry for biology.* J Chem Inf Model, 2012. **52**(7): p. 1757-68.
328. Dairaku, T., et al., *A practical fluorometric assay method to measure lysosomal acid lipase activity in dried blood spots for the screening of cholesteryl ester storage disease and Wolman disease.* Mol Genet Metab, 2014. **111**(2): p. 193-6.
329. Palocci, C., et al., *An approach to address Candida rugosa lipase regioselectivity in the acylation reactions of trytilated glucosides.* J Biotechnol, 2007. **128**(4): p. 908-18.
330. Grippa, E., et al., *Inhibition of Candida rugosa lipase by berberine and structurally related alkaloids, evaluated by high-performance liquid chromatography.* Biosci Biotechnol Biochem, 1999. **63**(9): p. 1557-62.
331. Ruiz, C., et al., *Inhibition of Candida rugosa lipase by saponins, flavonoids and alkaloids.* Journal of Molecular Catalysis B: Enzymatic, 2006. **40**(3-4): p. 138-143.
332. Debnath, S., et al., *Discovery of novel potential selective HDAC8 inhibitors by combine ligand-based, structure-based virtual screening and in-vitro biological evaluation.* Sci Rep, 2019. **9**(1): p. 17174.
333. Singh, N., B.O. Villoutreix, and G.F. Ecker, *Rigorous sampling of docking poses unveils binding hypothesis for the halogenated ligands of L-type Amino acid Transporter 1 (LAT1).* Sci Rep, 2019. **9**(1): p. 15061.
334. Pimentel, M.C., et al., *Immobilization of Candida rugosa lipase on magnetized Dacron: kinetic study.* Artif Cells Blood Substit Immobil Biotechnol, 2007. **35**(2): p. 221-35.

335. Gupta, P.K. and K.V. Sastry, *Effect of mercuric chloride on enzyme activities in the digestive system and chemical composition of liver and muscles of the catfish, Heteropneustes fossilis.* Ecotoxicol Environ Saf, 1981. **5**(4): p. 389-400.
336. Liu, N., et al., *Synthesis of Naturally Occurring Tropones and Tropolones.* Tetrahedron, 2014. **70**(49): p. 9281-9305.
337. Bei, W.J., et al., *Lipid-regulating effect of traditional chinese medicine: mechanisms of actions.* Evid Based Complement Alternat Med, 2012. **2012**: p. 970635.
338. Li, Y.L., et al., *The glycosides from Lomatogonium rotatum.* Nat Prod Res, 2008. **22**(3): p. 198-202.
339. Bao, L., et al., *Hypolipidemic effects of flavonoids extracted from Lomatogonium rotatum.* Exp Ther Med, 2016. **11**(4): p. 1417-1424.
340. Luo, S., et al., *The inhibitory effects of an eight-herb formula (RCM-107) on pancreatic lipase: enzymatic, HPTLC profiling and in silico approaches.* Heliyon, 2019. **5**(9): p. e02453.
341. Saez-Atienzar, S. and E. Masliah, *Cellular senescence and Alzheimer disease: the egg and the chicken scenario.* Nat Rev Neurosci, 2020. **21**(8): p. 433-444.
342. Vaz, M. and S. Silvestre, *Alzheimer's disease: Recent treatment strategies.* Eur J Pharmacol, 2020. **887**: p. 173554.
343. Askarova, S., et al., *The Links Between the Gut Microbiome, Aging, Modern Lifestyle and Alzheimer's Disease.* Front Cell Infect Microbiol, 2020. **10**: p. 104.
344. Haran, J.P., et al., *Alzheimer's Disease Microbiome Is Associated with Dysregulation of the Anti-Inflammatory P-Glycoprotein Pathway.* mBio, 2019. **10**(3).
345. Sochocka, M., et al., *The Gut Microbiome Alterations and Inflammation-Driven Pathogenesis of Alzheimer's Disease-a Critical Review.* Mol Neurobiol, 2019. **56**(3): p. 1841-1851.
346. Rea, K., T.G. Dinan, and J.F. Cryan, *The microbiome: A key regulator of stress and neuroinflammation.* Neurobiol Stress, 2016. **4**: p. 23-33.
347. Cerovic, M., G. Forloni, and C. Balducci, *Neuroinflammation and the Gut Microbiota: Possible Alternative Therapeutic Targets to Counteract Alzheimer's Disease?* Front Aging Neurosci, 2019. **11**: p. 284.
348. Chen, C., et al., *Gut dysbiosis contributes to amyloid pathology, associated with C/EBPbeta/AEP signaling activation in Alzheimer's disease mouse model.* Sci Adv, 2020. **6**(31): p. eaba0466.
349. Zhuang, Z.Q., et al., *Gut Microbiota is Altered in Patients with Alzheimer's Disease.* J Alzheimers Dis, 2018. **63**(4): p. 1337-1346.
350. Peng, M. and D. Biswas, *Short chain and polyunsaturated fatty acids in host gut health and foodborne bacterial pathogen inhibition.* Crit Rev Food Sci Nutr, 2017. **57**(18): p. 3987-4002.
351. Trang, T., J. Chan, and D.Y. Graham, *Pancreatic enzyme replacement therapy for pancreatic exocrine insufficiency in the 21(st) century.* World J Gastroenterol, 2014. **20**(33): p. 11467-85.
352. Graham, D.Y., *Enzyme replacement therapy of exocrine pancreatic insufficiency in man. Relations between in vitro enzyme activities and in vivo potency in commercial pancreatic extracts.* N Engl J Med, 1977. **296**(23): p. 1314-7.
353. Graham, D.Y., *An enteric-coated pancreatic enzyme preparation that works.* Dig Dis Sci, 1979. **24**(12): p. 906-9.
354. Greetham, H.L., et al., *Allobaculum stercoricanis gen. nov., sp. nov., isolated from canine feces.* Anaerobe, 2004. **10**(5): p. 301-7.
355. Bottacini, F., et al., *Diversity, ecology and intestinal function of bifidobacteria.* Microb Cell Fact, 2014. **13 Suppl 1**: p. S4.

356. Hernandez, M.A.G., et al., *The Short-Chain Fatty Acid Acetate in Body Weight Control and Insulin Sensitivity.* Nutrients, 2019. **11**(8).
357. Uhr, G.T., L. Dohnalova, and C.A. Thaiss, *The Dimension of Time in Host-Microbiome Interactions.* mSystems, 2019. **4**(1).
358. Lepara, O., et al., *Decreased serum lipids in patients with probable Alzheimer's disease.* Bosn J Basic Med Sci, 2009. **9**(3): p. 215-20.
359. Nagai, M., et al., *Effects of pancrelipase on nonalcoholic fatty liver disease after pancreaticoduodenectomy.* J Hepatobiliary Pancreat Sci, 2014. **21**(3): p. 186-92.
360. Slesinski, M.J., et al., *Lipid levels in adults with cystic fibrosis.* J Am Diet Assoc, 1994. **94**(4): p. 402-8.
361. Van Dyken, P. and B. Lacoste, *Impact of Metabolic Syndrome on Neuroinflammation and the Blood-Brain Barrier.* Front Neurosci, 2018. **12**: p. 930.
362. Cunnane, S.C., et al., *Plasma and brain fatty acid profiles in mild cognitive impairment and Alzheimer's disease.* J Alzheimers Dis, 2012. **29**(3): p. 691-7.
363. Spangenberg, E.E., et al., *Eliminating microglia in Alzheimer's mice prevents neuronal loss without modulating amyloid-beta pathology.* Brain, 2016. **139**(Pt 4): p. 1265-81.
364. Hong, S., et al., *Complement and microglia mediate early synapse loss in Alzheimer mouse models.* Science, 2016. **352**(6286): p. 712-716.
365. Kashon, M.L., et al., *Associations of cortical astrogliosis with cognitive performance and dementia status.* J Alzheimers Dis, 2004. **6**(6): p. 595-604; discussion 673-81.
366. Li, K., et al., *Reactive Astrocytes in Neurodegenerative Diseases.* Aging Dis, 2019. **10**(3): p. 664-675.
367. Satoh, J., et al., *TMEM119 marks a subset of microglia in the human brain.* Neuropathology, 2016. **36**(1): p. 39-49.
368. Neidert, N., et al., *Microglia-Specific Expression of Olfml3 Is Directly Regulated by Transforming Growth Factor beta1-Induced Smad2 Signaling.* Front Immunol, 2018. **9**: p. 1728.
369. Pelisch, N., et al., *CCL3 contributes to secondary damage after spinal cord injury.* J Neuroinflammation, 2020. **17**(1): p. 362.
370. Liddelow, S.A. and B.A. Barres, *Reactive Astrocytes: Production, Function, and Therapeutic Potential.* Immunity, 2017. **46**(6): p. 957-967.
371. Nichols, R.G. and E.R. Davenport, *The relationship between the gut microbiome and host gene expression: a review.* Hum Genet, 2021. **140**(5): p. 747-760.
372. Mancuso, C. and R. Santangelo, *Alzheimer's disease and gut microbiota modifications: The long way between preclinical studies and clinical evidence.* Pharmacol Res, 2018. **129**: p. 329-336.
373. Marizzoni, M., et al., *Short-Chain Fatty Acids and Lipopolysaccharide as Mediators Between Gut Dysbiosis and Amyloid Pathology in Alzheimer's Disease.* J Alzheimers Dis, 2020. **78**(2): p. 683-697.
374. Shimizu, K., et al., *Measurement of the Intestinal pH in Mice under Various Conditions Reveals Alkalization Induced by Antibiotics.* Antibiotics (Basel), 2021. **10**(2).
375. Lunagariya, N.A., et al., *Inhibitors of pancreatic lipase: state of the art and clinical perspectives.* EXCLI J, 2014. **13**: p. 897-921.
376. de Chaves, E.P. and V. Narayanaswami, *Apolipoprotein E and cholesterol in aging and disease in the brain.* Future Lipidol, 2008. **3**(5): p. 505-530.
377. Vaya, J. and H.M. Schipper, *Oxysterols, cholesterol homeostasis, and Alzheimer disease.* J Neurochem, 2007. **102**(6): p. 1727-1737.
378. Sienski, G., et al., *APOE4 disrupts intracellular lipid homeostasis in human iPSC-derived glia.* Sci Transl Med, 2021. **13**(583).

379. Gauthier, S.G., *Alzheimer's disease: the benefits of early treatment.* Eur J Neurol, 2005. **12 Suppl 3**: p. 11-6.
380. Broulikova, H.M., et al., *The Potential Impact of Alzheimer's Disease Early Treatment on Societal Costs of Care in Czechia: A Simulation Approach.* J Ment Health Policy Econ, 2018. **21**(4): p. 147-161.
381. Buckley, M.M., et al., *Glucagon-Like Peptide-1 Secreting L-Cells Coupled to Sensory Nerves Translate Microbial Signals to the Host Rat Nervous System.* Front Cell Neurosci, 2020. **14**: p. 95.
382. Sarkar, A., et al., *Psychobiotics and the Manipulation of Bacteria-Gut-Brain Signals.* Trends Neurosci, 2016. **39**(11): p. 763-781.
383. Bird, C.M. and N. Burgess, *The hippocampus and memory: insights from spatial processing.* Nat Rev Neurosci, 2008. **9**(3): p. 182-94.
384. Diepenbroek, C., et al., *Validation and characterization of a novel method for selective vagal deafferentation of the gut.* Am J Physiol Gastrointest Liver Physiol, 2017. **313**(4): p. G342-G352.
385. Fabelo, N., et al., *Evidence for premature lipid raft aging in APP/PS1 double-transgenic mice, a model of familial Alzheimer disease.* J Neuropathol Exp Neurol, 2012. **71**(10): p. 868-81.
386. Bai, Y.R., et al., *Alterations of fatty acid composition and metabolism in APP/PS1 transgenic mice.* Neurosci Lett, 2020. **738**: p. 135401.
387. Vestergaard, M., et al., *Cholesterol, lipids, amyloid Beta, and Alzheimer's.* Curr Alzheimer Res, 2010. **7**(3): p. 262-70.
388. Stuckey, J.I., et al., *Structure-Activity Relationships and Kinetic Studies of Peptidic Antagonists of CBX Chromodomains.* J Med Chem, 2016. **59**(19): p. 8913-8923.
389. Nguyen, T.L., et al., *How informative is the mouse for human gut microbiota research?* Dis Model Mech, 2015. **8**(1): p. 1-16.

APPENDIX

Chapter II

2.1: Supplementary figures

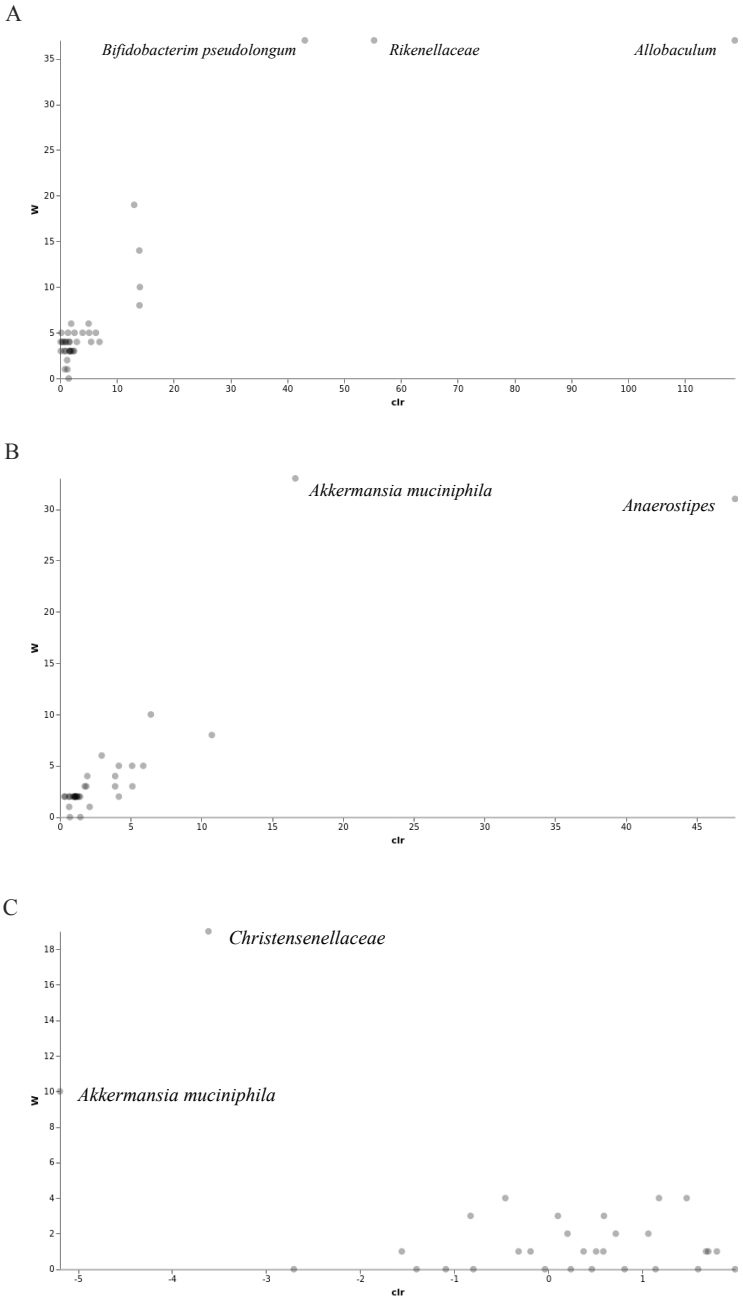

Supplementary figure 2.2.1: ANCOM *analysis in our short- and long-term study to determine significant species and genera driving the observed differences in diversity parameters. A. Short-term study (cecum) B. Long-term study (feces) C. Long-term study (cecum). ANCOM analysis and FDR correction was performed with Qiime2. For W-value determination pairwise comparisons of groups were performed. Significant taxa were classified and labelled when* $p_{FDR}<0.05$ *as determined by pairwise ANCOM.*

Chapter III

3.1: Supplementary figures

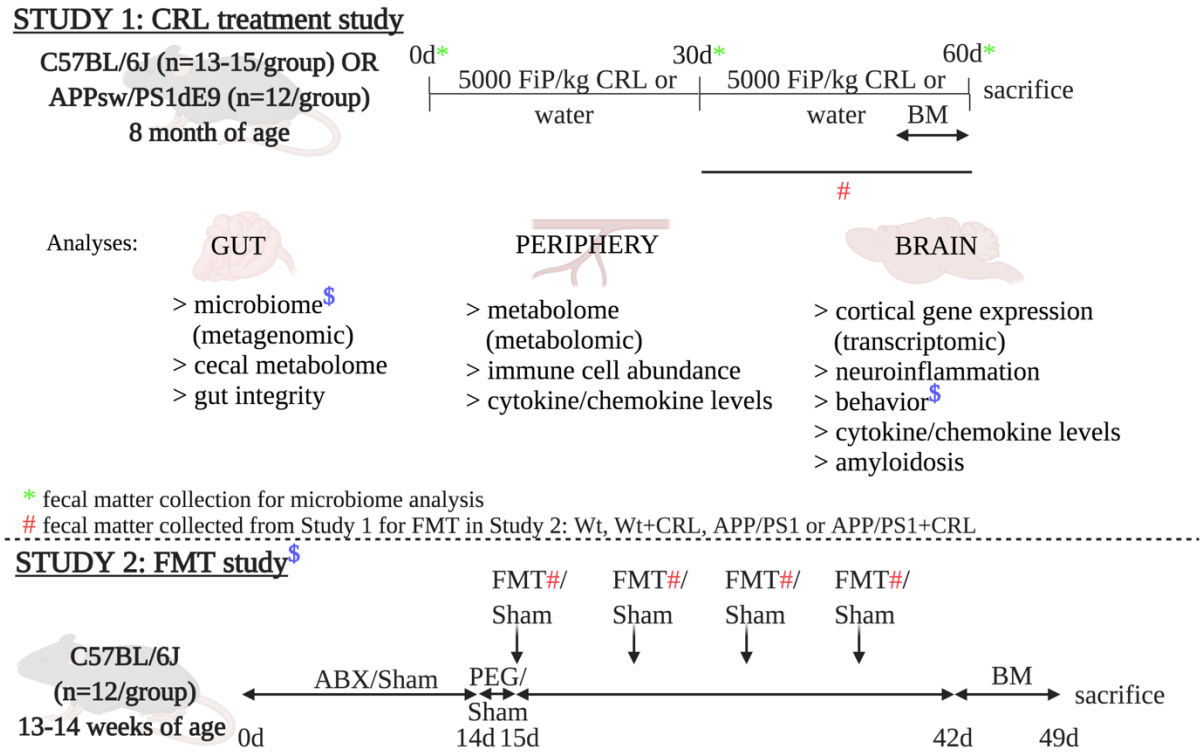

Abbreviations: ABX: antibiotic cocktail; PEG: bowel cleanse; FMT: fecal matter transplants; BM: Barnes maze

Supplementary figure 3.1.1: Overview of the conducted studies in Chapter III. In study 1, APP/PS1 and Wt mice received 5000 FIP/kg CRL in their drinking water or regular water for controls. Fecal samples were collected at 0, 30 and 60 days of treatment to analyse microbial changes throughout the treatment period. In addition, fecal samples were collected three times per week between treatment day 30 and 60 and live stocks maintained for Study 2. Two weeks before sacrifice mice were tested in the Barnes maze. After sacrifice the gut, periphery and brain were analysed to assess CRL's treatment effect on AD pathology compared to Wt mice. Finally, it was investigated in study 2, whether the treatment effects in the gut of Study 1 could be transferred ABX Wt mice, which have been reported to exhibit memory deficits via fecal matter transplants.

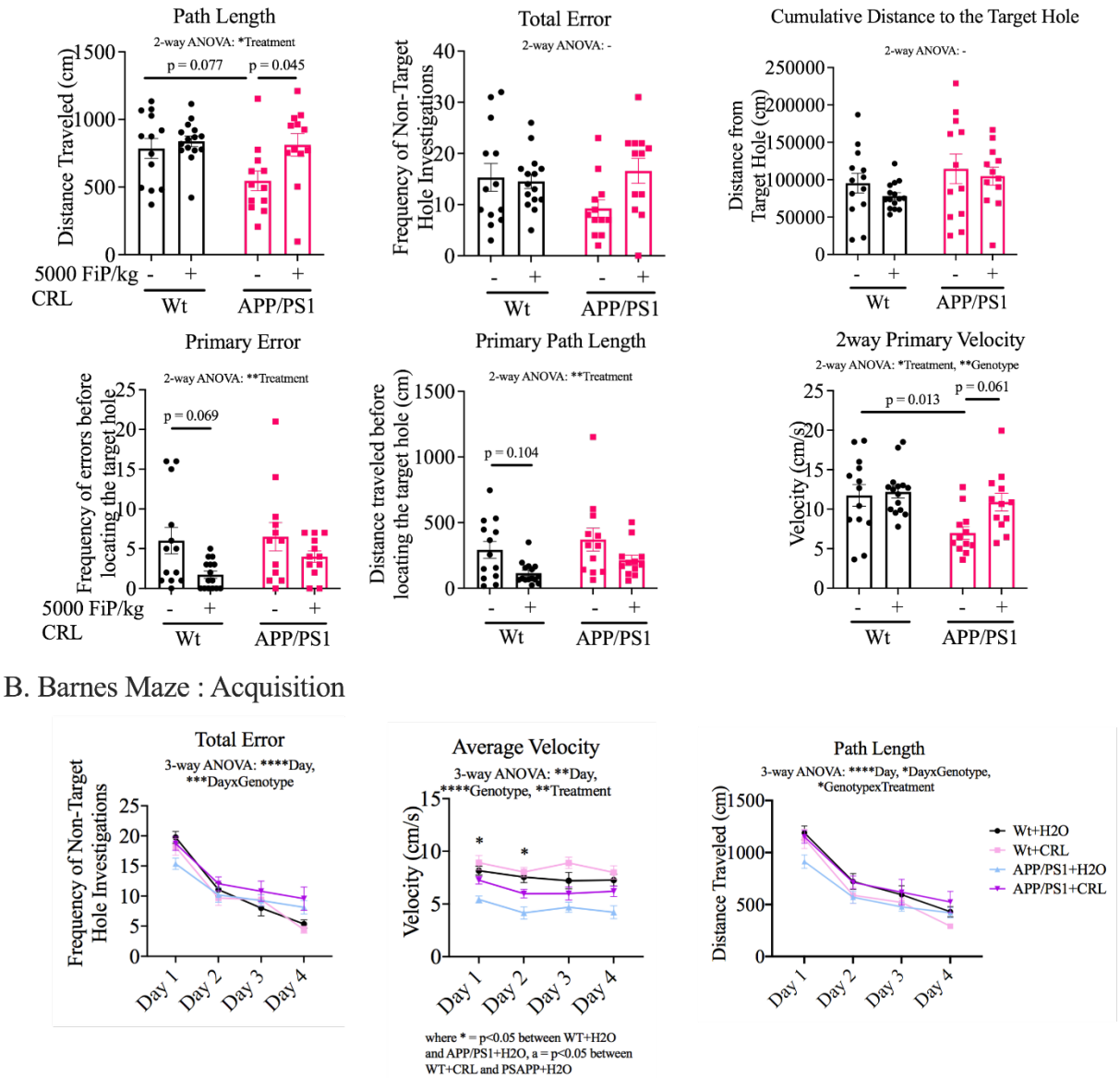

*Supplementary figure 3.1.2: Barnes maze parameters of Wt and APP/PS1 treated with CRL. A. Additional probe parameters showing treatment-dependent trends in primary error, primary pathway, and primary velocity (before first target hole interaction). Path length was reduced in untreated APP/PS1 mice similarly to velocity. No significant differences were determined for total error and cumulative distance to target hole. B. The acquisition data shows similarly to the probe significant differences for untreated APP/PS1 mice in average velocity but no difference in path length and total error. Significance of probe data was determined by 2-way ANOVA with Tukey correction, while acquisition data was analysed with 3-way ANOVA. Significance: * p<0.05, ** p<0.01, *** p<0.001, **** p<0.0001.*

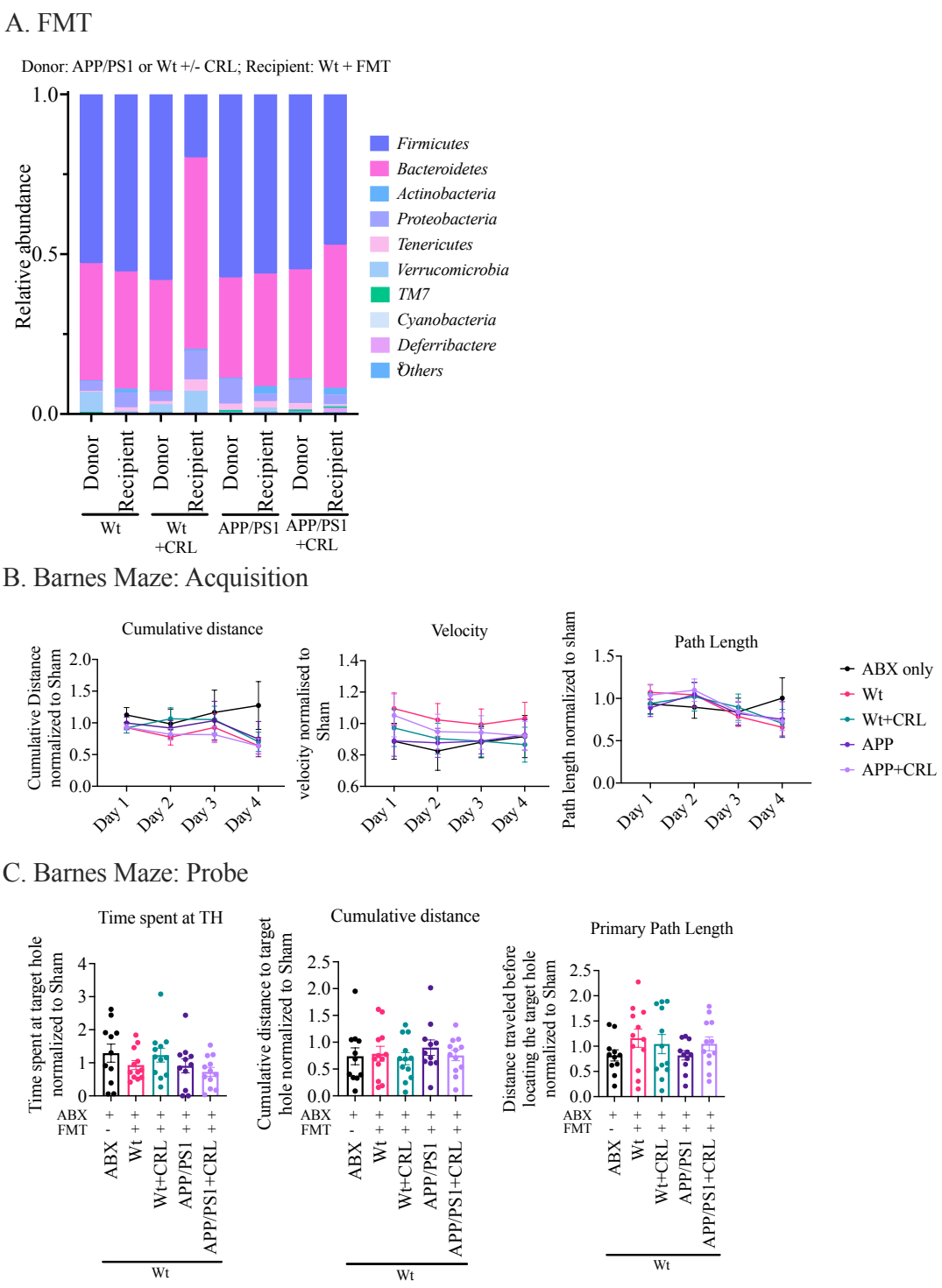

*Supplementary figure 3.1.2: FMT study and additional Barnes maze parameters. A. Taxonomy of donor and recipient of fecal matter revealed a great imbalance in Wt+CRL recipient mice, which might have been introduced during the oral gavage procedure. B. Additional probe parameters of the Barnes maze analysis revealed no further differences in primary path length, time spent at target hole or cumulative distance. C. The additional acquisition data of the Barnes maze analysis determined no significant difference in cumulative distance, path length or velocity. Probe data was analysed by 2-way ANOVA with Tukey correction, while acquisition data was analysed with 3-way ANOVA. Significance: * p<0.05, ** p<0.01, *** p<0.001, **** p<0.0001.*

Chapter IV

4.1: Supplementary figures

```
f= "splitme"
split_number= 25000
number_of_sdfs = split_number
i=0
j=0
f2=open(f+'_'+str(j)+'.sdf','w')
for line in open(f+'.sdf'):
        f2.write(line)
        if line[:4] == "$$$$":
                i+=1
        if i > number_of_sdfs:
                number_of_sdfs += split_number
                f2.close()
                j+=1
                f2=open(f+'_'+str(j)+'.sdf','w')
print(i)
```

Supplementary figure 4.1.1: Programming for splitting of sdf files including more than 50000 compounds into subfiles with a maximum of 25000 ligands. Hence, the Schrodinger software will be able to process these files without running out of memory during the docking calculation.

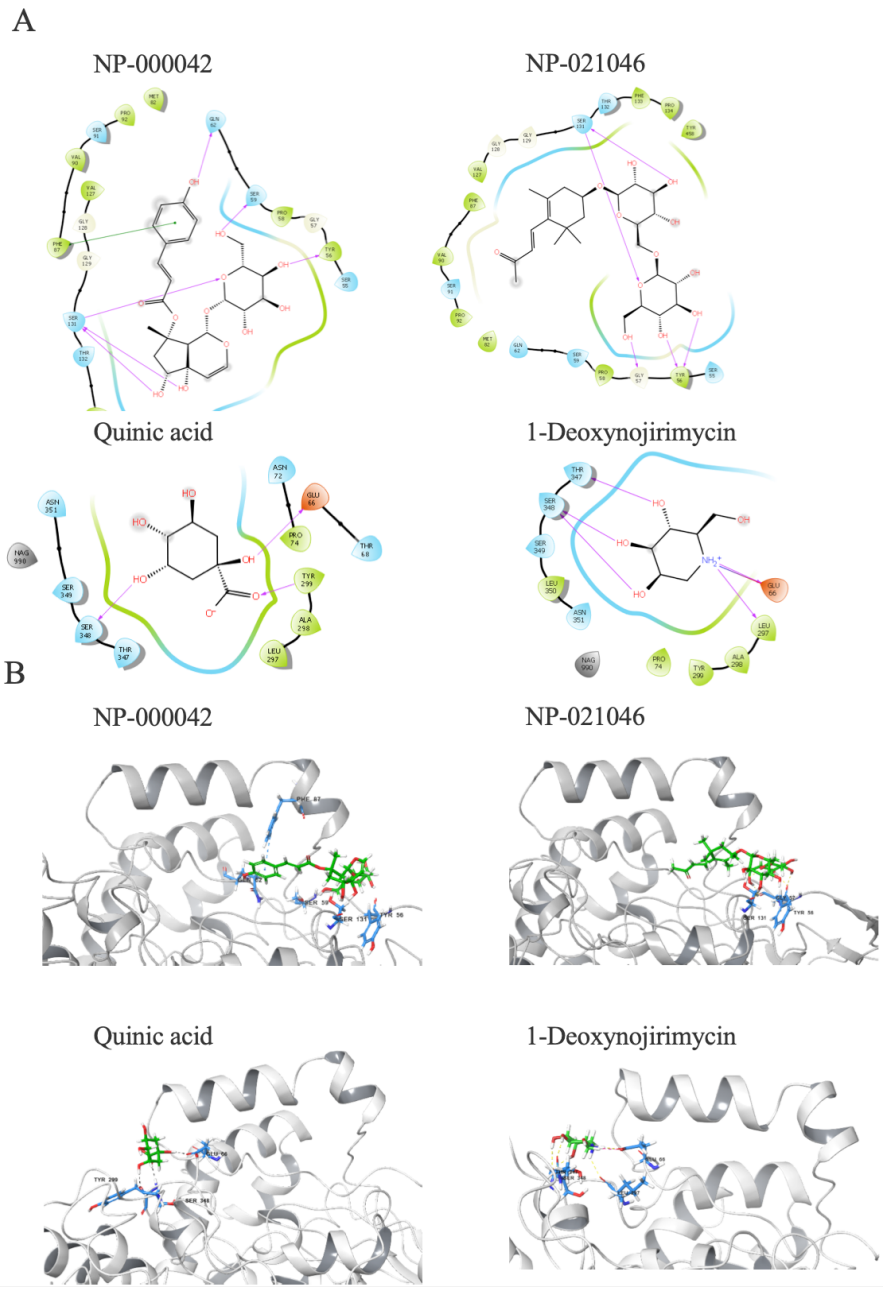

Supplementary figure 4.1.2: In silico screening results for less effective enhancer and inhibitors. A. 2-dimensional scheme of modulators in their respective binding sites 1 (quinic acid and 1-deoxynojirimycin) and 3 (NP-000042 and NP-021046). B. Three-dimensional image of modulators in respective binding sites.

A Inhibitor

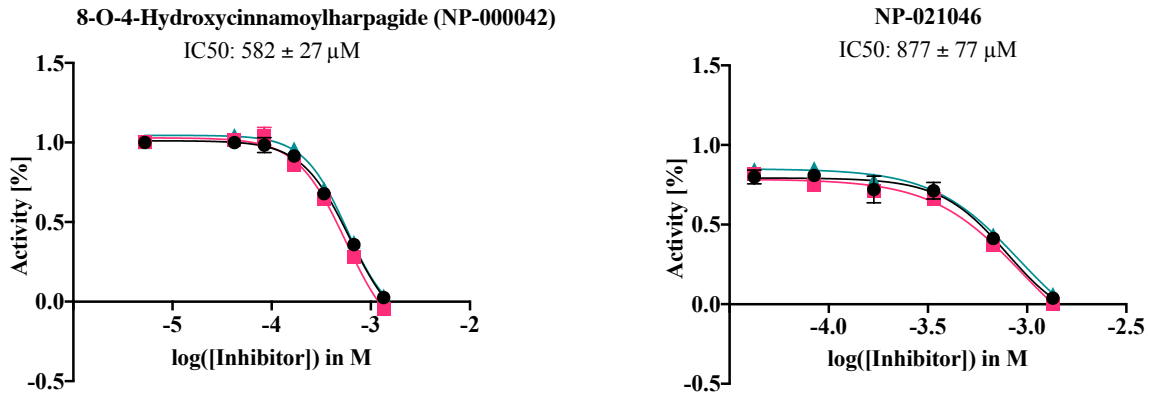

B Enhancer

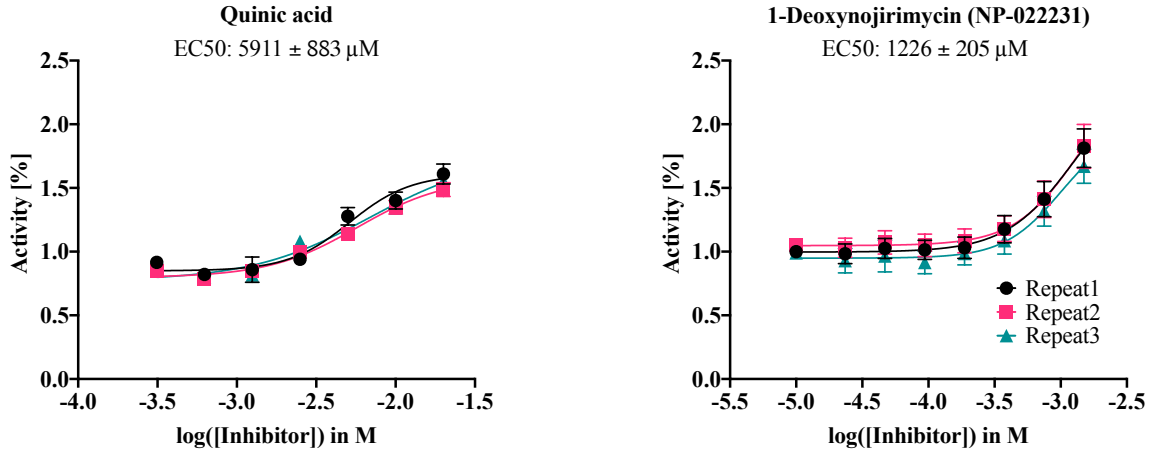

Supplementary figure 4.2.3: EC50 and IC50 of in silico-determined modulators with weaker interaction parameters. A. IC50 determination of weaker inhibitors in triplicate with IC50 0.6 – 0.9 mM. B. EC50 determination of weaker enhancers with EC50 of 1 – 6 mM. Enhancement effect of 1-Deoxynojirimycin could not be fully investigated due to unspecific effects of DMSO above 2 mM of modulator.

4.2: Supplementary table

Supplementary table 4.2.1: Summary of in vitro tested compounds. The selected modulators were identified as natural products and commercially available with XP Scores <-5. The in vitro analysis aided to determine the impact of the in silico selected modulators on CRL activity in vitro.

ID	Name	XP Score	MW (g/mol)	Allosteric site	Vendor	Order-number	Purity
1	D-manno-γ-lactone	-6.821	177.2	Site 1	TRC	M166000	98%
2	Deoxyaltronojirimycin	-6.673	199.6	Site 1	TRC	D231750	N/A
3	D-glucoronic acid	-5.514	216.1	Site 1	TRC	I252000	98%
4	Conduritol B	-5.339	164.1	Site 1	TRC	C665000	N/A
5	Deoxyfuconojirimycin	-5.730	183.6	Site 1	TRC	D236000	98%
6	D-Mannose	-5.768	180.2	Site 1	Sigma	M2069-25g	≥99%
7	**Tropolone**	**-5.603**	**122.1**	**Site 1**	**Sigma**	**T89702-1G**	**98%**
8	D-fructopyranose	-5.426	180.2	Site 1	Sigma	F0127-10MG	≥99%
9	D-Chiro-inositol	-6.240	180.2	Site 1	Sigma	74137-10MG	≥98%
10	DL-Alaninol	-5.236	75.1	Site 1	Sigma	192171-5G	98%
11	D-Quinic Acid	-5.620	192.2	Site 1	Sigma	138622-25g	98%
12	D-gulonic acid lactone	-5.510	178.1	Site 1	Sigma	310301-5G	95%
13	D-glucosamine	-8.163	215.6	Site 1	Sigma	G4875-10MG	≥99%
14	Gluconolactone	-5.510	178.1	Site 1	Sigma	G2164-100G	≥99%
15	3-Aminopropanamide HCl	-5.643	124.6	Site 1	Sigma	CDS000027	N/A
16	D-Arabinose	-5.278	150.1	Site 1	Sigma	A3131-10G	≥98%
17	L-Glucose	-5.807	180.2	Site 1	Sigma	G5500-250MG	≥99%
18	D-tagatose	-5.104	180.2	Site 1	Sigma	T2751-10MG	≥98.5%
19	1-Deoxymannojirimycin	-6.936	199.6	Site 1	Cayman	17178	≥98%
20	Conduritol B epoxide	-5.545	162.1	Site 1	Cayman	15216	≥95%
21	kanossamine hydrochloride	-5.814	215.6	Site 1	Cayman	16623	≥98%
22	1,4 Dideoxy-1,4-imino-D-arabinitol	-6.163	169.6	Site 1	Cayman	20939	≥95%
23	cysteamine hydrochloride	-5.508	113.6	Site 1	Cayman	22193	≥95%
24	D-Xylulose	-5.479	150.1	Site 1	Cayman	20830	≥95%
25	NP-001679	-8.071	406.4	Site 3	AnalytiCon	NP-001679	97%
26	NP-007267	-6.388	194.1	Site 2	AnalytiCon	NP-007267	70%
27	NP-012643	-9.262	620.6	Site 3	AnalytiCon	NP-012643	78%
28	NP-008789	-8.305	438.4	Site 3	AnalytiCon	NP-008789	86%
29	NP-017028	-8.979	343.3	Site 3	AnalytiCon	NP-017028	100%
30	NP-002623	-10.783	594.5	Site 3	AnalytiCon	NP-002623	70%
31	**Cynaroside**	**-8.818**	**448.4**	**Site 3**	**Sigma**	**PHL89724**	**≥95%**
32	NP-000042	-9.027	510.5	Site 3	AnalytiCon	NP-000042	90%
33	NP-016657	-8.611	534.5	Site 3	AnalytiCon	NP-016657	99%
34	NP-004213	-8.298	408.4	Site 3	AnalytiCon	NP-004213	89%
35	**NP-008496**	**-8.931**	**416.4**	**Site 3**	**AnalytiCon**	**NP-008496**	**99%**
36	**Rutin**	**-8.216**	**610.5**	**Site 3**	**Cayman**	**19868**	**≥98%**
37	NP-018732	-9.026	548.5	Site 3	AnalytiCon	NP-018732	99%
38	NP-001297	-8.072	584.5	Site 3	AnalytiCon	NP-001297	70%
39	NP-021046	-8.986	532.6	Site 3	AnalytiCon	NP-021046	82%
40	NP-005807	-8.352	538.5	Site 3	AnalytiCon	NP-005807	98%
41	NP-005114	-8.432	636.5	Site 3	AnalytiCon	NP-005114	100%
42	NP-011987	-9.320	630.5	Site 3	AnalytiCon	NP-011987	98%
43	1-Deoxynojirimycin	-7.519	163.2	Site 1	Cayman	21500	≥95%
44	NP-019608	-8.234	470.5	Site 3	AnalytiCon	NP-019608	100%
45	NP-016501	-9.138	564.5	Site 3	AnalytiCon	NP-016501	98%
46	Voglibose	-8.486	267.3	Site 2	Cayman	14179	≥95%
47	Methylhistamine	-7.169	198.1	Site 2	Cayman	19516	≥95%
48	Loganin	-8.232	390.4	Site 3	Cayman	19997	≥98%
49	Galactostatin	-7.551	199.6	Site 2	Cayman	17179	≥98%
50	Gentiobiose	-9.028	342.3	Site 3	Sigma	G3000	>95%
51	2- -D-Glucopyranosyl-a-D-glucopyranose	-8.358	342.3	Site 3	Sigma	R543772	N/A
52	Histamine dihydrochloride	-7.689	111.2	Site 2	Sigma	H7125-10M	≥97%
53	Nojirimycin	-7.671	243.2	Site 2	Sigma	N7779-5mg	≥98%

	Berberine	-	371.81	-	Sigma	B3251-5g	≥98%
	β-Aescin	-	1131.26	-	Santa Cruz	Sc-491651	≥90%
	Trigonelline	-	173.6	-	Cayman	11904	≥95%